

**Die Rolle des Sirtuins SIRT4 in der  
Zellzyklusprogression und mitotischen  
Zellteilung**

Inaugural-Dissertation

zur Erlangung des Doktorgrades  
der Mathematisch-Naturwissenschaftlichen Fakultät  
der Heinrich-Heine-Universität Düsseldorf

vorgelegt von

**Laura Bergmann**  
aus Faro

Düsseldorf, März 2022

aus dem Institut für Biochemie und Molekularbiologie II der Medizinischen Fakultät der  
Heinrich-Heine-Universität Düsseldorf

Gedruckt mit der Genehmigung der  
Mathematisch-Naturwissenschaftlichen Fakultät der  
Heinrich-Heine-Universität Düsseldorf

Referent: Prof. Dr. Mohammad Reza Ahmadian

Korreferent: Prof. Dr. Lutz Schmitt

Tag der mündlichen Prüfung: 18.07.2022

*„Logik, Logik, zur Wahrheit führt nur Logik!“*

*Professor Abronsius - Tanz der Vampire*

# Inhaltsverzeichnis

<b>1. Abbildungsverzeichnis</b> .....	<b>1</b>
<b>2. Zusammenfassung</b> .....	<b>3</b>
<b>3. Summary</b> .....	<b>5</b>
<b>4. Einleitung</b> .....	<b>7</b>
4.1. Mitotische Zellteilung und Zellzykluskontrolle .....	7
4.2. Der Spindelapparat.....	9
4.2.1. Das Zentrosom .....	9
4.2.2. Aufbau des $\gamma$ -Tubulin-Ring-Komplexes .....	13
4.2.3. Mikrotubuli-Dynamik .....	14
4.3. Krebsentstehung assoziiert mit Spindeldefekten und zentrosomaler Dysfunktion .....	16
4.4. Funktion der Sirtuine in der zellulären Stressantwort .....	18
4.4.1. Humane Sirtuine .....	18
4.4.2. Mitochondriale Sirtuine .....	19
4.4.3. Nukleäre und zytoplasmatische Sirtuine .....	24
4.4.4. Sirtuine und ihre Rolle im Zellzyklus .....	26
4.4.5. Sirtuine und Krebs .....	27
<b>5. Zielsetzung</b> .....	<b>30</b>
<b>6. Manuskripte</b> .....	<b>32</b>
6.1. SIRT4 interacts with OPA1 and regulates mitochondrial quality control and mitophagy.....	32
6.2. Ammonia inhibits energy metabolism in astrocytes in a rapid and glutamate dehydrogenase 2-dependent manner.....	62
6.3. Subcellular localization and mitotic interactome analyses identify SIRT4 as a centrosomally localized and microtubule associated protein .....	95
<b>7. Abschlussdiskussion</b> .....	<b>129</b>
7.1. Subzelluläre Lokalisierung von SIRT4.....	129
7.1.2. SIRT4( $\Delta$ N28) und die Bedeutung des N-Terminus von SIRT4.....	131
7.2. Extramitochondriales SIRT4 und seine Rolle im Zellzyklus.....	132
7.2.1. SIRT4 am Zentrosom und dessen Einfluss auf die Mikrotubuli-Dynamik.....	133
7.2.2. SIRT4 vermittelte Hemmung der Zellproliferation.....	136
7.3. SIRT4 als Regulator zwischen Mitochondrien-Aktivität und Mitose .....	138
7.3.1. Die SIRT4-OPA1-Achse in der Vorbereitung für die Mitose .....	138
7.3.2. Die SIRT4-CDK1 Achse im Mitochondrium und deren Einfluss auf Metabolismus und Zellzyklus .....	140
7.4. SIRT4 als metabolischer Tumorsuppressor .....	144
<b>8. Abkürzungsverzeichnis</b> .....	<b>146</b>
<b>9. Literaturverzeichnis</b> .....	<b>149</b>

<b>10. Danksagung</b> .....	<b>168</b>
<b>11. Lebenslauf</b> .....	<b>169</b>
<b>12. Eidesstattliche Erklärung</b> .....	<b>171</b>
<b>13. Anhang</b> .....	<b>173</b>
13.1. Aminosäuresequenzen und Alignments der Sirtuine 2, 3, 4 und 5 .....	173

# 1. Abbildungsverzeichnis

- Abbildung 1:** Darstellung des Zellzyklus. Erstellt mit BioRender.com ..... 7
- Abbildung 2:** Ablauf der mitotischen Zellteilung. Erstellt mit BioRender.com ..... 8
- Abbildung 3:** Die Zentriolenduplikation während des Zellzyklus. Erstellt mit BioRender.com ..... 11
- Abbildung 4:** Aufbau Zentrosom und PCM. **A:** Eine vereinfachte Darstellung des Zentrosoms. Das Zentrosom besteht aus zwei um 90° zueinander orientierten Zentriolen, die von einer Hülle aus Proteinen, dem sogenannten perizentriolären Material (PCM), umgeben sind. **B:** Ein einzelnes Zentriol in Seiten- und Draufsicht. Jedes Zentriol besteht aus (MT)-Triplets, die in einer Wagenradstruktur angeordnet sind. **C:** Schema der zentrosomalen Organisation, insbesondere der perizentriolären Schichten in der Interphase und Mitose. Während der Interphase sind die PCM-Komponenten in verschachtelten, konzentrischen Schichten organisiert. Vor der Mitose vermehrt sich das PCM und akquiriert Faktoren wie NEDD1 und  $\gamma$ TuRC, die MT-Nukleation ermöglichen. Verändert nach *Rale et al.* [49] und erstellt mit BioRender.com ..... 12
- Abbildung 5:** Mikrotubuli-Nukleation auf Grundlage des  $\gamma$ TuRC.  $\gamma$ -Tubulinmoleküle (gelb) innerhalb des  $\gamma$ TuRC sind über ihre Bindung an GCP-Proteine (braun) in einer Single-Turn-Helix positioniert.  $\gamma$ -Tubulinmoleküle binden ankommende  $\alpha/\beta$ -Tubulindimere (blau) aus dem Zytosol an. Der Zusammenbau der Mikrotubuli schreitet langsam durch eine instabile Phase voran, in der ein Zerlegen wahrscheinlicher ist als ein fortgesetzter Zusammenbau. Ein stabiles Stadium wird erreicht, sobald ein Mikrotubuli-Protofilament genügend Tubulindimere polymerisiert hat. Sobald der stabile Status erreicht ist, wird die Mikrotubuli-Polymerisation begünstigt und kann rasch voranschreiten. Verändert nach *Tovey und Conduit et al.* [51] und erstellt mit BioRender.com. .... 14
- Abbildung 6:** Übersicht der humanen Sirtuine anhand ihrer Struktur, molekularen Funktion und dominanten subzellulären Lokalisation [117, 118]. ..... 19
- Abbildung 7:** Schematische Darstellung der SIRT4 Hochregulierung im Mitochondrium und dessen Effekte auf die Morphologie und Qualität der Mitochondrien. Gemessen wurde eine Abnahme des O<sub>2</sub>-Verbrauchs, des Membranpotentials und eine erhöhte Produktion von mtROS. Zusätzlich wurde ein Zusammenhang zwischen einer reduzierten mitochondrialen Qualitätskontrolle und einer SIRT4 vermittelten Stabilisierung der aktiven L-OPA1-Variante beobachtet. Erstellt mit BioRender.com ..... 34
- Abbildung 8:** Darstellung des vorgeschlagenen Mechanismus der Rolle der Glutamat-Dehydrogenase (GDH) bei Ammoniak-induzierter Toxizität. Dabei wird eine Ammonium-Ionen induzierte Erschöpfung von  $\alpha$ -Ketoglutarat durch reduktive Aminierung zu Glutamat mittels GDH vorgeschlagen, was gleichzeitig zur Hemmung des Citratzyklus führt. SIRT4 nimmt in seiner natürlichen Funktion als GDH-Inhibitor einen regulatorischen Aspekt ein. Erstellt mit BioRender.com ..... 64

**Abbildung 9:** Darstellung der dualen Lokalisation von SIRT4 vorrangig im Mitochondrium und extramitochondrial am Zentrosom. Mit aufgeführt sind die in der massenspektrometrischen SIRT4-Interaktomanalyse identifizierten Interaktionspartner aus dem Bereich der Zentrosomenbestandteile, sowie Mikrotubuli Regulation. Erstellt mit BioRender.com ..... 96

**Abbildung 10:** Schematische Einordnung von SIRT4 am Zentrosom. Abgeleitet anhand der konfokalen Spinning Disk Aufnahmen und in Kombination mit den Co-Immunopräzipitationsdaten [263] ist zu vermuten, dass SIRT4 Teil des PCM oder aber Bestandteil des  $\gamma$ TuRC ist, um dort Einfluss auf die Nukleierung und Polymerisation der Spindelmikrotubuli zu nehmen [263]. Erstellt mit Biorender.com ..... 134

**Abbildung 11:** Vorgeschlagenes Modell der mitochondrialen SIRT4-Wirkmechanismen während der Interphase. Während der Interphase nimmt SIRT4 Einfluss auf die mitochondriale Bioenergetik, indem es antagonistisch zu SIRT3 die anaplerotische Reaktion des Citratzyklus über eine Inhibition der GDH reguliert. Ebenfalls wird der Atmungskomplex I negativ durch SIRT4 reguliert, wodurch die Energieproduktion gedrosselt wird [162]. Gleichzeitig nimmt SIRT4 Einfluss auf die Aufrechterhaltung eines verzweigten mitochondrialen Netzwerkes über Regulation des L-OPA1/S-OPA1 Gleichgewichts. Erstellt mit BioRender.com ..... 142

**Abbildung 12:** Vorgeschlagenes Modell der mitochondrialen SIRT4-Wirkmechanismen während der G<sub>2</sub>/M-Phase. In Vorbereitung auf die Mitose kommt es zur Translokation und Anreicherung von CDK1/ZyclinB in die Mitochondrien, wo es eine Reihe von Substraten (z.B. Mn-abhängige Superoxiddismutase, MnSOD) durch Phosphorylierung aktiviert, darunter auch die Untereinheiten des mitochondrialen Atmungskettenkomplexes I. Dies dient der Verbesserung der mitochondrialen Funktion und Energieproduktion, was den energiesensitiven G<sub>2</sub>/M-Übergang antreibt. CDK1 aktiviert ebenfalls über Phosphorylierung SIRT3, während gleichzeitig eine mögliche Phosphorylierung von SIRT4 zu dessen Abbau führen könnte. Dadurch wird das Gleichgewicht der anaplerotischen Reaktion deutlich stärker auf die Seite von  $\alpha$ -Ketoglutarat verschoben. In Zusammenhang mit einer Aktivierung des Atmungskettenkomplexes I kommt es zur erhöhten ATP Produktion, die für die mitotischen Vorgänge benötigt wird. Durch den Abbau oder die Deaktivierung von SIRT4 wird ebenfalls das Gleichgewicht auf die S-OPA1-Seite verschoben, wodurch eine verstärkte Fission des mitochondrialen Netzwerkes stattfinden kann, welche für die Distribution um den mitotischen Spindelapparat und auf die Tochterzellen notwendig ist. Erstellt mit BioRender.com ..... 143

## 2. Zusammenfassung

Der stress-induzierbare und seneszenz-assoziierte Tumorsuppressor Sirtuin 4 (SIRT4) reguliert die mitochondriale Bioenergetik und den Metabolismus über Nicotinamid-Adenin-Dinukleotid (NAD<sup>+</sup>)-abhängige enzymatische Aktivitäten.

Nach SIRT4 Überexpression wurde eine Zunahme der mitochondrialen Fusion und eine *Cluster*-Zunahme an Mitochondrien-Netzwerken beobachtet, die mit einer Reduktion des mitochondrialen Membranpotentials und einer Erhöhung von mitochondrialen *reactive oxygen species* (ROS) einhergeht. Diese Effekte wirken einer geregelten Mitophagie entgegen und stehen im Zusammenhang mit einer verminderten mitochondrialen Qualitätskontrolle. Tatsächlich konnte ein verschobenes Gleichgewicht zur langen L-Form der GTPase *Optic Atrophy 1* (L-OPA1) relativ zu der *short* Form (S-OPA1) bei SIRT4-eGFP Überexpression gemessen werden, was eine L-OPA1 abhängige Erhöhung der mitochondrialen Fusion bewirkt und die Zunahme an Mitochondrien-Netzwerken erklärt. Zusätzlich wurde nach einer SIRT4 Überexpression ein reduzierter O<sub>2</sub>-Verbrauch gemessen, der auf eine SIRT4-vermittelte Inhibition der Atmungskette schließen lässt.

Durch die Funktion von SIRT4 als Inhibitor der mitochondrialen Glutamat-Dehydrogenase (GDH) konnte ein Einblick in die Rolle von SIRT4 in der Entstehung der hepatischen Enzephalopathie gegeben werden. Hierbei konnte ein klarer Zusammenhang zwischen der SIRT4-vermittelten Hemmung der mitochondrialen GDH2-abhängigen reduktiven Aminierung von  $\alpha$ -Ketoglutarat und einer verbesserten mitochondrialen Atmung bei Hyperammonämie nachgewiesen werden.

Neben der mitochondriellen Rolle von SIRT4 wurde endogenes sowie ektopisch exprimiertes SIRT4, nicht aber SIRT3, über subzelluläre Fraktionierung und Mikroskopie-Aufnahmen extramitochondrial im Zytoplasma nachgewiesen. Des Weiteren zeigen Aufnahmen mittels konfokale *Spinning Disk* Mikroskopie, dass SIRT4 während des Zellzyklus dynamisch an Zentrosomen mit einem Intensitätsmaximum in den frühen mitotischen Stadien lokalisiert. Darüber hinaus bindet SIRT4 an Mikrotubuli und interagiert mit strukturellen ( $\alpha$ -Tubulin,  $\gamma$ -Tubulin, TUBGCP2 und TUBGCP3) und regulatorischen Mikrotubulikomponenten (HDAC6), die durch massenspektrometrische Analyse des mitotischen SIRT4-Interaktoms und Co-immunopräzipitation identifiziert und verifiziert wurden. Die Überexpression von SIRT4-eGFP führte zu einer deutlichen Abnahme des acetylierten  $\alpha$ -Tubulins (Lysin

40 [K40]) spezifisch in mitotischen (G<sub>2</sub>/M arretierten) HEK293-Zellen und damit wahrscheinlich zu einer veränderten Mikrotubuli-Dynamik während der Zellteilung. SIRT4 oder die Mutante SIRT4( $\Delta$ 28N), die nicht in die Mitochondrien translozieren kann, verzögerte die mitotische Progression und reduzierte die Zellproliferation. Daher ist zu vermuten, dass SIRT4 zusätzlich zu seiner bekannten Rolle im mitochondrialen Metabolismus auch als neues Zentrosomen- und Mikrotubuli-assoziiertes Protein fungiert, das an der Regulation der mitotischen Zellzyklusprogression beteiligt ist. Somit könnte stress-induziertes SIRT4 seine Rolle als Tumorsuppressor sowohl durch mitochondriale als auch mitochondrien-unabhängige, auf den mitotischen Spindelapparat lokalisierte, Funktionen ausüben.

In dieser Arbeit wird die Rolle von SIRT4 als mögliches Bindeglied zwischen Mitochondrienfunktion und Mitoseprogression diskutiert. Dabei sollte die subzelluläre Lokalisierung und Regulation von SIRT4 in Abhängigkeit von der Zellzyklusprogression betrachtet werden, um so auch die Relevanz von SIRT4 in seiner potenziellen dualen Form als Tumorsuppressor oder Onkogen zu verstehen.

### 3. Summary

The stress-inducible and senescence-associated tumor suppressor SIRT4 (SIRT4) regulates mitochondrial bioenergetics and metabolism *via* NAD<sup>+</sup>-dependent enzymatic activities.

Following SIRT4 overexpression an increase in overall mitochondrial fusion and mitochondrial networks was observed, accompanied by a reduction in mitochondrial membrane potential and an increase in mitochondrial *reactive oxygen species* (ROS). These effects counteract regulated mitophagy and are associated with reduced mitochondrial quality control.

Indeed, a shifted equilibrium to the long L form of the GTPase Optic Atrophy 1 (L-OPA1) relative to the *short* form (S)-OPA1 was measured upon SIRT4-eGFP overexpression, causing an L-OPA1-dependent increase in mitochondrial fusion and explaining an increased fused network. In addition, reduced O<sub>2</sub> consumption was measured after SIRT4 overexpression, suggesting SIRT4-mediated inhibition of the respiratory chain.

The function of SIRT4 as an inhibitor of mitochondrial glutamate dehydrogenase (GDH) provided insight into the role of SIRT4 in the development of hepatic encephalopathy. Here, a link between SIRT4-mediated inhibition of mitochondrial GDH2-dependent reductive amination of  $\alpha$ -ketoglutarate and enhanced mitochondrial respiration in hyperammonemia was demonstrated.

In addition to the mitochondrial role of SIRT4, endogenous as well as ectopically expressed SIRT4, but not SIRT3, could be detected extramitochondrially in the cytoplasm *via* subcellular fractionation and microscopy images. Furthermore, confocal spinning disk microscopy images show that SIRT4 dynamically localizes to centrosomes during the cell cycle with a maximum intensity at the early mitotic stages. Moreover, SIRT4 binds to microtubules and interacts with structural ( $\alpha$ -Tubulin,  $\gamma$ -Tubulin, TUBGCP2 and TUBGCP3) and regulatory microtubule components (HDAC6), which were detected and verified by coimmunoprecipitation and mass spectrometric analysis of the mitotic SIRT4 interactome. Overexpression of SIRT4-eGFP resulted in a significant decrease in acetylated  $\alpha$ -Tubulin (lysine 40 [K40]), specifically in mitotic (G<sub>2</sub>/M arrested) HEK293 cells, likely resulting in altered microtubule dynamics during cell division. SIRT4 or the mutant SIRT4( $\Delta$ 28N), which does not translocate into mitochondria, delayed mitotic progression and reduced cell proliferation. Therefore, in

addition to its known role in mitochondrial metabolism, SIRT4 may function as a novel centrosome- and microtubule-associated protein involved in the regulation of mitotic cell cycle progression. Thus, stress-induced SIRT4 may exert its role as a tumor suppressor through both mitochondrial and mitochondria-independent functions localized to the mitotic spindle apparatus.

The present work discusses the role of SIRT4 as a possible link between mitochondrial function and mitotic progression. Furthermore, the subcellular localization and regulation of SIRT4 is considered in relation to cell cycle progression in order to understand the relevance of SIRT4 in its potential dual function as a tumor suppressor or oncogene.

## 4. Einleitung

### 4.1. Mitotische Zellteilung und Zellzykluskontrolle

Die mitotische Zellteilung stellt einen komplexen und hochregulierten Prozess dar, der die gleichmäßige Aufteilung des duplizierten DNA-Gehalts einer Mutterzelle auf zwei Tochterzellen ermöglicht. Dies betrifft neben dem kompletten Chromosomensatz auch Zellorganellen und zahlreiche andere Bestandteile. Die für Zellteilung und die Aufrechterhaltung der zellulären Homöostase erforderliche DNA-Synthese, Mitose und Zytokinese sind im Zellzyklus eingebettet und werden durch viele extra- und intrazelluläre Stimuli und Signalwege gesteuert [1-5].

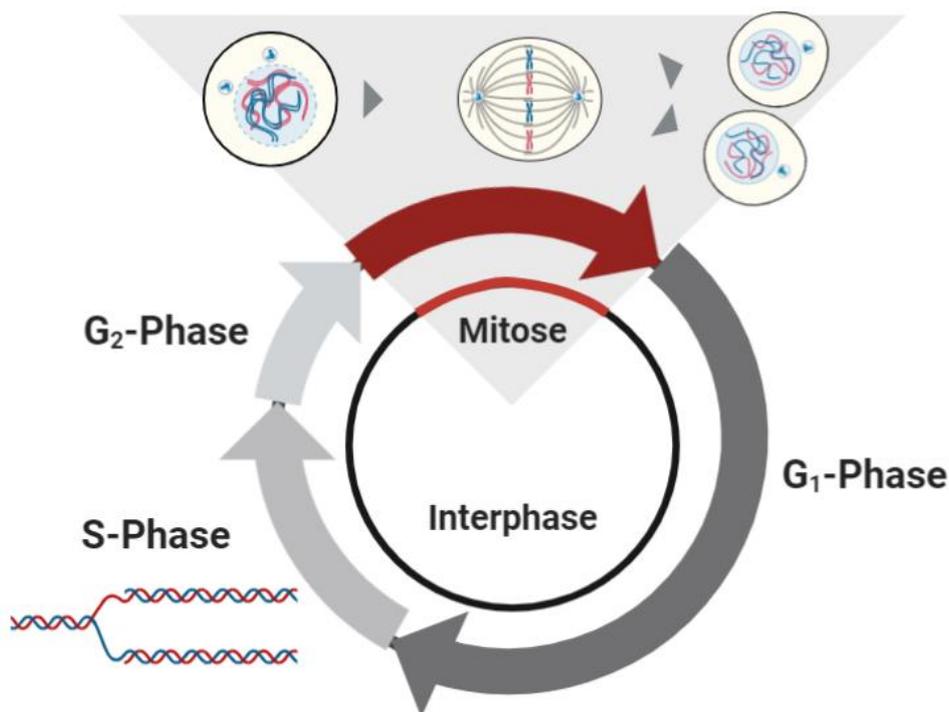


**Abbildung 1:** Darstellung des Zellzyklus. Erstellt mit BioRender.com

Der Zellzyklus lässt sich zunächst in vier Hauptphasen einteilen [6]. Die G<sub>1</sub>-Phase (engl. *gap*), in welcher die Zelle ihren zelltypspezifischen und metabolischen Aufgaben nachgeht, ist die Phase des Zellwachstums. Diese ist gekennzeichnet durch Vermehrung der Zellorganellen, Zunahme der Zytosolmenge, Proteinbiosynthese und schließlich Synthese aller Bestandteile, die im periodischen Verlauf für die kommende Mitose wieder aufgeteilt werden. In der Synthese-Phase (S-Phase) verdoppelt die

Zelle über den Prozess der DNA-Replikation ihr Erbgut. Die G<sub>2</sub>-Phase dient vorrangig als Kontrollpunkt, bevor die Zelle in die Mitose übergeht [7]. Dabei werden die G<sub>1</sub>-, S- und G<sub>2</sub>-Phasen als Interphase zusammengefasst und definieren damit den zeitlichen Abschnitt zwischen zwei Mitosen.

Die Mitose wird übergeordnet in Prophase, Metaphase, Anaphase und Telophase eingeteilt. Sie dauert bei Säugern ca. 60 Minuten und ist in proliferierenden Zellen die zeitlich kürzeste, und neben der DNA-Replikation, die stressempfindlichste Phase im Zellzyklus [8].

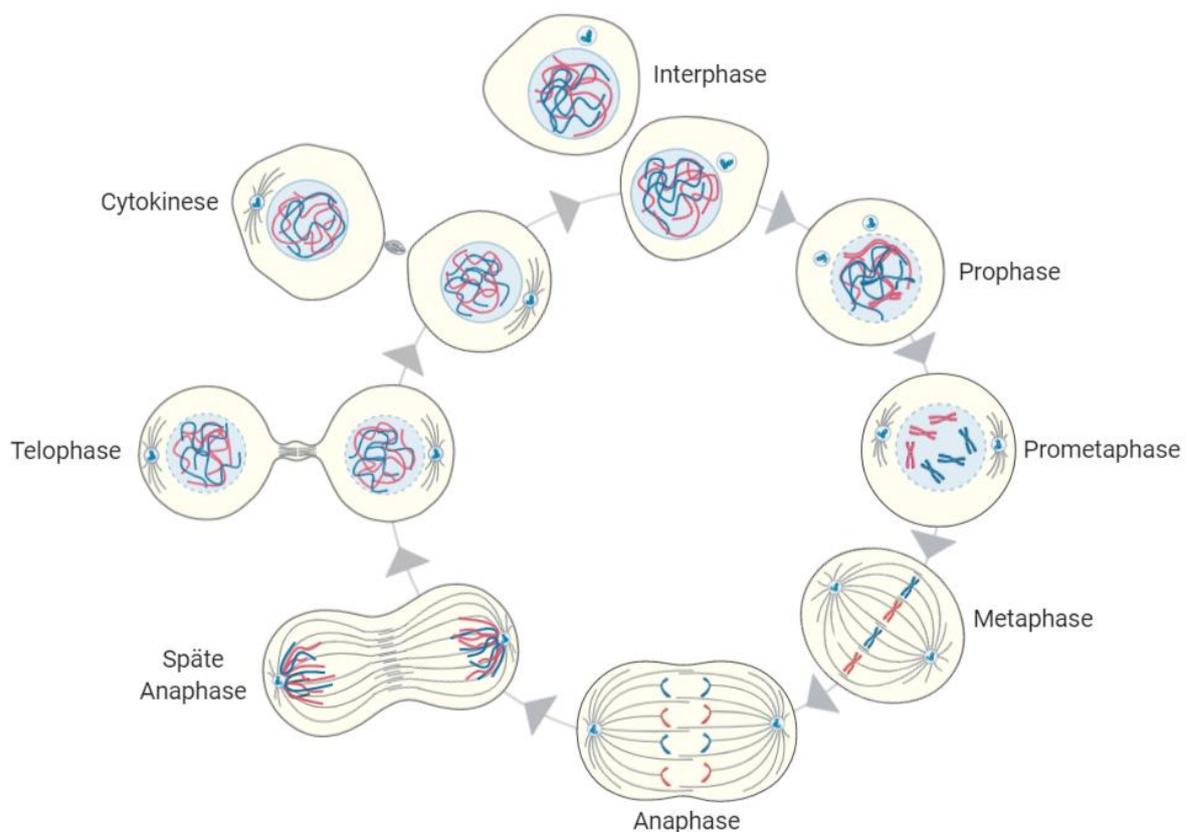


**Abbildung 2:** Ablauf der mitotischen Zellteilung. Erstellt mit BioRender.com

Jede Phase des Zellzyklus wird durch extrinsische und intrinsische Kontrollmechanismen, beispielsweise positiv durch Wachstumsfaktor-Stimuli oder negativ durch eine DNA-Schadensantwort, beeinflusst und ist durch die Aktivität regulatorischer Proteine gekennzeichnet [9, 10].

Das Fortschreiten durch eine der spezifischen Phasen wird hauptsächlich über die Komplexbildung der zyclin-abhängigen Kinasen (engl. *cyclin-dependent kinases*, CDKs) und deren Zykline, welche phasenabhängig in unterschiedlichen Konzentrationen vorliegen, gesteuert.

Ein enzymatisch aktiver Zyklin-CDK-Komplex besteht aus einer regulatorischen Untereinheit (Zyklin) und einer katalytischen Untereinheit (CDK) [11]. Die CDK Proteinkinasen steuern durch Phosphorylierung verschiedener Zielproteine das Fortschreiten durch die verschiedenen Phasen des Zellteilungszyklus [12, 13]. So leiten zum Beispiel in der frühen G<sub>1</sub>-Phase durch D-Typ-Zykline aktiviertes CDK4 und CDK6 die Phosphorylierung der Retinoblastom-Proteinfamilie ein [14, 15]. Dies führt zur Freisetzung von E2F-Transkriptionsfaktoren, was wiederum in der Aktivierung und Transkription von E2F-abhängigen Genen resultiert, die für den Zellzyklusfortschritt erforderlich sind [16, 17]. Auch der Prozess der Chromosomentrennung wird während der mitotischen Phase des Zellzyklus durch eine G<sub>2</sub>/M-abhängige Expression und einem rechtzeitigen Abbau von Zyklin B1 für die Metaphase-Anaphase Transition und zahlreichen anderen strukturellen Proteinen streng kontrolliert [5, 18].

## **4.2. Der Spindelapparat**

Zur fehlerfreien Segregation der Schwesterchromatiden bildet die Zelle den mitotischen Spindelapparat aus. Dieser besteht aus zwei Zentrosomen (eines an jedem Spindelpol), Astral- und Spindelmikrotubuli sowie den Mikrotubuli-assoziierten Protein (MAP)-Komplexen [19-21].

### **4.2.1. Das Zentrosom**

Das Zentrosom ist eine multifunktionale, strukturell komplexe makromolekulare Maschine, die aus hunderten von Proteinen besteht [22, 23]. Das Zentrosom stellt das wichtigste Mikrotubuli-Organisationszentrum (MTOC - engl. *microtubule organizing centre*) in tierischen Zellen dar und besteht aus einem Paar von Zentriolen, das von einer amorphen Proteinmatrix (dem PCM - perizentrioläres Material) als Hauptankerfaktor umgeben ist [24, 25]. In der Interphase trägt das Zentrosom zur Kontrolle des Mikrotubuli-Netzwerks bei, welches dem schnellen intrazellulären Transport von Proteinen und Organellen dient [26]. Des Weiteren ist das Zentrosom essenziell für die initiale bipolare Ausrichtung der mitotischen Spindel [23, 27]. Dabei bilden die Zentriolen mit ihrer typischen neunfachsymmetrischen Wagenradstruktur den Kern des Zentrosoms. Die zylindrische Struktur der Symmetrie folgend, besteht aus neun parallelen Mikrotubuli-Triplets, die längs der Achse des Zylinders verlaufen

[28-30]. Das die Zentriolen umgebende PCM nimmt mit den mitotischen Phasen an Masse zu oder ab und bildet das Nukleationszentrum für Spindel- und Astralmikrotubuli [31].

Während der G<sub>2</sub>/M-Phase des Zellzyklus durchlaufen die Zellen eine massive Mikrotubuli-Umlagerung, die als wichtiger regulatorischer Schalter fungiert und aus Mikrotubuli-Nukleation, -Dehnung, -Polymerisation und -Depolymerisation besteht [27, 32]. Zu Beginn der Anaphase beginnen Astral-Mikrotubuli in Richtung des Zellkortex zu wachsen, während sich eine gegenläufige, gebündelte Struktur aus Zentralspindel und Mittelzonenmikrotubuli zwischen den zu segregierenden Chromosomen bildet [27, 33]. Diese Anaphase-Spindelstrukturen induzieren eine lokalisierte Aktivierung der kleinen Guanosintriphosphatase (GTPase) Rho (RhoA bei Säugetieren), die wiederum die Bildung des kontraktiven Aktin-Myosin-Rings auslöst [34]. Nach Ausbildung der Spaltfurche im Zentrum der Zelle, bildet diese, zusammen mit den Mikrotubuli der Zentralspindel, eine spezialisierte Struktur, den sogenannten Mittelkörper [27]. Für eine erfolgreiche Teilung in zwei Zellen muss der Mittelkörper stabil gehalten werden, dabei scheint ein Zusammenhang zwischen der Komplettierung der Zytokinese und der Inaktivierung der Aurora B Kinase zu bestehen [35, 36]. Somit spielt das Zentrosom über die Kontrolle der Zentralspindel auch eine Schlüsselrolle bei der Zytokinese.

Der Verdopplungszyklus der Zentrosomen erfolgt parallel mit dem Zellzyklus und findet bereits gegen Ende der G<sub>1</sub>-Phase und zu Anfang der S-Phase statt [18, 37]; dargestellt in Abbildung 3. Postmitotische Zellen haben ein Paar Zentriolen, von denen die eine orthogonal in die andere greift [30, 37]. In der initialen Phase nach der Mitose - dem „*Disengagement*“ - lösen sich die beiden Zentriolen voneinander und sind nur noch durch eine lockere, faserige Struktur miteinander verbunden. Sie gelten nun als die Mutterzentriolen. Im nächsten Schritt erfolgt die Zentriolen-Duplikation im G<sub>1</sub>/S-Übergang, wobei der Zusammenbau einer Prozentriole senkrecht zu jeder Mutterzentriole erfolgt. Durch die G<sub>2</sub>-Phase hindurch wächst die Prozentriole heran, bis sie die gleiche Größe wie die Mutterzentriole erreicht hat.

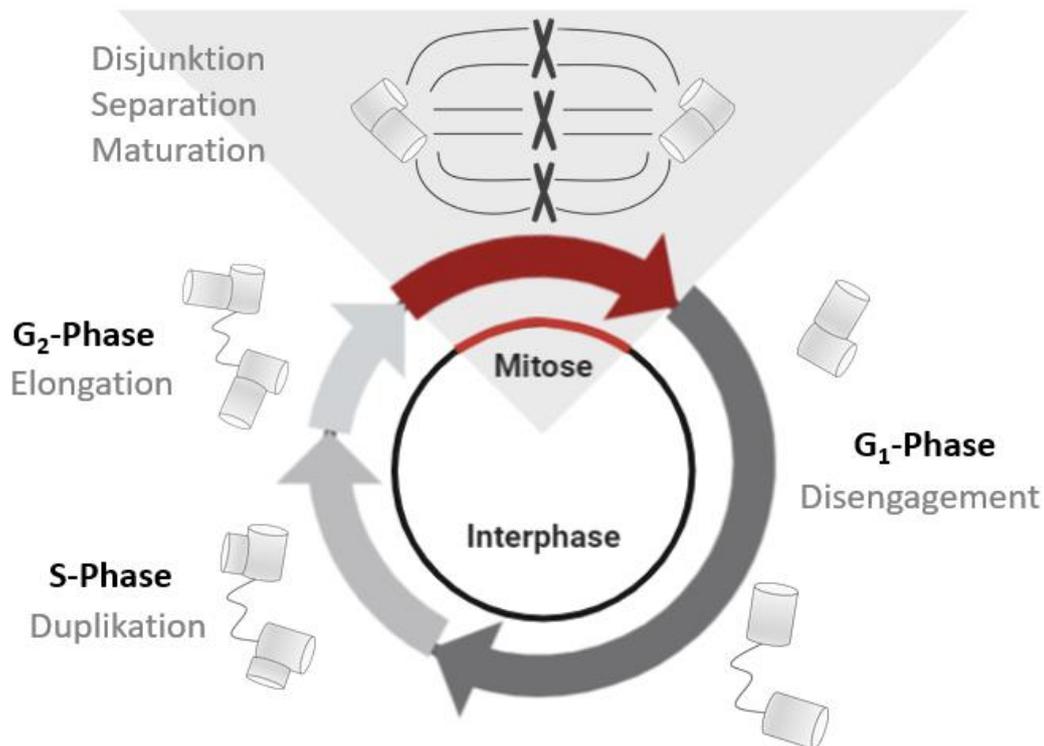


**Abbildung 3:** Die Zentriolenduplikation während des Zellzyklus. Erstellt mit BioRender.com

Vor der Mitose beginnen die Mutterzentriolen mehr PCM zu akkumulieren, und es kommt zunehmend zur Mikrotubulikondensation, um die Spindelmontage vorzubereiten [18]. Das PCM dient als Plattform für Proteinkomplexe, welche die mitotische Verteilung der Organellen, den Proteinabbau und den Aufbau des Spindelapparates regulieren. Im Gegensatz zu anderen Organellen, wie z.B. dem Zellkern und den Mitochondrien, ist das PCM jedoch nicht membrangebunden, sondern vielmehr eine dynamische Ansammlung von Proteinkomplexen, darunter auch lokal translatierte *messenger RNA* (mRNA) [38-40], die das Innere der Organelle bilden und ihre Abschnitte bestimmen [25, 31].

Eine der ersten identifizierten PCM-Komponenten ist Pericentrin, welches als zentrosomaler Rekrutierungs- und integraler Strukturfaktor dient und somit die korrekte Zentrosomen- und Mitosespindelbildung für einen ununterbrochenen Zellzyklusverlauf gewährleistet [24]. Die Entdeckung zusätzlicher PCM-Kernbestandteile wie Cep192/SPD-2, CDK5RAP2/Cnn, Cep152/Asterless und SPD-5 in verschiedenen Organismen zeigte, dass die einzige größere Ähnlichkeit unter den PCM-organisierenden Proteinen eine Fülle von *Coiled-coil*-Domänen ist [22, 31, 41-43]. Neben den Strukturproteinen enthält das PCM eine beträchtliche Anzahl verschiedener regulatorischer Proteine, wie beispielsweise die zentrosom-assoziierten

Kinasen der Plk- und Aurora-Familie, aber auch die kleine GTPase Ran und den Tumorsuppressor und Transkriptionsfaktor p53 [8, 44, 45]. Eine wichtige Rolle bei der Zentrosomenvervielfältigung spielt die Enzymfamilie der NAD<sup>+</sup>-abhängigen Poly-(ADP)-Ribosyltransferasen (PARPs), welche im Zellkern und an den Zentrosomen lokalisieren und Einfluss auf das Zentrosom, die Integrität der mitotischen Spindel sowie die Dauer der Mitose haben [46-48]. Insbesondere wird Zentrosomen-Hyperamplifikation häufig in mit PARP-Inhibitor behandelten Zellen sowie in Poly-(ADP-ribose)-Polymerase 1 (PARP-1)-Nullzellen beobachtet. Entsprechend wird diese Enzymfamilie mit der Aufrechterhaltung der chromosomalen Stabilität in Verbindung gebracht [45].

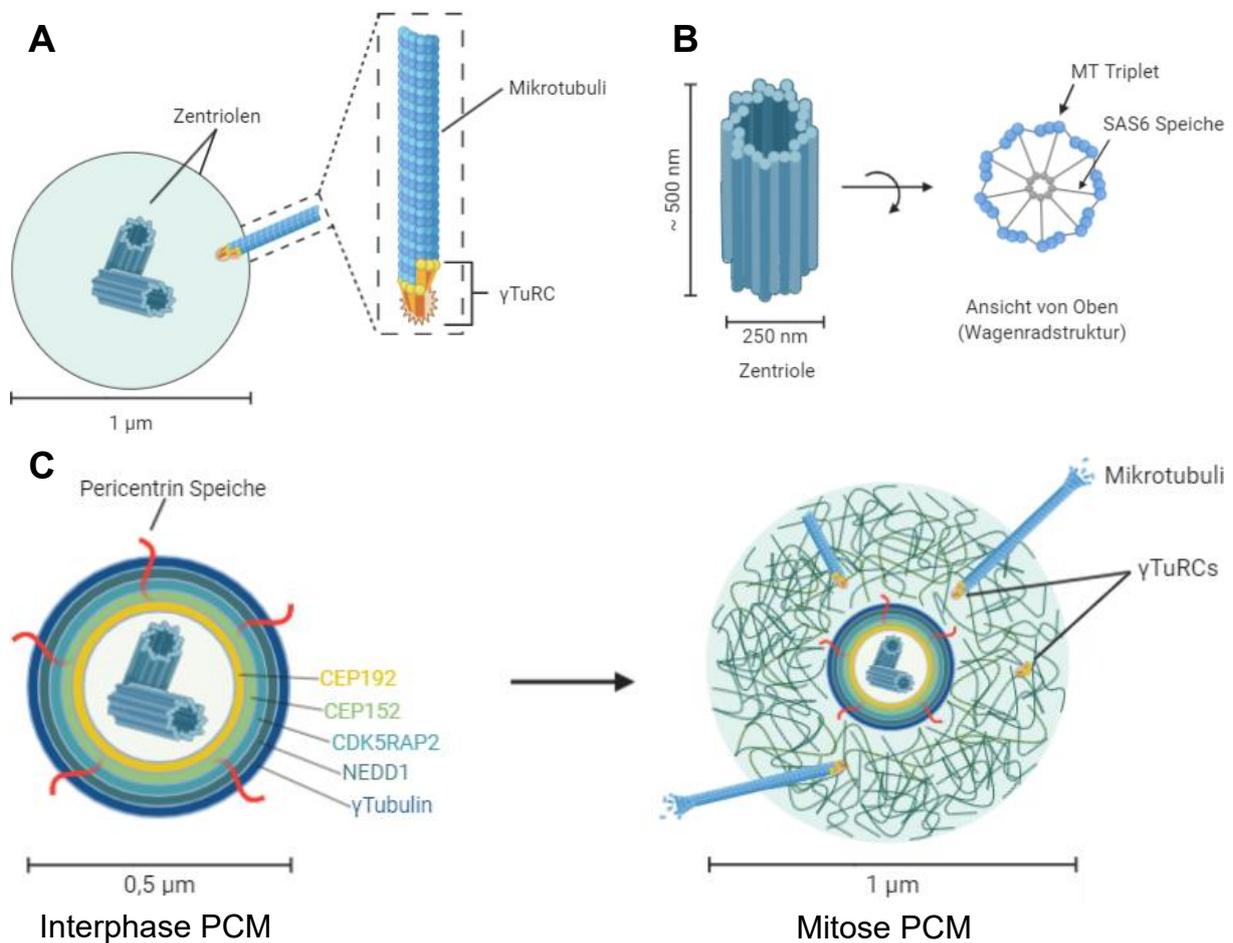


**Abbildung 4:** Aufbau Zentrosom und PCM. **A:** Eine vereinfachte Darstellung des Zentrosoms. Das Zentrosom besteht aus zwei um 90° zueinander orientierten Zentriolen, die von einer Hülle aus Proteinen, dem sogenannten perizentriolären Material (PCM), umgeben sind. **B:** Ein einzelnes Zentriol in Seiten- und Draufsicht. Jedes Zentriol besteht aus (MT)-Triplets, die in einer Wagenradstruktur angeordnet sind. **C:** Schema der zentrosomalen Organisation, insbesondere der perizentriolären Schichten in der Interphase und Mitose. Während der Interphase sind die PCM-Komponenten in verschichteten, konzentrischen Schichten organisiert. Vor der Mitose vermehrt sich das PCM und akquiriert Faktoren wie NEDD1 und  $\gamma$ TuRC, die MT-Nukleation ermöglichen. Verändert nach Rale *et al.* [49] und erstellt mit BioRender.com

## 4.2.2. Aufbau des $\gamma$ -Tubulin-Ring-Komplexes

Alle MTOCs basieren auf  $\gamma$ -Tubulin, einem Homolog von  $\alpha$ -Tubulin und  $\beta$ -Tubulin, welches zur Nukleation von Mikrotubuli benötigt wird. Die Nukleation der Mikrotubuli wird durch den  $\gamma$ -Tubulin-Ring-Komplex (engl.  *$\gamma$ -Tubulin ring complex* -  $\gamma$ TuRC) und verwandte  $\gamma$ -Tubulin-Komplexe reguliert, die eine räumliche und zeitliche Kontrolle über die Initiierung des Mikrotubuli-Wachstums ermöglichen [50, 51].

Der  $\gamma$ TuRC, bestehend aus  $\gamma$ -Tubulin und  $\gamma$ -Tubulinkomplex-Proteinen (GCPs, auch TUBGCPs genannt), nukleiert Mikrotubuli, indem er ein Template für den Zusammenbau von  $\alpha/\beta$ -Tubulin-Heterodimeren bereitstellt. Zellen enthalten  $\gamma$ -Tubulinkomplexe (engl.  *$\gamma$ -Tubulin complex* -  $\gamma$ TuC) von zwei verschiedenen Größen: den kleinen  $\gamma$ -Tubulinkomplex (engl.  *$\gamma$ -tubulin small complex* -  $\gamma$ TuSC) und den  $\gamma$ TuRC [50-56].

Der  $\gamma$ TuSC ist ein Tetramer, der sich aus zwei  $\gamma$ -Tubulinen und den zwei weiteren  $\gamma$ -Tubulinkomplex-Proteinen GCP2 und GCP3 zusammensetzt. Im  $\gamma$ TuRC sind mehrere Kopien des  $\gamma$ TuSC zu einer ringförmigen, makromolekularen Struktur mit zusätzlichen Proteinen, wie GCP4, GCP5 und GCP6, angeordnet [53]. Als Nukleationstemplate ist  $\gamma$ TuRC nicht nur wichtig für die Erzeugung von Mikrotubuli, sondern auch für die Kontrolle ihrer Position und Orientierung, was für die Bildung geordneter Mikrotubuli-Arrays von grundlegender Bedeutung ist. Daher wird die Aktivität von  $\gamma$ TuRC durch Aktivierungsfaktoren streng kontrolliert, welche die Nukleation räumlich auf mikrotubuli-organisierende Zentren wie das Zentrosom beschränken [50, 52]. GCP2 und GCP3 sind in fast allen Eukaryoten vertreten und bilden den Kern der Nukleationsmaschinerie. Die meisten Eukaryoten besitzen auch GCP4 und GCP5, während GCP6 evolutiv erst seit kurzem in der Tier- und Pilzwelt vertreten ist [50, 55]. Neben den Proteinen der GCP-Familie finden sich auch andere nicht-GCP Komponenten im  $\gamma$ TuRC. Dazu gehören die beiden Proteine MOZART1 (*mitotic-spindle organizing protein associated with a ring of  $\gamma$ -tubulin 1*) und MOZART2, welche als integrale Bestandteile des  $\gamma$ TuRC in menschlichen Zelllinien beschrieben wurden [52, 57-59].

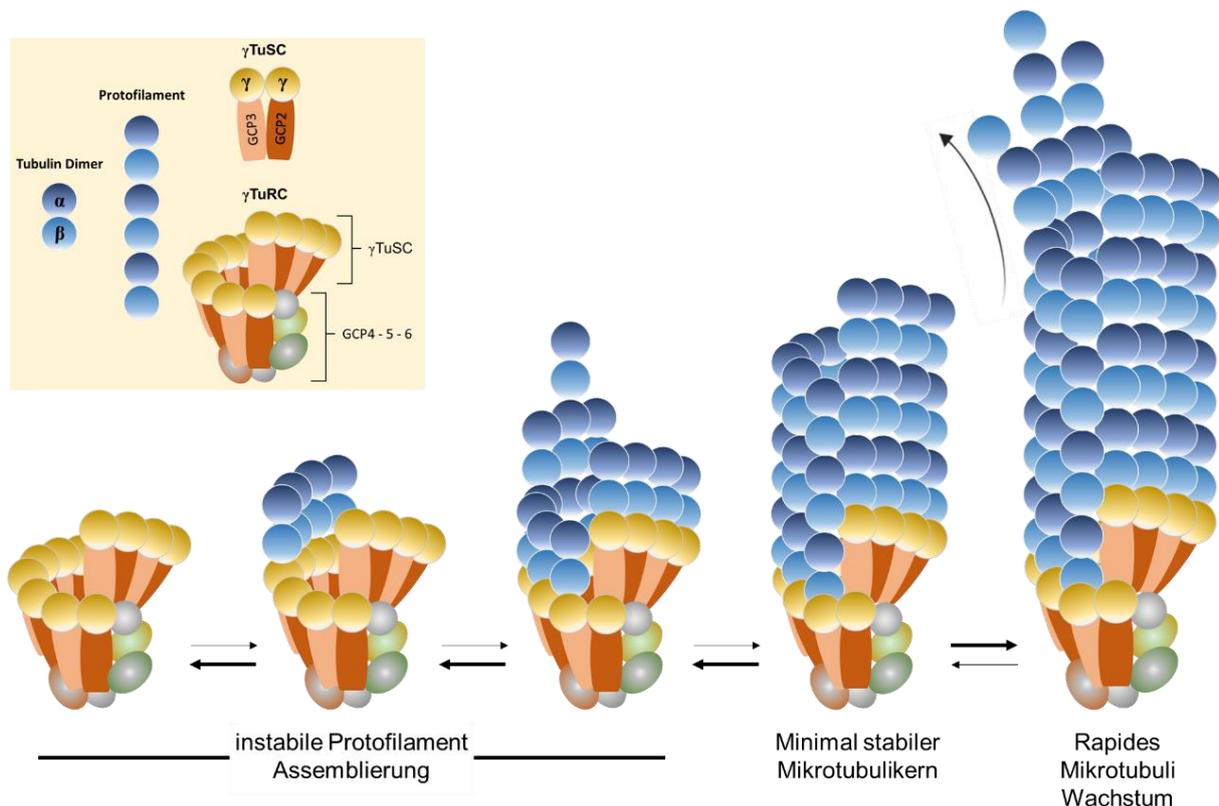


**Abbildung 5:** Mikrotubuli-Nukleation auf Grundlage des  $\gamma$ TuRC.  $\gamma$ -Tubulinmoleküle (gelb) innerhalb des  $\gamma$ TuRC sind über ihre Bindung an GCP-Proteine (braun) in einer Single-Turn-Helix positioniert.  $\gamma$ -Tubulinmoleküle binden ankommende  $\alpha/\beta$ -Tubulindimere (blau) aus dem Zytosol an. Der Zusammenbau der Mikrotubuli schreitet langsam durch eine instabile Phase voran, in der ein Zerlegen wahrscheinlicher ist als ein fortgesetzter Zusammenbau. Ein stabiles Stadium wird erreicht, sobald ein Mikrotubuli-Protofilament genügend Tubulindimere polymerisiert hat. Sobald der stabile Status erreicht ist, wird die Mikrotubuli-Polymerisation begünstigt und kann rasch voranschreiten. Verändert nach Tovey und Conduit *et al.* [51] und erstellt mit BioRender.com.

### 4.2.3. Mikrotubuli-Dynamik

Mikrotubuli sind fibrilläre Strukturen von etwa 250 Å Durchmesser, die den meisten eukaryotischen Zellen gemeinsam sind. Sie sind Polymere, die aus der heterodimeren  $\alpha$ -Tubulin- $\beta$ -Tubulin ( $\alpha/\beta$ -Tubulin) Grundeinheit in einer Guanosintriphosphat (GTP)-abhängigen Weise zusammengesetzt werden. Dabei bindet eine GTP-Tubulin Einheit an das positive Ende der Mikrotubuli. Nach kurzer Zeit hydrolysiert das GTP unter Freisetzung von Phosphat, während das Guanosindiphosphat (GDP)-Tubulin im polymerisierten Gerüst verbleibt [32, 60]. Zusätzlich bestehen die Mikrotubuli aus einer Vielzahl von Nebenbestandteilen, den sogenannten Mikrotubuli-assoziierten Proteinen [27, 50, 61]. Das Mikrotubuli-Zytoskelett ist für die räumliche und zeitliche Organisation eukaryotischer Zellen von entscheidender Bedeutung und spielt eine zentrale Rolle bei unterschiedlichen Funktionen, wie intrazellulärem Transport, Organellenpositionierung, Motilität, Signalgebung und Zellteilung [50].

Die Grundlage dieser Aufgabenvielfalt ist begründet in dem herausragenden Merkmal aller Mikrotubuli: ihrer dynamischen Instabilität (ausgenommen die stabilen Mikrotubuli der Zilien und Flagellen). Aufgrund eines schnellen Austauschs der  $\alpha/\beta$ -Tubulin-Heterodimere zwischen der polymeren Form und einem löslichen Tubulinpool [62-64], können diese hochdynamischen Polymere zwischen Wachstums- und Depolymerisationszyklen umschalten, was der Zelle eine schnelle Reorganisation des Mikrotubuli-Zytoskeletts im Verlauf der Zellpolarisation, Migration und mitotischen Teilung ermöglicht [61, 65-68].

Die Länge der Mikrotubuli und ihre "dynamische Instabilität" hängen von der Verschiebung des Gleichgewichts zwischen "Katastrophe" (Schrumpfung der Mikrotubuli) und "Rettung" (Wachstum der Mikrotubuli) ab, welches hauptsächlich durch mehrere MAPs reguliert wird [21, 60]. Der dynamische Zustand der Mikrotubuli und ihre (In-)Stabilität werden durch posttranslationale Modifikationen (PTM), u.a. die (De-)Acetylierung von  $\alpha$ -Tubulin (am Lysin 40 [K40]), reguliert [69-71]. Das Besondere an der  $\alpha$ -Tubulin-Acetylierung ist, dass sich das Lysin 40 im Inneren des Mikrotubulilumen befindet, wohingegen die anderen PTMs an der Mikrotubuli-Außenseite vollzogen werden [71]. Stabile Mikrotubuli sind über einen längeren Zeitraum beständig und weisen eine akkumulierte Acetylierung auf [71]. Die Modifikation ergibt sich daher als Akkumulationsmarker über die Zeit.

Das Sirtuin SIRT2 und die Histondeacetylase 6 (HDAC6) sind bekannte Deacetylasen, die in einer NAD<sup>+</sup>-abhängigen Weise  $\alpha$ -Tubulin am Lysin-40 deacetylieren [72] und dabei die Dynamik der Mikrotubuli über eine durch die Deacetylierung hervorgerufene Instabilität [71, 73] verändern.

### **4.3. Krebsentstehung assoziiert mit Spindeldefekten und zentrosomaler Dysfunktion**

Die Zelltransformation und Tumorentstehung ist ein mehrstufiger Prozess, der in einzelnen Zellen durch die Akkumulation von Mutationen entsteht, welche die Funktion kritischer Onkogene erhöhen, Tumorsuppressorgene vermindern, deregulieren oder stören, was wiederum zu autonomem Wachstum und Verlust der Homöostase führt.

Eine Eigenschaft von Tumorzellen ist unter anderem, dass es zu einer verstärkten Inhibition der Apoptose kommt, wodurch der gestörte Zellzyklus nicht mehr verlassen wird, obwohl entsprechende externe oder interne regulatorische Signale dies veranlassen würden [74, 75]. Ein abnormaler Chromosomensatz (Aneuploidie) ist dabei eines der ersten identifizierten Kennzeichen von Krebszellen [37, 45]. So dokumentierte Leo Hanseman schon 1890 das häufige Auftreten von asymmetrischen und multipolaren Mitosen in Karzinomgeweben [76, 77]. Aneuploidie und Chromosomeninstabilität stehen unter anderem direkt mit zentrosomalen Dysfunktionen im Zusammenhang [37, 45]. Eine Ausprägung ist das Phänomen der zentrosomalen Hyperamplifikation (mehr als zwei Zentrosomen), wodurch abnormal vervielfältigte Spindelpole in einer chromosomalen Fehlsegregation resultieren.

Bei einer zu hohen Fehlerakkumulation oder bei zu gravierenden Schäden kann es zur Initiierung der Apoptose kommen, um potentielle Erkrankungen zu verhindern (z.B. Zellentartung, chronische Inflammation, irreguläre Ausschüttung von Zytokinen oder andere Faktoren, welche die Zell-Zellorganisation stören) [78]. Alternativ geht die Zelle postmitotisch in der G<sub>1</sub>-Phase in die zelluläre Seneszenz über [79-81].

Die zelluläre Seneszenz beschreibt einen Prozess, bei dem Zellen aufhören sich zu teilen und ausgeprägte phänotypische Veränderungen aufweisen; zu diesen gehören entscheidende Chromatin- und Sekretomveränderungen, sowie die Aktivierung von Tumorsuppressoren [79, 82-84]. Die wichtigsten Merkmale seneszenten Zellen lassen sich als Seneszenz-assoziiertes sekretorischer Phänotyp (SASP) [85, 86] oder Seneszenz-assoziiertes Sekretom (SMS) [87] zusammenfassen. Senescente Zellen weisen Charakteristika wie Wachstumsstillstand, Apoptoseresistenz und veränderte Genexpression auf [78]. Dabei werden vor allem Gene hochreguliert, die hauptsächlich für Proteine kodieren, wie Zytokine und Chemokine mit proinflammatorischen

Eigenschaften, sowie verschiedene Wachstumsfaktoren und Proteasen, die zusammen die Gewebestruktur und -funktion verändern.

Durch Inhibition oder Depletion verschiedener mitotischer Proteine, mit Rollen in der Aufrechterhaltung der Zentrosom- und Kinetochor-Integrität und/oder mit mitotischer Checkpoint-Funktion, wird ein p53-p21WAF-getriebener Phänotyp der vorzeitigen Seneszenz aktiviert [81]. Zu diesen mitotischen Proteinen gehören unter anderem die in verschiedenen Prozessen der mitotischen Progression involvierte Aurora A Kinase [88, 89], das *transforming acidic coiled-coil-containing protein 3* (TACC3) [90] und der integrale Bestandteil und Rekrutierungsfaktor des Zentrosoms Pericentrin [91, 92].

Um Zellentartung zu verhindern und zu minimieren, haben sich über die Zeit verschiedene Zellzyklus-Kontrollmechanismen entwickelt. Dabei finden sich neben vielen kleineren *Feedbackloops* vier wichtige Hauptkontrollpunkte: Die G<sub>1</sub>/S, Intra-S-, G<sub>2</sub>/M- und Metaphase-Kontrollpunkte [6, 93, 94]. Bei Krebszellen sind diese Kontrollpunkte in der Regel außer Kraft gesetzt, sodass eine stetige Proliferation aufrecht gehalten werden kann.

Auch die Mitose hat verschiedene Kontrollpunkte, um eine korrekte Verteilung der Chromatiden auf die Tochterzellen zu gewährleisten. Wenn diese Kontrollpunkte nicht eingehalten werden und die Mitose trotz aufgetretener Fehler absolviert wird, kommt es zu Phänomenen, die zur Zelltransformation und schlussendlich auch Krebsentstehung beitragen.

Während einige Zellen in der Mitose absterben, verlassen andere die Mitose, ohne sich zu teilen und kehren in die Interphase zurück. Sobald sie sich wieder in der Interphase befinden, erleiden einige Zellen einen Zellzyklus-Stillstand, andere sterben ab, und wieder andere replizieren erneut ihr Genom und treten in einen sogenannten Endozyklus ein, der zu Polyploidie führt [95, 96]. Ein weiteres prominentes Phänomen ist „*Mitotic-Slippage*“; dabei kommt es zu einer Fortführung der Mitose, obwohl die Zelle während eines Arrestes im *Spindel-Assembly-Checkpoint* (SAC) über die verhinderte *Anaphase Promoting Complex* (APC)-vermittelte Proteolyse von Zyklin B, angehalten wurde. Ein Arrest im SAC tritt beispielsweise auf, wenn die Zelle zu schwach oder aber komplett ungebundene Kinetochore detektiert [97, 98].

## 4.4. Funktion der Sirtuine in der zellulären Stressantwort

Die Protein-Familie der Sirtuine leitet sich von ihrem Homolog, dem *Silent Information Regulator 2 (SIR2)* aus *Saccharomyces cerevisiae*, ab und findet sich konserviert in Pflanzen, Bakterien und Tieren wieder. In der Bäckerhefe konnte gezeigt werden, dass Sir2p positiven Einfluss auf die Lebensspanne hat, da es direkt an der Regulierung der Genomstabilität beteiligt ist [99-101]. Dabei wird Sir2p unter Stressinduktion in Form von Kalorienrestriktion als Histon-Deacetylase aktiv [102]. Auch in den anderen Organismen wie *Caenorhabditis elegans* [103] und *Drosophila melanogaster* [104, 105] steht das Sir2 Protein in direktem Zusammenhang mit der Förderung der Gesundheit und der Erweiterung der Lebensspanne [106, 107].

### 4.4.1. Humane Sirtuine

Die Säugetierproteinfamilie der Sirtuine besteht aus sieben Mitgliedern, die ihre NAD<sup>+</sup>-abhängige enzymatische Aktivität in mehreren Signalwegen hauptsächlich als Deacetylasen, Deacylasen oder ADP-Ribosyltransferasen in verschiedenen zellulären Kompartimenten ausüben [108-111]. SIRT-Proteine bilden unter den Lysin-Deacetylasen die evolutionär definierte Klasse III der Histon Deacetylasen aus [112, 113].

Die Sirtuine SIRT1-7 lassen sich anhand ihrer hochkonservierten NAD<sup>+</sup>-Bindestelle, die auch als Sirtuin-Kerndomäne bezeichnet wird und welche zentral in der katalytischen Domäne liegt, kategorisieren [112, 114].

Neben dem konservierten Bereich unterscheiden sich die Sirtuine stark in ihren N- und C- Termini, welche die subzelluläre Lokalisierung, die Bindungspartner und Substratspezifitäten, damit auch einhergehende enzymatischen Aktivitäten, der Sirtuine beeinflussen [106, 115, 116].

Aktivität		N-Terminus	Katalytische Domäne	C-Terminus	Länge (AS)	Vorrangige Lokalisation
Deacetylase	SIRT1	244	363	498	747	Zellkern
Deacetylase	SIRT2	65	187	340	389	Zytoplasma
Deacetylase	SIRT3	126	248	385	399	Mitochondrium
ADP-Ribosyltransferase, Deacetylase, Deacylase, Lipoamidase	SIRT4	45	161	314	314	Mitochondrium
Deacetylase, Desuccinylase, Demalonylase	SIRT5	41	158	309	310	Mitochondrium
Deacetylase, ADP-Ribosyltransferase, Demyristoylase	SIRT6	35	133	274	355	Zellkern
Deacetylase	SIRT7	90	187	331	400	Zellkern

Histidin

**Abbildung 6:** Übersicht der humanen Sirtuine anhand ihrer Struktur, molekularen Funktion und dominanten subzellulären Lokalisation [117, 118].

Die Säugetier-Sirtuin-Isoformen befinden sich hauptsächlich im Zellkern (SIRT1, 6 und 7), im Zytosol (SIRT2) oder in den Mitochondrien (SIRT3, 4 und 5) und regulieren Prozesse vom Stoffwechsel bis hin zu Stressreaktionen, indem sie an der epigenetischen Regulation und Kontrolle der Genexpression im Zellkern (SIRT1, 2, 6 und 7), dem mitochondrialen Metabolismus und der Bioenergetik (SIRT3, 4, 5) [106, 119-121], der Regulation der Proliferation/des Zellüberlebens und der Alterung und Regulierung der Lebensspanne (z.B. SIRT6) [106, 116, 119, 122-125] beteiligt sind. Insgesamt verteilen sich die Sirtuine auf mehrere Kompartimente der Zelle, und ihre Lokalisierung kann sich je nach Gewebe/Zelltyp und physiologischem Zustand dynamisch ausprägen oder aber auch ändern.

## 4.4.2. Mitochondriale Sirtuine

### 4.4.2.1. Mitochondrien

Die Mitochondrien stehen im Mittelpunkt der zellulären Energieproduktion, indem sie Sauerstoff zur Generierung von Adenosintriphosphat (ATP) verbrauchen. Das dafür benötigte Pyruvat wird aus der Glykolyse zur Verfügung gestellt und im Citratzyklus verstoffwechselt [126]. In diesem durchqueren Elektronen die Elektronen-Transportkomplexe (I-IV) der Atmungskette, um einen Protonengradienten aufrecht zu erhalten, der dazu dient, über die ATP-Synthase ATP zu erzeugen. Auch Fettsäuren und Aminosäuren werden in den Mitochondrien durch Fettsäure-Oxidation bzw. Aminotransferase-Reaktionen als Metabolite verarbeitet. Zusätzlich generieren sie

ROS und sind wichtiger Ankerpunkt für Signalwege während der Apoptose [127]. Daher ist es nicht überraschend, dass Defekte in den mitochondrialen Funktionen zu einem allgemeinen Ungleichgewicht in der metabolischen Homöostase führen und mit zellulären Alterserscheinungen in Verbindung stehen [128, 129].

Mitochondrien existieren als dynamische, miteinander verbundene Netzwerke, die durch ein Gleichgewicht von Fusion und Spaltung (Fission) aufrechterhalten werden. Diese kontinuierliche Verschmelzung und Spaltung ist notwendig für zellphysiologische Prozesse, einschließlich der Zellproliferation, Migration und dem Tumorwachstum [130-136] und wird streng über mehrere Schlüsselproteine reguliert. Ein System zur Qualitätskontrolle für Mitochondrien, die ihr elektrochemisches Potenzial nicht mehr erzeugen oder aufrechterhalten können, stellt dabei die spezifische Autophagie in Form der Mitophagie dar [137-139]. Bei diesem Vorgang werden dysfunktionale oder geschädigte Mitochondrien als solche zunächst von der Zelle markiert, um von dem Rest des Netzwerks isoliert und schließlich abgebaut werden zu können [140, 141]. Das Gleichgewicht zwischen Fusion und Fission wird hauptsächlich von Enzymen reguliert, die der Familie der monomeren GTPasen angehören [142]. Die mitotische Mitochondrienspaltung hängt sowohl von der Relokalisierung der großen zytoplasmatischen GTPase *Dynamin-1-like Protein* (DRP1) zur äußeren Mitochondrienmembran als auch von der Phosphorylierung von DRP1 durch Zyklin B-CDK1 ab [136, 142-145]. Im Gegenzug wird die Fusion der äußeren Mitochondrienmembran über die Proteine Mitofusin 1 (MFN1) und Mitofusin 2 (MFN2) vermittelt. Eine erhöhte Fission im Zusammenhang mit einer Hochregulation von DRP1 und herunterregulierter MFN-Expression verstärkt die Entstehung von Lungenkrebs durch Erhöhung der Proliferationskapazität und reduzierte Apoptose [146-148]. Ein weiterer entscheidender Regulator der Fusion ist das im Intermembranraum lokalisierte OPA1, welches bei Entkopplung des mitochondrialen Membranpotentials von seiner langen Form L-OPA1, welche die Fusion fördert, zu seiner kurzen, inaktiven Form S-OPA1 gespalten wird [139, 149, 150]. Durch das Verschieben des dynamischen Gleichgewichts zugunsten einer der beiden OPA1 Formen kommt es entweder zur Ausprägung des mitochondrialen Netzwerks oder zur Vereinzelung der Mitochondrien [151].

#### 4.4.2.2. Die Sirtuine 3,4 und 5

Als klassisch mitochondriale Sirtuine gelten die Vertreter SIRT3, SIRT4 und SIRT5, deren prädominante subzelluläre Lokalisation mithilfe von hochauflösenden mikroskopischen Aufnahmen bestimmt wurde [152]. Zusätzlich besitzen sie ein mitochondriales Translokationssignal (MTS), welches für den Import in das Mitochondrium kodiert, wo sie zahlreiche Aspekte der mitochondrialen Biologie regulieren, einschließlich des Redox-Gleichgewichts, der Stoffwechsellhomöostase und der mitochondrialen Dynamik [153]. Trotz einer gewissen funktionalen Redundanz unterscheiden sich die mitochondrialen Sirtuine recht stark voneinander, was sich in der Ausprägung ihrer jeweiligen enzymatischen Aktivitäten und in ihren unterschiedlichen Interaktomen zeigt. Dabei interagieren SIRT5 und SIRT4 mit deutlich weniger Proteinen als SIRT3, wobei SIRT5 nochmal weniger Interaktionspartner als SIRT4 aufweist. Dafür gibt es eine substanzielle Überlagerung bei den mitochondrialen Targets für SIRT3 und SIRT4, was für ein wechselseitiges Zusammenspiel bei der Regulierung des mitochondrialen Metabolismus spricht [154]. SIRT3 wird in allen Geweben exprimiert, wobei die höchsten Konzentrationen in metabolisch aktiven Geweben auftreten, wie braunes Fett, Muskel, Leber, Niere, Herz und Gehirn. SIRT3 ist die wichtigste mitochondriale Deacetylase und primäre Determinante des mitochondrialen Acetyl-Proteoms [155-161]. So assoziiert SIRT3 mit Proteinen, die am oxidativen Gleichgewicht, an der Fettsäureoxidation, an der Glykolyse, am Aminosäurestoffwechsel, dem Citratzyklus und den Elektronentransportketten-Komplexen beteiligt sind. Zusätzlich umfasst das SIRT3-Interaktom auch Proteine, die an der mitochondrialen DNA-Replikation (mtDNA-Replikation), Transkription und Translation beteiligt sind [154].

SIRT4 ist bislang als die einzige ADP-Ribosyltransferase in den Mitochondrien bekannt [162]; daneben zeigt SIRT4 auch Deacetylase-, Deacylase- und Lipoamidase-Aktivität [163, 164]. Die SIRT4-Reaktom-Wege umfassen oxidative Gleichgewichtsreaktionen, Fettsäure-Stoffwechsel, Aminosäure-Katabolismus sowie Biotin-Transport [154].

Obwohl alle drei Mitglieder Deacetylase-Aktivität aufweisen, ist die Deacetylase-Aktivität von SIRT3 höher als die von SIRT4 und SIRT5 [164]. Stattdessen ist SIRT5 eine NAD<sup>+</sup>-abhängige Lysin-Desuccinylase, Demalonylase und Deglutarylase [165, 166]. SIRT5 dient als globaler Regulator der Lysin-Succinylierung in den

Mitochondrien und zielt auf Enzyme, die in der Fettsäure-Oxidation, dem Harnstoffzyklus und der Ketonkörper-Produktion involviert sind [167, 168].

Im mitochondrialen Metabolismus treten Sirtuine als Gegen- und Mitspieler auf. SIRT4 bindet und unterdrückt über ADP-Ribosylierung die GDH-Aktivität, welche für die Umwandlung von L-Glutamat in  $\alpha$ -Ketoglutarat zuständig ist. Dadurch stellt SIRT4 einen direkten Regulator der anaplerotischen Reaktionen des Citratzyklus dar [162]. Antagonistisch dazu arbeitet SIRT3, welches durch die Deacetylierung der GDH deren enzymatische Aktivität verstärkt [169].

Auch in der Regulation des Pyruvat-Dehydrogenase Komplexes (PDC) treten SIRT3 und SIRT4 als Gegenspieler auf. Während SIRT3 durch Deacetylierung die Pyruvat-Dehydrogenase (PDH)-Untereinheit E1 $\alpha$  aktiviert und zu einem erhöhten Umsatz von Pyruvat zu Acetyl-Coenzym A (Acetyl-CoA) führt [170, 171], inhibiert SIRT4 die PDH Aktivität durch die Hydrolysierung des Liponamid-Restes an dessen Untereinheit E2 [164]. Zusätzlich ist bekannt, dass die SIRT5-vermittelte Lysin-Desuccinylierung die Aktivität des PDC ebenfalls, wie SIRT4, unterdrückt [166].

Die differenzierten Funktionen dieser verschiedenen mitochondrialen Sirtuine ergeben sich aus den Unterschieden in der primären enzymatischen Aktivität und der jeweiligen Substrate.

Zahlreiche Untersuchungen haben die Sirtuin-Funktionen mit der Regulierung der ROS-vermittelten Signalgebung sowie mit der Entgiftung von schädlichen ROS in Verbindung gebracht.

SIRT3 reduziert die ROS-Produktion durch indirekte Interaktion mit FoxO3a und in direkter Weise im Mitochondrium mit der Mangan-abhängigen Superoxiddismutase (MnSOD) sowie anderen Komponenten der mitochondrialen Atmungskette [154, 172]. Deacetyliertes FoxO3a transloziert in den Kern und erhöht anschließend die Expression der MnSOD und der Katalase, die Superoxid ( $O_2^-$ ) in  $H_2O_2$  umwandelt und oxidativen Stress reduziert [173, 174]. Im Mitochondrium deacetyliert SIRT3 MnSOD direkt. Die SIRT3-vermittelte Hypoacetylierung von MnSOD erhöht deren Aktivität zur Reduzierung des oxidativen Stresses [175, 176].

Auch SIRT5 zeigt eine antioxidative Kapazität, beispielsweise über die Desuccinylierung und Aktivierung der Kupfer-Zink-abhängigen Superoxiddismutase (CuZnSOD), was zu einer Verringerung des zellulären ROS-Spiegels führt [177].

Darüber hinaus desuccinyliert SIRT5 die Isocitrate-Dehydrogenase 2 (IDH2) und deglutaryliert Glukose-6-Phosphat-Dehydrogenase (G6PD), wodurch beide Nicotinamidadenindinukleotidphosphat (NADPH)-produzierenden Enzyme aktiviert werden, was der Aufrechterhaltung der Redox-Homöostase dient [178]. SIRT5 unterdrückt auch indirekt den mitochondrialen oxidativen Stress, indem es die Aktivität der Succinat-Dehydrogenase (SDH), eines Schlüsselenzyms im Citratzyklus und der Elektronentransportkette, reguliert [179].

Im Kontrast zu SIRT3 und SIRT5 agiert SIRT4 als ROS induzierendes Enzym, indem es, wieder antagonistisch zu SIRT3, die Deacetylierung der MnSOD inhibiert, wodurch es zu einer Erhöhung der mitochondrialen ROS kommt [180]. Auch eine Überexpression von SIRT4 unterstützt diese Beobachtung, da eine zunehmende ROS-Produktion in Mitochondrien mit einhergehender Reduktion in der Mitochondrienqualität aufgezeigt werden konnte [181].

Zusammengenommen wirken SIRT3 und SIRT5 als antioxidative Proteine, während SIRT4 die Bildung von mitochondrialem ROS scheinbar fördert.

#### **4.4.2.3. Die multisubzelluläre Lokalisation und Funktion der mitochondrialen Sirtuine**

Aufgrund der N-terminalen mitochondrialen Translokationssequenz wurde zunächst angenommen, dass die Sirtuine SIRT3, SIRT4 und SIRT5 lediglich in der mitochondrialen Matrix lokalisieren [152, 157, 182]. SIRT4 weist sein MTS innerhalb der ersten, N-terminalen 28 Aminosäuren auf. Wird die MTS entfernt, kann SIRT4 nicht länger in den Mitochondrien angereichert werden [162]. Anhand mehrerer Arbeiten in den letzten Jahren relativiert sich diese feste Lokalisation und es zeigt sich, dass SIRT3, SIRT4 und SIRT5 sich nicht nur im Zytoplasma oder Nukleus anreichern, sondern dort wahrscheinlich auch spezifische Funktionen aufgrund ihrer korrespondierenden Proteininteraktoren erfüllen [168, 183, 184].

So reguliert SIRT3 direkt oder indirekt (d.h. mitochondrienabhängig) die Mikrotubuli-Dynamik und die chromosomale Ausrichtung während der Mitose [185, 186]. Erste Arbeiten zeigen auch für SIRT4 eine extra-mitochondriale Lokalisation. Darunter ein Bericht, der SIRT4 am Spindelapparat während der Meiose nachweist [187], sowie ein Report, dass ein Transport von SIRT4 in den Nukleus möglicherweise unter Stressbedingungen stattfindet [188]. SIRT4 könnte auch eine extramitochondriale Rolle in der Dynamik der Mikrotubuli spielen, da SIRT4 mit dem *Leucin-rich Protein*

130 (LRP130) [154, 189] interagiert, einem Multidomänen- und Doppelfunktionsprotein, welches an das Mikrotubuli-assoziierte Protein MAP1S bindet und den mitochondrialen Transport und das Mikrotubuli-Zytoskelett in der Interphase koordiniert [190].

#### 4.4.3. Nukleäre und zytoplasmatische Sirtuine

SIRT1, SIRT6 und SIRT7 lokalisieren überwiegend im Zellkern, wo sie die Funktion haben, Histone zu deacetylieren und dadurch die Genexpression epigenetisch zu beeinflussen [191]. Im Gegensatz hierzu befindet sich SIRT2 vor allem im Zytoplasma [106]. Diese Sirtuine werden allerdings als nukleär und zytoplasmatisch zusammengefasst, da hier schon seit längerem bekannt ist, dass ein Wechsel in der Lokalisierung zwischen Zellkern und Zytoplasma stattfindet. So wurde beispielsweise festgestellt, dass SIRT1 und SIRT2 sowohl im Kern als auch im Zytoplasma lokalisieren und dort auch mit respektiven Proteinen interagieren [192, 193].

SIRT1 besitzt die höchste Homologie zum Sir2p der Hefe und ist das bislang bestuntersuchte humane Sirtuin, welches in erster Linie als direktes *Stress-Response-Signal*, als Aktivator für Transkriptionsfaktoren und Genregulierung [194-197] oder auch an der Erkennung und Reparatur von DNA-Schäden im Zellkern, beispielsweise an der Reparatur von Doppelstrangbrüchen [198, 199], beteiligt ist. Bei Mäuseembryonen führt das Fehlen von SIRT1 zu einer großen Menge an Chromosomenanomalien und die heterozygote Deletion von SIRT1 beschleunigt die Tumorentstehung bei p53<sup>+/-</sup> Mäusen [200]. Zudem vermittelt SIRT1 metabolische Vorteile in verschiedenen Geweben wie Leber, Herz, weißem Fettgewebe (engl. *white adipose tissue* - WAT) und der Skelettmuskulatur. So unterstützt SIRT1 z.B. in der Leber unter anderem die Gluconeogenese über den Peroxisom-Proliferator-aktivierten Rezeptor  $\gamma$  (PPAR $\gamma$ )-Coaktivator 1 $\alpha$  (PGC-1 $\alpha$ ) und das Forkhead-Box Protein O1 (FOXO1) [201, 202].

Bei Kalorienrestriktion fördert SIRT1 die Fettsäure-Oxidation, indem es Peroxisom-PPAR $\alpha$  aktiviert und die Fettsäuresynthese hemmt [203, 204]. Zusätzlich hemmt SIRT1 die Glykolyse in Leber- sowie auch Muskelzellen durch Unterdrückung der Phosphoglyceratmutase-1 (PGAM-1) [205]. Im WAT treibt SIRT1 die Fettbräunung an, um die Lipidverwertung in Leber und Muskel zu fördern und den Energieverbrauch zu

erhöhen [206, 207]. SIRT1 wirkt sich auch positiv auf das Herz aus, indem es die ischämische Toleranz über eine Aktivierung der endothelialen Stickstoffmonoxid-Synthase (eNOS) erhöht und zusätzlich vor kardialer Hypertrophie schützt [208, 209].

SIRT2 findet sich hauptsächlich im Zytoplasma, wo es NAD<sup>+</sup>-abhängig das Lysin-40 der Mikrotubuli der  $\alpha$ -Tubulin-Untereinheit deacetyliert und so für eine fehlerfreie mitotische Progression erforderlich ist [192, 210]. Die Lokalisation von SIRT2 im Zellkern wurde zunächst aufgrund eines nukleoplasmatischen *Shuttling*-Mechanismus vermutet. Zusätzlich konnte auch eine konstitutiv nukleäre SIRT2-Isoform nachgewiesen werden [211]. SIRT2 ist bislang sehr gut in seiner Rolle und Funktion in Mitose und Zellzyklus untersucht, da es an vielfältigen Prozessen in der Zellzykluskontrolle [212], Aufrechterhaltung der genomischen Integrität und Stabilität [213, 214], Mikrotubuli-Dynamik [214] sowie als Mitspieler in metabolischen Netzwerken [215, 216] und der Autophagie [217] oder aber Apoptose beteiligt ist [218]. Während des Zellzyklus erhöhen sich die SIRT2-Proteinmengen im Kern und SIRT2 assoziiert zudem mit mitotischen Strukturen: beginnend mit dem Zentrosom während der Prophase, der mitotischen Spindel während der Metaphase und dem *midbody* während der Zytokinese [219].

Einwirkung auf die Lipidsynthese nimmt SIRT2 durch die Deacetylierung von FOXO1, woraus eine Unterdrückung der Transkriptionsaktivität von PPAR $\gamma$  resultiert [220]. Im Weiteren konnte gezeigt werden, dass eine SIRT2-vermittelte Deacetylierung des Lysin709 von HIF-1 $\alpha$  (*Hypoxia-inducible factor* - HIF) unter hypoxischem Zellstress dessen Stabilität in Tumorzellen reguliert [221].

SIRT6 und SIRT7, die im Nukleus lokalisieren, interagieren mit Histonen und gelten als epigenetische Regulatoren.

Ein Merkmal der Alterung ist die Akkumulation von geschädigten Zell- und Organismuskomponenten im Laufe der Zeit, gerade auch in der nukleären und mitochondrialen DNA [222]. In diesem Kontext spielt SIRT6 eine wichtige Rolle, indem es die genomische Stabilität gewährleistet [223, 224]. SIRT6 wirkt durch Deacetylaseaktivität auf das Histon 3-Lysin 9, wodurch SIRT6 das Telomeren-Chromatin während der S-Phase moduliert [224, 225]. Eine SIRT6-Depletion führt zu einer Telomerdysfunktion mit End-to-End-Chromosomenfusionen und vorzeitiger zellulärer Seneszenz. Darüber hinaus weisen SIRT6-depletierte Zellen abnormale

Telomerstrukturen auf, die den beim Werner-Syndrom, einer vorzeitigen Alterungsstörung, beobachteten Defekten ähneln [226, 227]. Durch die Histon 3 Modifikation wirkt SIRT6 als Repressor des Transkriptionsfaktors HIF-1 $\alpha$ , wodurch verschiedene glykolytische Gene reguliert werden und SIRT6 somit zu einem Teil des Kontrollmechanismus in der Glukosehomöostase wird [228].

Wie auch SIRT6 lokalisiert SIRT7 im Zellkern und interagiert durch Deacetylierung mit dem Histon H3K18Ac (acetyliertes Lysin 18 des Histons H3), um den *DNA-Damage-Response* Faktor 53BP1 zu DNA-Doppelstrangbrüchen zu rekrutieren, um diese über *non-homologous end joining* (NHEJ) zu reparieren [229]. Dies steht auch im Zusammenhang mit der Stabilisierung des transformierten Zustands von Krebszellen [230]. Diese Rolle macht SIRT7 essenziell für die Aufrechterhaltung der Genomstabilität und -integrität, wodurch es sich funktionell ebenfalls als Tumorsuppressor auszeichnet.

Wieder in Ähnlichkeit zu SIRT6 interagiert SIRT7 auch mit Hypoxie beeinflussenden Faktoren, indem es die transkriptionelle Aktivität der Transkriptionsfaktoren HIF-1 und HIF-2 hemmt, da es die zellulären Proteingehalte ihrer jeweiligen Untereinheiten HIF-1 $\alpha$  und HIF-2 $\alpha$  senkt [231]. Des Weiteren wird SIRT7 mit aktiven rRNA-Genen assoziiert und vermittelt positive Regulation der Ribonukleinsäure-Polymerase I (RNA-Pol I) - Transkription. Die Depletion von SIRT7 stoppt die Zellproliferation und löst die Apoptose aus [232].

#### **4.4.4. Sirtuine und ihre Rolle im Zellzyklus**

Gerade im Fall von SIRT2, für das bereits viele Aufgaben in der Zellzykluskontrolle und gerade auch in der Mikrotubuli-Dynamik untersucht wurden [212, 213, 233], gibt es zunehmend Hinweise auf eine kritische Rolle der Sirtuine in der Zentrosomenbiologie und der mitotischen Regulation. SIRT2 beeinflusst unter anderem die Genomstabilität, indem es die Aktivität der CDK9, einem Protein, das stressbedingten Mitosearrest vermittelt, über Deacetylierung reguliert [234]. Es dient somit als Kontrollpunkt-Regulator in der Mitose, was nahelegt, dass SIRT2 eine Tumorsupressorfunktion einnimmt [235]. Zudem beeinflusst SIRT2 im Zellkern über Chromatinpackung - durch Regulation der Histon H4 Lysin-20 Methylierung

(H4K20me1) - die Mitoseprogression und deacetyliert spezifisch während der G<sub>2</sub>/M-Transition am Histon H4 das Lysin16 (H4K16Ac) [236, 237].

In Übereinstimmung damit wird die Expression von SIRT2 zellzyklusabhängig reguliert, wobei SIRT2 am Zentrosom und der mitotischen Spindel lokalisiert [192]. Die Phosphorylierung von SIRT2 durch Zyklin A-CDK2 reduziert die Bindung von SIRT2 am Zentrosom und fördert die G<sub>2</sub>/M-Progression [238]. Erhöhte SIRT2-Konzentrationen bei mitotischem Stress führen zu einer Verlängerung der mitotischen Phase [213]. Dies beruht wahrscheinlich auf einer regulatorischen Rolle von SIRT2 gegenüber dem *Anaphase Promoting Complex/Cyclosome* (APC/C) [235]. Hingegen kontrolliert SIRT1 z.B. über die Plk2-Achse die Zentrosomenverdoppelung [239]. Des Weiteren hat der durch SIRT1 und p300 regulierte Acetylierungszustand des Lysin-33 der CDK1 Einfluss auf dessen Bindung mit Zyklin-B und damit auf die Kinase-Aktivität des Komplexes. Wichtig ist, dass Zellen, die die Acetylierungsmutante von Cdc2/CDK1 exprimieren, in G<sub>2</sub> angehalten werden und sich nicht mehr teilen. Dies weist auf die Notwendigkeit des deacetylierten Zustands des katalytischen Lysins für die Zellteilung hin [240].

#### **4.4.5. Sirtuine und Krebs**

Aufgrund ihrer Assoziation mit alterungsbedingten Krankheiten wie Stoffwechselstörungen und Neurodegeneration gelten Sirtuine als potenzielle therapeutische Targets [241, 242]. Eine direkte Verknüpfung zwischen der neurologischen Alterung und der Mitochondrien-Homöostase konnte direkt mit der Regulation der Acetyl-CoA Level im Mitochondrium in Verbindung gebracht werden [243]. Die Alterung eines Organismus geht mit einem Rückgang der gesunden Funktion mehrerer Organsysteme einher, was zu einer erhöhten Inzidenz von beispielsweise Diabetes mellitus Typ II, neurodegenerativen Erkrankungen und Herz-Kreislauf-Erkrankungen führen kann [82, 244, 245].

Auch Krebs ist eine altersassoziierte Erkrankung, da dessen Entstehung durch eine zeitlich bedingte Häufung von Mutationen mit dem Alter zunimmt. Viele der Mutationen entstehen durch Fehler bei der DNA-Replikation, umweltbedingten Einflüssen wie UV-Strahlung, oder aber werden durch intrazelluläre reaktive Sauerstoffspezies hervorgerufen, welche direkt in Mitochondrien entstehen können und sich als Reaktion auf zellulären Stress bilden. So korreliert bei vielen Organismen eine längere

Lebensdauer mit geringeren Mengen an reaktiven Sauerstoffspezies in der Zelle. Dies geht beispielsweise auf eine grundlegend geringere zelluläre ROS-Produktion oder auf enzymatische Reaktionen, von Katalasen, Superoxid-Dismutasen oder Glutathion-Peroxidasen, zur Verringerung der ROS-Konzentration zurück [246].

Im Zusammenhang mit einer stärker alternden Gesellschaft werden Prävention und Behandlung von Tumorerkrankungen immer unerlässlicher. Es gibt zahlreiche experimentelle Ergebnisse, die eine Beziehung zwischen Sirtuinen und Krebs unterstützen. So wurde über mehrere Sirtuine berichtet, dass sie tumorsuppressive Aktivitäten aufweisen [195, 200, 247, 248].

#### **4.4.5.1. SIRT4, ein Tumorsuppressor und wichtiger Stoffwechselregulator in den Mitochondrien**

SIRT4 wurde ursprünglich in Bezug auf die Regulierung des Zellstoffwechsels (überwiegend aufgrund von dessen Funktion der GDH-Modifikation und Inhibierung im Mitochondrium) und Aufrechterhaltung der genomischen Stabilität identifiziert und untersucht [163, 249-253]. So hat SIRT4 eine wichtige Auswirkung auf Prozesse der menschlichen Alterspathologien, wie z.B. metabolische, kardiovaskuläre und neurodegenerative Erkrankungen sowie Krebs [254].

In den letzten Jahren haben Studien gezeigt, dass SIRT4 als metabolischer Tumorsuppressor fungiert, der Zellwachstum und Zellproliferation hemmt sowie die Zelltransformation durch Glutaminanaplerose unterdrücken kann [251, 255, 256]. Neben SIRT4 sind auch SIRT3 und SIRT6, aufgrund ihrer Regulation von Glykolyse und Glutaminolyse, als metabolische Tumorsuppressoren identifiziert worden. Bei vielen menschlichen Tumorarten konnte ein Verlust oder eine Reduktion der Expression dieser Sirtuine festgestellt werden [248, 251, 257]. So reprimieren SIRT3 und SIRT6 den Warburg-Effekt, der in vielen menschlichen Tumoren auftritt und bei dem die Deregulierung der Glykolyse das Tumorwachstum unterstützt. Der Verlust von SIRT3 [247] oder SIRT6 [248] induziert die Glykolyse und Glutaminolyse, während der Verlust von SIRT4 nur die Glutaminolyse induziert [251].

Entsprechend der Rolle von SIRT3 und SIRT4 als Tumorsuppressorproteinen entwickeln *Knock-Out*-Mauslinien für SIRT3 und SIRT4 insbesondere Brust- bzw. Lungentumore, [257, 258]. Dabei ist z.B. die SIRT4 Expression in 70 von 133 Fällen in *non-small cell lung cancer* (NSCLC) verringert [253].

Der Phänotyp der Tumorzellen ist mit einer erhöhten chromosomalen Fehlregulation und Aneuploidie/Polyploidie assoziiert, die in primären SIRT4<sup>(-/-)</sup> Maus-Embryofibroblasten nachgewiesen wurde [256, 259]. Im Vergleich zu Wildtyp-Zellen zeigen SIRT4<sup>(-/-)</sup> Zellen mehr DNA-Schäden und eine höhere Empfindlichkeit gegenüber chromosomaler Instabilität nach Behandlung mit Stressoren wie UV-Strahlung.

Insgesamt hemmt SIRT4 die Proliferation von Lungenkrebszellen, blockiert den Zellzyklus und unterdrückt die Zellinvasion und -migration. Zusammenfassend deuten diese Ergebnisse darauf hin, dass SIRT4 als wichtiges Antitumor-Protein bei NSCLC fungiert. Es ist unklar, ob die Tumorphänotypen von Mäusen, denen SIRT3 oder SIRT4 fehlt, primär auf mitochondrienabhängigen und/oder -unabhängigen (d.h. mitotisch/mikrotubuliassozierten) Mechanismen beruhen.

Bemerkenswert ist, dass SIRT4 kürzlich am meiotischen Spindelapparat während der Eizellreifung identifiziert wurde. Oozyten von gealterten Mäusen weisen höhere SIRT4-Level auf, was zu mehr meiotischen Defekten führt, die durch eine SIRT4-Depletion reduziert werden konnten [260]. Entsprechend seiner Akkumulation in gealterten Oozyten wird die Expression von SIRT4 während der replikativen und stressbedingten Seneszenz, die durch verschiedene DNA-schädigende Stressoren, wie beispielsweise *in vivo* in photogealterter menschlicher Haut, ausgelöst wird, hochreguliert [181, 258].

## 5. Zielsetzung

In der Literatur ist bereits für verschiedene Sirtuine bekannt, dass diese, abhängig von Zellstress und Zellzyklus, unterschiedlich in verschiedenen Zellkompartimenten lokalisieren, um dort spezifische Funktionen zu erfüllen. In vorangegangenen Untersuchungen von SIRT4 bezüglich seiner mitochondrialen Funktion wurden in mikroskopischen Aufnahmen vermehrt Strukturen beobachtet, die auf eine extramitochondriale Lokalisation schließen lassen. Dies legt die Vermutung nahe, dass auch SIRT4 nicht nur auf seine Funktion als Modulator der mitochondrialen Morphologie und des mitochondrialen Metabolismus beschränkt ist. Die vorliegende Arbeit hatte in diesem Zusammenhang zum Ziel folgende Punkte zu untersuchen und zu beantworten:

1. Gibt es ein extramitochondriales Reservoir an endogenem SIRT4 oder ektopisch exprimiertem SIRT4-eGFP und lokalisieren diese am Zentrosom und der mitotischen Spindel? Hierzu wurden hochauflösende, konfokale Mikroskopie-Analysen und subzelluläre Fraktionierungen herangezogen.
2. Wie wirkt sich eine SIRT4-Überexpression auf die mitotische Progression und Proliferation der Zellen aus? Ist ein eventuell beobachteter Effekt auf die mitochondriale oder extramitochondriale Funktion zurückzuführen?
3. Welche potenziellen Mechanismen und Interaktionspartner sprechen für eine extramitochondriale Funktion? Dieser Punkt sollte mit Hilfe einer Charakterisierung der massenspektrometrischen Analyse des zellulären SIRT4-Interaktoms G<sub>2</sub>/M-arretierter Zellen aufgeklärt werden.
4. Wo im perizentriolaren Material ist SIRT4 eingebettet? Hat es dort eine enzymatisch aktive Funktion oder gilt es nur als Stabilitäts- und Anker-Faktor? Nimmt SIRT4 über die posttranslationale Modifikation der Mikrotubuli (K40) Dynamik Einfluss auf die Mitose?

Die Beantwortung dieser Fragen sollte neue Einblicke in die vielfältigen Wirkweisen von SIRT4 im Hinblick auf die Lokalisation am Spindelapparat, die Regulation der Mikrotubuli Dynamik und die mitotische Progression geben. Weiterhin sollte die Relevanz von SIRT4 in seiner potenziellen extramitochondrialen Rolle besser verstanden werden, um so weiteren Mechanismen auf den Grund zu gehen, welche im Zusammenhang mit der Aufrechterhaltung der genomischen Stabilität und Krebsentstehung stehen und um das allgemeine Verständnis für altersbedingte Krankheiten zu erweitern.

## 6. Manuskripte

### 6.1. SIRT4 interacts with OPA1 and regulates mitochondrial quality control and mitophagy

Lang A, Anand R, Altinoluk-Hambüchen S, Ezzahoini H, Stefanski A, Iram A, **Bergmann L**, Urbach J, Böhler P, Hänsel J, Franke M, Stühler K, Krutmann J, Scheller J, Stork B, Reichert AS and Piekorz RP. *Aging* (Albany NY). 2017; 9:2160-2186. DOI: 10.18632/aging.101307 [261].

Die Arbeit charakterisiert die Rolle von SIRT4 in der mitochondrialen Dynamik und Qualitätskontrolle/Mitophagie. In vorherigen Experimenten wurde beobachtet, dass im Zusammenhang mit der Hochregulierung der SIRT4-Expression durch miR-15b-Inhibitoren negative Effekte auf die Morphologie und Qualität der Mitochondrien auftraten. Am prävalentesten war die Abnahme des Membranpotentials und die erhöhte Produktion von ROS [181].

Durch die ektopische Expression von SIRT4-eGFP und entsprechender Mutanten, der katalytisch inaktiven Mutante SIRT4(H161Y) und der SIRT4( $\Delta$ 28N) Variante, welche aufgrund ihrer fehlenden MTS nicht mehr in das Mitochondrium importiert wird, konnte gezeigt werden, dass SIRT4 die stressinduzierte mitochondriale ROS-Produktion fördert. Dazu wurde das Membranpotential ( $\Delta\Psi_m$ ) stabiler Zelllinien nach Carbonylcyanide-m-chlorophenylhydrazon (CCCP) Behandlung gemessen.

Zellen, die SIRT4-eGFP exprimierten, zeigten einen signifikanten Anstieg der Stress-induzierten mitochondrialen ROS (mtROS)-Werte, die im Vergleich zu den Kontrollzellen doppelt so hoch waren. Bei den korrespondierenden Mutanten war die mtROS Produktion deutlich schwächer als bei den SIRT4-eGFP Zellen. Um die mitochondriale Qualität in der Zelle zu gewährleisten, werden Mitochondrien mit anhaltender Depolarisation über den Mechanismus der selektiven Autophagie *i.e.* Mitophagie entfernt. Mithilfe konfokaler Laserscanning-Mikroskopie und Immunoblotanalyse des Autophagiemarkers LC3-II konnte gezeigt werden, dass die Expression von SIRT4 den stressbedingten Autophagieflux fördert, während jedoch

die Parkin-assoziierte Mitophagie unter Berücksichtigung der erhöhten Mitochondrienmasse verringert wird.

Ebenfalls konnte unter basalen Konditionen eine Hemmung der mitochondrialen Atmung (Reduktion des O<sub>2</sub>-Gehalts) nach SIRT4-Überexpression beobachtet werden. Massenspektrometrische Interaktionsanalysen identifizierten den mitochondrialen Fusionsregulator OPA1 als SIRT4-Interaktionspartner. Anhand von Co-Immunopräzipitationsexperimenten wurde die Interaktion bestätigt und zusätzlich eine Abhängigkeit der Interaktion mit der L-OPA1 Variante in Abhängigkeit von der katalytischen Aktivität von SIRT4 gezeigt.

Mithilfe von *Spinning Disk* Mikroskopie konnte beobachtet werden, dass nach einer erhöhten Expression von SIRT4 vermehrt verlängerte/verschmolzene Mitochondriennetzwerke auftreten, welche mit höheren Mengen der L-OPA1-Variante assoziiert sind. Eine veränderte mitochondriale Dynamik mit verminderter Autophagie oder Mitophagie sind Kennzeichen der zellulären Alterung. Auch in Fibroblasten, welche als Modell der zellulären Seneszenz herangezogen wurden, führte die Hochregulation endogener SIRT4-Expression zur Erhöhung der L-OPA1-Mengen und beeinflusste die mitochondriale Fusion und Morphologie in einer SIRT4-abhängigen Weise.

Zusammengefasst beschreibt die Publikation einen Zusammenhang zwischen einer reduzierten mitochondrialen Qualitätskontrolle und einer SIRT4 vermittelten Stabilisierung der aktiven L-OPA1-Variante. Dargestellt in Abbildung 7. Eine Verschiebung des Gleichgewichts zur aktiven L-OPA1-Variante führt zu einem stabileren bzw. fixiertem mitochondrialen Netzwerk, was eine Reduktion der Mitophagie beinhaltet. Da dieser Effekt der inhibierten mitochondrialen Qualitätskontrolle bei einer Hochregulation der SIRT4-Mengen auftritt, lässt sich ein Zusammenhang mit der zellulären Seneszenz und Alterung vermuten.

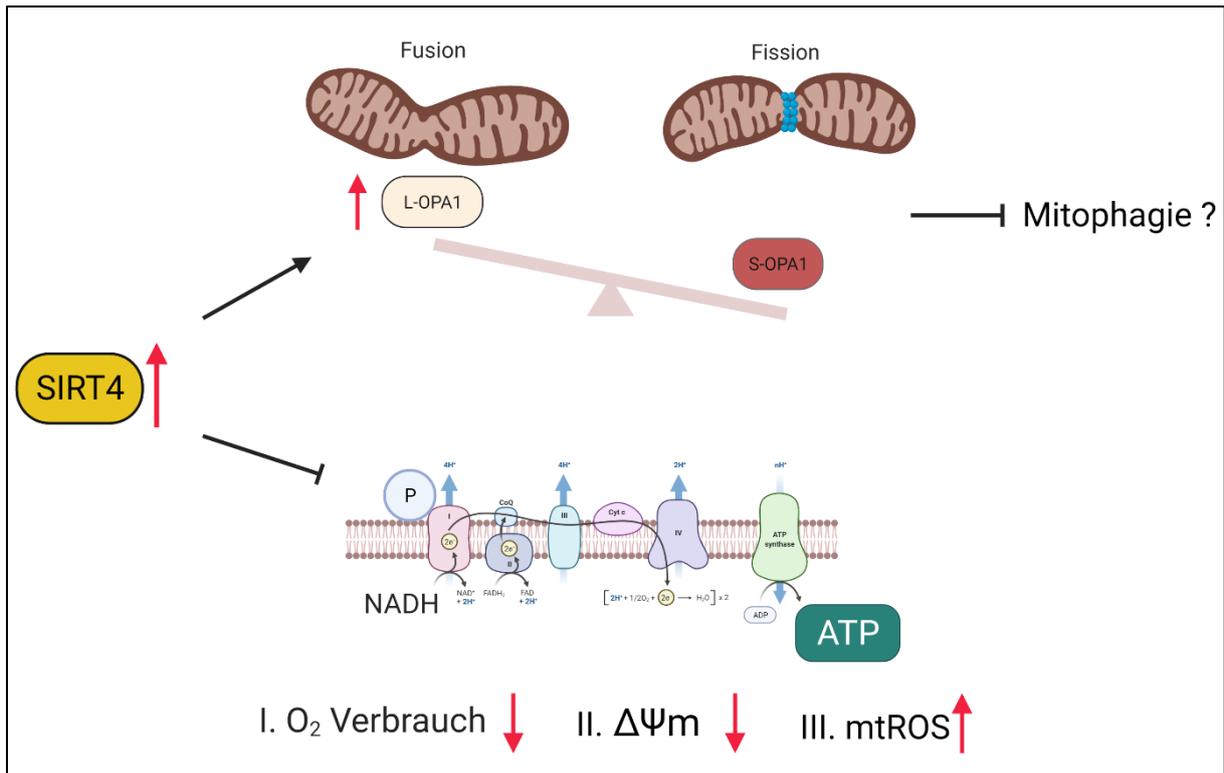


**Abbildung 7:** Schematische Darstellung der SIRT4 Hochregulierung im Mitochondrium und dessen Effekte auf die Morphologie und Qualität der Mitochondrien. Gemessen wurde eine Abnahme des O<sub>2</sub>-Verbrauchs, des Membranpotentials und eine erhöhte Produktion von mtROS. Zusätzlich wurde ein Zusammenhang zwischen einer reduzierten mitochondrialen Qualitätskontrolle und einer SIRT4 vermittelten Stabilisierung der aktiven L-OPA1-Variante beobachtet. Erstellt mit BioRender.com

Die Autorin der vorliegenden Dissertation erarbeitete ca. 10% der Befunde dieser Publikation. Der Beitrag bestand in der Zellkultivierung von HEK293 Zellen, die SIRT4-eGFP und seine respektiven Mutanten stabil überexprimieren, der Zellernte und Unterstützung bei der Western Blot Analyse und der Protein-Interaktions-Studien mithilfe der Nanobody oder OPA1-Co-Immünpräzipitations Methode.

## SIRT4 interacts with OPA1 and regulates mitochondrial quality control and mitophagy

Alexander Lang<sup>1</sup>, Ruchika Anand<sup>2</sup>, Simone Altinoluk-Hambüchen<sup>1</sup>, Hakima Ezzahoini<sup>1</sup>, Anja Stefanski<sup>3</sup>, Afshin Iram<sup>1</sup>, Laura Bergmann<sup>1</sup>, Jennifer Urbach<sup>2</sup>, Philip Böhler<sup>4</sup>, Jan Hänsel<sup>1</sup>, Manuel Franke<sup>1</sup>, Kai Stühler<sup>3</sup>, Jean Krutmann<sup>5</sup>, Jürgen Scheller<sup>1</sup>, Björn Stork<sup>4</sup>, Andreas S. Reichert<sup>2</sup>, and Roland P. Piekorz<sup>1</sup>

<sup>1</sup>Institut für Biochemie und Molekularbiologie II, Medizinische Fakultät der Heinrich-Heine-Universität, Düsseldorf, Germany

<sup>2</sup>Institut für Biochemie und Molekularbiologie I, Medizinische Fakultät der Heinrich-Heine-Universität, Düsseldorf, Germany

<sup>3</sup>Molecular Proteomics Laboratory (BMFZ), Medizinische Fakultät der Heinrich-Heine-Universität, Düsseldorf, Germany

<sup>4</sup>Institut für Molekulare Medizin I, Medizinische Fakultät der Heinrich-Heine-Universität, Düsseldorf, Germany

<sup>5</sup>IUF - Leibniz Institut für umweltmedizinische Forschung, Medizinische Fakultät der Heinrich-Heine-Universität, Düsseldorf, Germany

**Correspondence to:** Roland P. Piekorz; email: [Roland.Piekorz@hhu.de](mailto:Roland.Piekorz@hhu.de)

**Keywords:** Sirtuin-4/SIRT4, mitochondrial quality control, mitochondrial fusion/fission, mitophagy, OPA1, reactive oxygen species/ROS, senescence, fibroblast, aging

**Received:** July 16, 2017    **Accepted:** October 15, 2017    **Published:** October 29, 2017

**Correction:** This article has been corrected. See Aging 2018; 10(9) <https://doi.org/10.18632/aging.101570>

**Copyright:** Lang et al. This is an open-access article distributed under the terms of the Creative Commons Attribution License (CC BY 3.0), which permits unrestricted use, distribution, and reproduction in any medium, provided the original author and source are credited.

### ABSTRACT

The stress-responsive mitochondrial sirtuin SIRT4 controls cellular energy metabolism in a NAD<sup>+</sup>-dependent manner and is implicated in cellular senescence and aging. Here we reveal a novel function of SIRT4 in mitochondrial morphology/quality control and regulation of mitophagy. We report that moderate overexpression of SIRT4, but not its enzymatically inactive mutant H161Y, sensitized cells to mitochondrial stress. CCCP-triggered dissipation of the mitochondrial membrane potential resulted in increased mitochondrial ROS levels and autophagic flux, but surprisingly led to increased mitochondrial mass and decreased Parkin-regulated mitophagy. The anti-respiratory effect of elevated SIRT4 was accompanied by increased levels of the inner-membrane bound long form of the GTPase OPA1 (L-OPA1) that promotes mitochondrial fusion and thereby counteracts fission and mitophagy. Consistent with this, upregulation of endogenous SIRT4 expression in fibroblast models of senescence either by transfection with miR-15b inhibitors or by ionizing radiation increased L-OPA1 levels and mitochondrial fusion in a SIRT4-dependent manner. We further demonstrate that SIRT4 interacts physically with OPA1 in co-immunoprecipitation experiments. Overall, we propose that the SIRT4-OPA1 axis is causally linked to mitochondrial dysfunction and altered mitochondrial dynamics that translates into aging-associated decreased mitophagy based on an unbalanced mitochondrial fusion/fission cycle.

## INTRODUCTION

Aging is defined as a time-dependent loss of physiological integrity and organ function and is characterized by key hallmarks, among them genomic instability, stem cell exhaustion, mitochondrial dysfunction, and cellular senescence [1]. Senescence is either elicited endogenously, e.g. *via* telomere shortening in the case of replicative senescence [2-4], or triggered by extrinsic noxae such as UV radiation (stress-induced senescence) that is responsible for photo-aging of the skin [5-7]. Senescent cells occur and accumulate *in-vivo*, and clearance of senescent cells ameliorates aging-associated pathologies thereby extending healthy lifespan [8, 9]. The hallmarks of aging are functionally interconnected. For instance, upregulation of the cyclin-dependent kinase (CDK) and cell cycle inhibitor p21<sup>WAF</sup>, a p53 target gene and key effector of stress-induced cellular senescence [10, 11], leads to a reduced capacity of stem cell dependent tissue regeneration [12]. Moreover, p21<sup>WAF</sup> maintains a vicious circle in  $\gamma$ -irradiated fibroblasts by re-enforcing senescence signaling *via* the generation of more mitochondrial reactive oxygen species (mtROS) and thus more ROS induced DNA damage [13]. Overall, the pro-aging effects of senescence and the SASP (senescence associated secretory phenotype) seem to be at least in part dependent on the presence of mitochondria [14, 15].

The morphology and dynamics of mitochondria underlie a stringent quality control *via* fusion-fission cycles which are primarily mediated by the key large GTPases OPA1 (optic atrophy 1), mitofusins (MFN1 and 2), and DRP1 (dynamamin-related protein 1). Aging-associated changes in the expression levels of fusion proteins (OPA1, MFN1/2) or reduction of the fission factors DRP1 and FIS1 (a recruitment factor for DRP1 in the mitochondrial outer membrane) have been observed in senescent endothelial or mesenchymal stem cells, both resulting in increased mitochondrial elongation and fusion [16, 17]. As part of mitochondrial quality control, dysfunctional/depolarized, fragmented mitochondria are continuously eliminated by mitophagy, a form of selective autophagy [18-20]. However, there is accumulating evidence for a decline of autophagy and mitophagy during aging [18, 21-27] thereby impairing mitochondrial quality and function. For instance, mitophagy was greatly reduced in aged muscle stem cells (satellite cells) resulting in accumulation of dysfunctional mitochondria, increased ROS generation, and a senescent phenotype [28, 29].

Mitochondrial sirtuins (mtSIRT) comprise three members, SIRT3, SIRT4, and SIRT5 which are all involved in regulating energy metabolism and metabolic

homeostasis [30-33] and whose expression is regulated by transcriptional and post-transcriptional mechanisms, including miRNAs [34, 35]. Among the mtSIRTs, SIRT4 expression is upregulated during senescence triggered by different stimuli as well as *in-vivo* in photo-aged human skin [35]. Upregulation of SIRT4 expression can *per se* induce senescence as shown in trophoblast stem cells [36]. Only limited information exists about the role of mtSIRTs in the regulation of mitochondrial morphology/dynamics and quality control mechanisms. SIRT3, the major deacetylase of metabolic targets in mitochondria, promotes mitochondrial networking and function by activating the fusion factor OPA1 [37]. In the case of SIRT5, an enzyme with demalonylase, deglutarylase, and desuccinylase activities [38, 39] that regulates ammonia detoxification, mitochondrial size was increased and mitophagy decreased upon SIRT5 overexpression [40]. Lastly, overexpression of SIRT4 was linked to the regulation of mitochondrial dynamics *via* inhibition of ERK-mediated phosphorylation of the pro-fission factor DRP1, therefore inhibiting its activity and hence mitochondrial fission [41]. Similar to SIRT5, several enzymatic activities have been described for SIRT4, including ADP-ribosylation of glutamate dehydrogenase (GDH) [42], lipoamidase mediated targeting of the pyruvate dehydrogenase (PDH) complex [43], and lysine deacetylation in the control of leucine metabolism [44].

We demonstrated recently that up-regulation of endogenous SIRT4 expression inhibits the mitochondrial membrane potential ( $\Delta\Psi_m$ ), increases mtROS level, and alters mitochondrial morphology towards aggregation [35]. Here, we further addressed the molecular basis for this phenotype in cells stably expressing wild-type and mutant forms of SIRT4 at low levels and characterized the role of SIRT4 in mitochondrial morphology/quality control and mitophagy under basal and mitochondrial stress conditions.

## RESULTS

### SIRT4 promotes stress induced mitochondrial ROS production

In the present study, we addressed the role of SIRT4, a miR-15b repressed and stress-inducible senescence-associated mitochondrial sirtuin [35, 45], in the regulation of mitochondrial dynamics and quality control. We generated HEK293 cell lines stably expressing C-terminal eGFP fusion proteins of SIRT4, including its catalytically inactive version (H161Y) or SIRT4( $\Delta$ 28N) lacking the N-terminal mitochondrial targeting signal [46]. Expression and subcellular

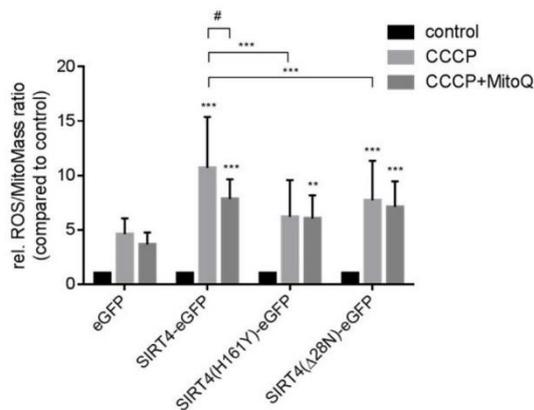


**Figure 1. Catalytically active SIRT4-eGFP increases mitochondrial ROS production after CCCP-induced mitochondrial uncoupling.** HEK293 cell lines stably expressing eGFP, SIRT4-eGFP, SIRT4(H161Y)-eGFP, or SIRT4( $\Delta$ 28N)-eGFP were treated with CCCP (10 nM) for two hours either with or without pretreatment with MitoQ (100 nM; 16 hours). Thereafter cells were stained with the cell-permeant dyes MitoTracker<sup>®</sup> Deep Red and MitoSOX<sup>™</sup> Red followed by flow cytometric analysis. Shown are mean  $\pm$  s.d. values from nine experiments. To evaluate statistical significance (comparison of eGFP vs. wild-type or mutant SIRT4 or comparisons indicated by brackets) two-way ANOVA followed-up by Tukey's test were performed (\*\* $p < 0.01$ ; \*\*\* $p < 0.001$ ). The effect of MitoQ treatment was evaluated using a paired t-test ( $^{\#}p < 0.05$ ).

localization of SIRT4-eGFP and its mutants were confirmed by confocal microscopy, immunoblotting, and flow cytometry analysis (Suppl. Fig. 1). We next subjected these cell lines to CCCP (Carbonylcyanide *m*-chlorophenylhydrazone) treatment and hence to dissipation of the mitochondrial membrane potential ( $\Delta\Psi_m$ ). As depicted in Fig. 1, cells expressing SIRT4-eGFP displayed a significant increase in stress-induced mitochondrial ROS (mtROS) levels which were two-times higher as compared to eGFP-expressing control cells and which could be significantly inhibited by co-treatment with the mitochondria-specific anti-oxidant mitoQ [47, 48]. In contrast, mtROS response was significantly weaker in cells expressing SIRT4(H161Y)-eGFP or SIRT4( $\Delta$ 28N)-eGFP (Fig. 1).

Here, co-treatment with mitoQ did not show an effect. Thus, consistent with the mtROS inducing and  $\Psi_m$ -decreasing role of SIRT4 in primary human dermal fibroblasts [35], SIRT4 expression promotes stress-induced mtROS production also in HEK293 cells *via* its enzymatic activity.

### SIRT4 expression promotes stress triggered autophagic flux, but decreases Parkin associated mitophagy considering the increased mitochondrial content

Mitochondria with sustained depolarization are removed by mitophagy, a selective degradation mechanism for damaged mitochondria, ensuring mitochondrial quality control [22, 49]. To assess the role of SIRT4 in this process we determined the autophagic flux in HEK293 cell lines stably expressing SIRT4-eGFP or its mutants by analyzing the levels of the autophagy marker LC3B-II after treatment with rapamycin (mTORC1 inhibitor and general autophagy inducer) or CCCP (a mitochondrial uncoupler and selective mitophagy inducer). As depicted in Fig. 2, LC3B-II levels were approximately two-fold-increased in CCCP-treated HEK293 SIRT4-eGFP cells, but did not change significantly in cells expressing SIRT4(H161Y)-eGFP or SIRT4( $\Delta$ 28N)-eGFP. We did not detect significant changes in the autophagic flux of any of these cell lines following rapamycin treatment. Consistent with the immunoblot analysis in Fig. 2, the number of LC3B dots per cell was also approximately two-fold higher in CCCP treated SIRT4-eGFP cells vs. eGFP controls as determined by confocal imaging analysis (data not shown). Given this potentially specific effect of SIRT4 on mitophagy, we next analyzed the translocation of the E3 ligase Parkin to damaged mitochondria, a process that promotes selective recruitment of mitochondria to the autophagic machinery [18]. HEK293 cells expressing SIRT4-eGFP (or its mutants) were transfected with a cDNA coding for mCherry-Parkin, subjected to treatment with CCCP and Bafilomycin A1 (BafA1), and analyzed by confocal microscopic imaging (Fig. 3A). Translocation of mCherry-Parkin to mitochondria was observed in all instances as expected after dissipation of the membrane potential. Yet, only for SIRT4-eGFP expressing cells the mitochondrial mass was increased when compared to the eGFP control (Fig. 3B). Taking this into account, we observed that HEK293 cells expressing SIRT4-eGFP, but not the catalytically inactive SIRT4(H161Y)-eGFP or the extra-mitochondrially localized SIRT4( $\Delta$ 28N)-eGFP mutants, displayed a relative decrease in mCherry-Parkin/MTC02 double-positive dots by approximately 40% when standardized against the mitochondrial content (*i.e.*, total MTC02 signal) (Fig. 3C). Taken together, these data indicate that under mitochondrial stress conditions SIRT4 despite promoting mtROS production leads to a net decrease in mitophagy and therefore subsequent decreased removal of dysfunctional mitochondria.

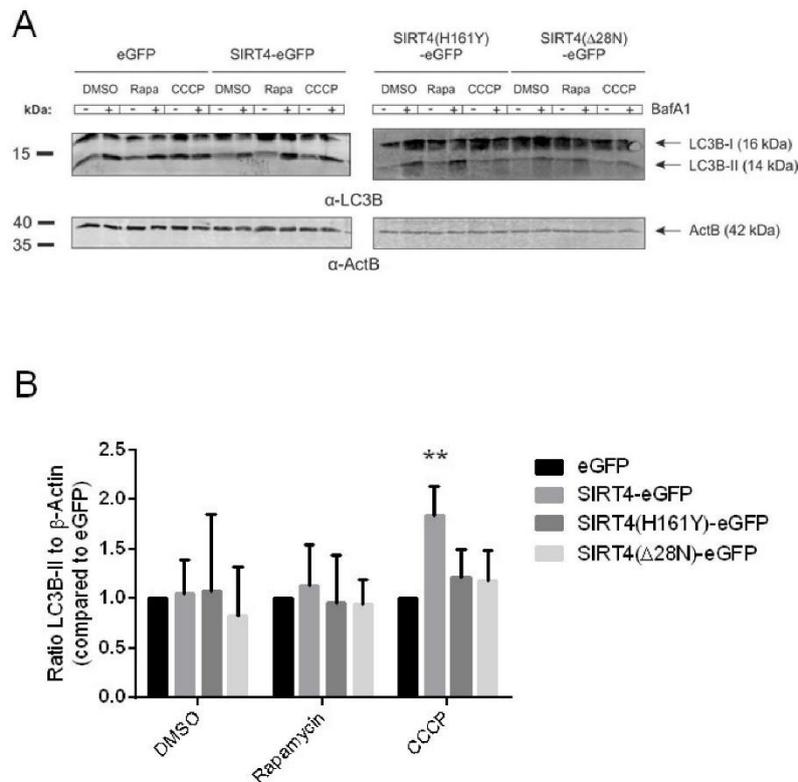


**Figure 2. SIRT4-eGFP expression leads to an increased autophagic flux upon CCCP-induced mitochondrial uncoupling.**

(A) HEK293 cell lines stably expressing eGFP, SIRT4-eGFP, SIRT4(H161Y)-eGFP, or SIRT4(Δ28N)-eGFP were treated with DMSO (control), rapamycin (100 nM), or CCCP (10 μM) for two hours. In addition, during the second hour cells were either untreated (-) or co-treated (+) with BafA1 (Bafilomycin A; 100 nM) that stalls autophagic flux *via* inhibition of the fusion between lysosomes and autophagosomes. A representative experiment is depicted in which LC3B-I and LC3B-II levels were analyzed by immunoblotting. (B) LC3B-II signals (co-treatment with BafA1) were compared to the protein levels of β-Actin/ACTB as loading control using ImageJ based quantification. Data shown are mean ± s.d. values from four to seven experiments. To evaluate statistical significance (treatment vs. DMSO) two-way ANOVA followed by Tukey's test was performed (\*\*p<0.01).

### SIRT4 expression inhibits mitochondrial respiration already under basal conditions

The findings above raised the question whether ectopic SIRT4 expression predisposes cells to mitochondrial stress by impacting already on basal mitochondrial functions such as oxidative phosphorylation. Conflicting results have been described regarding the impact of increased SIRT4 levels on mitochondrial oxygen consumption [50, 51]. We therefore measured the oxygen flow in HEK293 cells expressing SIRT4-eGFP (or its mutants) under basal conditions and upon inhibition of specific respiratory complexes of the electron transport chain (ETC) [52]. As depicted in Fig.

4A and B, HEK293 SIRT4-eGFP cells displayed a significantly reduced oxygen flow both under basal conditions and at maximum respiration, the latter mirroring a reduced electron transport system capacity (ETS) upon complete mitochondrial uncoupling of the electron transport system using CCCP. Surprisingly, cells expressing SIRT4(Δ28N)-eGFP, which cannot localize to mitochondria, showed a significantly increased O<sub>2</sub> flow both at basal and maximum respiration (Fig. 4C). This finding suggests a dominant-negative function of SIRT4(Δ28N) that could be caused by inhibition and/or trapping of endogenous SIRT4 in the cytosol. This interpretation is consistent with an increased oxygen flux and improved mitochondrial function upon SIRT4 depletion [51].

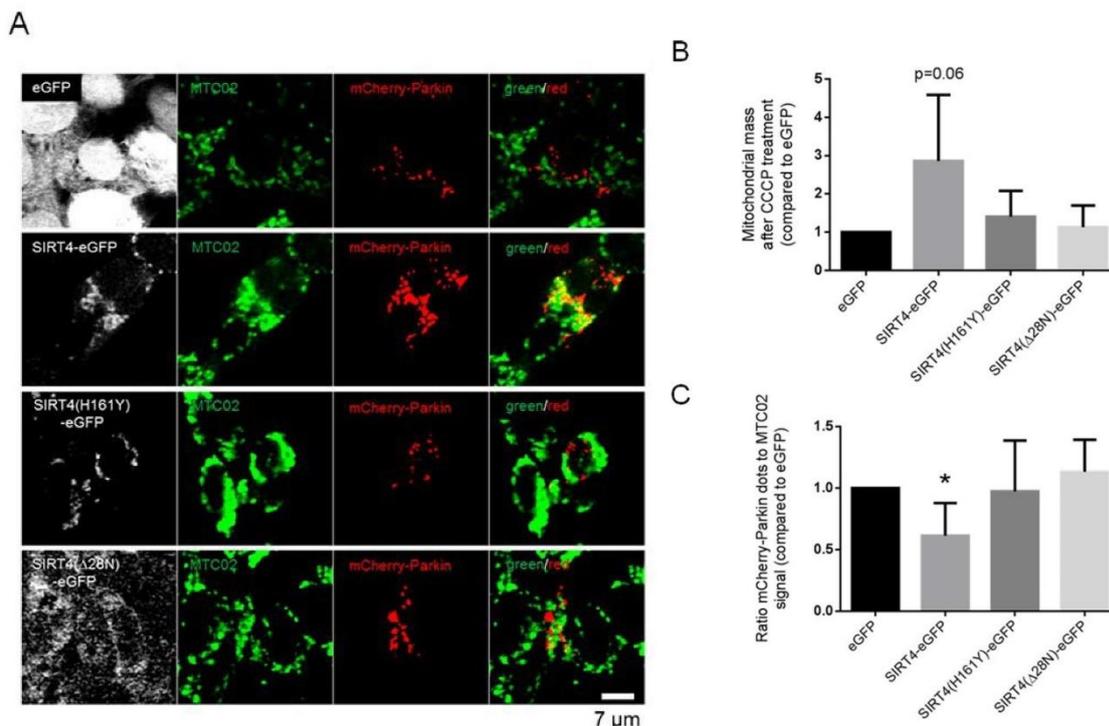


**Figure 3. SIRT4-eGFP expression results in overall decreased mitochondrial recruitment of mCherry-Parkin upon CCCP-induced mitochondrial uncoupling.** (A) HEK293 cell lines stably expressing eGFP, SIRT4-eGFP, SIRT4(H161Y)-eGFP, or SIRT4(Δ28N)-eGFP (GFP signal in white) were transfected with an expression construct for mCherry-Parkin (red). After one day, cells were treated with CCCP (10 μM) for two hours followed by co-treatment with BafA1 (100 nM) during the second hour. Cells were fixed and subjected to confocal microscopic analysis. Mitochondria were detected using the marker MTC02 (green). (B) Quantification of the mitochondrial content via MTC02 staining analysis using ImageJ software (Material & Methods and suppl. Material & Methods). (C) Quantification of mCherry-Parkin/MTC02 double-positive dots was performed based on the mitochondrial content as determined in (B) using ImageJ software (Material & Methods and suppl. Material & Methods). Numbers of cells analyzed in (B) and (C) from four experiments: eGFP, 57; SIRT4-eGFP, 55; SIRT4(H161Y)-eGFP, 43; SIRT4(Δ28N)-eGFP, 48. To evaluate statistical significance two-way ANOVA followed by Tukey's test was performed (\*p<0.05).

### SIRT4 expression leads to a higher degree of elongated/fused mitochondria associated with higher levels of the mitochondrial fusion regulator L-OPA1

Mitochondria, dependent on their (dys)functional status/depolarization, undergo either increased mitochondrial fusion or fission, the latter of which leads to mitophagic clearance upon excessive damage [20, 27]. To further analyze the impact of SIRT4 on mitochondrial quality control we analyzed the mitochondrial network, i.e. mass and structure, in HEK293 cells expressing SIRT4-eGFP (or its mutants). We employed confocal microscopy using staining with the anti-mitochondria antibody MTC02 and subsequent ImageJ based analysis. As depicted in Fig. 5A, cells expressing SIRT4-eGFP underwent an increased

mitochondrial aggregation already under basal (untreated) conditions. This aggregation was clearly less pronounced in GFP control cells or cells expressing the SIRT4 mutants. These findings were corroborated by flow cytometry where HEK293 SIRT4-eGFP cells, but not cells expressing SIRT4(H161Y)-eGFP or SIRT4(Δ28N)-eGFP, depicted significantly increased MitoTracker® staining intensity and hence an increased mitochondrial mass (Suppl. Fig. 2A and 2B). Further quantitative analysis revealed that the mean length of fused mitochondrial tubes was significantly increased only in SIRT4-eGFP expressing cells (Fig. 5B and Suppl. Fig. 3; Suppl. Movies 1 to 4). To corroborate this finding at the molecular level we analyzed the proteolytic processing of the large GTPase and key mitochondrial fusion/fission regulator OPA1 [53, 54].

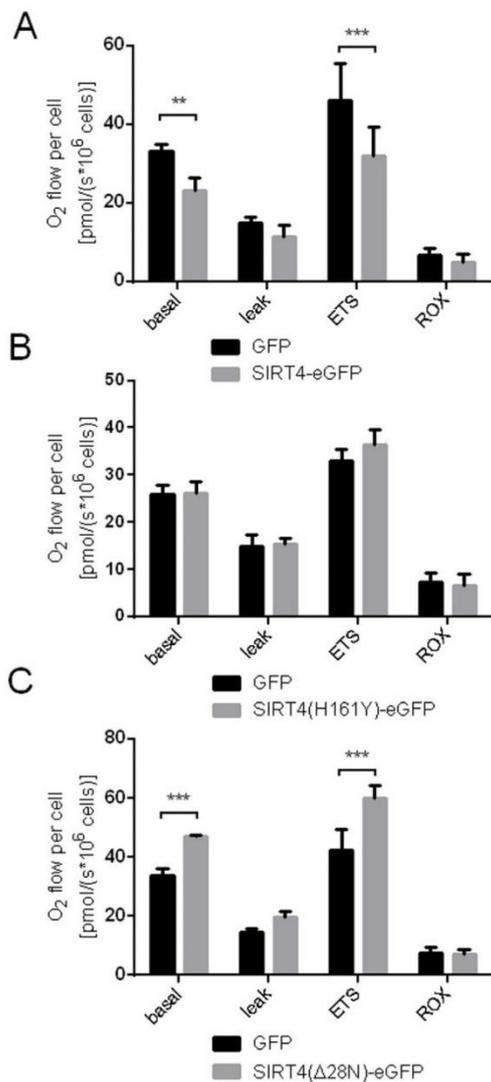


**Figure 4. Oxygen consumption is reduced in HEK293 cells expressing SIRT4-eGFP.** Respirometric measurements of oxygen consumption were performed in HEK293 cell lines stably expressing SIRT4-eGFP (A), SIRT4(H161Y)-eGFP (B), or SIRT4(Δ28N)-eGFP (C) as previously described [52, 64]. Oxygen consumption was measured under basal and stressed conditions (leak: treatment with oligomycin A, 2 μg/ml; ETS: mitochondrial uncoupling of the electron transport system using CCCP, 400-500 nM; residual oxygen consumption, ROX: treatment with 500 nM rotenone and 2.5 μM antimycin A) as compared to control cells expressing eGFP. To evaluate statistical significance two-way ANOVA followed by Tukey's test was performed [\*\*p<0.01, \*\*\*p<0.001; SIRT4-eGFP: n=5; SIRT4(H161Y)-eGFP, n=4; SIRT4(Δ28N)-eGFP: n=4].

Indeed, in HEK293 SIRT4-eGFP cells, the ratio of the proteolytically processed forms of OPA1 was significantly shifted from S-OPA1 (associated with mitochondrial fission and mitophagy) towards L-OPA1 (associated with mitochondrial fusion) (Fig. 6A and 6B). Taken together, these data suggest that SIRT4-eGFP expression inhibits mitochondrial respiration that in terms of mitochondrial quality control translates into increased mitochondrial fusion, the latter possibly resulting in reduced basal mitophagy.

#### SIRT4 interacts with the mitochondrial fusion regulator L-OPA1

To get further insight into the molecular mechanism of how SIRT4 regulates basal mitochondrial quality control we performed co-immunoprecipitation and mass spectrometry to identify interaction partners of SIRT4 in HEK293 cells. The mitochondrial fusion regulator OPA1 was identified to interact specifically with SIRT4-eGFP. Next, we verified this interaction by Western blot analysis after co-immunoprecipitation both in untreated and in CCCP-stressed cells using single-domain-anti-GFP antibodies (Fig. 7A). Here, both forms of OPA1, L-OPA1 and S-OPA1, co-immunoprecipitated with SIRT4-eGFP as well as with its mutants. However, we observed that the amount of L-OPA1 co-immunoprecipitating with SIRT4(H161Y)-eGFP was significantly lower as compared to wild-type SIRT4-eGFP when standardized to the total protein input (Fig. 7B). The (direct or indirect) interaction between SIRT4-eGFP and OPA1 could be confirmed *via* reverse co-immunoprecipitation using a rabbit anti-OPA1 antibody [55] (Suppl. Fig. 4). Taken together, SIRT4 may interact in an enzyme activity-dependent manner with L-OPA1 *via* a currently unknown mechanism and thereby regulate mitochondrial fusion.

#### Upregulation of endogenous SIRT4 expression in fibroblast models of cellular senescence increases L-OPA1 levels and mitochondrial fusion in a SIRT4-dependent manner

Altered mitochondrial dynamics with decreased autophagy or mitophagy are hallmarks to cellular aging [22-24, 27, 56]. We therefore expanded our analyses to primary human dermal fibroblasts to confirm the role of the SIRT4 – L-OPA1 axis in mitochondrial morphology and dynamics in a cellular model more relevant to aging. To upregulate the expression of SIRT4 fibroblasts were either transfected with miR-15b inhibitors or subjected to γ-irradiation (γIR; single dose of 20 Gy) [35]. Under both conditions fibroblasts showed an anti-proliferative response [13, 35], as *e.g.* measured by decreased BrdU incorporation (Suppl. Fig. 5). Thereafter, L-OPA1 vs. S-OPA1 levels and the

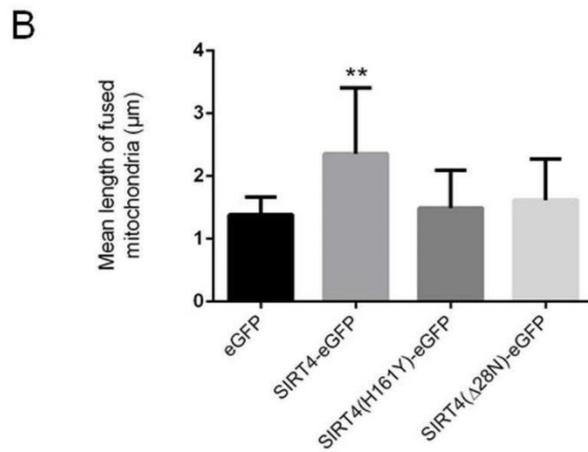
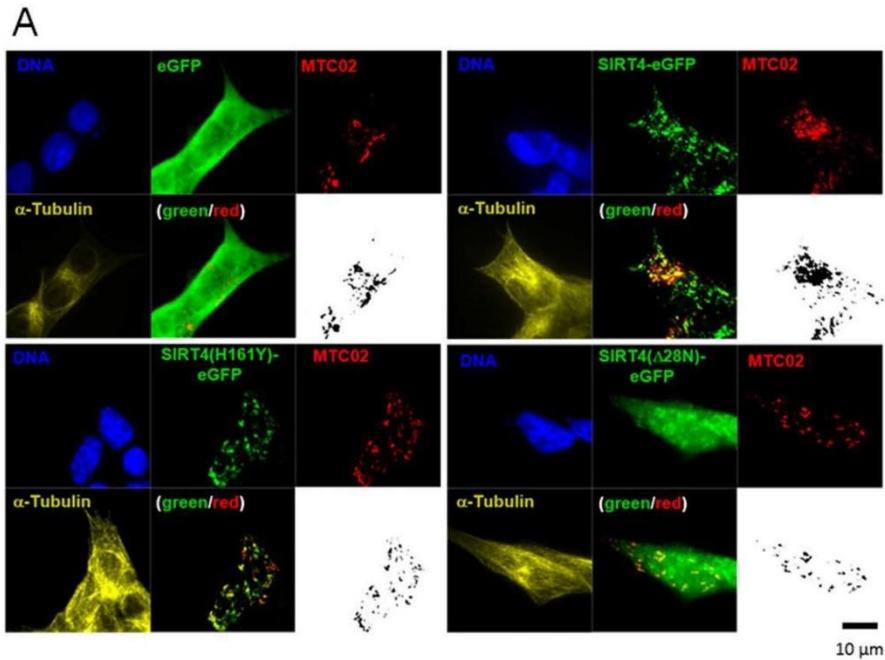


**Figure 5. SIRT4-eGFP expression leads to increased mitochondrial aggregation/fusion.** (A) Subcellular visualization of the mitochondrial marker MTC02 and  $\alpha$ -Tubulin was performed by confocal microscopy in HEK293 cells stably expressing eGFP, SIRT4-eGFP, SIRT4(H161Y)-eGFP, or SIRT4( $\Delta$ 28N)-eGFP. Mitochondrial profiles (MTC02; black/white pictures) were visualized using ImageJ software (Material & Methods and suppl. Material & Methods) to integrate microscopic confocal pictures. Cellular morphology/size was defined by  $\alpha$ -Tubulin staining. Representative images are depicted. (B) Quantification of the mean length of fused mitochondria in cells expressing SIRT4-eGFP or its mutants. Numbers of cells analyzed from four experiments: eGFP, 136; SIRT4-eGFP, 75; SIRT4(H161Y)-eGFP, 104; SIRT4( $\Delta$ 28N)-eGFP, 107. To evaluate statistical significance (compared to eGFP), two-way ANOVA followed-up by Tukey's test was performed (\*\* $p < 0.01$ )

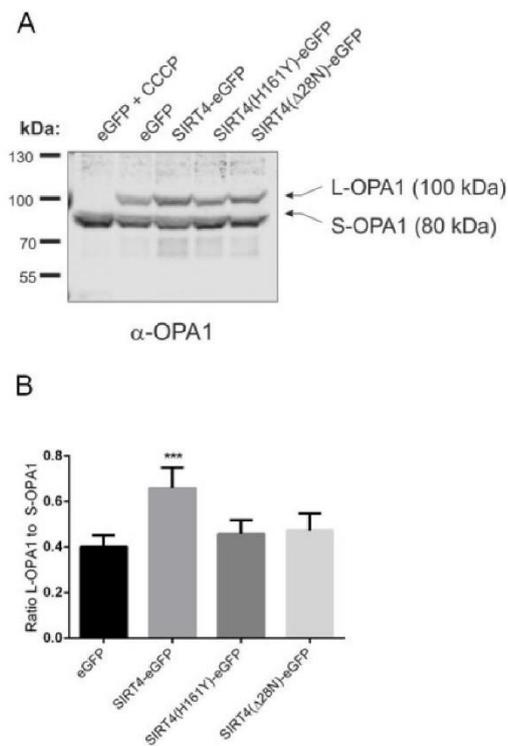


**Figure 6. SIRT4-eGFP expression stabilizes the mitochondrial fusion regulator L-OPA1.** (A) The expression of L-OPA1 vs. S-OPA1 was analyzed by immunoblotting in HEK293 cells stably expressing eGFP, SIRT4-eGFP, SIRT4(H161Y)-eGFP, or SIRT4(Δ28N)-eGFP. As a control for complete proteolytic processing of L-OPA1 to S-OPA1 eGFP-expressing control cells were treated with CCCP (10 μM) for two hours. (B) The ratio between the expression levels of L-OPA1 and S-OPA1 was determined by ImageJ-based densitometric analysis. To evaluate statistical significance (compared to eGFP), two-way ANOVA followed by Tukey's tests was performed (\*\* $p < 0.01$ ;  $n = 6$ ).

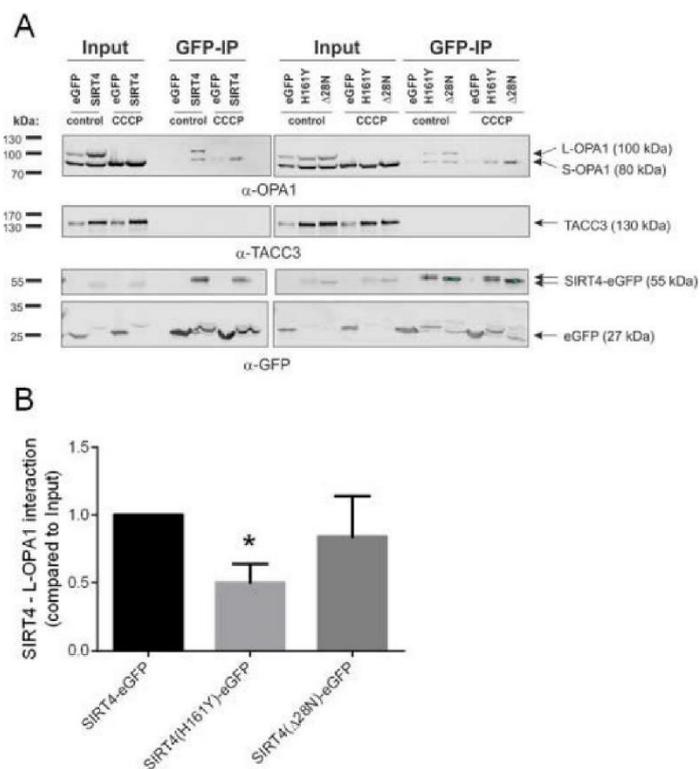


**Figure 7. SIRT4-eGFP interacts with OPA1.** (A) HEK293 cells stably expressing SIRT4-eGFP, SIRT4(H161Y)-eGFP, or SIRT4(Δ28N)-eGFP were either untreated or treated with CCCP (10 μM, 2h) and thereafter subjected to OPA1 co-immunoprecipitation (IP) analysis using sepharose beads coupled anti-GFP single-domain-antibodies (nanobodies). Total cell lysates were loaded as input control (5%). CCCP treatment caused a complete proteolytic processing of L-OPA1 to S-OPA1. TACC3 was detected using specific antibodies and served as a representative negative co-immunoprecipitation control. (B) SIRT4 enzymatic activity is required for efficient interaction of SIRT4 with L-OPA1. The amount of L-OPA1 co-immunoprecipitated with SIRT4-eGFP, SIRT4(H161Y)-eGFP, or SIRT4(Δ28N)-eGFP was determined in relation to the protein input and subjected to ImageJ-based densitometric analysis. To evaluate statistical significance, two-way ANOVA followed by Tukey's tests was performed (\* $p < 0.05$ ;  $n = 4$ ).

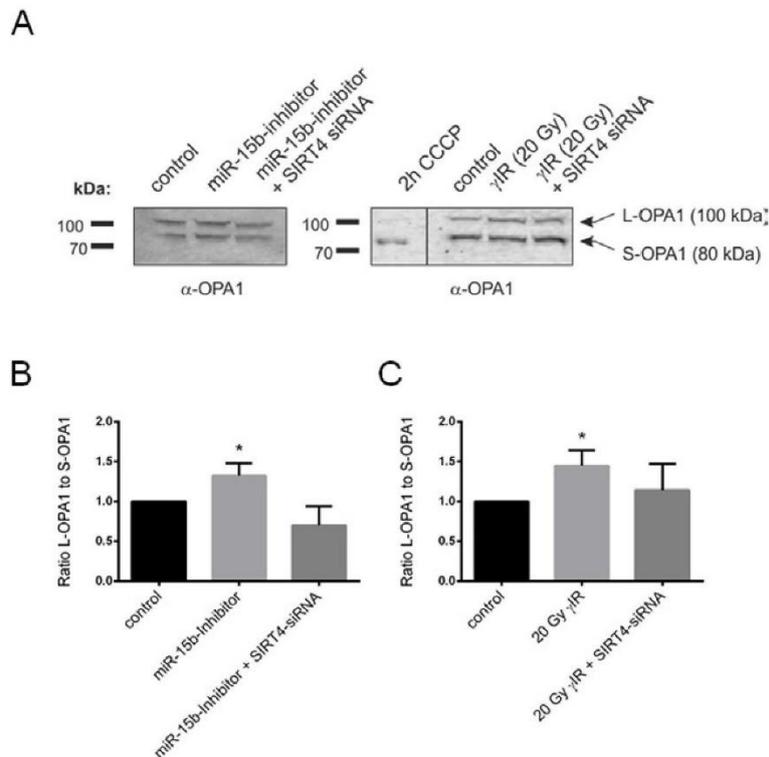


**Figure 8. Aging-associated SIRT4 upregulation leads to a shifted L-OPA1 to S-OPA1 ratio in two different fibroblast senescence models.** Primary human dermal fibroblasts were either transfected with miR-15b inhibitors (or control oligonucleotides) or subjected to  $\gamma$ -irradiation ( $\gamma$ IR; 20 Gy) (both in the presence or absence of siRNA duplexes against SIRT4) [35] followed by analysis of OPA1-L and OPA1-S expression by immunoblotting after four days (A) As a control for complete proteolytic processing of L-OPA1 to S-OPA1, fibroblasts were treated with CCCP (10  $\mu$ M) for two hours. The ratio between the expression levels of L-OPA1 and S-OPA1 was determined by ImageJ-based densitometric analysis in miR-15b inhibitor transfected fibroblasts (B) and cells subjected to  $\gamma$ IR (C). To evaluate statistical significance (compared to control), two-way ANOVA followed by Tukey's test was performed (\* $p$ <0.05;  $n$ =4).

mitochondrial profile/morphology were analyzed in the presence or absence of siRNA duplexes against SIRT4. Consistent with the findings in SIRT4-eGFP expressing HEK293 cells, in both fibroblast senescence models the ratio of L-OPA1 to S-OPA1 was significantly up-regulated, both in a SIRT4-dependent manner (Fig. 8A and 8B) and consistent with corresponding changes in the mitochondrial profiles as visualized by confocal microscopy and quantitative ImageJ based analysis. Increased mitochondrial mass and significantly elevated mitochondrial fusion (indicated by an increased mean length of fused mitochondrial tubes) were observed upon SIRT4 upregulation through miR-15b inhibition (Fig. 9, Suppl. Fig. 6, Suppl. Movies 5 to 7) or  $\gamma$ -irradiation (Fig. 10, Suppl. Fig. 7, Suppl. Movies 8 to 10).

## DISCUSSION

This study provides novel insight into the role of the mitochondrially localized and aging associated sirtuin SIRT4 in basal and stress-induced regulation of mitochondrial morphology and turnover mechanisms. Our data show that SIRT4 promotes mtROS generation triggered by dissipation of the membrane potential across the inner membrane. Although this led to an increase in autophagic flux, overall Parkin-linked mitophagy was apparently decreased due to an increased mitochondrial content. Mechanistically, we propose that SIRT4 functions *via* interacting with L-OPA1 representing a novel regulatory axis in mitochondrial quality control, *i.e.* promotion of

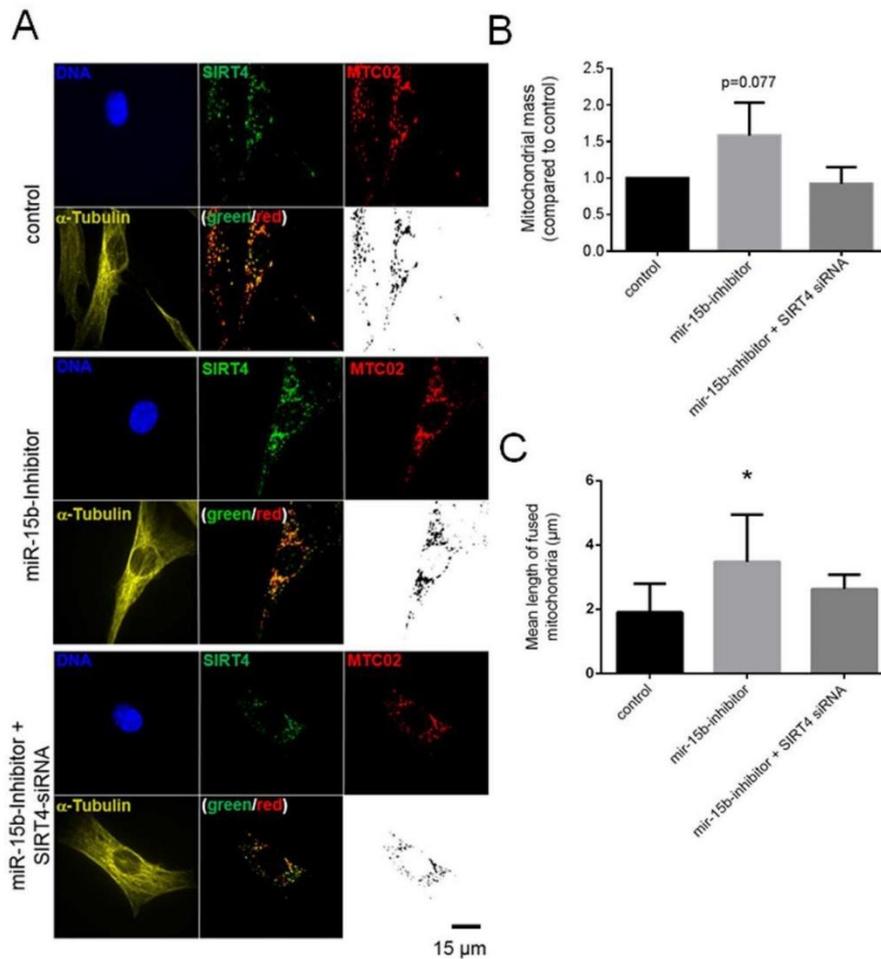


**Figure 9. SIRT4 upregulation through miR-15b inhibition increases L-OPA1 levels and promotes mitochondrial fusion in fibroblasts.** (A) Primary human dermal fibroblasts were transfected with miR-15b inhibitors (or control oligonucleotides) in the presence or absence of siRNA duplexes against SIRT4 [35] followed by subcellular visualization of SIRT4 (green), MTC02 (red), and  $\alpha$ -Tubulin (yellow) after four days. The mitochondrial profiles (MTC02; black/white) were further visualized as binary confocal pictures. Cellular morphology/size was defined by  $\alpha$ -Tubulin staining. Representative images are depicted. (B) Quantification of the mitochondrial mass *via* MTC02 staining analysis using ImageJ software (Material & Methods and suppl. Material & Methods). (C) Quantitative analysis of mitochondrial fusion/length of mitochondrial tubes (as exemplified in suppl. Fig. 6) using ImageJ software (Material & Methods and suppl. Material & Methods). To evaluate statistical significance, two-way ANOVA followed by Tukey's test was performed (\* $p < 0.05$ ;  $n = 12-14$  cells analysed by spinning disk confocal microscopy in three experiments).

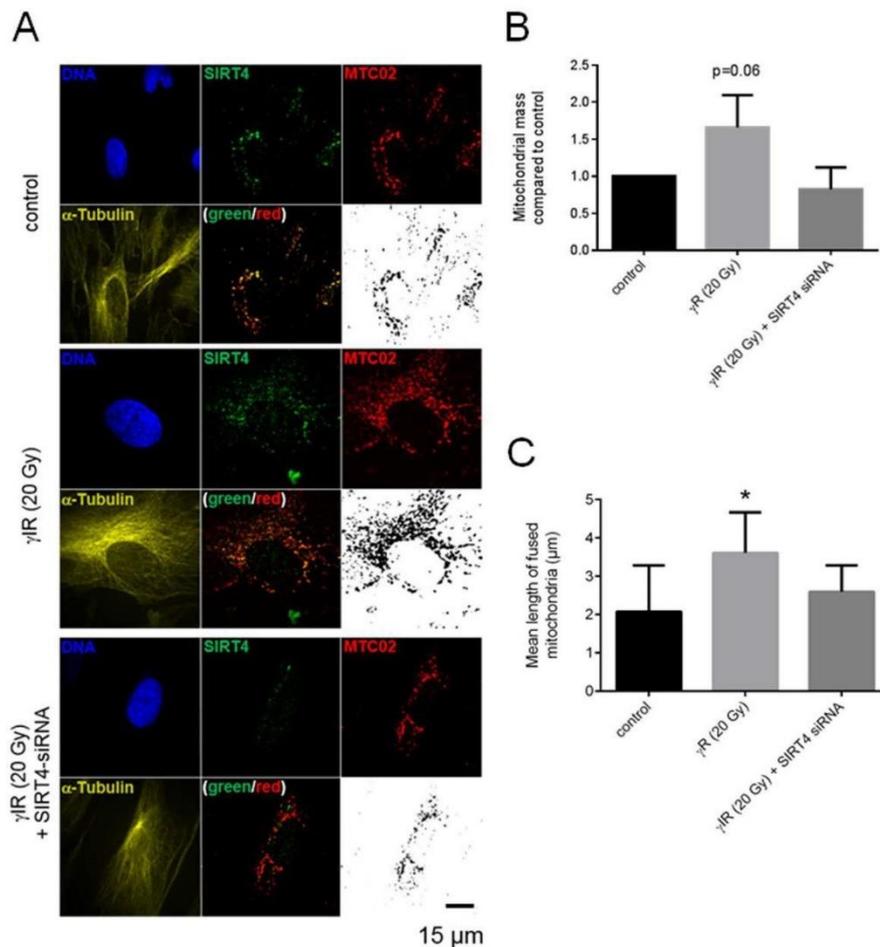


**Figure 10. SIRT4 upregulation upon ionizing radiation stress increases L-OPA1 levels and promotes mitochondrial fusion in fibroblasts.** (A) Primary human dermal fibroblasts were subjected to  $\gamma$ IR (20 Gy) both in either the presence or absence of siRNA duplexes against SIRT4 [35] followed by subcellular visualization of SIRT4 (green), MTC02 (red), and  $\alpha$ -Tubulin (yellow) after four days. The mitochondrial profiles (MTC02; black/white) were further visualized as binary confocal pictures. Cellular morphology/size was defined by  $\alpha$ -Tubulin staining. Representative images are depicted. (B) Quantification of the mitochondrial mass *via* MTC02 staining analysis using ImageJ software (Material & Methods and suppl. Material & Methods). (C) Quantitative analysis of mitochondrial fusion/length of mitochondrial tubes (as exemplified in suppl. Fig. 7) using ImageJ software (Material & Methods and suppl. Material & Methods). To evaluate statistical significance, two-way ANOVA followed by Tukey's test was performed (\* $p$ <0.05;  $n$ =13-19 cells analysed by spinning disk confocal microscopy in three experiments).

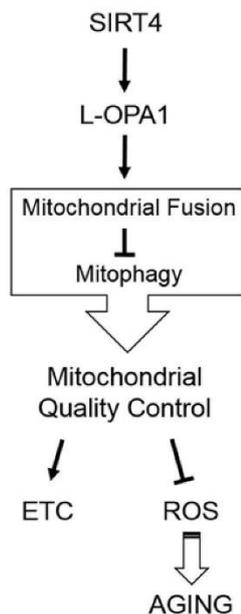


**Figure 11. Model summarizing the regulatory role of the SIRT4-OPA1 axis in mitochondrial quality control.** OPA1, optic atrophy gene 1; ETC, electron transport chain; ROS, reactive oxygen species.

mitochondrial fusion and therefore likely reduction of mitophagy (summarized in Fig. 11).

Mitochondria represent a major source of ROS [57] that dependent on its concentration negatively impacts on mitochondrial function eventually resulting in autophagic clearance of damaged mitochondria. MtROS are typically increased in cells overexpressing enzymatically active SIRT4 [35] (Fig. 1) together with a reduced oxygen consumption under basal and mitochondrial stress conditions (Fig. 4) [51]. In contrast, depletion of SIRT4 in HEK293 cells results in increased oxygen flux and improved mitochondrial function [51]. Consistent with this, we observed an increased O<sub>2</sub> flow in HEK293 SIRT4( $\Delta$ 28N)-eGFP cells both at basal and maximum respiration (Fig. 4), possibly reflecting a dominant-negative function of SIRT4( $\Delta$ 28N). The latter may bind to wild-type SIRT4 and prevent it from mitochondrial translocation (that is dependent on the first 28 a.a.), given that recombinant SIRT4 as well as SIRT4 expressed in HEK293 cells forms homo-oligomeric to multimeric complexes in gel filtration analysis (own unpublished results). The molecular basis for the inhibitory and promoting effects of SIRT4 on mitochondrial respiration and mtROS

generation, respectively, is likely connected to the functional inhibition of one or more SIRT4 targets in the inner mitochondrial membrane and matrix. For instance, SIRT4 negatively regulates key steps in anaplerosis of the citric acid cycle *via* different NAD<sup>+</sup>-dependent enzymatic reactions, *i.e.* ADP-ribosylation and inhibition of glutamate dehydrogenase (GDH) [42] or lipoamidase-mediated targeting and inhibition of the pyruvate dehydrogenase (PDH) complex [43]. Moreover, mass spectrometric characterization of the protein interaction network of SIRT4 identified components of mitochondrial complexes involved in oxidative phosphorylation, namely complex I, IV, and V [58], with complex I representing a major source of mtROS [59].

Besides their functions in energy metabolism and mitochondrial respiratory chain complexes [58], all three mtSIRTs participate in the regulation of mitochondrial morphology/dynamics and hence mitochondrial quality control through interaction with key fusion/fission regulators. SIRT3 promotes mitochondrial networking and functions by deacetylation and therefore activation of the fusion factor OPA1 thereby increasing its GTPase activity [37]. In the case of SIRT4, we now observed increased mitochondrial fusion (Fig. 5, 9, and 10) concomitant with an elevated mitochondrial content in cells overexpressing wild-type SIRT4, but not the catalytically inactive mutant H161Y. These findings were further corroborated by the novel physical link between SIRT4 and OPA1 that was evident in mass spectrometry analysis of SIRT4-eGFP binding partners (Lang et al., manuscript in preparation) and GFP-single-domain antibody (Fig. 7) as well as anti-OPA1 antibody (Suppl. Fig. 4) based co-immunoprecipitation experiments. The molecular mechanism leading to SIRT4 triggered increase in the L-OPA1/S-OPA1 ratio as well the interaction of SIRT4 with L-OPA1 (Fig. 7A and Suppl. Fig. 4) were dependent on the enzymatic activity of SIRT4 (Fig. 7B), and could involve the stabilization of L-OPA1 *via* (in)direct protein-protein interaction or protection from stress-induced and OMA1 mediated processing [60]. The elevated L-OPA1 levels in all cell models analyzed were associated with an increased mitochondrial fusion (Fig. 5, 9, and 10). Moreover, in line with our findings, a recent report linked SIRT4 to the regulation of mitochondrial dynamics *via* inhibition of ERK-mediated phosphorylation of the pro-fission factor DRP1, therefore inhibiting its activity and hence mitochondrial fission [41]. However, similar to the SIRT4-OPA1 interaction, the molecular mechanism by which SIRT4 impacts on the ERK-DRP1 axis is currently unclear and may require one or more of the known enzymatic activities of SIRT4 (ADP-ribosyltransferase, lipo-

amidase, or lysine deacylase; [42-44]). Lastly, in the case of SIRT5, mitochondrial size was increased and mitophagy decreased upon SIRT5 overexpression, whereas the opposite effect was observed in SIRT5 silenced cells or upon treatment with the SIRT5 inhibitor MC3482 [40]. SIRT5 overexpression led to increased levels of the fusion factors OPA1 and MFN2, whereas at the same time the positive mitophagy regulators PINK2 and PARK1 were downregulated [40]. Consistent with this, SIRT5 has a protective role by preventing mitochondrial fragmentation during starvation, given that SIRT5 deficiency increases mitochondrial DRP1 levels and mitophagy [61]. Taken together, all three mtSIRTs seem to promote mitochondrial fusion and/or inhibit fission, and thus might attenuate mitophagic clearance of dysfunctional mitochondria. Of note, Ho et al. observed that higher SIRT4 levels trigger increased retrograde AMPK/PGC1 $\alpha$  signaling from mitochondria to the nucleus [51]. However, this mechanism may rather mediate an increase in mitochondrial biogenesis to compensate for the accumulation of dysfunctional mitochondria which eventually did not undergo proper mitophagic clearance.

In summary, our findings are consistent with an inverse correlation between increased levels of the metabolic tumor suppressor SIRT4 in cellular senescence and aging [35, 45] and cumulative evidence for declining autophagy with advanced age [18, 22, 24-27, 56]. An increased content of mitochondria, which accumulate in a dysfunctional status, is characteristic for senescent cells [1, 13]. Thus, we propose that stress/senescence induced SIRT4 functions *via* L-OPA1 as a novel determinant in the down-regulation of mitophagy during aging by shifting the mitochondrial fusion/fission cycle towards fusion.

## MATERIALS AND METHODS

### Cell culture

HEK293 cells and primary human dermal fibroblasts isolated from foreskin [35] were cultured at 37°C and 5% CO<sub>2</sub> in DMEM (Dulbecco's Modified Eagle Medium) containing high glucose (4.5 g/L; 11965092, Thermo Fisher Scientific) with 10% fetal bovine serum (FBS) and penicillin (100 units/mL)/streptomycin (100  $\mu$ g/mL).

### Cloning of SIRT4-eGFP expression constructs and generation of stable HEK293 lines

Full-length human SIRT4 (from pCMV6-SIRT4-Myc, Origene) and its mutants (H161Y, catalytically inactive;  $\Delta$ 28N, lacking the N-terminal mitochondrial

translocation sequence) were cloned as C-terminal eGFP fusion proteins into pcDNA3.1. HEK293 cells were transfected using TurboFect (Thermo Fisher Scientific) and subjected to G418 (400  $\mu$ g/ml) selection to generate stable cell lines. Expression of SIRT4-eGFP fusion constructs was validated by confocal microscopy, immunoblotting, and flow cytometry (Suppl. Fig. 1).

### Measurement of mitochondrial reactive oxygen species (mtROS)

Cells were stained with cell-permeable dyes MitoTracker® Deep Red FM (100  $\mu$ M; M22426) and MitoSOX™ Red (5  $\mu$ M; M36008), both obtained from Thermo Fisher Scientific. The mitochondria-specific antioxidant MitoQ (10-(6'-ubiquinonyl) decyl triphenylphosphonium bromide) [47], kindly provided by Dr. Mike Murphy (Cambridge), was used to treat cells at a concentration of 100 nM for two days. Treatment of cells with the mitochondrial uncoupler CCCP (Carbonylcyanide *m*-chlorophenylhydrazone; 10  $\mu$ M) occurred for two hours followed by harvesting and staining living cells in 1x PBS for 20 min. Analyses were performed with a BD FACSCanto™ II system (BD Biosciences) employing Flowing Software 2.5.1 (University of Turku, Finland).

### Preparation of total cell lysates for immunoblot analysis

Cleared cell lysates were generated using lysis buffer containing 0.3% CHAPS (3-[(3-Cholamidopropyl) dimethylammonio]-1-propanesulfonate), 50 mM Tris-HCl (pH 7.4), 150 mM NaCl, 1 mM Na<sub>3</sub>VO<sub>4</sub>, 10 mM NaF, 1 mM EDTA, 1 mM EGTA, 2.5 mM Na<sub>4</sub>O<sub>7</sub>P<sub>2</sub>, 1  $\mu$ M DTT, 1x cOmplete™ protease inhibitor cocktail (CO-RO, Sigma-Aldrich). Lysates were cleared by centrifugation (11,000 x g at 4°C for 20 min). Protein concentration of the supernatants was determined using the Bradford assay (K015.1, Roth).

### Immunoprecipitation of eGFP fusion proteins

The single-domain-anti-GFP antibody ("nanobody") method [62, 63] was employed to immunoprecipitate SIRT4-eGFP fusion proteins. Total cell lysates from HEK293 cells stably expressing eGFP, SIRT4-eGFP, SIRT4(H161Y)-eGFP, or SIRT4( $\Delta$ 28N)-eGFP were prepared as described above. Two mg protein was diluted together with 10  $\mu$ l single-domain-anti-GFP antibody beads in a final volume of 400  $\mu$ l lysis buffer [0.3% CHAPS, 50 mM Tris-HCl (pH 7.4), 150 mM NaCl, 1 mM Na<sub>3</sub>VO<sub>4</sub>, 10 mM NaF, 1 mM EDTA, 1 mM EGTA, 2.5 mM Na<sub>4</sub>O<sub>7</sub>P<sub>2</sub>, 1  $\mu$ M DTT, 1x cOmplete™ protease inhibitor cocktail]. This mixture

was incubated overnight at 4°C under rotation. On the next day, the beads were washed four-times with 1 ml washing buffer (lysis buffer without cOmplete™ protease inhibitor cocktail) followed by incubation in Laemmli loading buffer at 95°C for 5 min. Samples and total cell lysates (5% of input) were subjected to SDS-PAGE (10% gels) and proteins were transferred on nitrocellulose membranes (Hybond C, GE Healthcare). Membranes were incubated overnight at 4°C with antibodies against OPA1 [55], TACC3 (sc-22773, Santa Cruz Biotechnology), or GFP (11814460001, Roche Molecular Systems) which were diluted 1:1000 in TBS containing 0.05% Tween 20.

### Measurement of autophagic flux by LC3B-II immunoblot analysis

HEK293 cells were seeded on six-well-plates and cultured for two days at 37°C and 5% CO<sub>2</sub>. To induce autophagy or selective autophagy of mitochondria (mitophagy) cells were treated with 100 nM Rapamycin or 10 μM CCCP (Carbonylcyanide *m*-chlorophenylhydrazone; 857815, Sigma-Aldrich), respectively, for two hours. During the second hour cells were co-treated with (Bafilomycin A; 100 nM; Invivogen) to stall autophagic flux *via* inhibition of the fusion between lysosomes and autophagosomes. Total cell lysates (50 μg) were analyzed on 13.5% SDS-PAGE gels. Antibodies detecting both LC3B-I/ LC3B-II (#2775, Cell Signaling Technology) and β-actin/ACTB (MAB1501, Millipore) were diluted 1:1000 in TBS-Tween (0.05%) and incubated on immunoblot membranes overnight at 4°C. Primary antibodies were detected by IRDye® 680RD goat anti-mouse IgG (P/N 925-68070, LI-COR) and IRDye® 800CW goat anti-rabbit IgG (P/N 925-32211, LI-COR) secondary antibodies using the Odyssey® Imaging System (LI-COR Biosciences).

### Immunofluorescence and confocal laser scanning microscopy to analyze mitophagy

HEK293 cells stably expressing eGFP, SIRT4-eGFP, SIRT4(H161Y)-eGFP, or SIRT4(Δ28N)-eGFP were transfected with pCMV6-mCherry-Parkin (PARK2) and treated with 10 μM CCCP together with 100 nM Bafilomycin A1 for two hours on the next day, as described above. Cells were fixed in 4% paraformaldehyde for 20 min and permeabilized with 0.2% Triton X-100 for 20 min followed by a blocking step with 4% BSA/0.05% saponin for 30 min at room temperature. Cells were co-stained with primary antibodies against the mitochondrial marker MTC02 (abcam, ab3298; 1:500), and α-Tubulin/TUBA1B (Acris antibodies, SM568P; 1:500) overnight at 4°C. Secondary antibodies (Alexa Fluor 546-conjugated goat

anti-mouse IgG and Alexa Fluor 633-conjugated goat anti-rat IgG) were from Life Technologies and used at a dilution of 1:500 for one hour at room temperature. Analyzes were performed with a LSM510-Meta confocal microscope (Zeiss) equipped with 40/1.3 immersion objectives and emission wavelengths of 468 nm, 488 nm, 543 nm, and 633 nm. Quantification of mCherry-Parkin dots was performed based on the mitochondrial content (MTC02 signal) using ImageJ software v1.49k and a specific macro (Suppl. Material & Methods).

### Immunofluorescence and confocal laser scanning microscopy to analyze mitochondrial morphology and mitochondrial fusion/tube formation

To obtain high resolution pictures for analysis of mitochondrial morphology HEK293 cells and primary human dermal fibroblasts were co-stained with antibodies against MTC02 (Abcam, ab3298; 1:500) and α-Tubulin (Abcam, ab52866, 1:500) overnight at 4°C. To increase detection of SIRT4-eGFP fusion proteins (in the case of stably transfected HEK293 cells) primary antibodies against GFP (Nacalai Tesque, Inc., GF090R, 1:1000) were employed. Secondary antibodies were Alexa Fluor 488-conjugated goat anti-rat, Alexa Fluor 546-conjugated goat anti-mouse IgG, and Alexa Fluor 633-conjugated goat anti-rabbit IgG. Acquisitions were performed with the UltraVIEW spinning disk confocal microscope (Perkin Elmer) with emission wavelengths of 468 nm, 488 nm, 543 nm, and 633 nm and the Volocity 6.3 software (Perkin Elmer). Pictures were further analyzed using ImageJ software v1.49k employing specific macros for the analysis of mitochondrial mass and mitochondrial tube formation/length analysis (Suppl. Material & Methods).

### Respirometric measurements

Oxygen consumption was determined in HEK293 cells (10<sup>6</sup>/ml media) stably expressing eGFP, SIRT4-eGFP, SIRT4(H161Y)-eGFP, or SIRT4(Δ28N)-eGFP under basal and stress conditions as compared to control cells expressing eGFP. Measurement were performed essentially as described [52, 64] (leak: treatment with oligomycin A, 2 μg/ml; ETS: mitochondrial uncoupling of the electron transport system using CCCP, 400-500 nM; residual oxygen consumption, ROX: treatment with 500 nM rotenone and 2.5 μM antimycin A).

### Transfection of oligonucleotides

Primary human dermal fibroblasts were transfected with miR-15b inhibitors (or control oligonucleotides) with or without SIRT4 siRNA duplexes to modulate SIRT4 expression essentially as described [35]. Transfection

efficiency was controlled by co-transfection of siGLO Red transfection indicators (GE Dharmacon).

### Ionizing $\gamma$ -irradiation ( $\gamma$ IR)

Primary human dermal fibroblasts were transfected with siRNA duplexes against SIRT4 essentially as described [35]. Following 24h, cells were exposed to  $\gamma$ IR (one dose of 20 Gy; 175 kV and 15 mA) using a Gulmay RS225 X-ray system from X-Strahl (Camberley, UK) and were cultured for another three days before analysis.

### Statistical analysis

Data are presented as mean  $\pm$  s.d. Multiple comparisons were analyzed by one-way or two-way analysis of variance (ANOVA) employing the GraphPad Prism software.

### ABBREVIATIONS

BafA1: Bafilomycin A1; CCCP: Carbonylcyanide *m*-chlorophenylhydrazone;  $\gamma$ IR: gamma-irradiation; ETC: electron transport chain; GDH: glutamate dehydrogenase; miRNA: microRNA; mitoQ: 10-(6'-ubiquinonyl) decyltriphenylphosphoniumbromide; mtSIRT: mitochondrially localized sirtuin; OPA1: optic atrophy gene 1;  $\Delta\Psi$ m: mitochondrial membrane potential; mtROS: mitochondrial reactive oxygen species; ROX: residual oxygen consumption; SASP: senescence associated secretory phenotype.

### ACKNOWLEDGEMENTS

We thank Katharina Schmitz, Chris Wichmann, Reza Ahmadian, and members of the institute for discussions and comments on the manuscript, Jan Borchert for help with ImageJ software, Axel Gödecke for use of the LICOR imaging system, and Mike Murphy (Cambridge) and Marc Majora for sharing MitoQ.

### CONFLICTS OF INTEREST

The authors state no conflict of interest.

### FUNDING

Strategischer Forschungsfond (grant 701.301.987) of the Heinrich-Heine-University (to R.P.P.), the research commission (grant 9772643) of the Medical Faculty of the Heinrich-Heine-University (to R.P.P.), and Deutsche Forschungsgemeinschaft SFB728 project A05 (to R.P.P). Deutsche Forschungsgemeinschaft SFB594 project B09 (to A.S.R) and research commission grant

2/2015 by the Medical Faculty of the Heinrich-Heine-University Düsseldorf (to R.A. and A.S.R.).

### REFERENCES

1. López-Otín C, Blasco MA, Partridge L, Serrano M, Kroemer G. The hallmarks of aging. *Cell*. 2013; 153:1194–217. <https://doi.org/10.1016/j.cell.2013.05.039>
2. Campisi J, d'Adda di Fagagna F. Cellular senescence: when bad things happen to good cells. *Nat Rev Mol Cell Biol*. 2007; 8:729–40. <https://doi.org/10.1038/nrm2233>
3. Hayflick L, Moorhead PS. The serial cultivation of human diploid cell strains. *Exp Cell Res*. 1961; 25:585–621. [https://doi.org/10.1016/0014-4827\(61\)90192-6](https://doi.org/10.1016/0014-4827(61)90192-6)
4. Rodier F, Campisi J. Four faces of cellular senescence. *J Cell Biol*. 2011; 192:547–56. <https://doi.org/10.1083/jcb.201009094>
5. Cavinato M, Jansen-Dürr P. Molecular mechanisms of UVB-induced senescence of dermal fibroblasts and its relevance for photoaging of the human skin. *Exp Gerontol*. 2017; 94:78–82. <https://doi.org/10.1016/j.exger.2017.01.009>
6. Krutmann J, Gilchrist BA. (2006). Photoaging of skin. In: *Skin Aging* (Gilchrist BA, Krutmann J). (New York: Springer), pp. 33-44.
7. Tigges J, Krutmann J, Fritsche E, Haendeler J, Schaal H, Fischer JW, Kalfalah F, Reinke H, Reifemberger G, Stühler K, Ventura N, Gundermann S, Boukamp P, Boege F. The hallmarks of fibroblast ageing. *Mech Ageing Dev*. 2014; 138:26–44. <https://doi.org/10.1016/j.mad.2014.03.004>
8. Baker DJ, Childs BG, Durik M, Wijers ME, Sieben CJ, Zhong J, Saltness RA, Jeganathan KB, Verzosa GC, Pezeshki A, Khazaie K, Miller JD, van Deursen JM. Naturally occurring p16(Ink4a)-positive cells shorten healthy lifespan. *Nature*. 2016; 530:184–89. <https://doi.org/10.1038/nature16932>
9. Baker DJ, Wijshake T, Tchkonja T, LeBrasseur NK, Childs BG, van de Sluis B, Kirkland JL, van Deursen JM. Clearance of p16Ink4a-positive senescent cells delays ageing-associated disorders. *Nature*. 2011; 479:232–36. <https://doi.org/10.1038/nature10600>
10. Georgakilas AG, Martin OA, Bonner WM. p21: A Two-Faced Genome Guardian. *Trends Mol Med*. 2017; 23:310–19. <https://doi.org/10.1016/j.molmed.2017.02.001>

11. Singh M, Piekorz RP. Senescence-associated lysosomal  $\alpha$ -L-fucosidase (SA- $\alpha$ -Fuc): a sensitive and more robust biomarker for cellular senescence beyond SA- $\beta$ -Gal. *Cell Cycle*. 2013; 12:1996. <https://doi.org/10.4161/cc.25318>
12. Ju Z, Choudhury AR, Rudolph KL. A dual role of p21 in stem cell aging. *Ann N Y Acad Sci*. 2007; 1100:333–44. <https://doi.org/10.1196/annals.1395.036>
13. Passos JF, Nelson G, Wang C, Richter T, Simillion C, Proctor CJ, Miwa S, Olijslagers S, Hallinan J, Wipat A, Saretzki G, Rudolph KL, Kirkwood TB, von Zglinicki T. Feedback between p21 and reactive oxygen production is necessary for cell senescence. *Mol Syst Biol*. 2010; 6:347. <https://doi.org/10.1038/msb.2010.5>
14. Correia-Melo C, Marques FD, Anderson R, Hewitt G, Hewitt R, Cole J, Carroll BM, Miwa S, Birch J, Merz A, Rushton MD, Charles M, Jurk D, et al. Mitochondria are required for pro-ageing features of the senescent phenotype. *EMBO J*. 2016; 35:724–42. <https://doi.org/10.15252/embj.201592862>
15. Wiley CD, Velarde MC, Lecot P, Liu S, Sarnoski EA, Freund A, Shirakawa K, Lim HW, Davis SS, Ramanathan A, Gerencser AA, Verdin E, Campisi J. Mitochondrial dysfunction induces senescence with a distinct secretory phenotype. *Cell Metab*. 2016; 23:303–14. <https://doi.org/10.1016/j.cmet.2015.11.011>
16. Mai S, Klinkenberg M, Auburger G, Bereiter-Hahn J, Jendrach M. Decreased expression of Drp1 and Fis1 mediates mitochondrial elongation in senescent cells and enhances resistance to oxidative stress through PINK1. *J Cell Sci*. 2010; 123:917–26. <https://doi.org/10.1242/jcs.059246>
17. Stab BR 2nd, Martinez L, Grismaldo A, Lerma A, Gutiérrez ML, Barrera LA, Sutachan JJ, Albarracín SL. Mitochondrial functional changes characterization in young and senescent human adipose derived MSCs. *Front Aging Neurosci*. 2016; 8:299. <https://doi.org/10.3389/fnagi.2016.00299>
18. Hamacher-Brady A, Brady NR. Mitophagy programs: mechanisms and physiological implications of mitochondrial targeting by autophagy. *Cell Mol Life Sci*. 2016; 73:775–95. <https://doi.org/10.1007/s00018-015-2087-8>
19. Komatsu M, Ichimura Y. Selective autophagy regulates various cellular functions. *Genes Cells*. 2010; 15:923–33. <https://doi.org/10.1111/j.1365-2443.2010.01433.x>
20. Twig G, Shirihai OS. The interplay between mitochondrial dynamics and mitophagy. *Antioxid Redox Signal*. 2011; 14:1939–51. <https://doi.org/10.1089/ars.2010.3779>
21. Diot A, Morten K, Poulton J. Mitophagy plays a central role in mitochondrial ageing. *Mamm Genome*. 2016; 27:381–95. <https://doi.org/10.1007/s00335-016-9651-x>
22. Gaziev AI, Abdullaev S, Podlutzky A. Mitochondrial function and mitochondrial DNA maintenance with advancing age. *Biogerontology*. 2014; 15:417–38. <https://doi.org/10.1007/s10522-014-9515-2>
23. Kalfalah F, Janke L, Schiavi A, Tigges J, Ix A, Ventura N, Boege F, Reinke H. Crosstalk of clock gene expression and autophagy in aging. *Aging (Albany NY)*. 2016; 8:1876–95. <https://doi.org/10.18632/aging.101018>
24. Korolchuk VI, Miwa S, Carroll B, von Zglinicki T. Mitochondria in cell senescence: is mitophagy the weak link? *EBioMedicine*. 2017; 21:7–13. <https://doi.org/10.1016/j.ebiom.2017.03.020>
25. López-Lluch G, Santos-Ocaña C, Sánchez-Alcázar JA, Fernández-Ayala DJ, Asencio-Salcedo C, Rodríguez-Aguilera JC, Navas P. Mitochondrial responsibility in ageing process: innocent, suspect or guilty. *Biogerontology*. 2015; 16:599–620. <https://doi.org/10.1007/s10522-015-9585-9>
26. Rubinsztein DC, Mariño G, Kroemer G. Autophagy and aging. *Cell*. 2011; 146:682–95. <https://doi.org/10.1016/j.cell.2011.07.030>
27. Weber TA, Reichert AS. Impaired quality control of mitochondria: aging from a new perspective. *Exp Gerontol*. 2010; 45:503–11. <https://doi.org/10.1016/j.exger.2010.03.018>
28. García-Prat L, Martínez-Vicente M, Perdiguero E, Ortet L, Rodríguez-Ubreva J, Rebollo E, Ruiz-Bonilla V, Gutarra S, Ballestar E, Serrano AL, Sandri M, Muñoz-Cánoves P. Autophagy maintains stemness by preventing senescence. *Nature*. 2016; 529:37–42. <https://doi.org/10.1038/nature16187>
29. García-Prat L, Muñoz-Cánoves P, Martínez-Vicente M. Dysfunctional autophagy is a driver of muscle stem cell functional decline with aging. *Autophagy*. 2016; 12:612–13. <https://doi.org/10.1080/15548627.2016.1143211>
30. Haigis MC, Sinclair DA. Mammalian sirtuins: biological insights and disease relevance. *Annu Rev Pathol*. 2010; 5:253–95. <https://doi.org/10.1146/annurev.pathol.4.110807.092250>

31. Li X, Kazgan N. Mammalian sirtuins and energy metabolism. *Int J Biol Sci.* 2011; 7:575–87. <https://doi.org/10.7150/ijbs.7.575>
32. Pirinen E, Lo Sasso G, Auwerx J. Mitochondrial sirtuins and metabolic homeostasis. *Best Pract Res Clin Endocrinol Metab.* 2012; 26:759–70. <https://doi.org/10.1016/j.beem.2012.05.001>
33. van de Ven RA, Santos D, Haigis MC. Mitochondrial sirtuins and molecular mechanisms of aging. *Trends Mol Med.* 2017; 23:320–31. <https://doi.org/10.1016/j.molmed.2017.02.005>
34. Buler M, Andersson U, Hakkola J. Who watches the watchmen? Regulation of the expression and activity of sirtuins. *FASEB J.* 2016; 30:3942–60. <https://doi.org/10.1096/fj.201600410RR>
35. Lang A, Grether-Beck S, Singh M, Kuck F, Jakob S, Kefalas A, Altinluk-Hambüchen S, Graffmann N, Schneider M, Lindecke A, Brenden H, Felsner I, Ezzahoini H, et al. MicroRNA-15b regulates mitochondrial ROS production and the senescence-associated secretory phenotype through sirtuin 4/SIRT4. *Aging (Albany NY).* 2016; 8:484–505. <https://doi.org/10.18632/aging.100905>
36. Castex J, Willmann D, Kanouni T, Arrigoni L, Li Y, Friedrich M, Schleicher M, Wöhrle S, Pearson M, Kraut N, Méret M, Manke T, Metzger E, et al. Inactivation of Lsd1 triggers senescence in trophoblast stem cells by induction of Sirt4. *Cell Death Dis.* 2017; 8:e2631. <https://doi.org/10.1038/cddis.2017.48>
37. Samant SA, Zhang HJ, Hong Z, Pillai VB, Sundaresan NR, Wolfgeher D, Archer SL, Chan DC, Gupta MP. SIRT3 deacetylates and activates OPA1 to regulate mitochondrial dynamics during stress. *Mol Cell Biol.* 2014; 34:807–19. <https://doi.org/10.1128/MCB.01483-13>
38. Osborne B, Bentley NL, Montgomery MK, Turner N. The role of mitochondrial sirtuins in health and disease. *Free Radic Biol Med.* 2016; 100:164–74. <https://doi.org/10.1016/j.freeradbiomed.2016.04.197>
39. Yang L, Ma X, He Y, Yuan C, Chen Q, Li G, Chen X. Sirtuin 5: a review of structure, known inhibitors and clues for developing new inhibitors. *Sci China Life Sci.* 2017; 60:249–56. <https://doi.org/10.1007/s11427-016-0060-7>
40. Polletta L, Vernucci E, Carnevale I, Arcangeli T, Rotili D, Palmerio S, Steegborn C, Nowak T, Schutkowski M, Pellegrini L, Sansone L, Villanova L, Runci A, et al. SIRT5 regulation of ammonia-induced autophagy and mitophagy. *Autophagy.* 2015; 11:253–70. <https://doi.org/10.1080/15548627.2015.1009778>
41. Fu L, Dong Q, He J, Wang X, Xing J, Wang E, Qiu X, Li Q. SIRT4 inhibits malignancy progression of NSCLCs, through mitochondrial dynamics mediated by the ERK-Drp1 pathway. *Oncogene.* 2017; 36:2724–36. <https://doi.org/10.1038/onc.2016.425>
42. Haigis MC, Mostoslavsky R, Haigis KM, Fahie K, Christodoulou DC, Murphy AJ, Valenzuela DM, Yancopoulos GD, Karow M, Blander G, Wolberger C, Prolla TA, Weindruch R, et al. SIRT4 inhibits glutamate dehydrogenase and opposes the effects of calorie restriction in pancreatic beta cells. *Cell.* 2006; 126:941–54. <https://doi.org/10.1016/j.cell.2006.06.057>
43. Mathias RA, Greco TM, Oberstein A, Budayeva HG, Chakrabarti R, Rowland EA, Kang Y, Shenk T, Cristea IM. Sirtuin 4 is a lipoamidase regulating pyruvate dehydrogenase complex activity. *Cell.* 2014; 159:1615–25. <https://doi.org/10.1016/j.cell.2014.11.046>
44. Anderson KA, Huynh FK, Fisher-Wellman K, Stuart JD, Peterson BS, Douros JD, Wagner GR, Thompson JW, Madsen AS, Green MF, Sivley RM, Ilkayeva OR, Stevens RD, et al. SIRT4 is a lysine deacetylase that controls leucine metabolism and insulin secretion. *Cell Metab.* 2017; 25:838–855.e15. <https://doi.org/10.1016/j.cmet.2017.03.003>
45. Jeong SM, Xiao C, Finley LW, Lahusen T, Souza AL, Pierce K, Li YH, Wang X, Laurent G, German NJ, Xu X, Li C, Wang RH, et al. SIRT4 has tumor-suppressive activity and regulates the cellular metabolic response to DNA damage by inhibiting mitochondrial glutamine metabolism. *Cancer Cell.* 2013; 23:450–63. <https://doi.org/10.1016/j.ccr.2013.02.024>
46. Ahuja N, Schwer B, Carobbio S, Waltregny D, North BJ, Castronovo V, Maechler P, Verdin E. Regulation of insulin secretion by SIRT4, a mitochondrial ADP-ribosyltransferase. *J Biol Chem.* 2007; 282:33583–92. <https://doi.org/10.1074/jbc.M705488200>
47. Murphy MP. Understanding and preventing mitochondrial oxidative damage. *Biochem Soc Trans.* 2016; 44:1219–26. <https://doi.org/10.1042/BST20160108>
48. Saretzki G, Murphy MP, von Zglinicki T. MitoQ counteracts telomere shortening and elongates lifespan of fibroblasts under mild oxidative stress. *Aging Cell.* 2003; 2:141–43. <https://doi.org/10.1046/j.1474-9728.2003.00040.x>

49. Held NM, Houtkooper RH. Mitochondrial quality control pathways as determinants of metabolic health. *BioEssays*. 2015; 37:867–76. <https://doi.org/10.1002/bies.201500013>
50. de Moura MB, Uppala R, Zhang Y, Van Houten B, Goetzman ES. Overexpression of mitochondrial sirtuins alters glycolysis and mitochondrial function in HEK293 cells. *PLoS One*. 2014; 9:e106028. <https://doi.org/10.1371/journal.pone.0106028>
51. Ho L, Titus AS, Banerjee KK, George S, Lin W, Deota S, Saha AK, Nakamura K, Gut P, Verdin E, Kolthur-Seetharam U. SIRT4 regulates ATP homeostasis and mediates a retrograde signaling via AMPK. *Aging (Albany NY)*. 2013; 5:835–49. <https://doi.org/10.18632/aging.100616>
52. Anand R, Strecker V, Urbach J, Wittig I, Reichert AS. Mic13 is essential for formation of crista junctions in mammalian cells. *PLoS One*. 2016; 11:e0160258. <https://doi.org/10.1371/journal.pone.0160258>
53. MacVicar T, Langer T. OPA1 processing in cell death and disease - the long and short of it. *J Cell Sci*. 2016; 129:2297–306. <https://doi.org/10.1242/jcs.159186>
54. MacVicar TD, Lane JD. Impaired OMA1-dependent cleavage of OPA1 and reduced DRP1 fission activity combine to prevent mitophagy in cells that are dependent on oxidative phosphorylation. *J Cell Sci*. 2014; 127:2313–25. <https://doi.org/10.1242/jcs.144337>
55. Barrera M, Koob S, Dikov D, Vogel F, Reichert AS. OPA1 functionally interacts with MIC60 but is dispensable for crista junction formation. *FEBS Lett*. 2016; 590:3309–22. <https://doi.org/10.1002/1873-3468.12384>
56. Biala AK, Dhingra R, Kirshenbaum LA. Mitochondrial dynamics: orchestrating the journey to advanced age. *J Mol Cell Cardiol*. 2015; 83:37–43. <https://doi.org/10.1016/j.yjmcc.2015.04.015>
57. Sies H, Berndt C, Jones DP. Oxidative Stress. *Annu Rev Biochem*. 2017; 86:715–48. <https://doi.org/10.1146/annurev-biochem-061516-045037>
58. Yang W, Nagasawa K, Münch C, Xu Y, Satterstrom K, Jeong S, Hayes SD, Jedrychowski MP, Vyas FS, Zaganjor E, Guarani V, Ringel AE, Gygi SP, et al. Mitochondrial Sirtuin network reveals dynamic SIRT3-dependent deacetylation in response to membrane depolarization. *Cell*. 2016; 167:985–1000.e21. <https://doi.org/10.1016/j.cell.2016.10.016>
59. Dröse S, Brandt U, Wittig I. Mitochondrial respiratory chain complexes as sources and targets of thiol-based redox-regulation. *Biochim Biophys Acta*. 2014; 1844:1344–54. <https://doi.org/10.1016/j.bbapap.2014.02.006>
60. Korwitz A, Merkwirth C, Richter-Dennerlein R, Tröder SE, Sprenger HG, Quirós PM, López-Otín C, Rugarli EI, Langer T. Loss of OMA1 delays neurodegeneration by preventing stress-induced OPA1 processing in mitochondria. *J Cell Biol*. 2016; 212:157–66. <https://doi.org/10.1083/jcb.201507022>
61. Guedouari H, Daigle T, Scorrano L, Hebert-Chatelain E. Sirtuin 5 protects mitochondria from fragmentation and degradation during starvation. *Biochim Biophys Acta*. 2017; 1864:169–76. <https://doi.org/10.1016/j.bbamcr.2016.10.015>
62. Franke M, Schröder J, Monhasery N, Ackfeld T, Hummel TM, Rabe B, Garbers C, Becker-Pauly C, Floss DM, Scheller J. Human and murine interleukin 23 receptors are novel substrates for a disintegrin and metalloproteases ADAM10 and ADAM17. *J Biol Chem*. 2016; 291:10551–61. <https://doi.org/10.1074/jbc.M115.710541>
63. Rothbauer U, Zolghadr K, Muyldermans S, Schepers A, Cardoso MC, Leonhardt H. A versatile nanotrap for biochemical and functional studies with fluorescent fusion proteins. *Mol Cell Proteomics*. 2008; 7:282–89. <https://doi.org/10.1074/mcp.M700342-MCP200>
64. Pesta G, Gnaiger E. (2012). High-Resolution Respirometry: OXPHOS Protocols for Human Cells and Permeabilized Fibers from Small Biopsies of Human Muscle. In: Palmeira C and Moreno AJ, eds. *Methods in Molecular Biology*: Springer Science+Business Media, pp. 25-58.

## SUPPLEMENTAL MATERIAL

### SUPPLEMENTARY MATERIALS AND METHODS

#### ImageJ based analysis of confocal microscopic pictures

The following macros were used to quantify mCherry-Parkin dots (A), mitochondrial mass (B), and the length of mitochondrial tubes (C):

(A) Confocal pictures were recorded in ten Z-stacks and analyzed with z-project [run("Z Project...", "projection=[Average Intensity]"); run("Split Channels");]. The MTC02 and mCherry-Parkin channels were made binary [selectWindow("Parkin.lsm"); run("Subtract Background...", "rolling=300 stack"); run("Auto Threshold", "method=MaxEntropy white"); selectWindow("MTC02.lsm"); run("Auto Threshold", "method=RenyiEntropy white");]. The number of mCherry-Parkin dots localized in the regions with MTC02 signals were analyzed with the plugin "Speckle Inspector" [2] [run("Speckle Inspector", "big=MTC02.tif small=Parkin.tif min\_object=3 min\_object\_circularity=0.3 min\_speckle\_size=3 max\_speckle\_size=50 exclude roi speckle");].

(B) Confocal pictures were recorded in ten and more Z-stacks and analyzed with z-project [run("Z Project...", "projection=[Average Intensity]"); run("Split Channels");]. Further on  $\alpha$ -Tubulin signal was reduced to a binary picture [run("Median...", "radius=4"); run("Subtract Background...", "rolling=200"); run("Auto Threshold", "method=Li dark");]. MTC02 signal was detected in regions of interest of the  $\alpha$ -Tubulin signal [run("Analyze Particles...", "size=50-Infinity add"); selectWindow(MTC02); roiManager("Measure");].

(C) Confocal pictures were recorded in ten and more Z-stacks and analyzed with z-project [run("Z Project...", "projection=[Average Intensity]"); run("Split Channels");]. The MTC02 channel was made binary [run("Subtract Background...", "rolling=300 stack"); run("Auto Threshold", "method=Default dark");]. The mitochondrial length was measured by "Particle Length (via Skeleton)" [2] [run("Analyze Particles...", "size=0,3-Infinity show=Outlines display");].

#### Measurement of BrdU incorporation

Primary human dermal fibroblasts were transfected with miR-15b-inhibitors with co-transfection of siRNA duplexes against SIRT4 or control siRNA duplexes.

Following two days, cells were incubated for another two days in culture media containing 10  $\mu$ M BrdU. Staining of fixed cells and further FACS analysis were performed as described in the BrdU staining kit (556029, BD Biosciences). DNA was stained for 10 min with 7-AAD (10  $\mu$ l/10<sup>6</sup> cells; 00-6993-50, eBioscience™).

#### Quantification of mitochondrial mass by MitoTracker® FACS

HEK293 cells were stained with the cell-permeable dye MitoTracker® Deep Red FM (100  $\mu$ M; Thermo Fisher Scientific) for 20 min followed by flow cytometry using a BD FACSCanto™ II system (BD Biosciences) and Flowing Software 2.5.1 (University of Turku, Finland) or FlowJo V10 (FlowJo, LLC).

#### Immunoprecipitation of OPA1 from stably transfected HEK293 cells

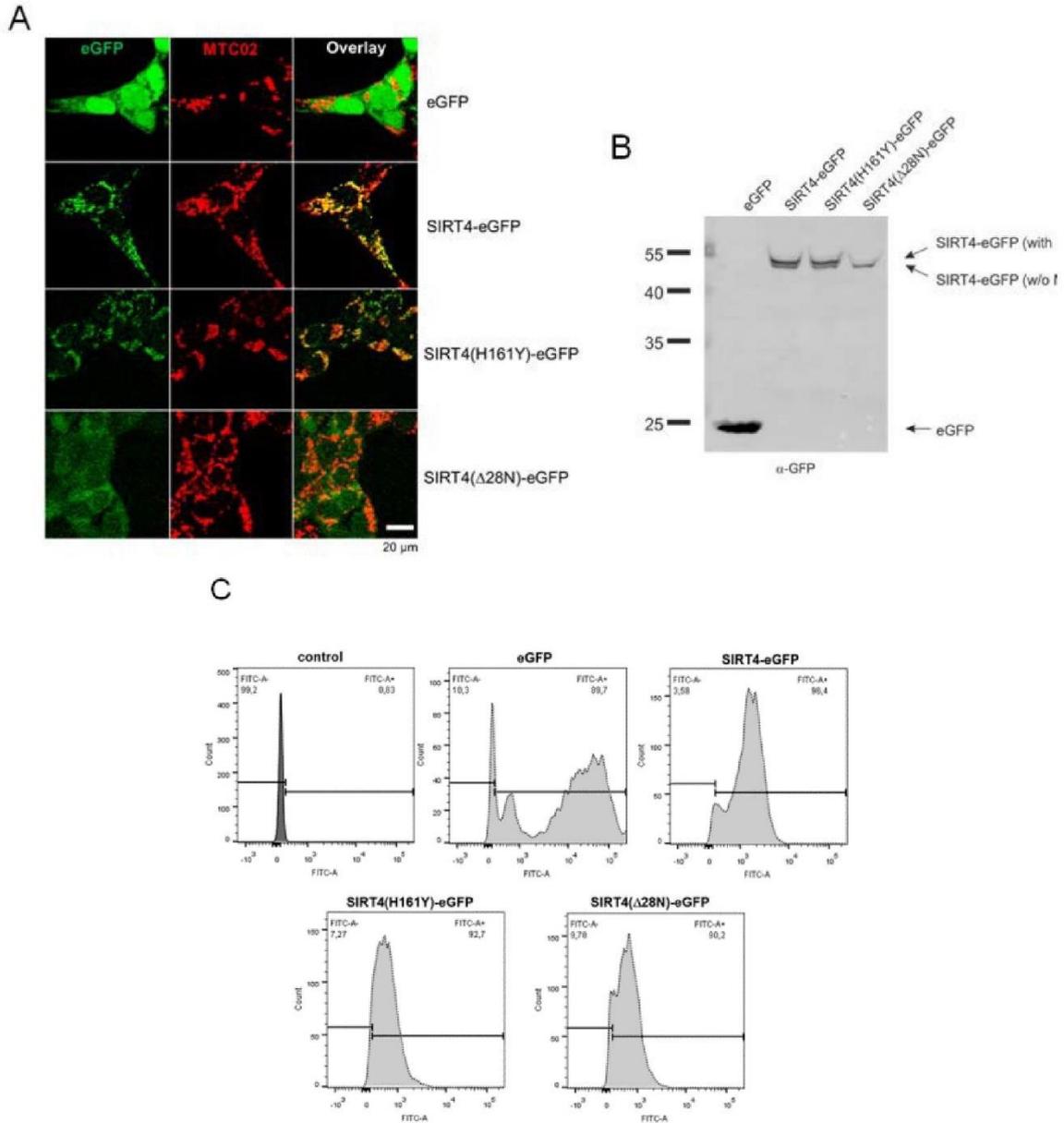
Total cell lysates from HEK293 cells stably expressing eGFP, SIRT4-eGFP, SIRT4(H161Y)-eGFP, or SIRT4( $\Delta$ 28N)-eGFP were prepared as described above. Two mg protein was incubated with 0.5  $\mu$ l rabbit anti-OPA1 antibody [3] in a total volume of 300  $\mu$ l lysis buffer [0.3% CHAPS, 50 mM Tris-HCl (pH 7.4), 150 mM NaCl, 1 mM Na<sub>3</sub>VO<sub>4</sub>, 10 mM NaF, 1 mM EDTA, 1 mM EGTA, 2.5 mM Na<sub>4</sub>O<sub>7</sub>P<sub>2</sub>, 1  $\mu$ M DTT, 1x cOmplete™ protease inhibitor cocktail (Roche)] overnight at 4°C. Protein A/G sepharose beads (Santa Cruz Biotechnology 10  $\mu$ l beads in 100  $\mu$ l lysis buffer) were added and followed by incubation for two hours at 4°C under rotation. The beads were washed four-times with 1 ml washing buffer (lysis buffer without cOmplete™ protease inhibitor cocktail) followed by incubation in Laemmli loading buffer at 95°C for 5 min. Samples and total cell lysates (5% of input) were subjected to SDS-PAGE (10% gels) and proteins were transferred to nitrocellulose membranes (Hybond C, GE Healthcare). Membranes were incubated overnight at 4°C with antibodies against GFP (11814460001, Roche Molecular Systems) and OPA1 (612607, BD Biosciences) diluted 1:1000 in TBS containing 0.05% Tween 20.

#### SUPPLEMENTARY REFERENCES

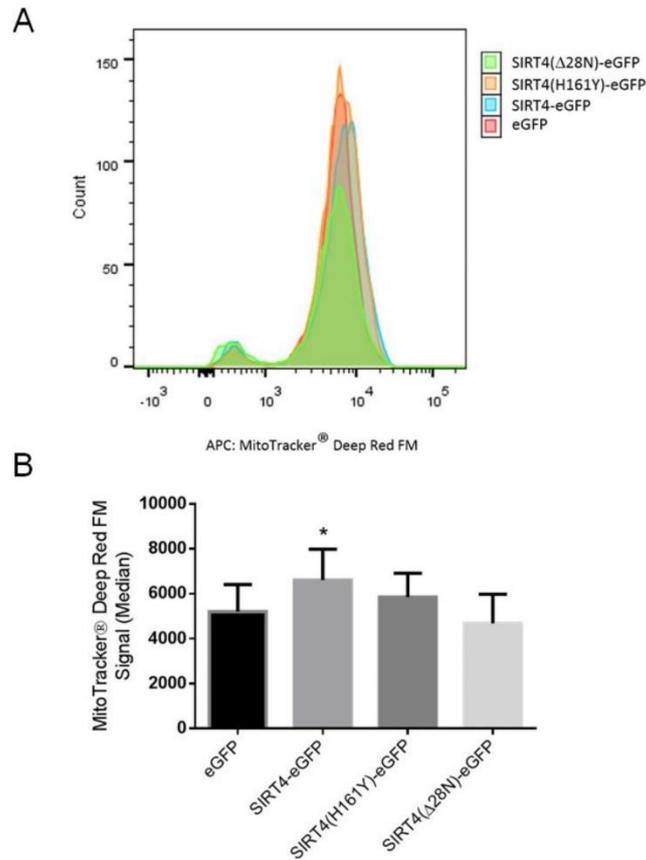
1. Lang A, Grether-Beck S, Singh M, Kuck F, Jakob S, Kefalas A, Altinluk-Hambuchen S, Graffmann N, Schneider M, Lindecke A, Brenden H, Felsner I, Ezzahoini H, et al. MicroRNA-15b regulates mitochondrial ROS production and the senescence-associated secretory phenotype through sirtuin 4/SIRT4. *Aging* (Albany NY). 2016; 8:534-559. <https://doi.org/10.18632/aging.100905>

2. Brocher J. The BioVoxel Image Processing and Analysis Toolbox. EuBIAS-Conference. 2015, Jan 5.
3. Barrera M, Koob S, Dikov D, Vogel F and Reichert AS. OPA1 functionally interacts with MIC60 but is dispensable for crista junction formation. FEBS Lett. 2016; 590(19):3309-3322.  
<https://doi.org/10.1002/1873-3468>

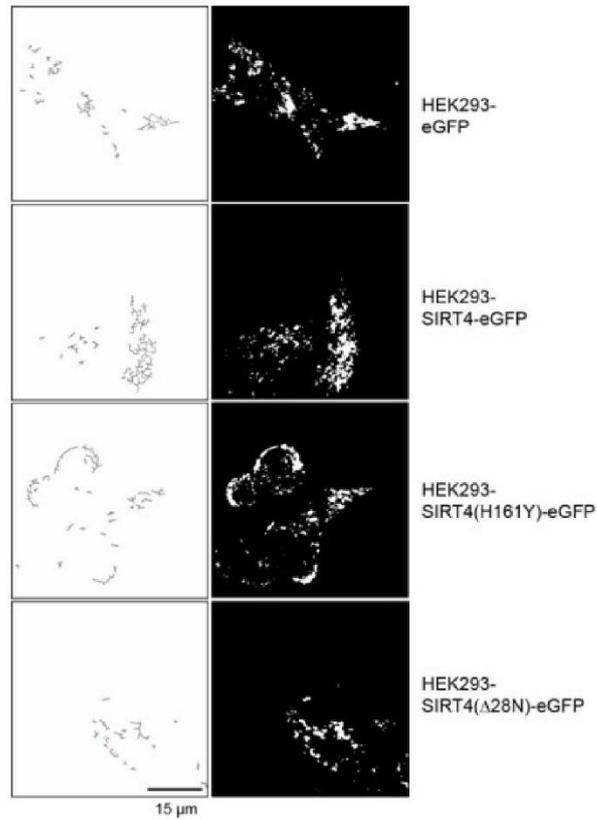
SUPPLEMENTARY FIGURES



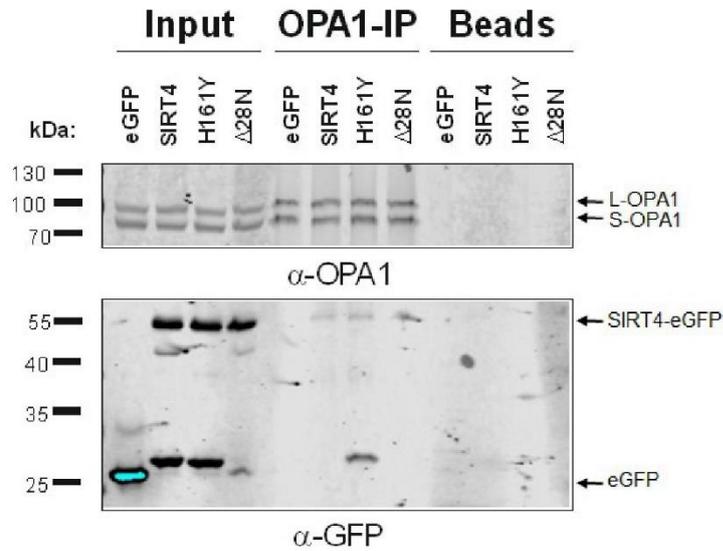
Supplementary Figure S1. Validation of subcellular localization and expression of eGFP, SIRT4-eGFP, SIRT4(H161Y)-eGFP, and SIRT4(Δ28N)-eGFP in HEK293 cells. HEK293 cells expressing eGFP, SIRT4-eGFP, SIRT4(H161Y)-eGFP, or SIRT4(Δ28N)-eGFP were subjected to confocal microscopic (A), immunoblot (B), and flow cytometric (C) analysis. MTS, mitochondrial translocation sequence. Representative experiments are depicted.



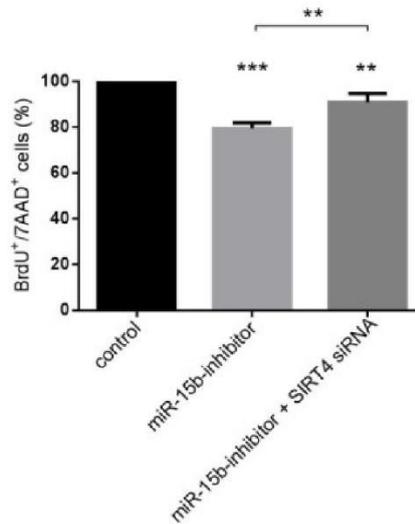
**Supplementary Figure S2. SIRT4-eGFP expression results in a higher mitochondrial mass in HEK293 cells.** (A) Representative flow cytometry profile of HEK293 cells expressing eGFP, SIRT4-eGFP, SIRT4(H161Y)-eGFP, or SIRT4(Δ28N)-eGFP stained with MitoTracker® Deep Red FM. (B) Quantitative analysis of MitoTracker® Deep Red FM signals. To evaluate statistical significance, two-way ANOVA followed-up Tukey's test was performed (\* $p < 0.05$ ;  $n = 3$  experiments).



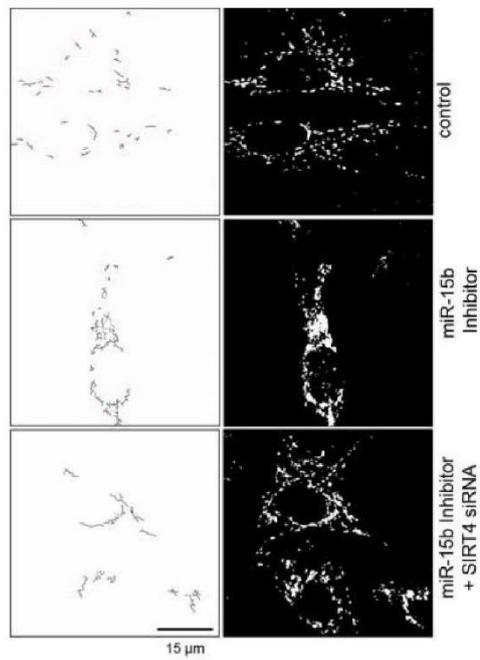
**Supplementary Figure S3. Visualization and analysis of the length of fused mitochondria in HEK293 cells stably expressing SIRT4-eGFP or its mutants.** Tracking of fused mitochondria which were detected by MTC02 staining (right panels) was analyzed by an ImageJ software based Macro (left panels; Material and Methods & suppl. Material and Methods).



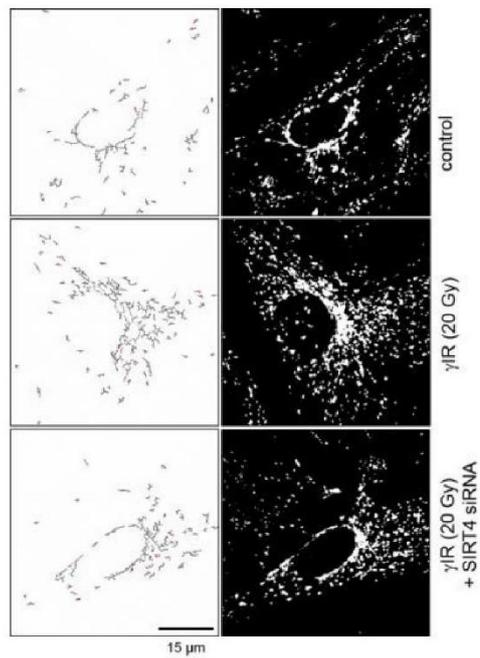
**Supplementary Figure S4. Co-immunoprecipitation of OPA1 and SIRT4-eGFP.** Total cell lysates from HEK293 cells stably expressing SIRT4-eGFP, SIRT4(H161Y)-eGFP, or SIRT4( $\Delta$ 28N)-eGFP were subjected to immunoprecipitation analysis (OPA1-IP) using a rabbit anti-OPA1 antibody (suppl. Material & Methods) followed by detection of co-immunoprecipitated SIRT4-eGFP. Total cell lysates were loaded as input control (5%) and samples w/o antibody employed as beads control.



**Supplementary Figure S5. SIRT4 upregulation upon transfection of miR-15b inhibitors inhibits BrdU incorporation in primary human dermal fibroblasts.** Primary human dermal fibroblasts were transfected with miR-15b inhibitors (or control oligonucleotides) in the presence or absence of siRNA duplexes against SIRT4 [35] and cultured for two days. Cells were thereafter pulsed with BrdU for another two days and thereafter subjected to FACS analysis. To evaluate statistical significance, two-way ANOVA followed by Tukey's test was performed (\* $p$ <0.05;  $n$ =3 experiments).



**Supplementary Figure S6. Visualization and analysis of the length of fused mitochondria in primary human dermal fibroblasts upon SIRT4 upregulation through miR-15b inhibition.** Tracking of fused mitochondria which were detected by MTC02 staining (right panels) was analyzed by an ImageJ software based Macro (left panels; Material and Methods & suppl. Material and Methods).



**Supplementary Figure S7. Visualization and analysis of the length of fused mitochondria in primary human dermal fibroblasts upon  $\gamma$ -irradiation.** Tracking of fused mitochondria which were detected by MTC02 staining (right panels) was analyzed by an ImageJ software based Macro (left panels; Material and Methods & suppl. Material and Methods).

## SUPPLEMENTARY MOVIES

Please browse the Full text version of this manuscript to see the Supplementary Movies 1-10.

**Suppl. Movie 1: 3D reconstruction of the mitochondrial network in HEK293-cGFP cells.** Mitochondria were detected by MTC02 staining and spinning disk confocal microscopic analysis.

**Suppl. Movie 2: 3D reconstruction of the mitochondrial network in HEK293-SIRT4-cGFP cells.** Mitochondria were detected by MTC02 staining and spinning disk confocal microscopic analysis.

**Suppl. Movie 3: 3D reconstruction of the mitochondrial network in HEK293-SIRT4(H161Y)-cGFP cells.** Mitochondria were detected by MTC02 staining and spinning disk confocal microscopic analysis.

**Suppl. Movie 4: 3D reconstruction of the mitochondrial network in HEK293-SIRT4( $\Delta$ 28N)-cGFP cells.** Mitochondria were detected by MTC02 staining and spinning disk confocal microscopic analysis.

**Suppl. Movie 5: 3D reconstruction of the mitochondrial network in primary human dermal fibroblasts.** Mitochondria were detected by MTC02 staining and spinning disk confocal microscopic analysis.

**Suppl. Movie 6: 3D reconstruction of the mitochondrial network in primary human dermal fibroblasts transfected with miR-15b inhibitors.** Mitochondria were detected by MTC02 staining and spinning disk confocal microscopic analysis.

**Suppl. Movie 7: 3D reconstruction of the mitochondrial network in primary human dermal fibroblasts transfected with miR-15b inhibitors and siRNA duplexes against SIRT4.** Mitochondria were detected by MTC02 staining and spinning disk confocal microscopic analysis.

**Suppl. Movie 8: 3D reconstruction of the mitochondrial network in primary human dermal fibroblasts (sham treated).** Mitochondria were detected by MTC02 staining and spinning disk confocal microscopic analysis.

**Suppl. Movie 9: 3D reconstruction of the mitochondrial network in primary human dermal fibroblasts subjected to  $\gamma$ -irradiation (20 Gy).** Mitochondria were detected by MTC02 staining and spinning disk confocal microscopic analysis.

**Suppl. Movie 10: 3D reconstruction of the mitochondrial network in primary human dermal fibroblasts subjected to transfection with siRNA duplexes against SIRT4 and  $\gamma$ -irradiation (20 Gy).** Mitochondria were detected by MTC02 staining and spinning disk confocal microscopic analysis.

## 6.2. Ammonia inhibits energy metabolism in astrocytes in a rapid and glutamate dehydrogenase 2-dependent manner

Drews L, Zimmermann M, Westhoff P, Brillhaus D, Poss RE, **Bergmann L**, Wiek C, Brenneisen P, Piekorz RP, Mettler-Altmann T, Weber APM, Reichert AS. Dis Model Mech. 2020 Nov 4;13(10):dmm047134. doi: 10.1242/dmm.047134. PMID: 32917661; PMCID: PMC7657470 [262].

Die Arbeit behandelt im ersten Schritt die mitochondriale Morphologie in Modellen der zellulären hepatischen Enzephalopathie (HE) unter erhöhtem Ammoniumgehalt, welche mittels konfokaler Fluoreszenzmikroskopie untersucht wurde. Bei der hepatischen Enzephalopathie ist die Astrozytendysfunktion ein primärer Faktor, der im Verlauf die neuronale Aktivität bei Hyperammonämie beeinträchtigt. Es konnte beobachtet werden, dass Ammonium-Ionen die mitochondriale Fragmentierung auf eine schnelle und reversible Weise in der menschlichen Astrozytom-Zelllinie MOG-G-CCM und primären Ratten-Astrozyten induziert. Dabei änderte sich die Morphologie der Mitochondrien schneller in den primären Ratten-Astrozyten als in den menschlichen Astrozytomzellen.

Um zu untersuchen, ob die beobachtete Veränderung der mitochondrialen Morphologie mit einer mitochondrialen Dysfunktion einhergeht, wurde die zelluläre Sauerstoffverbrauchsrate gemessen. Bei menschlichen Astrozyten war die freie Atmungskapazität sowie die maximale Atmung bereits nach einer Stunde  $\text{NH}_4\text{Cl}$ -Behandlung im Vergleich zu der Kontrolle signifikant reduziert. Zusätzlich wurden die mitochondriale Atmung und die Glykolyse pH-unabhängig behindert.

Da Ammonium-Ionen zu einer schnellen und drastischen Veränderung des Energiestoffwechsels führen, wurde mit einer gezielten Metabolomik-Analyse geprüft, ob Metabolite, wie Aminosäuren und Zwischenprodukte des Citratzyklus, durch Ammonium-Ionen verändert werden. Es wurde bereits nach 24 Stunden ein signifikanter Anstieg des Gehalts an Isozitrone Säure und/oder Zitronensäure und verzweigtkettigen Aminosäuren wie z.B. Isoleucin/Leucin/Valin beobachtet. Andere essenzielle Aminosäuren wie Methionin, Phenylalanin, Threonin und Tryptophan, sowie die nicht-essenziellen Aminosäuren Alanin, Aspartat, Cystein, Prolin, Serin und

Tyrosin waren nach 24 Stunden bzw. erst nach 48 Stunden erhöht, während Glycin schon nach 4 Stunden Behandlung einen signifikanten Anstieg zeigte.

Dieses Muster deutet darauf hin, dass die mitochondriale Glutamat-Dehydrogenase 2 (GDH2, kodiert durch das *GLUD2*-Gen), welche die reduktive Aminierung von  $\alpha$ -Ketoglutarat und  $\text{NH}_4\text{Cl}$  zu Glutamat katalysiert, an der anfänglichen Fixierung von  $\text{NH}_4\text{Cl}$  in den Mitochondrien beteiligt sein könnte. Um diese Hypothese zu testen, wurde GDH2 in menschlichen Astrozytomzellen mittels siRNA herunterreguliert und die mitochondriale Atmung nach einer einstündigen  $\text{NH}_4\text{Cl}$ -Behandlung gemessen. Dabei konnte gezeigt werden, dass die  $\text{NH}_4\text{Cl}$ -induzierte Beeinträchtigung der mitochondrialen Atmung GDH2-abhängig ist.

Die Hemmung der GDH-abhängigen reduktiven Aminierung von  $\alpha$ -Ketoglutarat durch Supplementation mit Glutamat, Glutamin oder durch die Erhöhung der SIRT4-Mengen mittels Überexpression, welches die GDH hemmt, verbessert die mitochondriale Atmung bei Hyperammonämie. Schematische Zusammenfassung in Abbildung 8. Die Sauerstoffverbrauchsrate in HeLa- sowie menschlichen Astrozytom-Zellen wurde mit oder ohne Behandlung mit 5 mM  $\text{NH}_4\text{Cl}$  für eine Stunde gemessen. Die freie Atmungskapazität von unbehandelten HeLa-SIRT4-eGFP und HeLa-eGFP Zellen wurde nicht beeinträchtigt, während die Atmung nach der  $\text{NH}_4\text{Cl}$ -Behandlung bei HeLa-eGFP-Zellen signifikant abnahm. Dies war nicht der Fall bei Zellen, die SIRT4-eGFP überexprimierten. Aus mechanistischer Sicht wird vermutet, dass GDH2 für die Ammonium-Ionen induzierte Erschöpfung von  $\alpha$ -Ketoglutarat durch reduktive Aminierung zu Glutamat erforderlich ist, was gleichzeitig zur Hemmung des Citratzyklus führt.

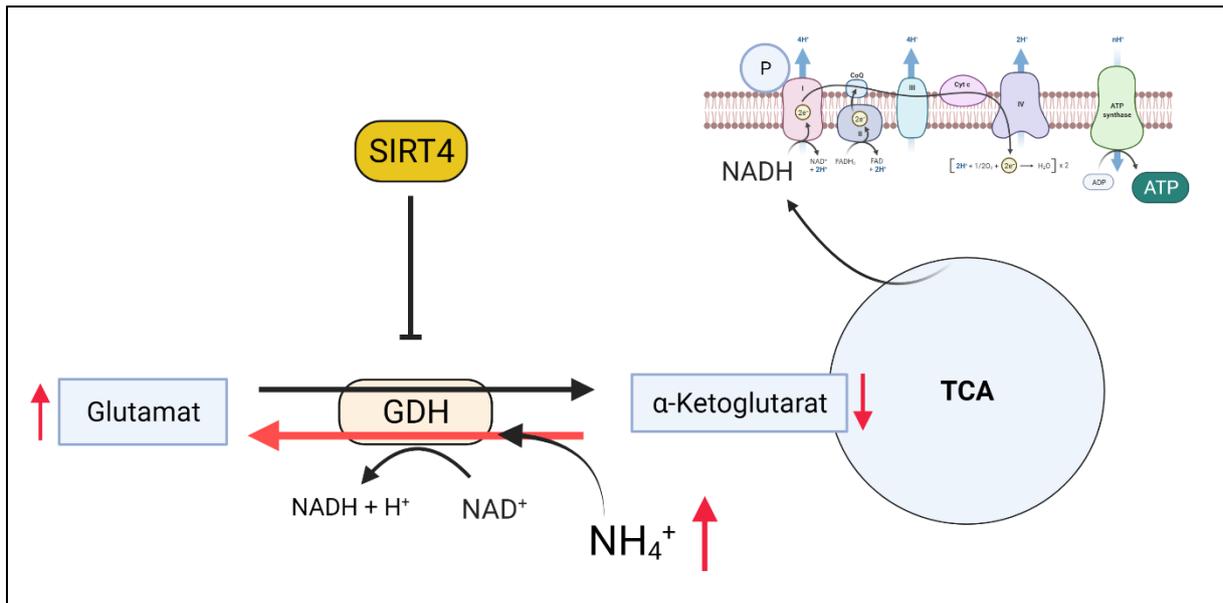


**Abbildung 8:** Darstellung des vorgeschlagenen Mechanismus der Rolle der Glutamat-Dehydrogenase (GDH) bei Ammoniak-induzierter Toxizität. Dabei wird eine Ammonium-Ionen induzierte Erschöpfung von  $\alpha$ -Ketoglutarat durch reduktive Aminierung zu Glutamat mittels GDH vorgeschlagen, was gleichzeitig zur Hemmung des Citratzyklus führt. SIRT4 nimmt in seiner natürlichen Funktion als GDH-Inhibitor einen regulatorischen Aspekt ein. Erstellt mit BioRender.com

Insgesamt werden in dieser Arbeit mehrere Anhaltspunkte dafür geliefert, dass hohe Mengen an  $\text{NH}_4\text{Cl}$  zu einer raschen, metabolischen Reprogrammierung von Astrozyten führen, insbesondere durch eine GDH-abhängige Beeinträchtigung des Citratzyklus. Dabei ist ein mitochondrienabhängiger Mechanismus zu vermuten, der zu den frühen Schritten in der Pathogenese von HE beiträgt, in dem das Zusammenspiel zwischen Energiestoffwechsel und  $\text{NH}_4\text{Cl}$ -Reduktion eine zentrale Rolle spielt.

Die Autorin der vorliegenden Dissertation erarbeitete ca. 10% der Befunde dieser Publikation. Der Beitrag bestand in der Generierung, Heranzucht und basalen Charakterisierung der stabil SIRT4-eGFP und eGFP überexprimierenden HeLa-Zelllinien. Des Weiteren wurde die Überexpression und mitochondriale Lokalisation von SIR4-eGFP mittels konfokaler Laserscanning-Mikroskopie analysiert.

## RESEARCH ARTICLE

# Ammonia inhibits energy metabolism in astrocytes in a rapid and glutamate dehydrogenase 2-dependent manner

Leonie Drews<sup>1</sup>, Marcel Zimmermann<sup>1</sup>, Philipp Westhoff<sup>2,3</sup>, Dominik Brilhaus<sup>2,3</sup>, Rebecca E. Poss<sup>1</sup>, Laura Bergmann<sup>4</sup>, Constanze Wiek<sup>5</sup>, Peter Brenneisen<sup>1</sup>, Roland P. Piekorz<sup>4</sup>, Tabea Mettler-Altman<sup>2,3</sup>, Andreas P. M. Weber<sup>2,3</sup> and Andreas S. Reichert<sup>1,\*</sup>

**ABSTRACT**

Astrocyte dysfunction is a primary factor in hepatic encephalopathy (HE) impairing neuronal activity under hyperammonemia. In particular, the early events causing ammonia-induced toxicity to astrocytes are not well understood. Using established cellular HE models, we show that mitochondria rapidly undergo fragmentation in a reversible manner upon hyperammonemia. Further, in our analyses, within a timescale of minutes, mitochondrial respiration and glycolysis were hampered, which occurred in a pH-independent manner. Using metabolomics, an accumulation of glucose and numerous amino acids, including branched chain amino acids, was observed. Metabolomic tracking of <sup>15</sup>N-labeled ammonia showed rapid incorporation of <sup>15</sup>N into glutamate and glutamate-derived amino acids. Downregulating human *GLUD2* [encoding mitochondrial glutamate dehydrogenase 2 (GDH2)], inhibiting GDH2 activity by SIRT4 overexpression, and supplementing cells with glutamate or glutamine alleviated ammonia-induced inhibition of mitochondrial respiration. Metabolomic tracking of <sup>13</sup>C-glutamine showed that hyperammonemia can inhibit anaplerosis of tricarboxylic acid (TCA) cycle intermediates. Contrary to its classical anaplerotic role, we show that, under hyperammonemia, GDH2 catalyzes the removal of ammonia by reductive amination of  $\alpha$ -ketoglutarate, which efficiently and rapidly inhibits the TCA cycle. Overall, we propose a critical GDH2-dependent mechanism in HE models that helps to remove ammonia, but also impairs energy metabolism in mitochondria rapidly.

**KEY WORDS:** Hepatic encephalopathy, Hyperammonemia, Mitochondria, TCA cycle, Glutamate dehydrogenase, Brain energy metabolism

**INTRODUCTION**

Hepatic encephalopathy (HE) is a severe neuropsychiatric disorder caused by hyperammonemia due to acute or chronic liver dysfunction, most commonly liver cirrhosis. Another major cause of HE is portosystemic shunting, leading to the distribution of portal blood without removal of toxins in the liver (Cash et al., 2010). It is estimated that 50–70% of all patients suffering from liver cirrhosis develop minimal HE or HE (Patidar and Bajaj, 2015). Given that more than 600,000 people are estimated to suffer from liver cirrhosis in the USA (Scaglione et al., 2015), this corresponds to ~300,000 to 420,000 people with HE in the USA alone. The symptoms can vary from mild to severe, ranging from confusion to hepatic coma and death (Ferenci et al., 2002). So far, the only curative treatment is liver transplantation (Larsen et al., 1995). Treatment options to reduce symptoms are manifold, but insufficient, and have often not been subject to randomized control studies (Ferenci, 2017). A major precipitation factor in HE is hyperammonemia resulting from the impaired ability of the liver to eliminate ammonia via the urea cycle (Ferenci, 2017). Ammonia passes the blood-brain barrier (Lockwood et al., 1979, 1980), causing swelling and production of reactive oxygen species (ROS)/reactive nitrogen species in astrocytes (Görg et al., 2013; Norenberg et al., 2005). Increased ROS levels lead to mitochondrial dysfunction, energy failure, formation of the mitochondrial transition pore (Bai et al., 2001; Stewart et al., 2000; Frank et al., 2012) or RNA oxidation (Görg et al., 2008). Several studies demonstrated that hyperammonemia primarily disturbs astrocyte function, resulting in subsequent neurological dysfunction (Görg et al., 2018; Norenberg, 1987). Astrocytes have an essential role in ensuring neuronal function, such as by providing nutrients, recycling the neurotransmitter glutamate (Sontheimer, 1995; Zalc, 1994) and detoxifying ammonia in the brain, which is thought to occur primarily via ammonia fixation by glutamine synthetase (Martinez-Hernandez et al., 1977). However, the molecular mechanism of ammonia-induced neurological impairment and the role of known ammonia detoxification pathways are unclear.

An increase in mitochondrial fission was reported to occur in mice with severe liver damage in the substantia nigra, but not in the prefrontal cortex (Bai et al., 2018). In various HE rat models, it was shown that the activity of respiratory chain complexes was decreased in different brain regions (Boer et al., 2009; Dhanda et al., 2017). Additionally, an impact on the TCA cycle under hyperammonemia has been discussed, given that some TCA cycle enzymes, e.g. pyruvate dehydrogenase and isocitrate dehydrogenase, were reported to be inhibited by ammonia (Katunuma et al., 1966; Zwingmann et al., 2003). The role of the TCA cycle in the pathogenesis of HE is controversially discussed (reviewed in Rama Rao and Norenberg, 2012). Additionally, a recent analysis of the metabolome of cerebrospinal fluid (CSF) of HE patients points towards alterations

<sup>1</sup>Institute for Biochemistry and Molecular Biology I, Medical Faculty, Heinrich Heine University Düsseldorf, Universitätsstr. 1, 40225 Düsseldorf, Germany. <sup>2</sup>Institute of Plant Biochemistry, Cluster of Excellence on Plant Sciences (CEPLAS), Heinrich Heine University Düsseldorf, Universitätsstr. 1, 40225 Düsseldorf, Germany. <sup>3</sup>Plant Metabolism and Metabolomics Laboratory, Cluster of Excellence on Plant Sciences (CEPLAS), Heinrich Heine University Düsseldorf, Universitätsstr. 1, 40225 Düsseldorf, Germany. <sup>4</sup>Institute for Biochemistry and Molecular Biology II, Medical Faculty, Heinrich Heine University Düsseldorf, Universitätsstr. 1, 40225 Düsseldorf, Germany. <sup>5</sup>Department of Otorhinolaryngology and Head/Neck Surgery (ENT), Medical Faculty, Heinrich Heine University Düsseldorf, Moorenstr. 5, 40225 Düsseldorf, Germany.

\*Author for correspondence (reichert@hhu.de)

© D.B., 0000-0001-9021-3197; P.B., 0000-0003-3405-0287; A.S.R., 0000-0001-9340-3113

This is an Open Access article distributed under the terms of the Creative Commons Attribution License (<https://creativecommons.org/licenses/by/4.0>), which permits unrestricted use, distribution and reproduction in any medium provided that the original work is properly attributed.

Handling Editor: Monica J. Justice  
Received 17 August 2020; Accepted 2 September 2020

in metabolic pathways linked to energy metabolism (Weiss et al., 2016). Overall, disturbances in mitochondrial morphology and imbalances in various energy metabolism pathways have been suggested as a consequence of hyperammonemia; however, their possible contributions to the pathogenesis of HE are still unclear. In most HE models, prolonged treatments with ammonia (such as 24 h and beyond) have been used and are quite well studied (Görg et al., 2015; Hazell and Norenberg, 1998; Oenarto et al., 2016). However, the early events upon exposure to high ammonia concentrations are unclear. Here, we focused on effects after short durations of ammonia treatment and immediate outcomes thereof.

The mitochondrial network constantly undergoes fission and fusion events, which are important to maintain mitochondrial quality control (Nunnari et al., 1997; Schäfer and Reichert, 2009). It was shown that different stress conditions, such as heat shock or increased ROS, can trigger fission of mitochondria, leading to a fragmented mitochondrial morphology (Frank et al., 2012; Duvezin-Caubet et al., 2006). Polletta et al. (2015) have shown the appearance of small, round mitochondria in MDA-MB-231 human breast cancer and C2C12 mouse myoblast cells after treatment with  $\text{NH}_4\text{Cl}$ , among other stressors. Overall, it is not well understood whether and how altered mitochondrial function and energy metabolism could contribute to the pathogenesis of HE. Here, we decided to address the early effect of hyperammonemia on mitochondrial function and energy metabolism using cellular models of HE. We show that ammonia impairs mitochondrial oxidative phosphorylation (OXPHOS) very rapidly and provide several lines of evidence that ammonia is primarily fixed by reductive amination of  $\alpha$ -ketoglutarate to generate glutamate, catalyzed by the mitochondrial glutamate dehydrogenase 2 (GDH2). This provides a novel view on the early steps of ammonia-induced toxicity and will likely help to better understand the pathogenesis of HE in future studies.

## RESULTS

### Ammonia induces mitochondrial fragmentation in a rapid and reversible manner

In order to test whether modulation of mitochondrial morphology by ammonia represents an early event in ammonia-induced effects in astrocytes, we transfected the human astrocytoma cell line MOG-G-CCM with pEGFP-Mito, a GFP variant targeting the mitochondrial matrix (Weber et al., 2013). Cells were treated with 5 mM  $\text{NH}_4\text{Cl}$  for 1–72 h and changes in mitochondrial morphology were quantified using confocal fluorescence microscopy. Similar conditions are used in numerous established *in vitro* HE models (Görg et al., 2015; Warskulat et al., 2002), and a similar ammonia concentration (5.4 mM) was present in the brain of an *in vivo* rat model (Swain et al., 1992). The appearance of cells showing enhanced mild (intermediate) or severe (highly fragmented) mitochondrial fragmentation (Fig. 1A) was evident after 6 h of treatment, compared to controls or to earlier time points (Fig. 1B,C). Mitochondrial fragmentation became more prominent after 24 h, reaching a high steady-state level. Treatment with  $\text{NH}_4\text{Cl}$  for 48 h and 72 h did not further increase mitochondrial fragmentation (Fig. 1C). To corroborate this in primary cells, we used an established *in vitro* HE model, namely primary rat astrocytes treated with 5 mM  $\text{NH}_4\text{Cl}$ . In these astrocytes, mitochondrial morphology [visualized by immunostaining against Tom20 (also known as Tomm20)] was rapidly altered by  $\text{NH}_4\text{Cl}$  (Fig. 1B). The change towards mitochondrial fragmentation was even more rapid as it already became evident after 1 h of ammonia treatment (Fig. 1D). Hence, mitochondrial morphology is altered very rapidly by hyperammonemia and primary rat astrocytes appear to react even

faster than human astrocytoma cells. Next, we asked whether mitochondrial fragmentation is reversible upon removal of ammonia. Indeed, we observed in primary rat astrocytes that mitochondrial morphology, which was highly fragmented after 72 h treatment with  $\text{NH}_4\text{Cl}$ , recovered within 24 h to a highly tubular morphology when the medium was exchanged to fresh medium lacking  $\text{NH}_4\text{Cl}$  (Fig. S2). We conclude that mitochondrial fragmentation is rapidly induced by hyperammonemia within 1–6 h and is nearly fully reversible within 24 h after the removal of ammonia.

### Ammonia causes an immediate inhibition of mitochondrial respiration in a pH-independent manner

Mitochondrial fragmentation is one of the early hallmarks indicating mitochondrial dysfunction (Frank et al., 2012; Duvezin-Caubet et al., 2006; Jheng et al., 2012). To investigate whether the change in mitochondrial morphology comes hand in hand with mitochondrial dysfunction, we determined the cellular oxygen consumption rate (OCR) in human astrocytoma cells and in primary rat astrocytes after treatment with 5 mM  $\text{NH}_4\text{Cl}$  for variable time periods. We applied a Mito Stress Test Kit using a Seahorse XFe96 Extracellular Flux Analyzer to determine different parameters of mitochondrial respiration, including spare respiratory capacity and maximal respiration (see Fig. 2A and the ‘Cellular metabolism analysis’ section of the Materials and Methods). These two parameters represent the mitochondrial respiration in a challenged state by uncoupling using carbonyl-cyanide-4-(trifluoromethoxy)-phenylhydrazone (FCCP). In human astrocytoma cells, the spare respiratory capacity (Fig. 2B) and the maximal respiration (Fig. S1A) were significantly reduced after 1 h of ammonia treatment compared to non-treated controls. There was a trend showing a similar effect for basal respiration but this was not statistically significant (Fig. S1E). Prolonged ammonia pretreatments up to 48 h likewise resulted in significant impairment of mitochondrial respiration. It appeared that respiration is more affected with short times of ammonia pretreatment compared to longer times (Fig. 2B; Fig. S1A). To elaborate this further and to check how fast ammonia can affect mitochondrial respiration, we measured the OCR immediately after  $\text{NH}_4\text{Cl}$  was added. Indeed, this was sufficient to impair mitochondrial respiration as spare respiratory capacity (Fig. 2C) and maximal respiration (Fig. S1B) in primary rat astrocytes were significantly reduced. This reduction without pretreatment (0 h) was even stronger when compared to 1 h, 4 h or 6 h ammonia pretreatment, demonstrating that ammonia has an immediate strong effect on mitochondrial respiration, which moderately decreases with incubation time. We next tested whether this effect is dose dependent. This is indeed the case as concentrations as low as 1 mM  $\text{NH}_4\text{Cl}$  were sufficient to induce a substantial drop in respiration, which increased with higher concentrations (Fig. 2D; Fig. S1C). Ammonia is a potent base, causing alkalization of extra- and intracellular compartments even under buffering conditions. To analyze whether the observed effect is simply a pH-mediated effect, we repeated the assay using 5 mM  $\text{CH}_3\text{NH}_3\text{Cl}$ , which cannot be metabolized but acts as a pH mimetic to  $\text{NH}_4\text{Cl}$ . This did not impair mitochondrial respiration to any significant extent, independent of the duration of pretreatment, except for maximal respiration after 48 h (Fig. 2E; Fig. S1D). This excludes that the observed effect of ammonia results from changes in the pH. We also did not observe any gross changes in the steady-state levels of marker proteins required for OXPHOS that could explain the observed effects (Fig. S9C,D). Moreover, we tested whether removal of ammonia for 1 h is sufficient to restore mitochondrial respiration in human astrocytoma cells that have been pretreated for 1–48 h. One hour in medium without ammonia led to a full recovery of mitochondrial respiration independent of the duration of pretreatment

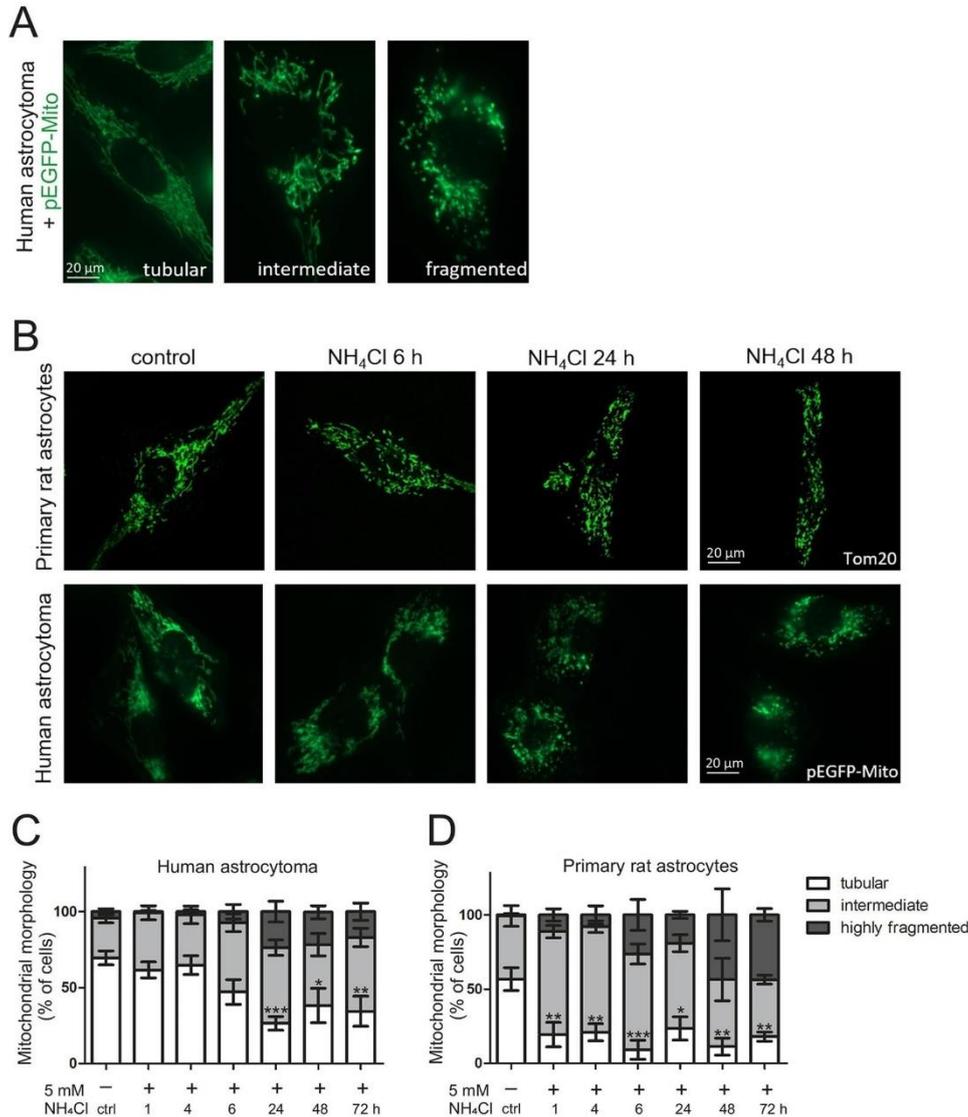


**Fig. 1. Mitochondrial morphology is altered by ammonia.** Human astrocytoma cells were transfected with pEGFP-Mito to visualize mitochondria. In primary rat astrocytes, visualization was achieved by immunostaining against Tom20. Cells were treated with 5 mM NH<sub>4</sub>Cl for respective durations. At least 20 pictures were taken per sample, showing approximately three to five cells each. Mitochondria were categorized as tubular, intermediate and fragmented morphological phenotype. (A) Representative images of morphological phenotype characterization in human astrocytoma cells. (B) Changes in morphology of mitochondria after treatment with 5 mM NH<sub>4</sub>Cl in primary rat astrocytes (top row) and human astrocytoma (bottom row). (C,D) Time course of changes in mitochondrial morphology in human astrocytoma ( $n=3-6$ ) (C) and primary rat astrocytes ( $n=3$ ) (D). Data are presented as mean±s.e.m. Statistics: one-way ANOVA with Dunnett's post test (all treatments versus control) for tubular morphology. \* $P<0.05$ , \*\* $P<0.01$ , \*\*\* $P<0.001$ .

(Fig. S3). This is consistent with our data showing that mitochondrial fragmentation is restored after removal of ammonia from the medium.

#### Ammonia impairs glycolysis in astrocytes in a rapid manner

We examined the influence of ammonia on glycolytic flux and glycolytic capacity using a Glycolysis Stress Test with the Seahorse XFe96 Analyzer. Here, the extracellular acidification rate (ECAR) is measured under different conditions and used to estimate glycolysis (see Fig. 3A and the 'Cellular metabolism analysis' section of the Materials and Methods). Treatment of human astrocytoma cells with

ammonia led to a significant and rapid reduction in both glycolytic flux (Fig. 3B) and glycolytic capacity (Fig. 3C) compared to controls. This was largely independent of the duration of ammonia pretreatment. Treatment with the pH mimetic CH<sub>3</sub>NH<sub>3</sub>Cl did not have any detrimental effect on glycolysis, further corroborating the specific role of ammonia, independent of its property to alter pH. Overall, we conclude that ammonia results in a very rapid, pH-independent impairment of two major bioenergetic metabolic pathways, namely OXPHOS and glycolysis. The observation that both pathways are inhibited by ammonia could be explained by an impairment at the level

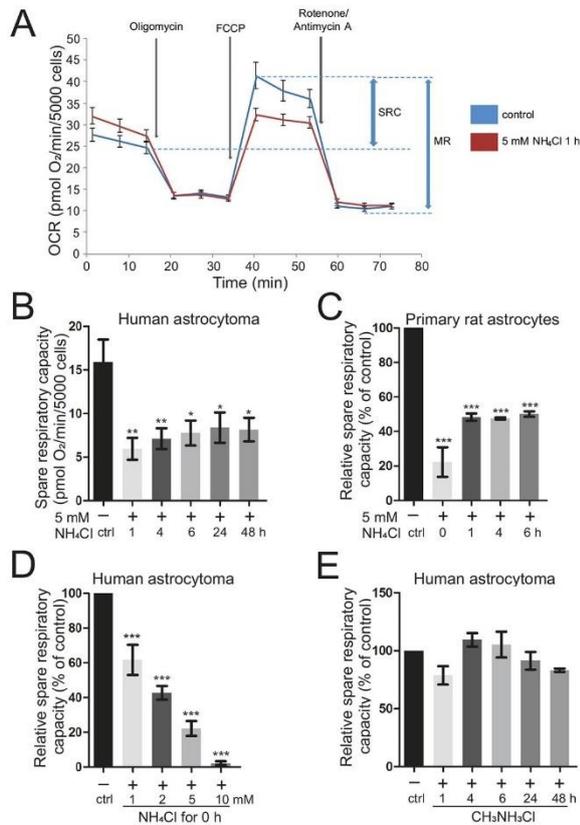


**Fig. 2. Mitochondrial respiration is immediately impaired by ammonia in a pH-independent manner.** Oxygen consumption rate (OCR) of human astrocytoma cells and primary rat astrocytes was analyzed in a Seahorse XFe96 Extracellular Flux Analyzer with a Mito Stress Test Kit after treatment with ammonia at the indicated molarity for the indicated duration. (A) Scheme of Seahorse Mito Stress Test with injections. MR, maximal respiration; SRC, spare respiratory capacity. (B) SRC of human astrocytoma cells after 5 mM NH<sub>4</sub>Cl treatment for 1–48 h ( $n=5-7$ ). (C) Relative SRC of primary rat astrocytes after 5 mM NH<sub>4</sub>Cl treatment for 1–6 h and live (0 h) ( $n=3-4$ ). (D) Relative SRC of human astrocytoma cells after live treatment with 1, 2, 5 and 10 mM NH<sub>4</sub>Cl ( $n=3$ ). (E) Relative SRC of human astrocytoma cells after 5 mM CH<sub>3</sub>NH<sub>3</sub>Cl (pH-mimetic) treatment for 1–48 h ( $n=3$ ). Individual biological replicates normalized to control (100%) (C–E). Data are presented as mean  $\pm$  s.e.m. Statistics: one-way ANOVA with Dunnett's post test (all treatments versus control). \* $P<0.05$ , \*\* $P<0.01$ , \*\*\* $P<0.001$ .

of the TCA cycle. The latter would not only impair formation of NADH/FADH<sub>2</sub> used during OXPHOS but also lead to an accumulation of acetyl-CoA and pyruvate. Without a rapid metabolic shift to convert pyruvate to lactate by lactate dehydrogenase, this would inhibit the glycolytic flux via product inhibition. In addition, NAD<sup>+</sup> is neither regenerated by the latter reaction nor the TCA cycle in sufficient amounts, also explaining reduced glycolysis. Nonetheless, the possibility exists that glycolysis is directly inhibited by ammonia, which we cannot exclude at this stage.

#### Targeted metabolomics analysis suggests alteration of the TCA cycle

Ammonia leads to a rapid and drastic change in energy metabolism. To check whether metabolites linked to energy metabolism,

including amino acids and TCA cycle intermediates, are altered by ammonia, we treated human astrocytoma cells with 5 mM NH<sub>4</sub>Cl for 1–48 h and subjected them to a targeted metabolomics analysis (Fig. 4A,B; Fig. S4, Tables S1 and S2). We observed a significant increase in the level of isocitric and/or citric acid, which are indistinguishable by the gas chromatography–mass spectrometry (GC-MS) system used here, after 48 h of ammonia treatment (Fig. S4). Moreover, the branched-chain amino acids (BCAAs) isoleucine/leucine/valine were significantly increased after 24 h. Other essential amino acids – methionine, phenylalanine, threonine and tryptophan – were increased after 24 h and/or 48 h, respectively. The non-essential amino acids – alanine, aspartate, cysteine, proline, serine and tyrosine – were increased after 24 h and/or 48 h, whereas glycine showed a significant increase only after 4 h of treatment. We noted a slight improvement in mitochondrial respiration coinciding with the increase in numerous amino acids at late time points (Fig. 2B; Fig. S1A), which could point to a delayed role of these amino acids in a compensatory response. To test the fate of ammonia further, we traced the incorporation of NH<sub>4</sub><sup>+</sup> in human astrocytoma cells using isotopically labeled <sup>15</sup>NH<sub>4</sub>Cl under the same conditions as before. Using liquid chromatography–mass spectrometry (LC-MS) analysis we found the strongest enrichment of <sup>15</sup>N-isotopologues for glutamate, followed by aspartate, proline and BCAAs (Fig. 5A–E; Fig. S5, Tables S3 and S4). Of note, a strong enrichment occurred after 1 h, emphasizing a rapid effect of hyperammonemia. Interestingly, the synthesis of glutamate and its downstream metabolites aspartate and proline, as well as the BCAAs, are catalyzed by the enzyme glutamate dehydrogenase (GDH), or downstream reactions, e.g. transaminase reactions, to form BCAAs (Fig. 5F). Overall, these results indicate that mitochondrial glutamate dehydrogenase 2 (GDH2, encoded by *GLUD2*), which catalyzes the reductive amination of  $\alpha$ -ketoglutarate and ammonia to glutamate, could be involved in the initial fixation of ammonia in mitochondria.

#### Ammonia-induced impairment of mitochondrial respiration depends on GDH2

To test this hypothesis, GDH2 was downregulated in human astrocytoma cells by targeting *GLUD2* gene expression using small interfering RNA (siRNA). Knockdowns were validated via western blotting (Fig. 6A; Fig. S6A), quantitative PCR (Fig. S6B) and determination of specific GDH activity (Fig. S10B). Cells depleted for GDH2 and corresponding controls were subjected to analysis of OCR using the Mito Stress Test. Depletion of GDH2 prevented the reduction of mitochondrial respiration upon treatment for 1 h with ammonia (Fig. 6B), suggesting that GDH2 is specifically required for the observed rapid ammonia-induced impairment of mitochondrial respiration. To investigate this further, GDH2 was overexpressed and subjected to OCR measurements. Overexpression of GDH2 was confirmed via western blotting (Fig. 6A; Fig. S6C) and determination of specific GDH activity (Fig. S10C). An additional band of higher molecular weight (Fig. 6A) can be attributed to a fraction of non-imported GDH2 precursor protein due to the overexpression. Treatment of GDH2-overexpressing cells with 5 mM NH<sub>4</sub>Cl for 1 h exacerbated the decrease in mitochondrial respiration observed before (Fig. 6C). To corroborate this, and to exclude off-target effects of the *GLUD2* siRNA used earlier, we also overexpressed GDH2 in the presence of the *GLUD2* siRNA. It should be noted that the sequence of *GLUD2* encoded on the plasmid is resistant to the used siRNA. Indeed, overexpression of GDH2 from a plasmid restored the sensitivity of human astrocytoma cells

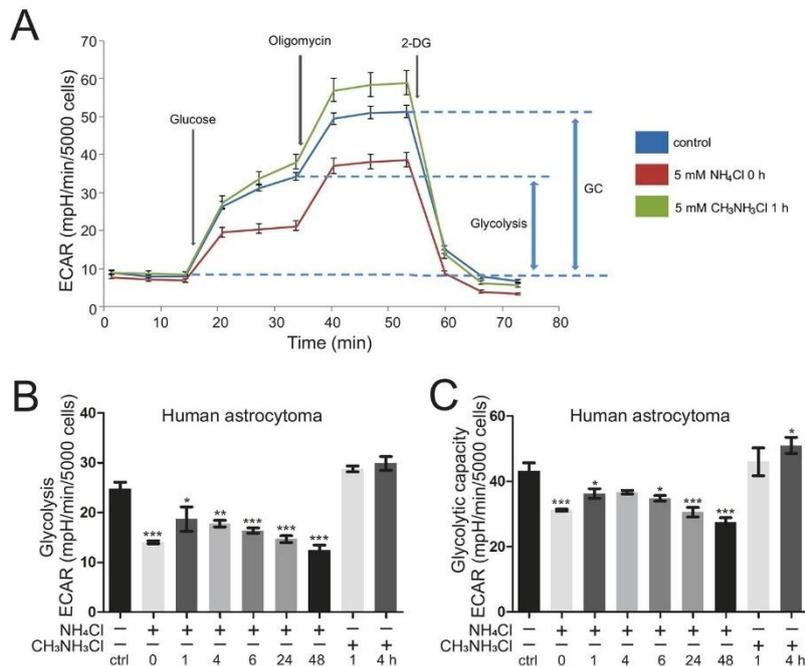


**Fig. 3. Ammonia impairs glycolytic function.**

Extracellular acidification rate (ECAR) was measured in human astrocytoma cells as a proxy for glycolysis using a Glycolysis Stress Test Kit and Seahorse XFe96 Extracellular Flux Analyzer. (A) Scheme of the Seahorse Glycolysis Stress Test with respective injections indicated. GC, glycolytic capacity; 2-DG, 2-deoxyglucose. (B,C) Glycolysis (B) and glycolytic capacity (C) of human astrocytoma cells after treatment with 5 mM NH<sub>4</sub>Cl for 1–48 h and live (0 h) ( $n=3$ ); treatment with 5 mM pH-mimetic CH<sub>3</sub>NH<sub>3</sub>Cl for 1 h and 4 h ( $n=2$ ). Data are presented as mean  $\pm$  s.e.m. Statistics: one-way ANOVA with Dunnett's post test (all treatments versus control). \* $P<0.05$ , \*\* $P<0.01$ , \*\*\* $P<0.001$ .

depleted for endogenous GDH2 to ammonia, excluding off-target effects of the *GLUD2* siRNA, and further supported that GDH2 is specifically required for ammonia to impair mitochondrial respiration (Fig. 6D). Moreover, in accordance with the GDH2 knockdown results presented earlier (Fig. 6B), the transfection with *GLUD2* siRNA in the presence of empty vector (ev) again prevented NH<sub>4</sub>Cl-induced impairment of respiration (Fig. 6D), thus confirming our knockdown results. Intrigued by these results, pointing to a critical role of GDH2, and by the metabolomics data showing a long-term increase in numerous amino acids, we reasoned that, in particular, glutamate levels might be altered in a rapid manner by ammonia. Astrocytoma cells indeed showed a gross increase in glutamate levels immediately after exposure to ammonia (Fig. 6G). This was not due to altered protein levels of GDH2 or its regulator SIRT4 (Fig. S9A,B), nor due to altered specific GDH activity induced by the addition of ammonia (Fig. S10A). Taken together, these results provide strong evidence that GDH2 is a critical factor in the rapid impairment of mitochondrial respiration caused by hyperammonemia.

#### Inhibition of GDH-dependent reductive amination of $\alpha$ -ketoglutarate by supplementation with glutamate or glutamine, or by SIRT4 overexpression, improves mitochondrial respiration under hyperammonemia

To further test the role of GDH in ammonia-induced toxicity of mitochondrial respiration, we aimed to test whether the detrimental effects of ammonia can be reduced using different amino acids. Pretreatment with 10 mM glutamine or glutamate directly before treatment with 5 mM NH<sub>4</sub>Cl for 1 h both led to reduction of the ammonia-mediated decrease in OCR (Fig. 6H,I). This is consistent with the rapid ability to produce  $\alpha$ -ketoglutarate directly from glutamate or indirectly by producing glutamate from glutamine by mitochondrial glutaminase. The rapid incorporation of ammonia-derived nitrogen in glutamate (Fig. 5A–F), the increase in total glutamate levels upon ammonia treatment (Fig. 6G) and our siRNA

experiments (Fig. 6A–D) strongly suggest a crucial role of GDH2 in mediating glutamate- and glutamine-dependent restoration of mitochondrial respiration. To corroborate this further, we applied a metabolic tracing experiment using <sup>13</sup>C-glutamine, allowing us to study glutamine-dependent anaplerosis of TCA intermediates, or glutaminolysis, under norm- and hyperammonemic conditions. Human astrocytoma cells were treated with a medium containing 2 mM or 10 mM fully <sup>13</sup>C-isotope-labeled glutamine with or without 5 mM NH<sub>4</sub>Cl for 40 min. After ammonia treatment at normal (2 mM) glutamine concentrations, the total levels of  $\alpha$ -ketoglutarate, fumarate and malate were significantly decreased, confirming an ammonia-induced depletion of TCA cycle intermediates within 40 min (Fig. S11, Table S5). This depletion was significantly inhibited by high concentrations (10 mM) of glutamine (Fig. S11), explaining why glutamine can restore mitochondrial respiration (Fig. 6I). The anaplerotic incorporation of <sup>13</sup>C derived from glutamine into TCA cycle intermediates such as  $\alpha$ -ketoglutarate (M+5), malate (M+4) and fumarate (M+4) was significantly inhibited by hyperammonemia only when glutamine concentration were normal, but not when glutamine concentrations were high in the medium (Fig. S11). This confirms that, under hyperammonemia, promoting glutaminolysis is a possible strategy to overcome mitochondrial toxicity of ammonia.

GDH is known to be inhibited by ADP ribosylation catalyzed by the mitochondrial sirtuin SIRT4 (Haigis et al., 2006). We employed HeLa-SIRT4-eGFP cells, a stable cell line overexpressing SIRT4, and the corresponding control cells (HeLa-eGFP) to test whether inhibition of mitochondrial GDH by SIRT4 can also restore mitochondrial respiration and/or mitochondrial morphology upon hyperammonemia. First, we confirmed that SIRT4-GFP overexpression (Fig. S7) caused a significant reduction in specific GDH activity compared to control cells expressing only GFP (Fig. 6E). Mitochondrial morphology and response to ammonia were not affected by expression of SIRT4-GFP (Fig. S8). Also, the

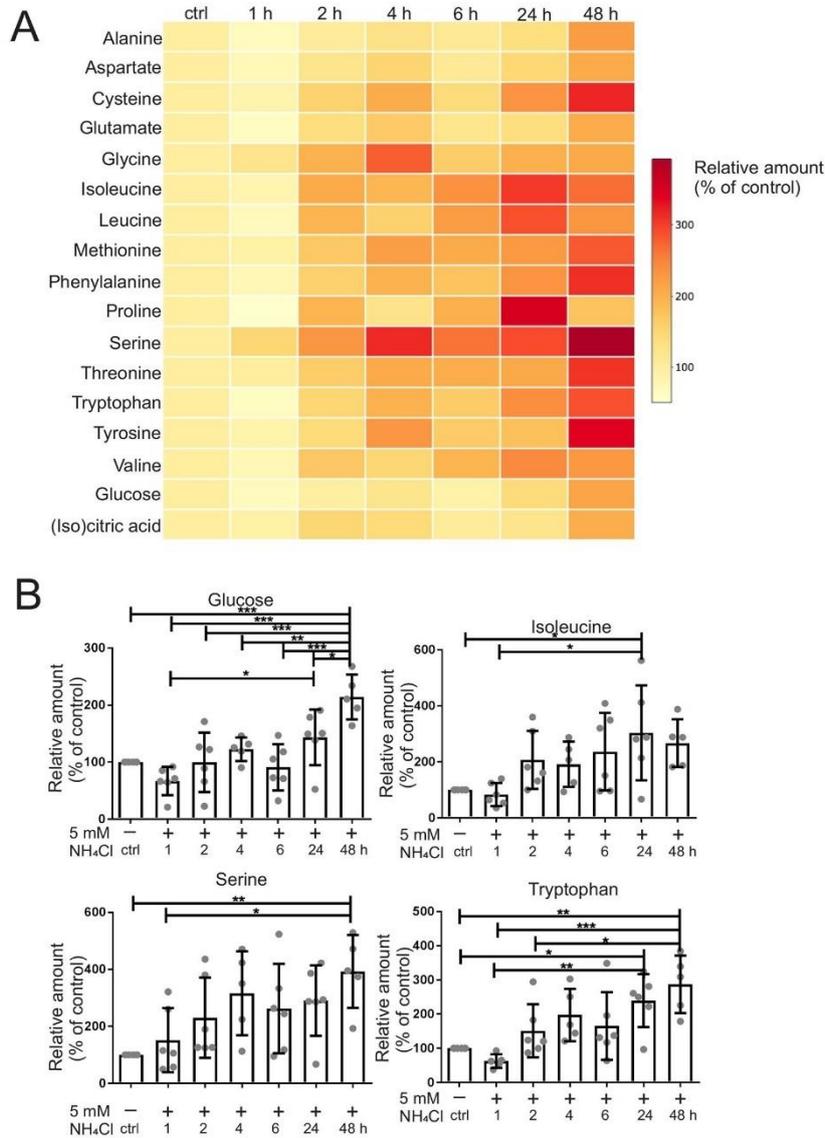


**Fig. 4. Ammonia alters energy and amino acid metabolism.** Mass spectrometry for steady-state metabolites was performed in human astrocytoma cells on a GC-QTOF. Treatment was with 5 mM  $\text{NH}_4\text{Cl}$  for 1-48 h. (A) Heat map showing the relative abundance of amino acids, glucose and (iso)citric acid compared to control (100%) over time. (B) Selected metabolites as indicated from A with additional details. Data are presented as mean  $\pm$  s.d. ( $n=4-6$ ). Statistics: one-way ANOVA with Tukey's post test (all samples versus all samples). \* $P<0.05$ , \*\* $P<0.01$ , \*\*\* $P<0.001$ .

spare respiratory capacities of untreated HeLa-SIRT4-eGFP and HeLa-eGFP cells were not affected. The fact that mitochondrial morphology was not restored by SIRT4 overexpression supports the view that ammonia exerts additional, detrimental effects that are independent of GDH. In line with this, ammonia results in a reduction in the mitochondrial membrane potential and in increased ROS formation, two parameters known to cause mitochondrial fragmentation (Görg et al., 2013; Duvezin-Caubet et al., 2006; Lu et al., 2019; Legros et al., 2002). However, after 1 h ammonia treatment, respiration dropped significantly in HeLa-eGFP cells but not in cells overexpressing SIRT4 (Fig. 6F), demonstrating that SIRT4 overexpression efficiently prevented ammonia-induced detrimental effects on mitochondrial respiration.

Overall, several lines of evidence indicate an essential role of mitochondrial GDH2 in the rapid impairment of mitochondrial

respiration under hyperammonemia. Mechanistically, we propose that GDH2 is required for ammonia-induced depletion of  $\alpha$ -ketoglutarate by reductive amination to glutamate, and that promoting anaplerosis of the TCA cycle via glutaminolysis can overcome the detrimental effects of ammonia on mitochondrial respiration (Fig. 7A,B).

## DISCUSSION

HE is a common complication occurring upon severe liver dysfunction. Although it is largely accepted that hyperammonemia-induced impairment of astrocytes plays a major role in mediating neurological disturbances (Görg et al., 2018; Norenberg, 1987), the underlying molecular mechanisms are unknown and numerous models have been proposed (Cash et al., 2010; Cordoba, 2014; Ott and Vilstrup, 2014). One particular aspect that is controversially

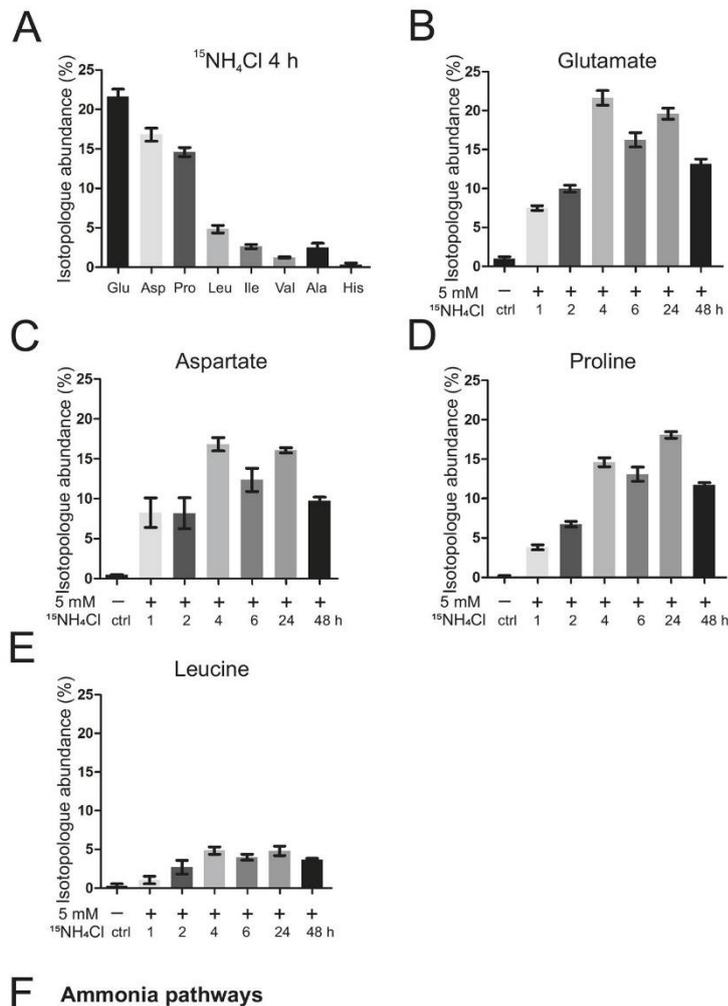
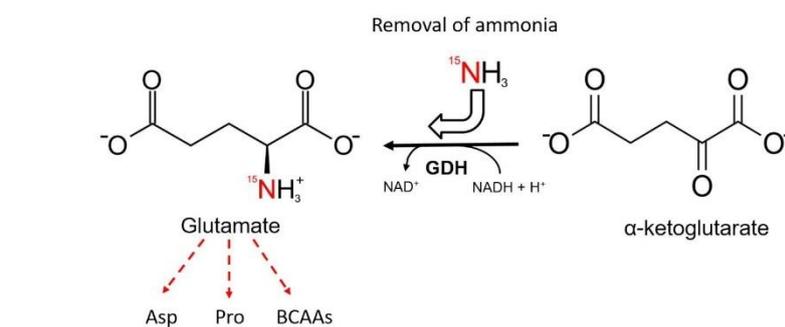


**Fig. 5. Ammonia is incorporated into GDH-dependent metabolites.** Mass spectrometry for ammonia flux was performed in human astrocytoma cells on an LC-QTOF. Treatment was with  $^{15}\text{NH}_4\text{Cl}$  for 1–48 h. (A) Amino acids found to be enriched in  $^{15}\text{N}$ -isotopologue abundance, representative after 4 h treatment. Values are corrected for natural abundance of heavy isotopes. (B–E) Isotopologue abundance of  $^{15}\text{N}$  in glutamate (B), aspartate (C), proline (D) and leucine (E) over time. (F) Pathway of  $^{15}\text{N}$ -ammonia recycling and utilization via glutamate dehydrogenase (GDH) and secondary reactions. Red arrows indicate the path of nitrogen. Data are presented as mean  $\pm$  s.d. ( $n=3$ ). BCAA, branched-chain amino acid.



discussed is the role of altered brain energy metabolism caused by hyperammonemia. Alterations in the CSF metabolome of HE patients (Weiss et al., 2016), differences in respiratory chain enzyme activities in rat HE models (Boer et al., 2009; Dhanda et al., 2017), and variable results on altered levels/activities of TCA cycle metabolites and enzymes have been reported (Rama Rao and

Norenberg, 2012). We noticed that the large majority of studies investigating acute or chronic *in vitro* and *in vivo* HE models address the toxic effects of hyperammonemia after 1 day, a few days or even weeks (Görg et al., 2015; Hazell and Norenberg, 1998; Oenarto et al., 2016). Little is known about the immediate effect of ammonia on brain energy metabolism. Here, we provide several lines of evidence

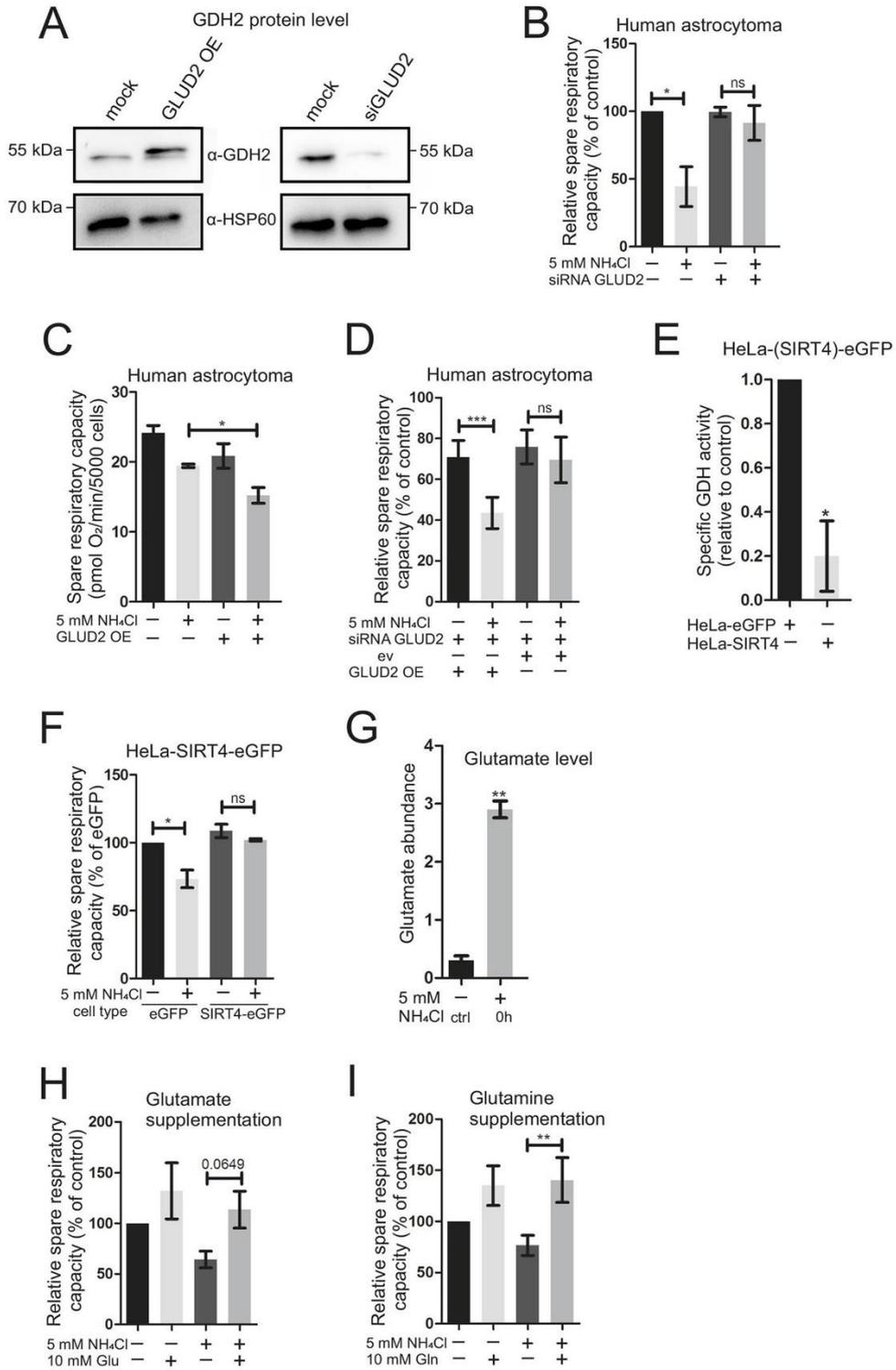


Fig. 6. See next page for legend.

**Fig. 6. Knockdown of *GLUD2* and anaplerotic supplementation reverses, whereas overexpression exacerbates, the detrimental effect of  $\text{NH}_4\text{Cl}$  on mitochondrial respiration.** (A) Representative western blot analysis of human astrocytoma cell lysates from *GLUD2* overexpression (48 h) and knockdown (48 h) versus mock samples (transfection reagent only).  $\alpha$ -HSP60 was used as a loading control. (B) Oxygen consumption rate (OCR), represented as relative spare respiratory capacity, in human astrocytoma cells was analyzed on a Seahorse XFe96 Extracellular Flux Analyzer with a Mito Stress Test Kit. *GLUD2* knockdown via siRNA transfection for 48 h  $\pm$  5 mM  $\text{NH}_4\text{Cl}$  treatment for 1 h. Individual biological replicates normalized to control (100%). Statistics: one-sample *t*-test. (C) Spare respiratory capacity of human astrocytoma cells. Treatment with 5 mM  $\text{NH}_4\text{Cl}$  for 1 h. *GLUD2* overexpression (OE) for 48 h ( $n=5$ ). (D) Relative spare respiratory capacity of human astrocytoma cells. Treatment with 5 mM  $\text{NH}_4\text{Cl}$  for 1 h. Knockdown of *GLUD2* for 48 h when indicated (siRNA), overexpression of *GLUD2* plasmid (OE) or empty vector (ev) for 48 h when indicated. Individual biological replicates normalized to control (100%, not shown) ( $n=5$ ). (E) GDH activity was measured in HeLa-eGFP cells and HeLa-SIRT4-eGFP cells. GDH activity was determined by a commercial assay detecting NADH production. Values were individually normalized to control and corrected for protein content using Bradford assays. Data are presented as mean  $\pm$  s.e.m. ( $n=3$ ). Statistics: one-sample *t*-test. (F) Relative spare respiratory capacity (%) measured with a Seahorse Analyzer using a Mito Stress Test Kit. HeLa-eGFP and HeLa-SIRT4-eGFP cells treated with 5 mM  $\text{NH}_4\text{Cl}$  for 1 h and respective controls. Individual biological replicates normalized to HeLa-eGFP cells (100%) ( $n=3$ ). (G) Targeted metabolomics quantification of glutamate in human astrocytoma cells immediately after treatment with 5 mM  $\text{NH}_4\text{Cl}$  (0 h). Measurement was performed on a GC-QTOF ( $n=3$ ). (H,I) Human astrocytoma cells were subject to Mito Stress Kit measurement on Seahorse XFe96 Extracellular Flux Analyzer. Treatment with (+) or without (-) 10 mM respective compound [H, glutamate ( $n=4-5$ ); I, glutamine ( $n=5$ )] with (+) or without (-) 5 mM  $\text{NH}_4\text{Cl}$  for 1 h. Relative spare respiratory capacity is represented by OCR. Individual biological replicates normalized to control (100%). Data are presented as mean  $\pm$  s.e.m. Statistics: one-tailed Student's *t*-test comparing two groups. \* $P<0.05$ , \*\* $P<0.01$ , \*\*\* $P<0.001$ ; ns, not significant.

that high ammonia levels lead to a rapid metabolic reprogramming of astrocytes, in particular via GDH-dependent impairment of the TCA cycle, raising the possibility that this represents an early event in the pathogenesis of HE.

The following arguments strongly support this view: (1) our data show that ammonia introduces rapid mitochondrial fragmentation in two cell types, human astrocytoma cells and primary rat astrocytes; (2) in primary cells, the effect was more rapidly observed, which could be attributed to metabolic differences in tumor cells (Hsu and Sabatini, 2008); (3) hyperammonemia resulted in an instantaneous impairment of mitochondrial respiration in both cell types; (4) the effect was not mediated by possible changes in pH as a pH mimetic did not impair respiration; (5) glycolysis was markedly hampered during hyperammonemia as a consequence of TCA cycle inhibition; (6) metabolomic analyses revealed a delayed increase of several amino acids, including those that can directly or indirectly engage in anaplerotic reactions feeding the TCA cycle; (7) glucose levels were increased, consistent with the observation that glycolysis is inhibited rapidly by ammonia; (8) isotope labeling of ammonia and metabolic  $^{15}\text{N}$  tracing showed that ammonia is rapidly fixed in glutamate (and metabolites derived from glutamate), which prompted us to investigate the role of the GDH that catalyzes the reductive amination of  $\alpha$ -ketoglutarate and ammonia to glutamate; (9) ammonia-induced inhibition of mitochondrial respiration is strongly dependent on the mitochondrial GDH2, suggesting that removal of ammonia may occur via GDH2; (10) GDH2 inhibition by overexpression of the mitochondrial sirtuin SIRT4 has the same effect as GDH2 knockdown; (11) GDH2 overexpression resulted in a sensitization of astrocytes to ammonia; (12) glutamate levels increased instantaneously after administration of ammonia and a

decrease in TCA intermediates was observed 40 min after ammonia addition; (13) glutamate/glutamine addition rescued respiratory effects, suggesting that promoting anaplerosis of the TCA cycle via GDH2 can reduce ammonia-induced toxicity; and (14) this was confirmed by  $^{13}\text{C}$ -metabolic tracing of glutamine under norm- and hyperammonemia, showing that promoting glutaminolysis under hyperammonemia was able to restore TCA cycle intermediates. Taken together, we have multiple lines of evidence that a critical entry point of excessive ammonia is the reductive amination of  $\alpha$ -ketoglutarate by GDH2, causing impairment of the TCA cycle and thus of respiration as well as glycolysis. GDH2 is known to play an important part specifically in astrocytes, yet its role under hyperammonemia is not well understood. It was reported that *GLUD2* expression in astrocytes increases the capacity for uptake and oxidative metabolism of glutamate, particularly during increased workload and aglycemia, implying that GDH2 is an important mediator allowing the replenishment of the TCA cycle by glutamate (Nissen et al., 2018). This is in line with our data showing that glutamate can indeed ameliorate the effects of hyperammonemia. A recent study showed that metabolic differences between transgenic mice carrying the human gene *GLUD2* and control mice during postnatal brain development center on metabolic pathways surrounding the TCA cycle (Li et al., 2016). These results support the importance of the GDH2-dependent modulation of energy metabolism in the brain.

In contrast to the prevailing view for norm conditions, our data show that, under hyperammonemic conditions, the net conversion of  $\alpha$ -ketoglutarate occurs primarily towards glutamate and not vice versa. To our knowledge, this direction of the GDH reaction has not been considered to be relevant for the pathogenesis of HE so far. This does not contradict the role of GDH as an important enzyme for anaplerosis, which is undisputed under normal conditions. An ammonia-detoxifying role of GDH has been shown in the liver (Williamson et al., 1967) and was proposed based on a mathematical model employed to investigate the mechanism of ammonia detoxification (Ghallab et al., 2016). Consistent with this, injection of GDH and  $\alpha$ -ketoglutarate with cofactors into mice reduced ammonia blood levels to normal levels within 15 min (Ghallab et al., 2016). Additionally, a rapid decrease in  $\alpha$ -ketoglutarate concentration in rat liver was reported after injection of  $\text{NH}_4\text{Cl}$  solution (Williamson et al., 1967). To our knowledge, the role of GDH-dependent ammonia detoxification in tissues other than the liver has not been addressed so far. Thus, our data now show that GDH2 in human astrocytes, on one hand, helps to remove the ammonia load, but, on the other hand, impairs the TCA cycle. GDH2-mediated removal of ammonia is not only beneficial, as commonly expected, but also detrimental to astrocytes. As a result of impairing the TCA cycle, we can well explain why glycolysis, as well as OXPHOS, is rapidly inhibited in hyperammonemia. We see a clear concentration dependency of ammonia-induced effects on respiration. This is in accordance with most patient data showing a correlation between blood ammonia levels and severity of disease (Ong et al., 2003).

It is interesting to note that humans and apes (hominoids), but not other mammals, have two genes encoding GDH1 and GDH2, namely *GLUD1* and *GLUD2*, respectively. GDH1 is found in all mammals in the cytosol and mitochondria and is widely expressed in all tissues. *GLUD2* encodes a mitochondrial form of GDH that is expressed solely in the testes, epithelial kidney cells and astrocytes of hominoids. It is proposed that *GLUD2* appeared in evolution after retroposition of the *GLUD1* gene, probably in an ape ancestor less than 23 million years ago (Burki and Kaessmann, 2004). The mature

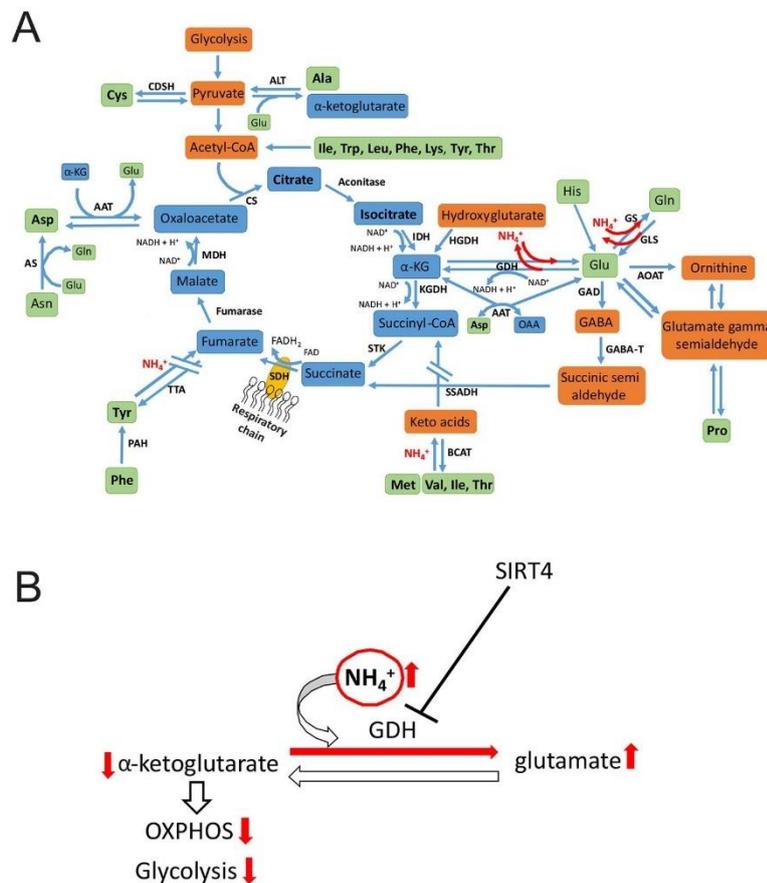


**Fig. 7. Proposed mechanism of the influence of ammonia on mitochondrial metabolism.**

(A) TCA cycle and anaplerotic reactions including the role of ammonia. Amino acids and TCA cycle intermediates increased in steady-state metabolites are depicted in bold. (B) Proposed mechanism on the role of GDH in ammonia-induced toxicity.  $\alpha$ -KG,  $\alpha$ -ketoglutarate; AAT, aspartate aminotransferase; ALT, alanine aminotransferase; AOAT, acetyl ornithine aminotransferase; AS, asparaginase; BCAT, branched-chain amino acid transferase; CDSH, cysteine desulfhydrase; CS, citrate synthase; GABA-T, GABA-transaminase; GAD, glutamate decarboxylase; GDH, glutamate dehydrogenase; GLS, glutaminase; GS, glutamine synthetase; HGDH, hydroxyglutarate dehydrogenase; IDH, isocitrate dehydrogenase; KGDH,  $\alpha$ -ketoglutarate dehydrogenase; MDH, malate dehydrogenase; OAA, oxaloacetate; OXPPOS, oxidative phosphorylation; PAH, phenylalanine hydroxylase; SDH, succinate dehydrogenase; SSADH, succinate semialdehyde dehydrogenase; STK, succinate thiokinase; TTA, tyrosine transaminase.

forms of human GDH1 and GDH2 are highly homologous, with a sequence similarity of  $\sim 97\%$ . Under physiological conditions, the GDH reaction mainly catalyzes the oxidative deamination to form  $\alpha$ -ketoglutarate (Adeva et al., 2012). GDH is regulated by SIRT4, a mitochondrial enzyme that uses  $\text{NAD}^+$  to ADP-ribosylate GDH and that inhibits GDH activity (Haigis et al., 2006). Here, we show that overexpression of SIRT4 can phenocopy the effect of GDH2 knockdown, corroborating our model.

One strong argument allowing us to conclude that ammonia is utilized in the GDH reaction towards glutamate was obtained from  $^{15}\text{N}$  label incorporation mainly in glutamate, aspartate and proline, as well as to a lower extent in leucine, isoleucine, valine, alanine and histidine after administration of  $^{15}\text{NH}_4\text{Cl}$ . Glutamate, aspartate, proline and the BCAAs are directly associated with GDH downstream reactions or acquire the  $^{15}\text{N}$  label through secondary reactions. It is interesting to note that breast cancer cells have also been shown to fix ammonia via the GDH reaction; Spinelli et al. (2017) reported that, in breast cancer cell lines, ammonia is primarily assimilated through reductive amination catalyzed by GDH, and the high accumulation of labeled nitrogen in glutamate, proline, aspartate and alanine, among others, is strongly reminiscent of our data in astrocytes.

Other studies support the critical role of the TCA cycle in HE. Weiss et al. (2016) examined metabolomics to highlight the dysfunctions of metabolic pathways in CSF samples of HE patients. This revealed an accumulation of acetylated compounds, which also

points towards a defect in the TCA cycle. Additionally, the increased metabolites are involved in ammonia, amino acid and energy metabolism; for example, glutamate, glutamine, methionine, phenylalanine and others (Weiss et al., 2016), many of which we also found elevated. Patient data show an association between arterial hyperammonemia and increase in glutamine concentration in the brain (Tofteng et al., 2006), which could result from GDH activity towards glutamate and, subsequently, glutamine. It was further shown that, under normal conditions, GDH is important to sustain the catalytic activity of the TCA cycle in mouse astrocytes by mediating the net formation of TCA intermediates, and that reduced GDH expression induces the usage of alternative substrates such as BCAAs (Nissen et al., 2015).

In contrast, we show that, at high ammonia levels, with increased time the concentration of amino acids such as BCAAs increases. Why is the effect of ammonia on mitochondrial respiration most prevalent at short time points but becomes less pronounced with time? We attribute this to a compensatory mechanism that involves the induction of anaplerotic reactions other than the one catalyzed by GDH. Such a mechanism could be enhanced proteolysis by autophagy or proteasomal degradation of proteins. A recent study reported that autophagic flux is altered in astrocytes in various HE models (Lu et al., 2019). Autophagy was also found to be induced in the substantia nigra of mice with liver damage and subsequent hyperammonemia (Bai et al., 2018). In our study, when ammonia was washed out for only 1 h, the detrimental effect on mitochondrial

respiration had not only gone, but mitochondrial respiration had reached levels above control levels, in particular after longer pretreatments with ammonia. This could be due to the fact that accumulated amino acids can rapidly engage in anaplerotic reactions and drive the TCA cycle as soon as ammonia is removed. Further, the detrimental effects of ammonia are rapidly reversible, which was also seen in mitochondrial morphology.

The importance of GDH for mitochondrial respiration is also known from *in vivo* studies. In *Cns-Glut1<sup>-/-</sup>* mice (GDH1 knockout in synaptosomes), the basal respiration in brain mitochondria in the presence of glutamate and malate was significantly reduced (Hohnholt et al., 2017). In GDH1 knockout neurons without stimulation of respiration (e.g. by FCCP treatment), there is no effect of GDH1 knockout on respiration, whereas upon stimulation by FCCP, the cells do not respond with an increase in respiration (Hohnholt et al., 2017). This is in line with our results showing that hyperammonemia does not grossly affect basal mitochondrial respiration but rather only affects it when respiratory activity is induced.

Our *in vitro* findings have identified two novel factors, GDH2 and SIRT4, and demonstrate a crucial role of the TCA cycle in the pathogenesis of HE. This may help to develop new treatment options in HE, e.g. supplementation of certain amino acids promoting anaplerosis, such as glutamate or glutamine. Targeting sirtuins, in particular SIRT1-3 and SIRT5, is already being studied intensively in cancer research. SIRT4 is regulated by miR15a/b (Lang et al., 2016), but a specific compound inhibiting SIRT4 activity is not known so far. Targeting SIRT4 could present another promising future therapeutic target for treating patients suffering from HE. Further studies, especially on the potential role of SIRT4 and GDH regulation, are needed for the development of improved treatment strategies for HE symptoms.

## MATERIALS AND METHODS

### Cell lines

Human astrocytoma cells (MOG-G-CCM) from European Collection of Authenticated Cell Cultures (ECACC; Public Health England, Salisbury, UK) were established from an anaplastic astrocytoma of human adult brain. Cells were grown in Dulbecco's modified eagle medium (DMEM) with 1 g/l glucose (Sigma-Aldrich, Taufkirchen, Germany), with 10% fetal calf serum (PAN-Biotech, Aidenbach, Germany), 2 mM GlutaMax (Thermo Fisher Scientific, Carlsbad, CA, USA), 2 mM sodium pyruvate (Thermo Fisher Scientific) and penicillin/streptomycin (Merck Millipore, Burlington, MA, USA) at 37°C and 5% humidified CO<sub>2</sub>. Primary rat astrocytes were prepared from the cerebral hemispheres of newborn Wistar rats and grown under the same conditions. The care and use of experimental animals complied with all relevant local animal welfare laws, guidelines and policies. SIRT4-eGFP-overexpressing HeLa cells and respective eGFP control cells were established as described here and in the Supplementary Materials and Methods and grown under the same conditions in the presence of 2 µg/ml puromycin (Thermo Fisher Scientific).

### Cellular metabolism analysis

A Mito Stress Test Kit and a Glycolysis Stress Test Kit (Agilent Technologies, Santa Clara, CA, USA) were applied according to the manufacturer's instructions using a Seahorse XFe96 Extracellular Flux Analyzer (Agilent Technologies). FCCP concentration and cell density were titrated/determined for each cell type prior to the experiments. Treatment with NH<sub>4</sub>Cl (VWR, Radnor, PA, USA) or CH<sub>3</sub>NH<sub>3</sub>Cl (Merck Millipore) at the given molarity was performed for 1, 4, 6, 24 and 48 h, or immediately prior to analysis (0 h). After measurement, cell numbers were quantified by absorption spectrometry (excitation, 361 nm; emission, 486 nm) using Hoechst 33342 (Thermo Fisher Scientific) staining using a plate reader (Tecan Infinite 200 PRO, Switzerland) and normalized to cell number. Basal

respiration is defined as the respiration before the first injection by the Seahorse system.

Maximal respiration was defined as the OCR after FCCP injection (maximal OCR) – the OCR after blocking mitochondrial respiration (non-mitochondrial OCR). Spare respiratory capacity was defined as the maximal OCR – basal respiration. Spare respiratory capacity (%) was defined as maximal respiration/basal respiration×100. Maximal respiration and spare respiratory capacity are challenged states of respiration. Glycolysis was the ECAR: the maximum rate measurement before oligomycin injection – the last rate of measurement before glucose injection. Glycolytic capacity was the maximum rate measurement after injection of oligomycin – the last rate measurement before glucose injection.

### Plasmids and transfection of cell lines

To visualize mitochondria, the construct pEGFP-Mito (Clontech Laboratories, Mountain View, CA, USA) was used. Transfection was performed using Effectene Transfection Reagent (Qiagen, Hilden, Germany) according to the manufacturer's instructions 24 h before imaging. Knockdown of GDH2 using siRNAs (#NM\_012084: 5'-CUAACCUCUUACACGUGUAA-3' and 5'-UUACACGUGAAGAGGUUAG-3', Sigma-Aldrich) and transfection of *GLUD2* plasmid/empty vector controls were performed using Lipofectamine RNAiMAX (Thermo Fisher Scientific) for 48 h in Seahorse plates, according to the manufacturer's instructions using the reverse transfection protocol. Human *GLUD2* was cloned into pcDNA3.1(+) (clone ID OHu18663, obtained from GenScript USA, Piscataway, NJ, USA). Control vector was pcDNA3.1(+) (Invitrogen, Thermo Fisher Scientific). The DNA sequence in the *GLUD2* overexpression plasmid was on purpose not targeted by the siRNA by introducing suitable silent mutations.

### Microscopy

Human astrocytoma cells were seeded in 3 cm glass bottom dishes (MatTek Corporation, Ashland, MA, USA), transfected with pEGFP-Mito and treated with 5 mM NH<sub>4</sub>Cl for 1, 4, 6, 24, 48 or 72 h. For Fig. S8, HeLa-(SIRT4)-eGFP cells were seeded in the same dishes described above and treated with 5 mM NH<sub>4</sub>Cl for 24 h or 48 h. Imaging was performed with a Zeiss Axiovert Observer D1 microscope with a 63×/1.4 NA oil objective (Filter: excitation, 450-490 nm; emission, 500-550 nm) (Zeiss, Oberkochen, Germany) and AxioVision Software. Twenty images per dish were taken and cells were categorized and quantitatively scored according to the degree of fragmentation; (tubular, intermediate, fragmented: cells with >90%, 90-10%, <10% of total mitochondrial signal with tubular morphology, respectively; Fig. 1A). For reversibility of the mitochondrial phenotype, primary rat astrocytes transfected with pEGFP-Mito were grown in the presence of 5 mM NH<sub>4</sub>Cl for 72 h and analyzed for mitochondrial fragmentation. Medium was exchanged and cells were analyzed for mitochondrial morphology 24 h, 48 h and 72 h after the removal of NH<sub>4</sub>Cl. To determine mitochondrial morphology changes in primary rat astrocytes, mitochondria were visualized by immunostaining against Tom20 (primary antibody: sc-11415, Santa Cruz Biotechnology, Dallas, TX, USA; secondary antibody: Alexa Fluor 488, #A27034, Thermo Fisher Scientific). To determine SIRT4 localization in HeLa-(SIRT4)-eGFP cells, the nucleus was stained with DAPI (Sigma-Aldrich), and for mitochondrial visualization immunostaining was performed against Tom20 (primary antibody: see above; secondary antibody: Alexa Fluor 546 #A11035, Invitrogen, Thermo Fisher Scientific). Analysis was performed as described above. Images were taken using a Spinning Disk Confocal microscope (PerkinElmer, Waltham, MA, USA) using the 405 nm, 488 nm and 561 nm lasers, 60×/1.4 NA oil objective and Volocity software. Images were processed with Fiji (Schindelin et al., 2012).

### Metabolite analysis

Cells were grown in 175-cm<sup>2</sup> flasks (Greiner Bio-One, Kremsmünster, Austria). For metabolite screening and <sup>15</sup>N-metabolic tracing, cells were treated with 5 mM NH<sub>4</sub>Cl for 48, 24, 6, 4, 2 or 1 h or harvested immediately after treatment (0 h). For <sup>13</sup>C-metabolic tracing, cells were treated with medium containing 2 mM or 10 mM [U-<sup>13</sup>C]-glutamine (#605166, Millipore Sigma, Taufkirchen, Germany) and 5 mM NH<sub>4</sub>Cl or water as control for 40 min. Cells were washed with PBS, trypsinized and resuspended in DMEM for cell counting. For metabolite screening and

<sup>15</sup>N-metabolic tracing, 1×10<sup>6</sup> cells were pelleted, and for <sup>13</sup>C-metabolic tracing, 3×10<sup>6</sup> cells were pelleted. Pellets were washed twice with ice-cold PBS and resuspended in a pre-cooled (−20°C) 1:2.5:1 mixture of H<sub>2</sub>O: methanol:chloroform (both VWR, Radnor, PA, USA), mixed at 4°C for 10 min, and centrifuged at 9300 g for 5 min at 4°C. The supernatant was subject to metabolite profiling. Polar metabolites were analyzed by gas chromatography coupled to a time-of-flight (TOF) mass spectrometer (GC-QTOF) (7200 GC-QTOF, Agilent Technologies) as published (Fiehn and Kind, 2007). For relative quantification, peak areas of the compounds were normalized to the internal standard ribitol (Sigma-Aldrich) added to the extraction buffer. To follow accumulation of <sup>15</sup>N label, cells were treated with <sup>15</sup>NH<sub>4</sub>Cl as described above. Metabolites were analyzed by liquid chromatography coupled to a TOF mass spectrometer (LC-QTOF) (1290 UHPLC 6530 QTOF, Agilent Technologies) according to Gu et al. (2007). Relative <sup>15</sup>N label enrichment was calculated after accounting for natural isotopic distribution. Peak integration and analysis were performed using the Agilent Mass Hunter Workstation B07 (Agilent Technologies). Further details are provided in Tables S1–S3. For ion chromatography-mass spectrometry (IC-MS) analysis, a combination of a Dionex ICS-6000 HPLC and a Thermo Fisher Scientific Q Exactive Plus mass spectrometer was used following the method described by Schwaiger et al. (2017) with slight modifications. In brief, the dried sample was reconstituted in 100 μl deionized water, of which 5 μl was injected via a Dionex AS-AP autosampler. For the anion exchange chromatography, a Dionex IonPac AS11-HC column (2 mm×250 mm, 4 μm particle size, Thermo Fisher Scientific) equipped with a Dionex IonPac AG11-HC guard column (2 mm×50 mm, 4 μm, Thermo Fisher Scientific) was used, and the mobile phase was generated using an eluent generator with a potassium hydroxide cartridge. The mass spectrometer operated in negative mode with a combination of full mass scan and a data-dependent Top5 MS<sup>2</sup> (ddMS<sup>2</sup>) experiment with a resolution of 140,000 and 17,500, respectively. Data analysis was conducted using a Compound Discoverer (version 3.1, Thermo Fisher Scientific). For data analysis, the standard workflow for stable isotope labeling from the Compound Discoverer was chosen and the default settings were used: 5 ppm mass tolerance, 30% intensity tolerance and 0.1% intensity threshold for isotope pattern matching. As an additional level of validation, an in-house database for retention times and MS<sup>2</sup> spectra was created using mzVault (Thermo Fisher Scientific) and implemented in the annotation workflow.

#### GDH activity kit

To determine changes in the activity of GDH under various conditions, a colorimetric Glutamate Dehydrogenase (GDH) Activity Assay Kit (MAK099, Sigma-Aldrich) was employed according to the manufacturer's instructions. In brief, cells were treated with the respective condition [5 mM NH<sub>4</sub>Cl for 1 h and 24 h; *GLUD2* knockdown and overexpression as described above; HeLa-(SIRT4)-eGFP cells untreated] and 1×10<sup>6</sup> cells per sample were used for the assay. Cells were homogenized in ice-cold assay buffer and used as described in the instructions. From colorimetric measurements, the amount of NADH generated in nmol and the GDH activity in mU/ml were determined using a standard curve. Bradford measurement was performed for all samples and results were corrected for protein concentration to obtain specific enzyme activities.

#### Statistics

Statistics were performed using GraphPad Prism 7.04 for Windows (GraphPad Software, La Jolla, CA, USA). For multiple comparisons, one-way ANOVA with Dunnett's, Tukey's or Sidak's post hoc test or paired one-way ANOVA with Geisser–Greenhouse correction and Sidak's multiple comparison post hoc test was performed. To compare two groups, Student's *t*-test was applied. To compare one group to a normalized value, one-sample *t*-test was used. Data are shown as mean±s.e.m. or s.d., as indicated in the figure legends.

#### Acknowledgements

We thank Prof. Dr Dieter Häussinger and Dr Boris Görg for providing primary rat astrocytes and continuous support; Prof. Wilhelm Stahl for scientific discussions; Andrea Borchardt and Tanja Portugal for excellent technical assistance; and

Dr Nahal Brocke-Ahmadinejad for bioinformatics support. We are grateful to Dr Helmut Hanenberg for providing cloning vectors. We appreciate the excellent technical assistance from Katrin Weber, Elisabeth Klemp and Maria Graf in mass spectrometric analysis.

#### Competing interests

The authors declare no competing or financial interests.

#### Author contributions

Conceptualization: L.D., M.Z., A.S.R.; Methodology: L.D., M.Z., P.W., D.B., R.E.P., L.B., C.W., R.P.P., T.M., A.P.M.W., A.S.R.; Formal analysis: L.D., M.Z., P.W., D.B., R.E.P., L.B., C.W., P.B., R.P.P., T.M.-A., A.S.R.; Investigation: L.D., M.Z., P.W., D.B., R.E.P., L.B., C.W., R.P.P., T.M.-A., A.S.R.; Resources: L.B., C.W., A.P.M.W., A.S.R.; Data curation: L.D., M.Z., P.W., D.B., R.E.P., L.B., C.W., P.B., R.P.P., T.M.-A., A.S.R.; Writing - original draft: L.D., M.Z., A.S.R.; Writing - review & editing: M.Z., D.B., R.E.P., L.B., P.B., R.P.P., T.M.-A., A.P.M.W.; Visualization: L.D., M.Z.; Supervision: R.P.P., A.P.M.W., A.S.R.; Project administration: L.D., A.S.R.; Funding acquisition: R.P.P., A.P.M.W., A.S.R.

#### Funding

This work was funded by Deutsche Forschungsgemeinschaft (DFG) CRC 974 project B09 (A.S.R.) and CRC 1208 (A.P.M.W.); and Stiftung für Altersforschung der Heinrich-Heine-Universität Düsseldorf project 701 810 783 (R.P.P.). The CEPPLAS Plant Metabolism and Metabolomics Laboratory is funded by DFG under Germany's Excellence Strategy (EXC-2048/1; project ID 390686111).

#### Supplementary information

Supplementary information available online at <https://dmm.biologists.org/lookup/doi/10.1242/dmm.047134.supplemental>

#### References

- Adeva, M. M., Souto, G., Blanco, N. and Donapetry, C. (2012). Ammonium metabolism in humans. *Metabolism* **61**, 1495–1511. doi:10.1016/j.metabol.2012.07.007
- Bai, G., Rama Rao, K. V., Murthy, C. R., Panickar, K. S., Jayakumar, A. R. and Norenberg, M. D. (2001). Ammonia induces the mitochondrial permeability transition in primary cultures of rat astrocytes. *J. Neurosci. Res.* **66**, 981–991. doi:10.1002/jnr.10056
- Bai, Y., Wang, Y. and Yang, Y. (2018). Hepatic encephalopathy changes mitochondrial dynamics and autophagy in the substantia nigra. *Metab. Brain Dis.* **33**, 1669–1678. doi:10.1007/s11011-018-0275-6
- Boer, L. A., Panatto, J. P., Fagundes, D. A., Bassani, C., Jeremias, I. C., Daufenbach, J. F., Rezin, G. T., Constantino, L., Dal-Pizzol, F. and Streck, E. L. (2009). Inhibition of mitochondrial respiratory chain in the brain of rats after hepatic failure induced by carbon tetrachloride is reversed by antioxidants. *Brain Res. Bull.* **80**, 75–78. doi:10.1016/j.brainresbull.2009.04.009
- Burki, F. and Kaessmann, H. (2004). Birth and adaptive evolution of a hominoid gene that supports high neurotransmitter flux. *Nat. Genet.* **36**, 1061–1063. doi:10.1038/ng1431
- Cash, W. J., McConville, P., McDermott, E., McCormick, P. A., Callender, M. E. and McDougall, N. I. (2010). Current concepts in the assessment and treatment of Hepatic Encephalopathy. *QJM* **103**, 9–16. doi:10.1093/qjmed/hcp152
- Cordoba, J. (2014). Hepatic encephalopathy: from the pathogenesis to the new treatments. *ISRN Hepatology* **2014**, 236268. doi:10.1155/2014/236268
- Dhanda, S., Sunkaria, A., Halder, A. and Sandhir, R. (2017). Mitochondrial dysfunctions contribute to energy deficits in rodent model of hepatic encephalopathy. *Metab. Brain Dis.* **33**, 209–223. doi:10.1007/s11011-017-0136-8
- Duvezin-Caubet, S., Jagasia, R., Wagener, J., Hofmann, S., Trifunovic, A., Hansson, A., Chomyn, A., Bauer, M. F., Attardi, G., Larsson, N.-G. et al. (2006). Proteolytic processing of OPA1 links mitochondrial dysfunction to alterations in mitochondrial morphology. *J. Biol. Chem.* **281**, 37972–37979. doi:10.1074/jbc.M606059200
- Ferenci, P. (2017). Hepatic encephalopathy. *Gastroenterol. Rep.* **5**, 138–147. doi:10.1093/gastro/gox013
- Ferenci, P., Lockwood, A., Mullen, K., Tarter, R., Weissenborn, K. and Blei, A. T. (2002). Hepatic encephalopathy—definition, nomenclature, diagnosis, and quantification: final report of the working party at the 11th world congresses of gastroenterology, Vienna, 1998. *Hepatology* **35**, 716–721. doi:10.1053/jhep.2002.31250
- Fiehn, O. and Kind, T. (2007). Metabolite profiling in blood plasma. *Methods Mol. Biol.* **358**, 3–17. doi:10.1007/978-1-59745-244-1\_1
- Frank, M., Duvezin-Caubet, S., Koob, S., Occhipinti, A., Jagasia, R., Petcherski, A., Ruonala, M. O., Priault, M., Salin, B. and Reichert, A. S. (2012). Mitophagy is triggered by mild oxidative stress in a mitochondrial fission dependent manner. *Biochim. Biophys. Acta* **1823**, 2297–2310. doi:10.1016/j.bbamcr.2012.08.007
- Ghallab, A., Cellière, G., Henkel, S. G., Driesch, D., Hoehme, S., Hofmann, U., Zellmer, S., Godoy, P., Sachinidis, A., Blaszkewicz, M. et al. (2016). Model-

- guided identification of a therapeutic strategy to reduce hyperammonemia in liver diseases. *J. Hepatol.* **64**, 860-871. doi:10.1016/j.jhep.2015.11.018
- Görg, B., Qvartskhava, N., Keitel, V., Bidmon, H. J., Selbach, O., Schliess, F. and Häussinger, D. (2008). Ammonia induces RNA oxidation in cultured astrocytes and brain in vivo. *Hepatology* **48**, 567-579. doi:10.1002/hep.22345
- Görg, B., Schliess, F. and Häussinger, D. (2013). Osmotic and oxidative/nitrosative stress in ammonia toxicity and hepatic encephalopathy. *Arch. Biochem. Biophys.* **536**, 158-163. doi:10.1016/j.abb.2013.03.010
- Görg, B., Karababa, A., Shafiqullina, A., Bidmon, H. J. and Häussinger, D. (2015). Ammonia-induced senescence in cultured rat astrocytes and in human cerebral cortex in hepatic encephalopathy. *Glia* **63**, 37-50. doi:10.1002/glia.22731
- Görg, B., Karababa, A. and Häussinger, D. (2018). Hepatic encephalopathy and astrocyte senescence. *J. Clin. Exp. Hepatol.* **8**, 294-300. doi:10.1016/j.jceh.2018.05.003
- Gu, L., Jones, A. D. and Last, R. L. (2007). LC-MS/MS assay for protein amino acids and metabolically related compounds for large-scale screening of metabolic phenotypes. *Anal. Chem.* **79**, 8067-8075. doi:10.1021/ac070938b
- Haigis, M. C., Mostoslavsky, R., Haigis, K. M., Fahie, K., Christodoulou, D. C., Murphy Andrew, J., Valenzuela, D. M., Yancopoulos, G. D., Karow, M., Blander, G. et al. (2006). SIRT4 inhibits glutamate dehydrogenase and opposes the effects of calorie restriction in pancreatic  $\beta$  cells. *Cell* **126**, 941-954. doi:10.1016/j.cell.2006.06.057
- Hazell, A. S. and Norenberg, M. D. (1998). Ammonia and manganese increase arginine uptake in cultured astrocytes. *Neurochem. Res.* **23**, 869-873. doi:10.1023/A:1022411012512
- Hohnholt, M. C., Andersen, V. H., Andersen, J. V., Christensen, S. K., Karaca, M., Maechler, P. and Waagepetersen, H. S. (2017). Glutamate dehydrogenase is essential to sustain neuronal oxidative energy metabolism during stimulation. *J. Cereb. Blood Flow Metab.* **38**, 1754-1768. doi:10.1177/0271678X17714680
- Hsu, P. P. and Sabatini, D. M. (2008). Cancer cell metabolism: warburg and beyond. *Cell* **134**, 703-707. doi:10.1016/j.cell.2008.08.021
- Jheng, H.-F., Tsai, P.-J., Guo, S.-M., Kuo, L.-H., Chang, C.-S., Su, I.-J., Chang, C.-R. and Tsai, Y.-S. (2012). Mitochondrial fission contributes to mitochondrial dysfunction and insulin resistance in skeletal muscle. *Mol. Cell. Biol.* **32**, 309-319. doi:10.1128/MCB.05603-11
- Katunuma, N., Okada, M. and Nishii, Y. (1966). Regulation of the urea cycle and TCA-cycle by ammonia. *Adv. Enzyme Regul.* **4**, 317-336. doi:10.1016/0065-2571(66)90025-2
- Lang, A., Grether-Beck, S., Singh, M., Kuck, F., Jakob, S., Kefalas, A., Altinluk-Hambüchen, S., Graffmann, N., Schneider, M., Lindecke, A. et al. (2016). MicroRNA-15b regulates mitochondrial ROS production and the senescence-associated secretory phenotype through sirtuin 4/SIRT4. *Aging* **8**, 484-505. doi:10.18632/aging.100905
- Larsen, F. S., Ranek, L., Hansen, B. A. and Kirkegaard, P. (1995). Chronic portosystemic hepatic encephalopathy refractory to medical treatment successfully reversed by liver transplantation. *Transpl. Int.* **8**, 246-247. doi:10.1111/j.1432-2277.1995.tb01513.x
- Legros, F., Lombès, A., Frachon, P. and Rojo, M. (2002). Mitochondrial fusion in human cells is efficient, requires the inner membrane potential, and is mediated by mitofusins. *Mol. Biol. Cell* **13**, 4343-4354. doi:10.1091/mbc.e02-06-0330
- Li, Q., Guo, S., Jiang, X., Bryk, J., Naumann, R., Enard, W., Tomita, M., Sugimoto, M., Khaitovich, P. and Pääbo, S. (2016). Mice carrying a human *GLUD2* gene recapitulate aspects of human transcriptome and metabolome development. *Proc. Natl. Acad. Sci. USA* **113**, 5358-5363. doi:10.1073/pnas.1519261113
- Lockwood, A. H., Finn, R. D., Campbell, J. A. and Richman, T. B. (1980). Factors that affect the uptake of ammonia by the brain: the blood-brain pH gradient. *Brain Res.* **181**, 259-266. doi:10.1016/0006-8993(80)90611-3
- Lockwood, A. H., McDonald, J. M., Reiman, R. E., Gelbard, A. S., Laughlin, J. S., Duffy, T. E. and Plum, F. (1979). The dynamics of ammonia metabolism in man. Effects of liver disease and hyperammonemia. *J. Clin. Invest.* **63**, 449-460. doi:10.1172/JCI109322
- Lu, K., Zimmermann, M., Görg, B., Bidmon, H.-J., Biermann, B., Klöcker, N., Häussinger, D. and Reichert, A. S. (2019). Hepatic encephalopathy is linked to alterations of autophagic flux in astrocytes. *EBioMedicine* **48**, 539-553. doi:10.1016/j.ebiom.2019.09.058
- Martinez-Hernandez, A., Bell, K. P. and Norenberg, M. D. (1977). Glutamine synthetase: glial localization in brain. *Science* **195**, 1356-1358. doi:10.1126/science.14400
- Nissen, J. D., Pajęcka, K., Stridh, M. H., Skytt, D. M. and Waagepetersen, H. S. (2015). Dysfunctional TCA-cycle metabolism in glutamate dehydrogenase deficient astrocytes. *Glia* **63**, 2313-2326. doi:10.1002/glia.22895
- Nissen, J. D., Lykke, K., Bryk, J., Stridh, M. H., Zaganas, I., Skytt, D. M., Schousboe, A., Bak, L. K., Enard, W., Pääbo, S. et al. (2018). Expression of the human isoform of glutamate dehydrogenase, hGDH2, augments TCA-cycle capacity and oxidative metabolism of glutamate during glucose deprivation in astrocytes. *Glia* **65**, 474-488. doi:10.1002/glia.23105
- Norenberg, M. D. (1987). The role of astrocytes in hepatic encephalopathy. *Neurochem. Pathol.* **6**, 13-33. doi:10.1007/BF02833599
- Norenberg, M. D., Rao, K. V. R. and Jayakumar, A. R. (2005). Mechanisms of ammonia-induced astrocyte swelling. *Metab. Brain Dis.* **20**, 303-318. doi:10.1007/s11011-005-7911-7
- Nunnari, J., Marshall, W. F., Straight, A., Murray, A., Sedat, J. W. and Walter, P. (1997). Mitochondrial transmission during mating in *Saccharomyces cerevisiae* is determined by mitochondrial fusion and fission and the intramitochondrial segregation of mitochondrial DNA. *Mol. Biol. Cell* **8**, 1233-1242. doi:10.1091/mbc.8.7.1233
- Oenarto, J., Karababa, A., Castoldi, M., Bidmon, H. J., Görg, B. and Häussinger, D. (2016). Ammonia-induced miRNA expression changes in cultured rat astrocytes. *Sci. Rep.* **6**, 18493. doi:10.1038/srep18493
- Ong, J. P., Aggarwal, A., Krieger, D., Easley, K. A., Karafa, M. T., Van Lente, F., Arroliga, A. C. and Mullen, K. D. (2003). Correlation between ammonia levels and the severity of hepatic encephalopathy. *Am. J. Med.* **114**, 188-193. doi:10.1016/S0002-9343(02)01477-8
- Ott, P. and Vilstrup, H. (2014). Cerebral effects of ammonia in liver disease: current hypotheses. *Metab. Brain Dis.* **29**, 901-911. doi:10.1007/s11011-014-9494-7
- Patidar, K. R. and Bajaj, J. S. (2015). Covert and overt hepatic encephalopathy: diagnosis and management. *Clin. Gastroenterol. Hepatol* **13**, 2048-2061. doi:10.1016/j.cgh.2015.06.039
- Polletta, L., Vernucci, E., Carnevale, I., Arcangeli, T., Rotili, D., Palmerio, S., Steegborn, C., Nowak, T., Schutkowski, M., Pellegrini, L. et al. (2015). SIRT5 regulation of ammonia-induced autophagy and mitophagy. *Autophagy* **11**, 253-270. doi:10.1080/15548627.2015.1009778
- Rama Rao, K. V. and Norenberg, M. D. (2012). Brain energy metabolism and mitochondrial dysfunction in acute and chronic hepatic encephalopathy. *Neurochem. Int.* **60**, 697-706. doi:10.1016/j.neuint.2011.09.007
- Scaglione, S., Kliethermes, S., Cao, G., Shoham, D., Durazo, R., Luke, A. and Volk, M. L. (2015). The epidemiology of cirrhosis in the United States: a population-based study. *J. Clin. Gastroenterol.* **49**, 690-696. doi:10.1097/MCG.0000000000000208
- Schäfer, A. and Reichert, A. S. (2009). Emerging roles of mitochondrial membrane dynamics in health and disease. *Biol. Chem.* **390**, 707-715. doi:10.1515/BC.2009.086
- Schindelin, J., Arganda-Carreras, I., Frise, E., Kaynig, V., Longair, M., Pietzsch, T., Preibisch, S., Rueden, C., Saalfeld, S., Schmid, B. et al. (2012). Fiji: an open-source platform for biological-image analysis. *Nat. Methods* **9**, 676-682. doi:10.1038/nmeth.2019
- Schwaiger, M., Rampler, E., Hermann, G., Miklos, W., Berger, W. and Koellensperger, G. (2017). Anion-exchange chromatography coupled to high-resolution mass spectrometry: a powerful tool for merging targeted and non-targeted metabolomics. *Anal. Chem.* **89**, 7667-7674. doi:10.1021/acs.analchem.7b01624
- Sontheimer, H. (1995). Review: glial neuronal interactions: a physiological perspective. *Neuroscientist* **1**, 328-337. doi:10.1177/107385849500100605
- Spinelli, J. B., Yoon, H., Ringel, A. E., Jeanfavre, S., Clish, C. and Haigis, M. C. (2017). Metabolic recycling of ammonia via glutamate dehydrogenase supports breast cancer biomass. *Science* **358**, 941-946. doi:10.1126/science.aam9305
- Stewart, V. C., Sharpe, M. A., Clark, J. B. and Heales, S. J. (2000). Astrocyte-derived nitric oxide causes both reversible and irreversible damage to the neuronal mitochondrial respiratory chain. *J. Neurochem.* **75**, 694-700. doi:10.1046/j.1471-4159.2000.0750694.x
- Swain, M., Butterworth, R. F. and Blei, A. T. (1992). Ammonia and related amino acids in the pathogenesis of brain edema in acute ischemic liver failure in rats. *Hepatology* **15**, 449-453. doi:10.1002/hep.1840150316
- Tofteng, F., Hauerberg, J., Hansen, B. A., Pedersen, C. B., Jørgensen, L. and Larsen, F. S. (2006). Persistent arterial hyperammonemia increases the concentration of glutamine and alanine in the brain and correlates with intracranial pressure in patients with fulminant hepatic failure. *J. Cereb. Blood Flow Metab.* **26**, 21-27. doi:10.1038/sj.jcbfm.9600168
- Warskulat, U., Görg, B., Bidmon, H. J., Müller, H. W., Schliess, F. and Häussinger, D. (2002). Ammonia-induced heme oxygenase-1 expression in cultured rat astrocytes and rat brain in vivo. *Glia* **40**, 324-336. doi:10.1002/glia.10128
- Weber, T. A., Koob, S., Heide, H., Wittig, I., Head, B., Van Der Bliek, A., Brandt, U., Mittelbronn, M. and Reichert, A. S. (2013). APOOL is a cardiolipin-binding constituent of the Mitofilin/MINOS protein complex determining cristae morphology in mammalian mitochondria. *PLoS ONE* **8**, e63683. doi:10.1371/journal.pone.0063683
- Weiss, N., Barbier Saint Hilaire, P., Colsch, B., Isnard, F., Attala, S., Schaefer, A., Amador, M. M., Rudler, M., Lamari, F., Sedel, F. et al. (2016). Cerebrospinal fluid metabolomics highlights dysregulation of energy metabolism in overt hepatic encephalopathy. *J. Hepatol.* **65**, 1120-1130. doi:10.1016/j.jhep.2016.07.046
- Williamson, D. H., Lund, P. and Krebs, H. A. (1967). The redox state of free nicotinamide-adenine dinucleotide in the cytoplasm and mitochondria of rat liver. *Biochem. J.* **103**, 514-527. doi:10.1042/bj1030514
- Zalc, B. (1994). Astrocytes. *Pharmacol. Funct. J. Neurochem.* **63**, 1186. doi:10.1046/j.1471-4159.1994.63031186.x
- Zwingmann, C., Chatauret, N., Leibfritz, D. and Butterworth, R. F. (2003). Selective increase of brain lactate synthesis in experimental acute liver failure: results of a [ $^3\text{H}$ -lactate] nuclear magnetic resonance study. *Hepatology* **37**, 420-428. doi:10.1053/jhep.2003.50052

## Supplementary Material and Methods

### qPCR for *GLUD* knock-down validation

Human astrocytoma cells were seeded and transfected as described before. RNA extraction with All Prep RNA/Protein Kit (Qiagen, Hilden, Germany) according to the manufacturer's instructions. RNA was reverse transcribed to cDNA with QuantiNova Reverse Transcription Kit (Qiagen, Hilden, Germany) according to the manufacturer's instructions. 10 ng cDNA was used for qPCR with Rotorgene 6000 system (Corbett Research, now Qiagen, Hilden, Germany) with the QuantiNova SYBR Green PCR Kit (Qiagen, Hilden, Germany) according to the manufacturer's instructions. Analysis was performed using Rotor-Gene Q Series Software (Qiagen, Hilden, Germany) employing the  $\Delta\Delta C_t$  method. HPRT1 was used as housekeeping gene. qPCR primer: GLUD2 forward: 5'-cggcagagtccaagacagt-3'; GLUD2 reverse: 5'-gaacgctccattgtatgc-3'; HPRT1 forward: 5'-cctggcgtcgtgattagtg-3'; HPRT1 reverse: 5'-tgaggataaacacccctttcca-3'.

### Construction of HeLa-SIRT4-eGFP cells

The cDNAs for eGFP and the human SIRT4-eGFP fusion protein were generated by PCR using pEGFP-N1 and pcDNA3.1-SIRT4-eGFP [1] as templates, respectively, and subsequently cloned via *NheI* and *XhoI* restriction sites into puc2CL12IPwo derived from plasmids generated earlier [2, 3]. Constructs were verified by Sanger DNA sequencing. HEK293T cells were transfected as described [2, 3] using polyethylenimine transfection reagent (Sigma-Aldrich, Taufkirchen, Germany) with HIV1 helper plasmid (pCD/NL-BH) [4], envelope vector (pczVSV-G) [5], and the newly generated plasmids puc2CL12eGFPIPwo or puc2CL12SIRT4-eGFPIPwo (both containing an IRES-PuroR cassette). Viral supernatants were harvested 48 h after transfection, filtered through 0.45  $\mu$ m filters (Sartorius AG, Göttingen, Germany), and used to transduce HeLa cells. Selection with 2  $\mu$ g/ml puromycin (InvivoGen, San Diego CA, USA) was started 96 h after transduction and eGFP positivity was tracked by flow cytometry (BD FACSCanto II, BD Biosciences, Franklin Lakes NJ, USA) in the FITC-A channel using non-transduced HeLa cells as negative control.

### Western Blot

Cells were treated as described previously and harvested with RIPA-buffer (Tris-HCl, NaCl, Triton X-100, sodium deoxycholate, SDS, EDTA, pH 7.4) with Complete protease inhibitor (Roche Diagnostics, Basel, Switzerland) and protein concentration was measured using a Bradford assay (Sigma-Aldrich, Taufkirchen, Germany). Proteins were separated with SDS-PAGE (12 % for GDH2 and SIRT4-eGFP, 10 % for SIRT4, 15 % for UQCRC2, COX8A and NDUFB4), blotted on a nitrocellulose membrane (Amersham, VWR, Radnor PA, USA), and blocked for 1 h with 5% fat-free milk powder solution (Carl Roth GmbH & Co. KG, Karlsruhe, Germany) in TBS. In case of SIRT4 membrane was blocked in 3% BSA (Sigma-Aldrich, Taufkirchen, Germany) solution in TBS-T. Primary antibody against GDH2 (Santa Cruz Biotechnology, Dallas TX, USA, sc-293459) was used at a 1:250 dilution over night; HSP60 antibody (Sigma-Aldrich, Taufkirchen, Germany, SAB4501464) as loading control was used at a 1:10,000 dilution for 1 h at RT. SIRT4 antibody (Proteintech, Rosemont IL, USA, 66543-1-Ig) was used 1:20,000 in TBS-T over night; UQCRC2 (Abcam, Cambridge, UK, ab14745) and COX8A (Thermo Fisher Scientific, Carlsbad CA, USA, PA567695) 1:1000 in 5% fat-free milk powder solution and NDUFB4 (Abcam, Cambridge, UK, ab110243) 1:2000 in 5% milk solution overnight. Loading controls GAPDH (Sigma-Aldrich, Taufkirchen, Germany, G8795) and Tubulin (Cell Signalling Technology, Danvers MA, USA, 2128S) were detected with 1:2000 antibody dilution in 5% milk solution overnight. Respective secondary antibody was decorated in 5% milk solution 1:10,000 at room temperature for 1 h, for SIRT4 antibody was diluted in TBS-T. Blots were developed using Signal Fire ECL Reagent (Cell Signaling Technology, Danvers MA, USA) and visualized using the Fusion SL Gel Documentation System (PEQLAB, Germany).

## References

- [1] Lang A, Anand R, Altinluk-Hambüchen S, Ezzahoini H, Stefanski A, Iram A, et al. SIRT4 interacts with OPA1 and regulates mitochondrial quality control and mitophagy. *Aging*. 2017;9:2163-89.
- [2] Roellecke K, Virts EL, Einholz R, Edson KZ, Altvater B, Rossig C, et al. Optimized human CYP4B1 in combination with the alkylator prodrug 4-ipomeanol serves as a novel suicide gene system for adoptive T-cell therapies. *Gene therapy*. 2016;23:615-26.
- [3] Wiek C, Schmidt EM, Roellecke K, Freund M, Nakano M, Kelly EJ, et al. Identification of Amino Acid Determinants in CYP4B1 for Optimal Catalytic Processing of 4-Ipomeanol. *The Biochemical journal*. 2015;465:103-14.
- [4] Zhang X-Y, Russa VFL, Reiser J. Transduction of Bone-Marrow-Derived Mesenchymal Stem Cells by Using Lentivirus Vectors Pseudotyped with Modified RD114 Envelope Glycoproteins. *Journal of virology*. 2004;78:1219-29.
- [5] Pietschmann T, Heinkelein M, Heldmann M, Zentgraf H, Rethwilm A, Lindemann D. Foamy Virus Capsids Require the Cognate Envelope Protein for Particle Export. *Journal of virology*. 1999;73:2613-21.



**Table S2. Raw data for targeted metabolite abundances measured via GC-MS from human astrocytoma cells treated with 5 mM NH<sub>4</sub>Cl and harvested immediately afterwards (0 h).**

	Glutamic acid
control_1	0.1904
control_2	0.2758
control_3	0.4481
0 h_1	3.0199
0 h_2	3.0735
0 h_3	2.6139

**Table S3. Summary of quantification method for <sup>15</sup>N-labeled amino acids measured via LC-QTOF.** Shown are all theoretically possible isotopomers after <sup>15</sup>N-labeling. Isotopomer masses colored in red could not be determined in any sample due to sensitivity or absence in the sample. Natural abundances were retrieved from MassHunter Isotope Distribution Calculator version B7024.29.

Compound	Formula	Retention time (min)	Mass of isotopomer (m/z)				Natural abundance of isotopomer (%)					
			m0	m1	m2	m3	m4	m0	m1	m2	m3	m4
alpha-Alanine	C3H7NO2	2.92	90.05495	91.05779				95.91521	3.62391			
Arginine	C6H14N4O2	20	175.11895	176.12125	177.12328	178.12547	179.12755	91.7848	7.52586	0.65109	0.03661	0.00158
Asparagine	C4H8N2O3	3.39	133.06077	134.06332	135.06512			94.30294	4.97424	0.68922		
Aspartate	C4H7NO4	2.2	134.04478	135.04775				94.42833	4.66098			
Cysteine	C3H7NO2S	2.58	122.02703	123.02926				91.10993	4.16172			
Glutamate	C5H9NO4	2.66	148.06043	149.06348				93.39646	5.64169			
Glutamine	C5H10N2O3	3.63	147.07642	148.07912	149.08089			93.27244	5.95014	0.73626		
Glycine	C2H5NO2	2.5	76.0393	77.0419				96.97491	2.59279			
Histidine	C6H9N3O2	14.36	156.07675	157.07927	158.08125	159.08356		92.1731	7.16796	0.62333	0.03412	
Isoleucine	C6H13NO2	6.2	132.10191	133.10501				92.8051	6.58171			
Leucine	C6H13NO2	5.72	132.10191	133.10501				92.8051	6.58171			
Lysine	C6H14N2O2	11.37	147.11128	148.11562	149.11753			92.45666	6.9054	0.60417		
Methionine	C5H11NO2S	4.2	150.05833	151.06095				89.12962	6.04027			
Phenylalanine	C9H11NO2	6.56	166.08626	167.08943				89.87849	9.26979			
Proline	C5H9NO2	2.88	116.0706	117.07364				93.85202	5.5977			
Serine	C3H7NO3	2.32	106.04987	107.05272				95.68214	3.65155			
Threonine	C4H9NO3	2.6	120.06552	121.06849				94.63657	4.65698			
Tryptophan	C11H12N2O2	11.13	205.09715	206.10019	207.10256			87.63511	11.26432	1.02654		
Tyrosine	C9H11NO3	4.2	182.08117	183.08435				89.66009	9.28141			
Valine	C5H11NO2	4	118.08626	119.0893				93.83044	5.618			

**Table S4. Raw data from quantification method for <sup>15</sup>N-labeled amino acids measured via LC-QTOF.**

rel. enrichment m+1	alpha-Alanine	Aspartate	Glutamate	Histidine	Isoleucine	Leucine	Proline	Valine
control_1	0	0.40090837	0.47125559	0.91527038	0	0.05577544	0	0.20031903
control_2	0	0.48510137	1.19260657	0.37448333	0	0.80310617	0.34308631	0
control_3			1.29267167	0	0	0	0	0
1 h_1	1.04923406	7.42071568	7.30439269	2.4884458	1.10860703	1.10742484	3.82161783	0
1 h_2	1.1342786	5.57061267	8.08730538	1.33380341	0.51222767	0.16596954	4.38318515	0.54090537
1 h_3	1.4235847	11.7719037	7.05797965	2.94279624	1.56580823	1.87013479	3.25527612	0
2 h_1	1.02353373	4.94454043	10.6995843	0	1.6910971	2.21479582	7.38352294	0.94699479
2 h_2	1.50847976	11.6258644	9.14597736	0.15150108	2.01387955	4.44076122	6.13227587	0.77000518
2 h_3	1.63380619	7.96397967	10.0765488	3.40861241	1.21635719	1.44060611	6.73474321	0.31476989
4 h_1	2.77573225	17.8409345	22.2289823	0.73633046	2.64423697	4.70825532	15.2264821	1.21290403
4 h_2	1.58387165	15.1567539	19.8113117	0.27736634	2.20542332	4.1037447	13.5017598	1.15444201
4 h_3	3.25053851	17.4705266	22.8746761	0	3.05079323	5.74084546	15.1134947	1.43422227
6 h_1	1.48273715	11.1146972	15.724708	0.07174415	2.13343836	3.26234773	12.6294388	1.31192073
6 h_2	1.04540805	10.6964563	14.9846617	0.40007852	2.37162829	4.13902977	11.8173998	1.51042917
6 h_3	1.81965465	15.2847053	18.0640338	0	3.12946529	4.56325965	14.8371646	1.8754336
24 h_1	1.91397889	15.4363329	20.3238226	0.52366814	2.48802449	3.60320655	18.6531695	1.21526608
24 h_2	2.22740472	16.250518	20.3090225	0	2.99205761	5.24440308	18.3253367	1.25429893
24 h_3	2.47775372	16.5117326	18.2038927	1.00092673	3.74397819	5.57323623	17.2402266	2.17686156
48 h_1	1.50324848	8.96337872	12.0635386	0.29616694	2.46188169	3.6951194	11.187649	0.76294907
48 h_2	1.31638932	9.8710555	13.2015612	0	2.05882482	3.43128094	12.2095382	0.93567938
48 h_3	1.2572175	10.4702217	14.2606943	0.48794577	2.39205954	3.96856915	11.7648981	3.40078421

Shown are only metabolites with a relative enrichment of <sup>15</sup>N of at least 1 % at any time point.

**Data analysis for <sup>15</sup>N-labeled amino acids.** Amino acid peaks in the samples were identified at mass-to-charge (m/z) ratios and retention times (RT) listed above and with external amino acid standards measured in parallel. Peaks were integrated via Agilent Mass Hunter Workstation B07 (Agilent Technologies, Santa Clara CA, USA). Peak intensities of m1 (i.e. incorporation of one <sup>15</sup>N-label) were corrected for their natural abundance via the following calculation.

m0<sub>int</sub>, peak intensity of non-labelled amino acid; m1<sub>int</sub>, peak intensity of amino acid with one <sup>15</sup>N-label (m+1); m1<sub>nat</sub>, natural abundance of isotopomer (see above);  
 $m1_{background} = m0_{int} \cdot m1_{nat} \cdot 100$ ;  $m1_{enrichment} = m1_{int} - m1_{background}$ ;  $m1_{relative.enrichment} = m1_{enrichment} : m0_{int} \cdot 100$

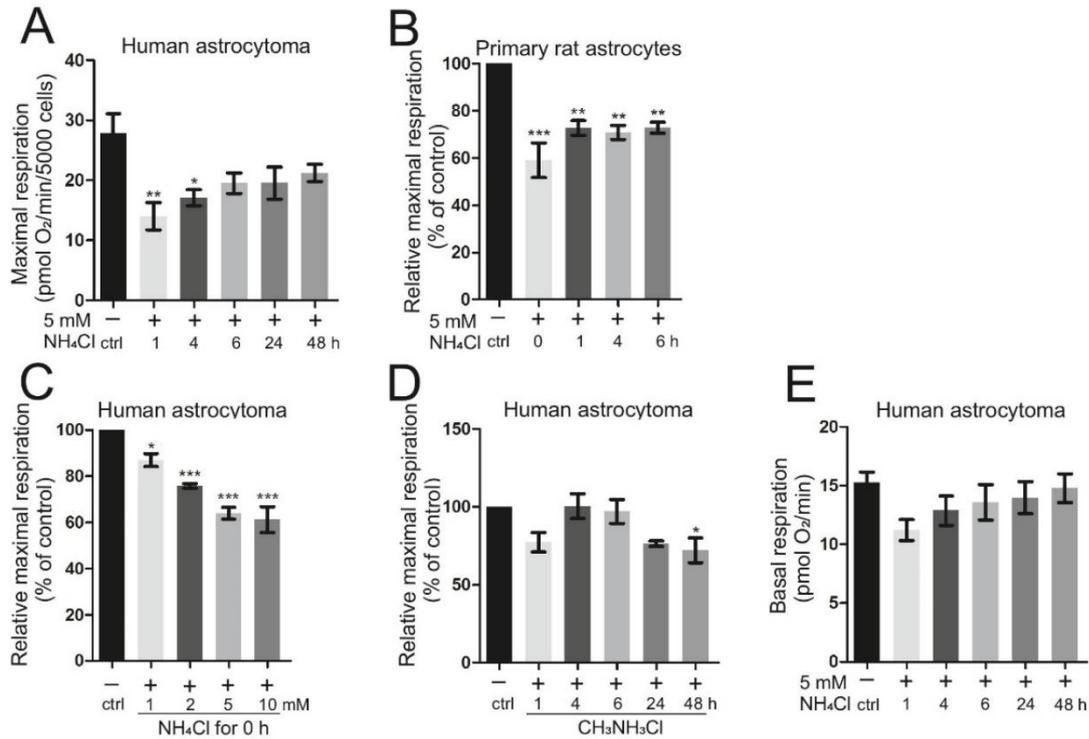


**Figure S1: Mitochondrial respiration is immediately impaired by ammonia in a pH-independent manner.** Oxygen consumption rate (OCR) of human astrocytoma cells and primary rat astrocytes was analyzed in Seahorse XFe96 Extracellular Flux Analyzer with the Mito Stress Test Kit after treatment with ammonia at indicated molarities or durations. (A) Maximal respiration of human astrocytoma cells after treatment with 5 mM NH<sub>4</sub>Cl for 1-48 h (n=5-7). (B) Relative maximal respiration of primary rat astrocytes after treatment with 5 mM NH<sub>4</sub>Cl for 1-6 h and directly after treatment (0 h) (n=3-4). (C) Relative maximal respiration of human astrocytoma cells and directly after treatment (0 h) with 1, 2, 5, or 10 mM NH<sub>4</sub>Cl (n=3). (D) Relative maximal respiration of human astrocytoma cells was determined after treatment with 5 mM CH<sub>3</sub>NH<sub>2</sub>Cl (pH-mimetic) for 1-48 h (n=3). (E) Basal respiration of human astrocytoma cells treated with 5 mM NH<sub>4</sub>Cl for 1-48 h (n=8). (B), (C), (D) Individual biological replicates normalized to control (100%) are depicted. Data presented as mean ± SEM. Statistics: One-way ANOVA with Dunnett's post test (all treatments vs. control). \*P < 0.05, \*\*P < 0.01, \*\*\*P < 0.001.

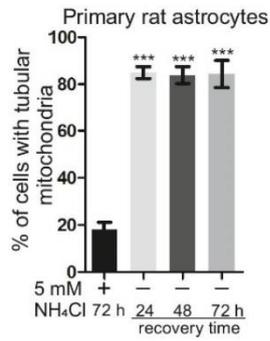


**Figure S2: Ammonia-induced mitochondrial fragmentation is reversible.** Primary rat astrocytes transfected with pEGFP-Mito. Baseline quantification was performed after 72 h treatment with 5 mM NH<sub>4</sub>Cl. Other time points represent recovery time periods after removal of ammonia. Characterization of mitochondria with respect to fragmented versus tubular morphology. Data represented mean  $\pm$  SD (n=3). One-way ANOVA with Dunnett's post test (all treatments vs. control). \*\*\*P < 0.001.

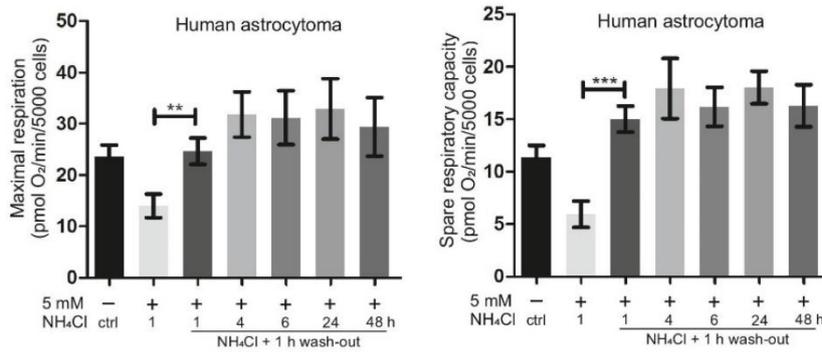
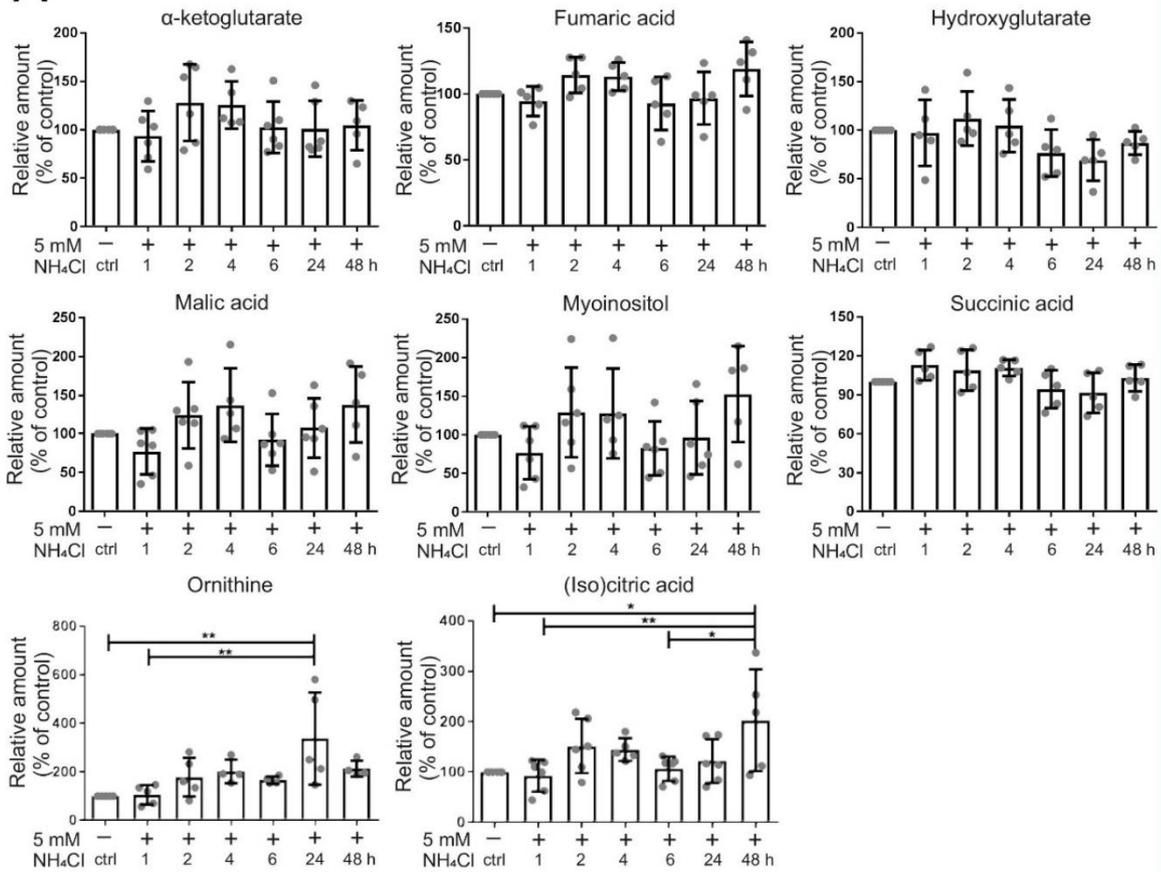


**Figure S3: Ammonia-induced decrease in oxygen consumption rate is rapidly reversible.** Human astrocytoma cells were analyzed using the Mito Stress Test Kit on Seahorse XFe96 Extracellular Flux Analyzer. Oxygen consumption rate (OCR) of maximum respiration (left) and spare respiratory capacity (right) were determined after 1 h wash-out of ammonia treated with 5 mM NH<sub>4</sub>Cl for 1-48 h and compared to 1 h treatment 5 mM NH<sub>4</sub>Cl. Data represented as mean ± SEM (n=3). Student's t-test, one-tailed, unpaired. \*\* P < 0.01, \*\*\* P < 0.001.

A



Disease Models & Mechanisms • Supplementary information

Figure S4A

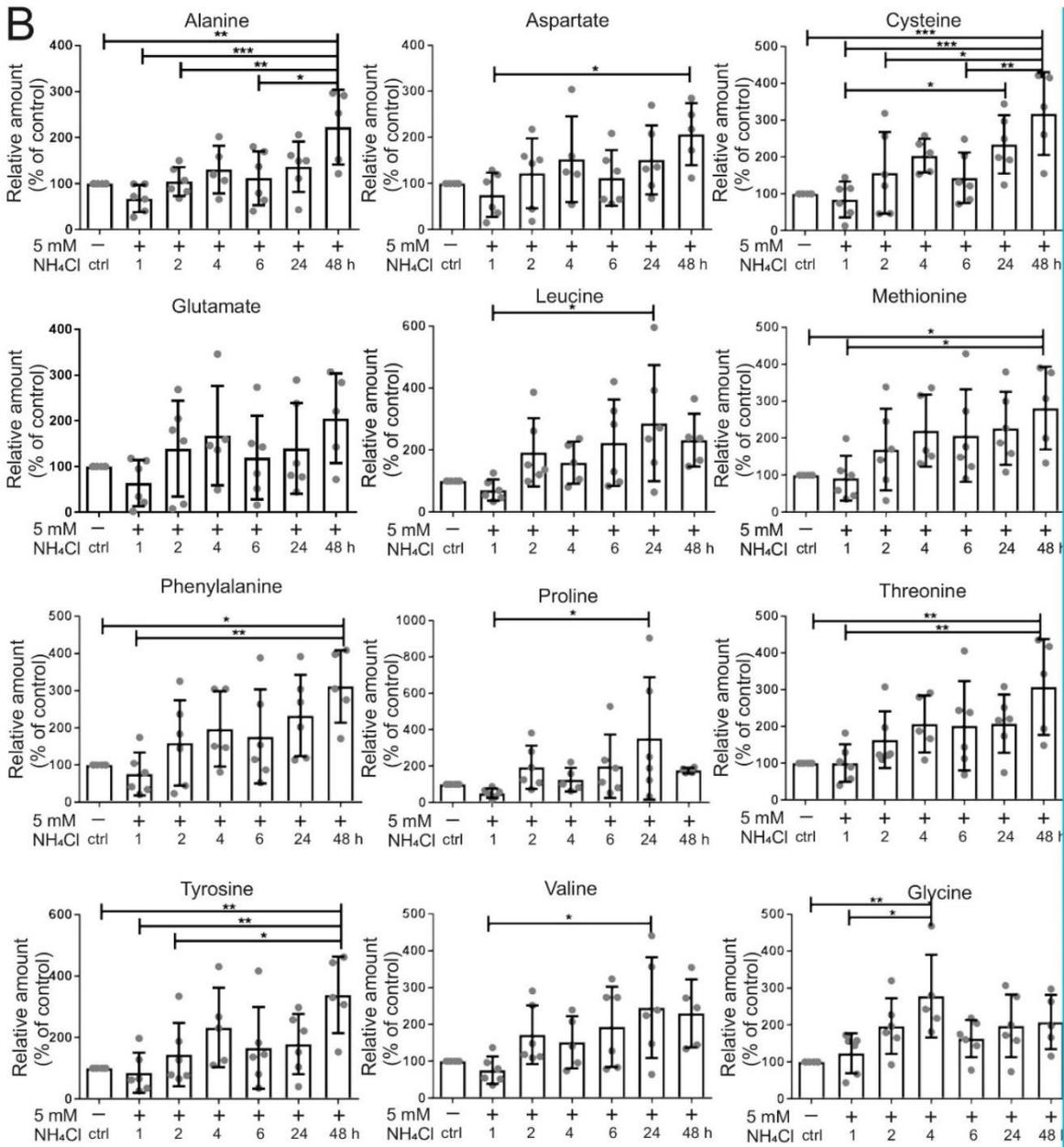


**Figure S4: Extended data from steady-state metabolomics.** Mass Spectrometry for steady-state metabolites was done in human astrocytoma cells on GC-QTOF. Treatment with 5 mM NH<sub>4</sub>Cl for 1-48 h. Relative abundance of respective metabolites compared to controls (100 %) over time. (A) Additional non-amino-acid metabolites and details not shown in the heat map of Fig. 4A or Fig. 4B. (B) Additional details for detected amino acids shown in the heat map of Fig. 4A or Fig. 4B. Data represent mean  $\pm$  SD (n=4-6). Statistics: One-way ANOVA with Tukey's post test (all samples vs. all samples). \*P < 0.05, \*\*P < 0.01, \*\*\*P < 0.001.

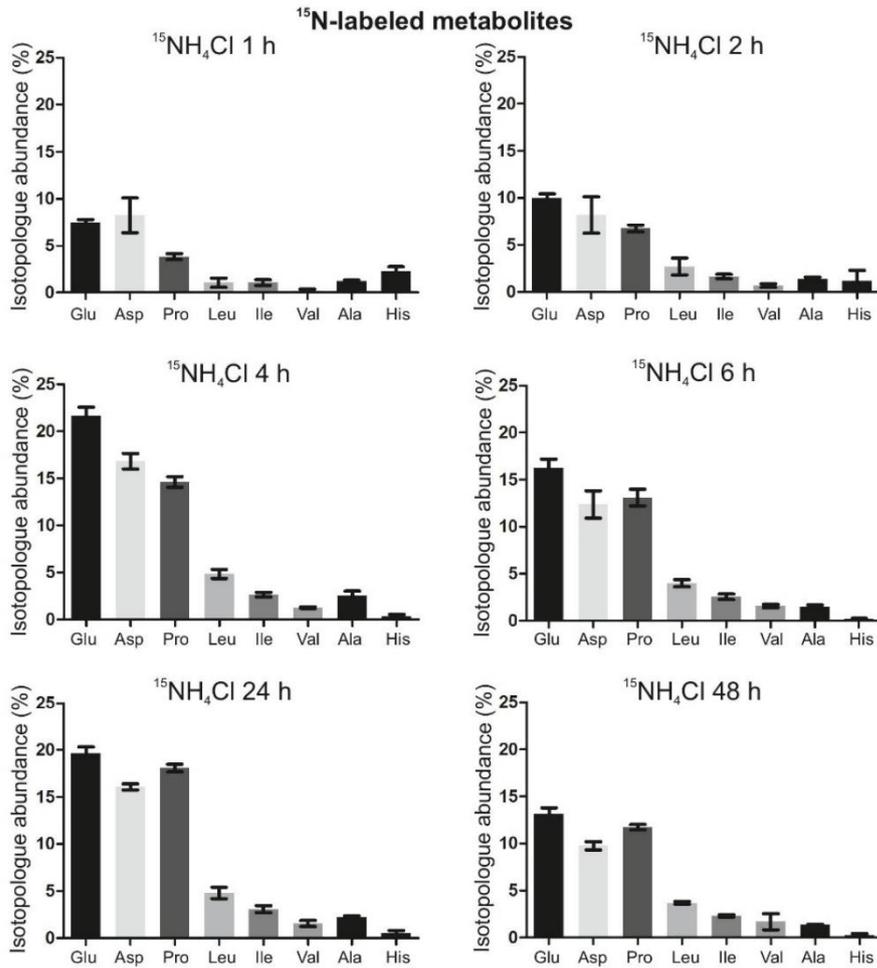


**Figure S5: <sup>15</sup>N-isotopologue abundance of labeled amino acids over time.** Mass Spectrometry for ammonia flux was done in human astrocytoma cells on LC-QTOF. Cells were treated with <sup>15</sup>NH<sub>4</sub>Cl for 1-48 h and isotopologue abundance of <sup>15</sup>N in Glu, Asp, Pro, Leu, Ile, Val, Ala and His was determined over time. Data represent mean ± SD (n=3).

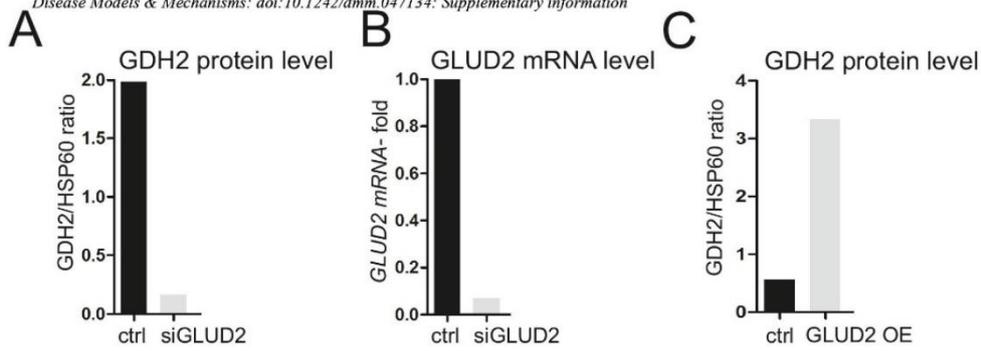


**Figure S6: Protein and/or mRNA level of glutamate dehydrogenase after *GLUD2* knock-down and overexpression.** *GLUD2* knock-down validation in human astrocytoma cells. (A) Densitometry of protein levels determined by Western blot analysis (Fig. 6A) using HSP60 as loading control. Ratios of GDH2 to HSP60 levels are shown in knock-down vs. control cells. (B) mRNA level was determined by qPCR using HPRT1 as housekeeping gene. *GLUD2* expression levels are depicted in knock-down cells as compared to control and normalized to 1. (C) Densitometry of protein levels determined by Western blot analysis (Fig. 6A) to validate overexpression (OE) of *GLUD2* normalized to loading control HSP60. Representative experiments are shown.

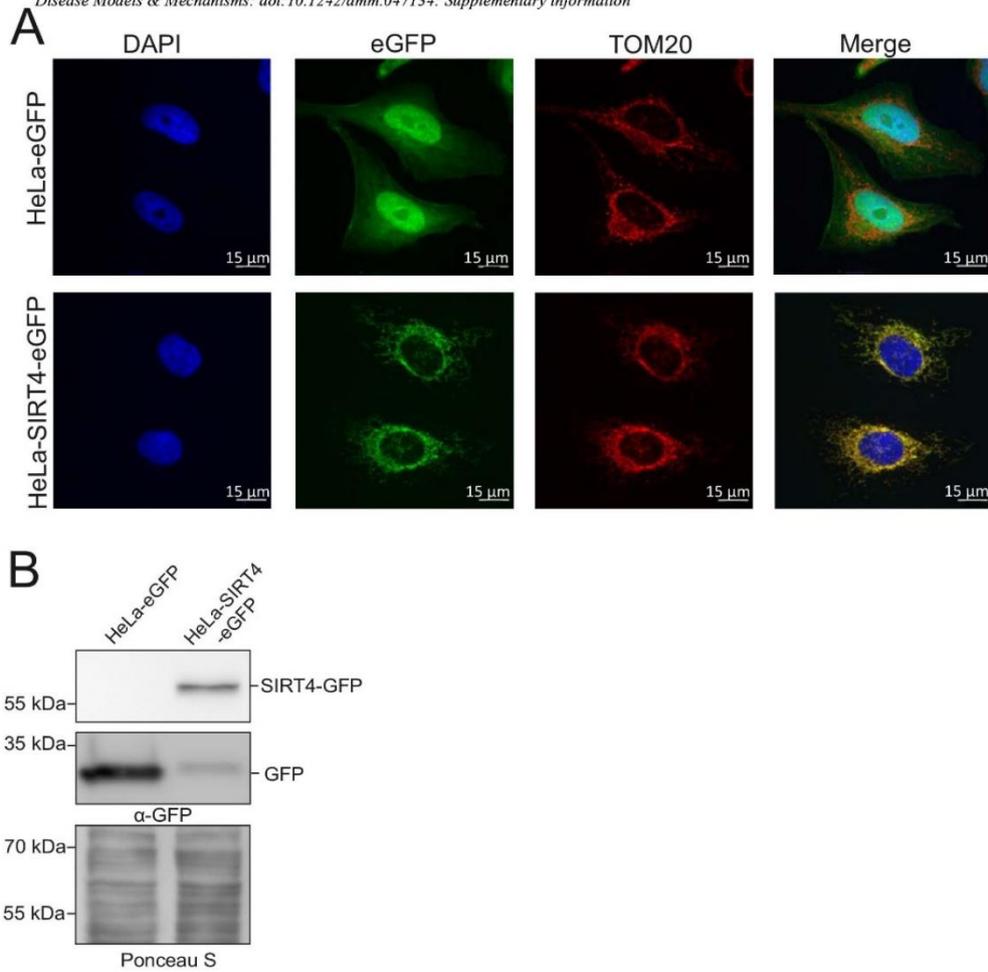


**Figure S7: Expression of SIRT4 and localization to mitochondria.** (A) Representative images showing the localization of SIRT4-GFP to mitochondria. Immunostaining against TOM20 (mitochondria) and DAPI (nucleus) staining in HeLa-eGFP and HeLa-SIRT4-eGFP cells. (B) Western blot showing the overexpression of SIRT4-eGFP construct in HeLa-eGFP vs. HeLa-SIRT4-eGFP cells. Ponceau S staining to control for loading.

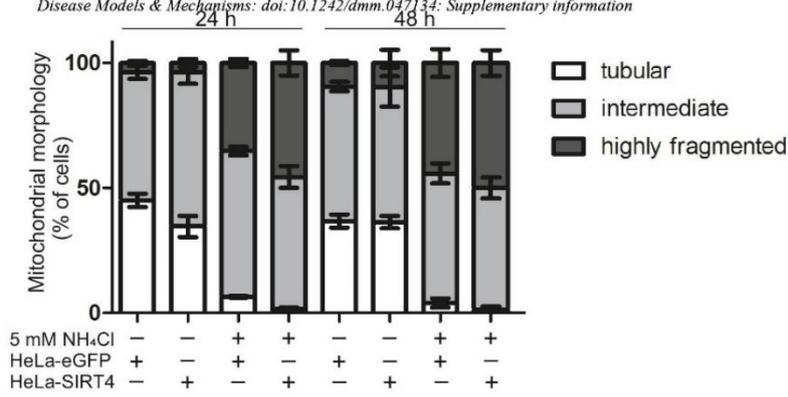


**Figure S8: SIRT4 overexpression does not restore ammonia-induced changes in mitochondrial morphology.** Mitochondria in HeLa-eGFP and HeLa-SIRT4-eGFP cells were visualized by immunostaining against TOM20. Cells were treated with 5 mM NH<sub>4</sub>Cl for respective duration 24 or 48 h. At least 20 pictures were taken per sample showing approximately 10-15 cells each. Mitochondria were categorized to tubular, intermediate and fragmented morphological phenotype and morphological changes are depicted over time. Percentage of cells with respective phenotype are shown. Data presented as mean ± SEM (n=3).

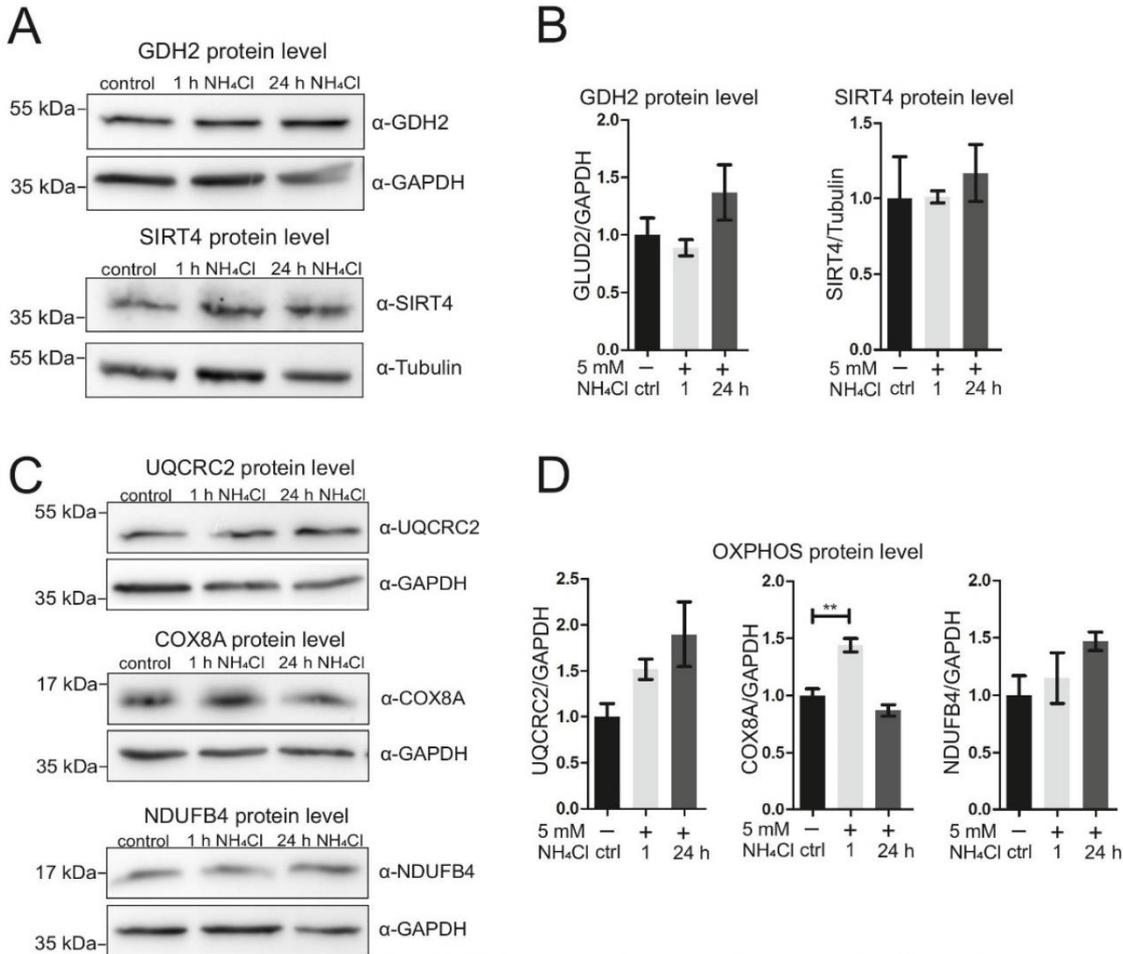


**Figure S9: Changes in protein levels of GDH2, SIRT4 and OXPPOS enzymes.** (A) Representative Western blots of GDH2 and SIRT4 protein levels after treatment with 5 mM NH<sub>4</sub>Cl for 1 or 24 h compared to control. GAPDH and Tubulin are used as a loading control, respectively. (B) Densitometry of Western blots shown in A corrected to respective loading control and normalized to control. (C) Representative Western blots showing protein levels of UQCRC2 (complex III), COX8A (complex IV) and NDUFB4 (complex I) after treatment with 5 mM NH<sub>4</sub>Cl for 1 or 24 h compared to control. GAPDH is used as a loading control. (D) Densitometry of Western blots shown in C corrected to GAPDH and normalized to control. Data presented as mean ± SEM (n=3). Statistics: One-way ANOVA with Dunnett's post test (all treatments vs. control). \*\*P < 0.01.

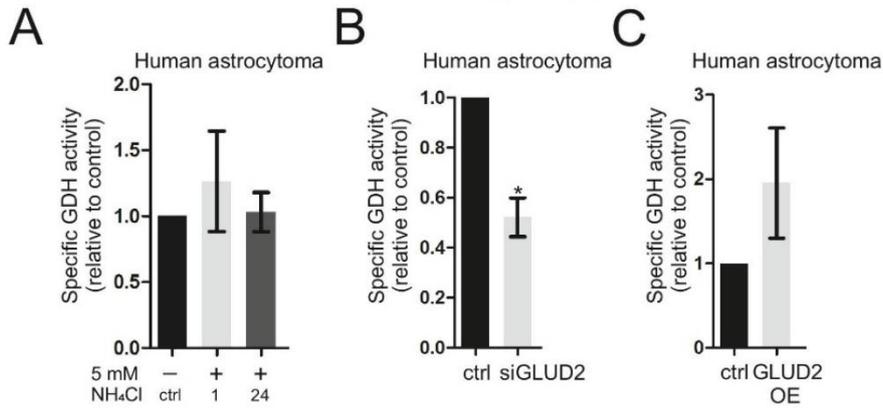


**Figure S10: Ammonia treatment alone does not grossly affect specific GDH activity.** (A) Human astrocytoma cells were treated with 5 mM NH<sub>4</sub>Cl for 1 or 24 h and GDH activity was measured in  $1 \times 10^6$  cells. (B) *GLUD2* knock-down was done in human astrocytoma cells using a GDH-targeting siRNA for 48 h. Knockdown is validated by reduction in GDH activity. (C) GDH2 was overexpressed in human astrocytoma cells for 48 h. Overexpression of GDH2 is corroborated by increased GDH activity. GDH activity was determined by a commercial assay detecting NADH production. Values were individually normalized to control and normalized to total protein content using a Bradford assay. Data is presented as mean  $\pm$  SEM (n=3). Statistics: One-sample t-test. \* P < 0.05.

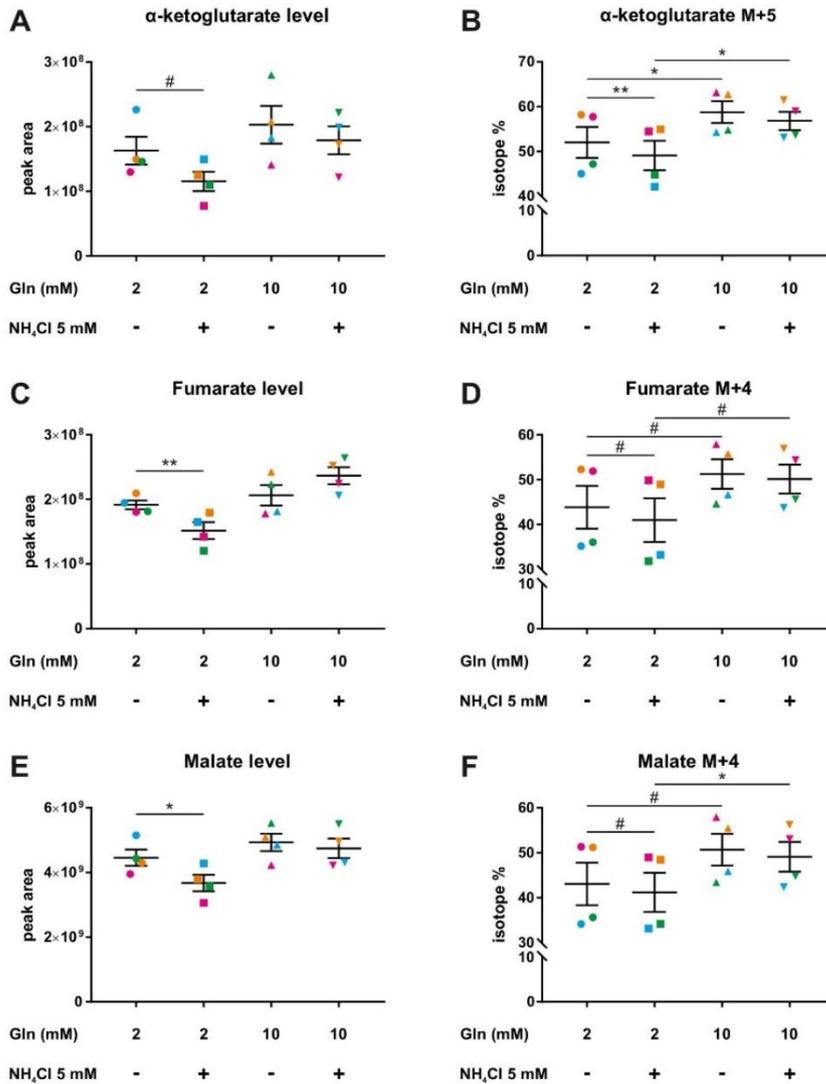


**Figure S11. Ammonia reduces the influx of carbon into the TCA-cycle from isotope labeled glutamine.** MOG-G-CCM cells were grown to confluency and were exposed to fresh growth medium containing 2 or 10 mM <sup>13</sup>C-labeled glutamine and 0 or 5 mM NH<sub>4</sub>Cl for 40 minutes before cell harvest. The levels of aKG, fumarate and malate as well as their isotope distributions were analyzed via IC-MS in 4 independent experiments. Results are shown as individual experiments in different colors and mean ±SEM. Statistical analysis was conducted with paired one-way ANOVA with Geisser-Greenhouse correction and Sidak's multiple comparison post-hoc test comparing 2 mM Gln vs. 2 mM Gln + NH<sub>4</sub>Cl, 2 mM Gln vs. 10 mM Gln, 2 mM Gln + NH<sub>4</sub>Cl vs. 10 mM Gln + NH<sub>4</sub>Cl, and 10 mM Gln vs. 10 mM Gln + NH<sub>4</sub>Cl. Only significant comparisons are indicated (# P<0.1, \* P<0.05, \*\* P<0.01). At 10 mM Gln addition of ammonia shows no significant alterations of TCA-cycle intermediates.

Figure S11

### 6.3. Subcellular localization and mitotic interactome analyses identify SIRT4 as a centrosomally localized and microtubule associated protein

**Bergmann L**, Lang A, Bross C, Altinoluk-Hambüchen S, Fey I, Overbeck N, Stefanski A, Wiek C, Kefalas A, Verhülsdonk P, Mielke C, Sohn D, Stühler K, Hanenberg H, Jänicke RU, Scheller J, Reichert AS, Ahmadian MR, Piekorz RP. *Cells*. 2020 Aug 24;9(9):1950. doi: 10.3390/cells9091950. PMID: 32846968; PMCID: PMC7564595. [263]

Diese Arbeit identifiziert eine zusätzliche und bisher unbekannte Funktion für das mitochondrial klassifizierte Sirtuin SIRT4 als zentrosomales und spindelassoziertes Enzym. Die Befunde sprechen insgesamt für eine neue extramitochondriale Funktion von SIRT4 als Tumorsuppressor in der Zellzyklusprogression und mitotischen Zellteilung, wobei letzteres im Zusammenhang mit chromosomaler Stabilität und Zelltransformation steht.

Eine subzelluläre Lokalisierung von endogen exprimiertem SIRT4 konnte mittels spezifischer Antikörper und konfokaler *Laserscanning*- und *Spinning Disk*-Mikroskopie an Interphasen- und mitotischen Zentrosomen und teilweise an der mitotischen Spindel in verschiedenen menschlichen Zelllinien beobachtet werden. Zusätzlich zu endogenem SIRT4 wurde auch ein C-terminales SIRT4-eGFP-Fusionsprotein lokalisiert an Zentrosomen im Zellzyklus nachgewiesen.

Eine quantitative Signalanalyse nach *Spinning Disk* Mikroskopie zeigte in HeLa-Zervixkarzinomzellen, dass endogenes SIRT4 eine dynamische Lokalisationskinetik am Zentrosom während der Zellzyklusprogression aufweist. Dabei wurde die höchste Signalintensität in der G<sub>2</sub>-Phase und frühen Mitose detektiert, gefolgt von einem signifikanten Abfall der Signalintensität von der Prophase bis zur späten Mitose/Zytokinese. Zusätzlich konnte mittels einer subzellulären Fraktionierung eine zytosolische Anreicherung von SIRT4, nicht aber von SIRT3, außerhalb der Mitochondrien bestätigt werden.

Angesichts der in der Literatur beschriebenen Stress-induzierten/DNA-Schaden-assoziierten Hochregulation von SIRT4 und seiner antiproliferativen Rolle wurde im nächsten Schritt die hemmende Funktion von SIRT4 auf die mitotische Zellteilung und Zellproliferation mittels Lebendzellaufnahmen (*live cell imaging*) und der Messung von Proliferationskinetiken analysiert. Die ektopische Überexpression von SIRT4-eGFP

oder der ausschließlich extramitochondrial lokalisierten Deletionsmutante SIRT4( $\Delta$ N28)-eGFP hemmt hierbei die Progression durch die mitotische Zellteilung und somit die Zellproliferation von HEK293 Zellen. Bemerkenswert ist, dass die Expression von SIRT4( $\Delta$ N28)-eGFP mit einem fast dreifachen Anstieg von bi- bis multinukleären Zellen als wahrscheinliche Folge einer gestörten Mitose einherging. Um die molekularen Mechanismen der extramitochondrialen SIRT4-Funktion aufzuklären, wurde eine massenspektrometrische SIRT4-Interaktomanalyse an G<sub>2</sub>/M-synchronisierten, SIRT4-eGFP exprimierenden HEK293-Zellen vorgenommen. Hierbei ließen sich neben mehreren mitochondrialen, SIRT4-bindenden bzw. interagierenden Proteinen und potenziellen Substraten (OPA1, ATP5F1A, ANT2, IDE) auch meist neuartige, extramitochondrial lokalisierte SIRT4-Interaktoren identifizieren. Letztere umfassen  $\alpha$ - und  $\beta$ -Tubulin als Untereinheiten von Mikrotubuli, Komponenten des zentrosomal lokalisierten  $\gamma$ TuRC ( $\gamma$ -Tubulin, TUBGCP2, TUBGCP3), die Mikrotubuli-Deacetylase HDAC6, die entscheidend an der Regulation der Stabilität und Dynamik der Mikrotubuli beteiligt ist, sowie den G<sub>2</sub>/M-Zellzyklus-Regulator CDK1. Eine schematische Übersicht der dualen Lokalisation von SIRT4 ist in Abbildung 9 aufgeführt.

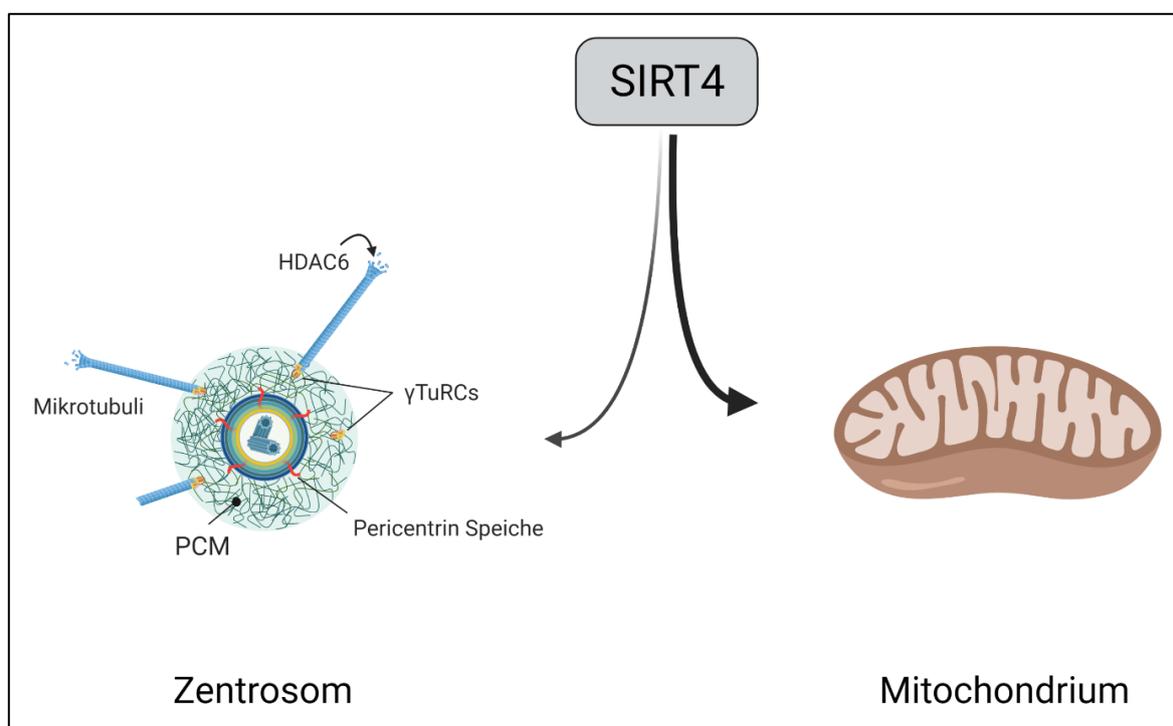


**Abbildung 9:** Darstellung der dualen Lokalisation von SIRT4 vorrangig im Mitochondrium und extramitochondrial am Zentrosom. Mit aufgeführt sind die in der massenspektrometrischen SIRT4-Interaktomanalyse identifizierten Interaktionspartner aus dem Bereich der Zentrosomenbestandteile, sowie Mikrotubuli Regulation. Erstellt mit BioRender.com

Angesichts der Interaktion zwischen SIRT4 und Proteinen des Mikrotubuli-Netzwerkes wurde die Bindung von SIRT4 an zelluläre Mikrotubuli und die Rolle von SIRT4 bei der HDAC6-vermittelten Regulation der Mikrotubuli-Dynamik untersucht. Dabei konnte beobachtet werden, dass es nach Überexpression von SIRT4-eGFP, nicht aber der katalytisch inaktiven Mutante SIRT4(H161Y)-eGFP, zu einer starken Abnahme des Lysin 40 (K40)-acetylierten  $\alpha$ -Tubulin in G<sub>2</sub>-synchronisierten HEK293-Zellen kam. Diese Ergebnisse lassen vermuten, dass die SIRT4-HDAC6 Achse in SIRT4 enzymatisch abhängiger Weise über die Deacetylierung von K40  $\alpha$ -Tubulin die Mikrotubuli-Dynamik in der G<sub>2</sub>/M-Phase des Zellzyklus reguliert. Hierbei wird anscheinend die Stabilität der Mikrotubuli verringert, was in einer Hemmung der mitotischen Progression und Proliferation resultieren könnte.

Zusammengenommen konnte in der Arbeit gezeigt werden, dass SIRT4 neben seinen bereits bekannten regulatorischen Aufgaben im mitochondrialen Metabolismus sehr wahrscheinlich auch eine regulatorische Rolle in der Zellzyklusprogression einnimmt. Dabei könnte diese durch die hier erstmals beschriebenen extramitochondrialen Mechanismen, aber auch mitochondrial durch eine bioenergetische Regulation vermittelt werden.

Die Autorin der vorliegenden Dissertation erarbeitete ca. 75% der Befunde dieser Publikation. Hierbei wurde der Großteil der Experimente durchgeführt und ausgewertet. Die Koautoren halfen bei Methoden wie der Massenspektrometrie, Lebendzellaufnahmen, Wachstumskurven, Nanobody- und  $\alpha$ -Tubulin-Co-Immunopräzipitation, Mikrotubuli-Pulldown Experimenten und unterstützenden Mikroskopie-Aufnahmen. Des Weiteren waren die Koautoren in die Zusammenstellung, Diskussion und Revision der Publikation involviert.

Article

# Subcellular Localization and Mitotic Interactome Analyses Identify SIRT4 as a Centrosomally Localized and Microtubule Associated Protein

Laura Bergmann <sup>1</sup>, Alexander Lang <sup>1,†</sup>, Christoph Bross <sup>1</sup>, Simone Altinluk-Hambüchen <sup>1</sup>, Iris Fey <sup>1</sup>, Nina Overbeck <sup>2</sup>, Anja Stefanski <sup>2</sup>, Constanze Wiek <sup>3</sup>, Andreas Kefalas <sup>1</sup>, Patrick Verhülsdonk <sup>1</sup>, Christian Mielke <sup>4</sup>, Dennis Sohn <sup>5</sup>, Kai Stühler <sup>2,6</sup>, Helmut Hanenberg <sup>3,7</sup>, Reiner U. Jänicke <sup>5</sup>, Jürgen Scheller <sup>1</sup>, Andreas S. Reichert <sup>8</sup>, Mohammad Reza Ahmadian <sup>1</sup> and Roland P. Piekorz <sup>1,\*</sup>

<sup>1</sup> Institute of Biochemistry and Molecular Biology II, Medical Faculty, Heinrich Heine University Düsseldorf, 40225 Düsseldorf, Germany; laura.bergmann@hhu.de (L.B.); alexander.lang@hhu.de (A.L.); christoph.bross@hhu.de (C.B.); simonealtinluk@gmail.com (S.A.-H.); Iris.fey@hhu.de (I.F.); andreas.kefalias@web.de (A.K.); Patrick.Verhuelsonk@uni-duesseldorf.de (P.V.); jscheller@hhu.de (J.S.); reza.ahmadian@hhu.de (M.R.A.)

<sup>2</sup> Molecular Proteomics Laboratory, Heinrich Heine University Düsseldorf, 40225 Düsseldorf, Germany; nina.overbeck@hhu.de (N.O.); anja.stefanski@hhu.de (A.S.); Kai.Stuehler@uni-duesseldorf.de (K.S.)

<sup>3</sup> Department of Otolaryngology and Head/Neck Surgery, Medical Faculty, Heinrich Heine University Düsseldorf, 40225 Düsseldorf, Germany; Constanze.Wiek@med.uni-duesseldorf.de (C.W.); Helmut.Hanenberg@uni-duesseldorf.de (H.H.)

<sup>4</sup> Institute of Clinical Chemistry and Laboratory Diagnostics, Medical Faculty, Heinrich Heine University Düsseldorf, 40225 Düsseldorf, Germany; Christian.Mielke@med.uni-duesseldorf.de

<sup>5</sup> Laboratory of Molecular Radiooncology, Clinic and Polyclinic for Radiation Therapy and Radiooncology, Medical Faculty, Heinrich Heine University Düsseldorf, 40225 Düsseldorf, Germany; Dennis.Sohn@hhu.de (D.S.); janicke@uni-duesseldorf.de (R.U.J.)

<sup>6</sup> Institute for Molecular Medicine I, Medical Faculty, Heinrich Heine University Düsseldorf, 40225 Düsseldorf, Germany

<sup>7</sup> Department of Pediatrics III, University Hospital Essen, University Duisburg-Essen, 45112 Essen, Germany

<sup>8</sup> Institute of Biochemistry and Molecular Biology I, Medical Faculty, Heinrich Heine University Düsseldorf, 40225 Düsseldorf, Germany; reichert@hhu.de

\* Correspondence: Roland.Piekorz@hhu.de; Tel.: +49-211-8112739; Fax: +49-211-8112726

† Current address: Department of Cardiology, Pulmonology, and Vascular Medicine, Medical Faculty, Heinrich Heine University Düsseldorf, 40225 Düsseldorf, Germany.

Received: 25 May 2020; Accepted: 21 August 2020; Published: 24 August 2020



**Abstract:** The stress-inducible and senescence-associated tumor suppressor SIRT4, a member of the family of mitochondrial sirtuins (SIRT3, SIRT4, and SIRT5), regulates bioenergetics and metabolism via NAD<sup>+</sup>-dependent enzymatic activities. Next to the known mitochondrial location, we found that a fraction of endogenous or ectopically expressed SIRT4, but not SIRT3, is present in the cytosol and predominantly localizes to centrosomes. Confocal spinning disk microscopy revealed that SIRT4 is found during the cell cycle dynamically at centrosomes with an intensity peak in G<sub>2</sub> and early mitosis. Moreover, SIRT4 precipitates with microtubules and interacts with structural ( $\alpha$ , $\beta$ -tubulin,  $\gamma$ -tubulin, TUBGCP2, TUBGCP3) and regulatory (HDAC6) microtubule components as detected by co-immunoprecipitation and mass spectrometric analyses of the mitotic SIRT4 interactome. Overexpression of SIRT4 resulted in a pronounced decrease of acetylated  $\alpha$ -tubulin (K40) associated with altered microtubule dynamics in mitotic cells. SIRT4 or the N-terminally truncated variant SIRT4( $\Delta$ N28), which is unable to translocate into mitochondria, delayed mitotic progression and reduced cell proliferation. This study extends the functional roles of SIRT4 beyond mitochondrial metabolism and provides the first evidence that SIRT4 acts

as a novel centrosomal/microtubule-associated protein in the regulation of cell cycle progression. Thus, stress-induced SIRT4 may exert its role as tumor suppressor through mitochondrial as well as extramitochondrial functions, the latter associated with its localization at the mitotic spindle apparatus.

**Keywords:** sirtuin; SIRT4; interactome; centrosome; mitosis; HDAC6

## 1. Introduction

Mitotic cell division represents a complex and highly regulated process that allows the equal partitioning of duplicated DNA content from a mother cell into two daughter cells. The mitotic spindle apparatus is comprised of two centrosomes, one at each spindle pole, astral and spindle microtubules, and microtubule-associated protein (MAP) complexes [1–3]. Centrosomes are the main microtubule organizing centers in animal cells comprising a pair of centrioles that are surrounded by pericentriolar material (PCM) components with pericentrin as the major anchoring factor [4]. During the G<sub>2</sub>/M-phase of the cell cycle, cells undergo a massive microtubule rearrangement that functions as an important regulatory switch and consists of microtubule nucleation, elongation, polymerization, and depolymerization [5]. The length of microtubules and their “dynamic instability” depend on an equilibrium shift between “catastrophe” (microtubule shrinkage) and “rescue” (microtubule growth) that is primarily regulated by several MAPs [3]. The dynamic status of microtubules and their (in)stability are critically regulated by post-translational modifications, including (de)acetylation of  $\alpha$ -tubulin (in particular lysine 40 [K40]) [6,7]. The sirtuin SIRT2 and histone deacetylase 6 (HDAC6) are known deacetylases that target K40-acetylated  $\alpha$ -tubulin in a NAD<sup>+</sup>-dependent manner [8], thereby altering microtubule dynamics by decreasing microtubule stability [9,10].

The mammalian protein family of NAD<sup>+</sup>-dependent sirtuins (SIRT) comprises seven members which function in different cellular compartments mainly as deacetylases, deacylases, or ADP-ribosyltransferases. SIRT proteins are implicated in multiple pathways involved in epigenetic regulation and gene expression in the nucleus (SIRT1, 2, 6, and 7), proliferation/cell survival, aging, and life-span regulation (e.g., SIRT6) [11–16], as well as mitochondrial metabolism and bioenergetics (SIRT3, 4, 5) [15–18]. SIRT3, a major mitochondrial deacetylase, and SIRT5 promote mitochondrial energy production, whereas SIRT4 exerts the opposite effect [19–22]. In particular, the metabolic gatekeepers glutamate dehydrogenase (GDH) and pyruvate dehydrogenase (PDH) [23,24] are inhibited by SIRT4 by its ADP-ribosyltransferase and Lipoamidase activities, respectively [25]. Furthermore, SIRT4 displays target-specific deacetylase [26,27] and deacylase [25,28] enzymatic activities.

Possible extra-mitochondrial roles of SIRT3 and SIRT5 are most likely due to their not well understood nuclear and cytosolic localization and their corresponding protein targets [29–31]. SIRT3 regulates, in a direct or indirect (i.e., mitochondria-dependent) manner, microtubule dynamics and chromosomal alignment during mitosis by currently unknown mechanism(s) [32,33]. SIRT4 could also play an extramitochondrial role in microtubule dynamics, given that SIRT4 interacts with Leucine-rich protein 130 (LRP130) [24,34], a multi-domain and dual-function protein that interacts with the microtubule-associated protein MAP1S and integrates mitochondrial transport and the microtubule cytoskeleton in interphase [35]. Moreover, recent work visualized a partial localization of SIRT4 into the nucleus that is even increased upon mitochondrial stress [36].

Consistent with a role for SIRT3 and SIRT4 as tumor suppressor proteins, knock-out mouse lines for SIRT3 and SIRT4 develop mammary and lung tumors, respectively [37,38]. The tumorigenic phenotype of SIRT4 knock-out mice is associated with an increased chromosomal missegregation and aneuploidy/polyploidy that was also detected in primary SIRT4<sup>-/-</sup> mouse embryonic fibroblasts [37]. Compared to wild-type cells, SIRT4<sup>-/-</sup> cells show increased DNA damage and sensitivity toward chromosomal instability upon treatment with stressors like UV radiation [37]. It is unknown, whether the tumor phenotypes of mice lacking SIRT3 or SIRT4 are primarily based on mitochondria-dependent

and/or -independent (i.e., mitotic/microtubule-associated) mechanisms. Moreover, SIRT4 was recently identified at the meiotic spindle apparatus during oocyte maturation. Oocytes from aged mice display higher SIRT4 levels leading to increased meiotic defects [39], which can be ameliorated by SIRT4 depletion. Consistent with its accumulation in aged oocytes, expression of SIRT4 is upregulated during replicative and stress-induced senescence, the latter triggered by different DNA-damaging stressors [37] as well as *in vivo* by UV radiation in photo-aged human skin [40].

Here, we performed subcellular localization and mitotic interactome analyses of SIRT4. Our findings indicate that besides its role in mitochondrial metabolism, SIRT4 functions also as a new centrosomally localized and microtubule-associated protein possibly involved in the regulation of mitotic cell cycle progression. In particular, ectopically expressed SIRT4 precipitates with microtubules, interacts with  $\alpha$ , $\beta$ -Tubulin and HDAC6 in co-immunoprecipitation experiments, and downregulates the levels of acetyl  $\alpha$ -tubulin (K40) in G<sub>2</sub>-synchronized cells. Thus, both mitochondrial localized and extra-mitochondrial SIRT4 (presumably via metabolic inhibition/ROS generation [41] and alteration of mitotic regulation and/or microtubule dynamics, respectively) may trigger the anti-proliferative tumor suppressor function(s) of SIRT4 upon replicative/mitotic stress.

## 2. Materials and Methods

### 2.1. Cell Culture

HEK293, HT1080, and HeLa cell lines were cultured at 37 °C and 5% CO<sub>2</sub> in DMEM (Dulbecco's Modified Eagle Medium) containing high glucose (4.5 g/L; Thermo Fisher Scientific, Schwerte, Germany) with 10% fetal bovine serum (FBS) and penicillin (100 units/mL)/streptomycin (100 µg/mL). Cell lines were obtained from the German Collection of Microorganisms and Cell Cultures GmbH (DSMZ, Braunschweig, Germany) (HEK293: ACC 305; HeLa: ACC 57; HT1080: ACC 315).

### 2.2. Generation of SIRT4 Expressing Cell Lines

HEK293 cell lines stably expressing SIRT4-eGFP from the pcDNA3.1 vector and mutants [enzymatically inactive SIRT4(H161Y)-eGFP and SIRT4( $\Delta$ N28)-eGFP lacking the N-terminal mitochondrial targeting signal] have been described [42] and cultured in media containing 800 µg/mL Geneticin/G418 (Genaxxon bioscience GmbH, Ulm, Germany) as permanent selection agent. HEK293 and HeLa cell lines stably expressing SIRT4-eGFP from the retroviral vector puc2CL12IPwo were generated as described elsewhere [43] and further enriched by fluorescence-activated cell sorting (FACS). Expression of SIRT4-eGFP fusion constructs was validated by immunoblotting and flow cytometry.

### 2.3. Cell Proliferation Kinetics

HEK293 cells expressing eGFP, SIRT4-eGFP, or mutants thereof were seeded at  $1.5 \times 10^4$  cells/well in triplicates (6-well plates). Total numbers of viable cells were determined after 2 and 4 days using the TC10 cell counter (Bio-Rad, München, Germany).

### 2.4. Live Cell Imaging

HEK293 cells expressing eGFP or SIRT4-eGFP ( $3 \times 10^5$ ) were seeded on  $\mu$ -Dish 35 mm plates (ibidi GmbH, Martinsried, Planegg). For live cell imaging, cells were cultured in CO<sub>2</sub>-independent HEPES containing media (Life Technologies/Thermo Fisher Scientific, Schwerte, Germany) at 37 °C in an isolated incubation chamber essentially as described [44]. Cells were initially imaged at brightfield and 488 nm and thereafter only at brightfield every 12 min using a Nikon Eclipse TE2000-E microscope under control of the NIS Elements Advanced Research software (Nikon; version 4.20).

### 2.5. Preparation of Total Cell Lysates for Immunoblot Analysis

Cleared cell lysates were generated using lysis buffer containing either 0.3% CHAPS (3-[(3-Cholamidopropyl) dimethylammonio]-1-propanesulfonate) or 0.5% NP-40, 50 mM Tris-HCl

(pH 7.4), 150 mM NaCl, 1 mM Na<sub>3</sub>VO<sub>4</sub>, 10 mM NaF, 1 mM EDTA, 1 mM EGTA, 2.5 mM Na<sub>4</sub>O<sub>7</sub>P<sub>2</sub>, 1 μM DTT, 1 × cOmplete™ protease inhibitor cocktail (Sigma-Aldrich). Lysates were cleared by centrifugation (11,000× g at 4 °C for 20 min). Protein concentration of the supernatants was determined using the Bradford assay (K015.1, Carl Roth GmbH, Karlsruhe, Germany). Cell lysates subjected to immunoblot analysis were obtained by lysing cells in lysis buffer containing 0.5% NP-40 (see above). Antibodies used for immunoblot analysis are listed in Table S2.

#### 2.6. Immunoprecipitation of GFP Fusion Proteins Using the Anti-GFP Nanobody or Standard Immunoprecipitation Protocols

The single-domain-anti-GFP antibody (“nanobody”) method [45] was employed to immunoprecipitate SIRT4-eGFP fusion proteins essentially as described [42]. Co-immunoprecipitation of α-tubulin interacting proteins was performed from total cell lysates using α-Tubulin specific antibodies (rabbit anti-α-tubulin, ab52899, Abcam, Berlin, Germany) and Protein A/G Sepharose beads (Santa Cruz Biotechnology, Heidelberg, Germany). Cell lysates subjected to immunoprecipitation were obtained by lysing cells in lysis buffer containing 0.3% CHAPS (see above).

#### 2.7. Subcellular Fractionation Analysis

Subcellular fractionation of total cell lysates was performed essentially as described [46] with additional centrifugation steps to obtain a cytosolic fraction together with a mitochondrially enriched particulate fraction. Cells were suspended in HEPES buffered solution [20 mM HEPES, pH 7.5; 220 mM mannitol; 70 mM sucrose; 1 mM EDTA; 1 × protease inhibitor cocktail (Sigma-Aldrich, München, Germany)] and mechanically lysed by repeatedly passing through 20 G syringe needles. The total cell lysate was centrifuged (600× g, 10 min), and the resulting crude cytoplasmic fraction without cellular debris was subjected to at least eight further centrifugation steps (600× g, 1000× g, 16,000× g) thereby collecting mitochondria enriched pellets and a pure cytosolic fraction. Mitochondria containing pellets were resuspended in HEPES buffered solution containing 10 mM MgCl<sub>2</sub> and 250 mM sucrose, centrifuged (12,000× g, 10 min) twice through a sucrose cushion (HEPES buffered solution containing 0.5 mM MgCl<sub>2</sub> and 880 mM sucrose). The resulting highly mitochondria enriched pellets were resuspended [40 mM Tris HCl, pH 7.5; 150 mM NaCl; 3% glycerol; 0.5 mM DTT; 1 × protease inhibitor cocktail (Sigma-Aldrich, München, Germany)] and analyzed by SDS-PAGE. Antibodies used for immunoblot analysis of subcellular marker proteins are listed in Table S2.

#### 2.8. Microtubule Pulldown Experiments

Pelleting of Taxol-stabilized microtubules from cytosolic fractions was performed essentially as described [47]. Asynchronously growing HEK293 cells expressing eGFP or SIRT4-eGFP were lysed in PHEM buffer [60 mM PIPES, 25 mM HEPES, 1 mM EGTA, 1 mM magnesium acetate, pH 6.8; 1 × cOmplete™ protease inhibitor cocktail (Sigma-Aldrich, München, Germany)] using a Dounce homogenizer. Following centrifugation (14,000× g for 30 min) of the total cell lysate, the supernatant (cytosolic fraction) was supplemented with GTP (1 mM) and Paclitaxel/Taxol (20 μM) (both from Sigma-Aldrich, München, Germany). Samples were incubated at room temperature for 30 min and subjected to centrifugation (14,000× g for 15 min) through a sucrose layer (15% sucrose in PHEM buffer) to obtain supernatant and the microtubules containing pellet fraction. The latter was washed one time in Taxol containing PHEM buffer, centrifuged, and sample fractions were analyzed by SDS-PAGE.

#### 2.9. Ro3306 Mediated G<sub>2</sub> Cell Cycle Arrest

Cells were treated for 14 h with the CDK1 inhibitor Ro3306 (10 μM; Selleckchem/BIOZOL, München, Germany) to achieve synchronization at G<sub>2</sub>. When indicated, cells were released into mitosis by one time washing and addition of fresh media, harvested 45 min later, and analyzed as indicated.

### 2.10. Mass Spectrometric Analysis of the Mitotic SIRT4 Interactome

Sample preparation for proteomic analysis, LC-MS analysis, computational mass spectrometric data analysis, and gene ontology/protein network analysis are specified in the Supplementary Materials and Methods section. Primary data obtained from mass spectrometric analysis of SIRT4-eGFP interacting proteins are listed in Table S1.

### 2.11. Confocal Laser Scanning Microscopy and Signal Quantification Using ImageJ Software

Cells were fixed in 4% paraformaldehyde for 20 min and permeabilized with 0.2% Triton X-100 for 20 min followed by a blocking step with 4% BSA/0.05% saponin for 30 min at room temperature. Alternatively, for spinning disk confocal analysis, cells were fixed in 4% paraformaldehyde for 20 min and permeabilized with 0.25% Triton X-100 for 5 min followed by a blocking step with 3% BSA in PBS (phosphate buffered saline) for two hours at room temperature. Cells were stained with primary antibodies in 1% BSA in PBS overnight at 4 °C. All primary and secondary antibodies used for confocal imaging analysis are listed in Table S3. DNA was detected by DAPI staining followed by mounting of coverslips with ProLong Gold antifade reagent (P36934; Invitrogen/Thermo Fisher Scientific, Germany). Analyses were performed with a LSM510-Meta confocal microscope (Carl Zeiss AG, Oberkochen, Germany) equipped with 40/1.3 immersion objectives and excitation wavelengths of 468 nm, 488 nm, 543 nm, and 633 nm. In addition, an UltraVIEW spinning disk confocal microscope (Perkin Elmer, Waltham, MA, USA) with excitation wavelengths of 405 nm, 488 nm, 561 nm, and 633 nm, a 60 ×/1.4 NA oil objective, and the Volocity 6.3 software (Perkin Elmer, Rodgau, Germany) was employed. To increase detection of SIRT4-eGFP fusion proteins, primary antibodies against GFP (GF090R; Nacalai Tesque, Inc./GERBU Biotechnik GmbH, Heidelberg, Germany; 1:1000) were employed in spinning disk confocal microscopy when indicated. Image processing and quantification of centrosomal SIRT4 and Pericentriolar signal intensities were performed based on ImageJ software v1.49k.

### 2.12. Statistical Analysis

Data are presented as mean ± s.d. Multiple comparisons were analyzed by one-way analysis of variance (ANOVA) followed by Tukey's post-hoc test to identify group differences in variance analysis using the GraphPad Prism software. Results with  $p \leq 0.05$  were considered significant.

## 3. Results

### 3.1. Endogenous SIRT4 and Ectopically Expressed SIRT4-eGFP Localize at Interphase and Mitotic Centrosomes

During our studies on the expression and mitochondrial function of SIRT4 [40,42,48], we noticed an extra-mitochondrial localization of SIRT4 primarily at centrosomes and apparently in part at the mitotic spindle in confocal laser scanning and spinning disk microscopy-based analyses of various human cell lines. We employed two anti-human SIRT4 antibodies, H-234 (sc-135053, rabbit polyclonal; Santa Cruz Biotechnology, Heidelberg, Germany) raised against a N-terminally truncated version of human SIRT4 (a.a. 81–314), and SAB1407208 (mouse monoclonal; Sigma-Aldrich, München, Germany) raised against full-length human SIRT4 (a.a. 1–314). As indicated in Figures S1 and S2, we observed a clear centrosomal localization of SIRT4 during interphase/G<sub>2</sub> and mitosis in HeLa and HT1080 cells when using the SIRT4 antibody from Santa Cruz Biotechnology in single antibody stainings and DAPI-mediated DNA detection. Moreover, staining with the SIRT4 antibody from Sigma-Aldrich revealed also a centrosomal/mitotic spindle pole associated localization of endogenous SIRT4 in HeLa cells (Figure S3). Similar to endogenously expressed SIRT4, C-terminal eGFP fusion proteins of SIRT4 and SIRT4( $\Delta$ N28), the latter representing an N-terminally (a.a. 1–28) truncated SIRT4 mutant unable to translocate into mitochondria [42,49], were also detected at interphase centrosomes of HT1080 fibrosarcoma and HeLa cervix carcinoma cells (Figure S4 and Video S1). The bona fide centrosomal localization of SIRT4 and SIRT4-eGFP has been verified in further experiments described below by co-staining against Pericentriolar (Figures 1 and 2; Videos S2–S4). Besides its extramitochondrial/centrosomal localization, SIRT4 was

also observed as described in mitochondria [23,42] using co-staining against the mitochondrial marker MTC02 (Figure S5; [40,42]). In clear contrast to SIRT4, SIRT3 was not detectable at interphase or mitotic centrosomes or at the mitotic spindle apparatus, but displayed solely a mitochondrial localization (Figure S6) as previously described [50].

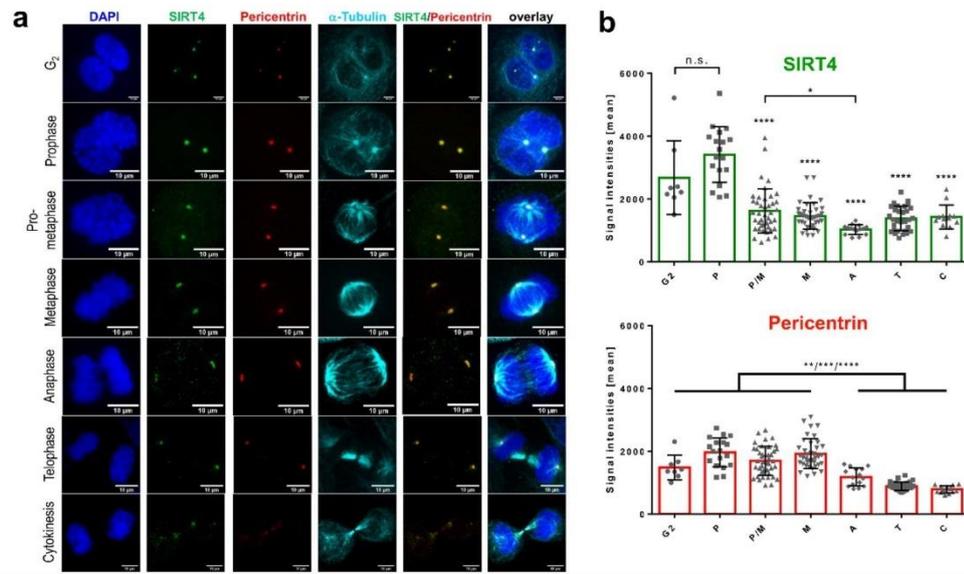


**Figure 1.** Centrosomal localization pattern of SIRT4 during G<sub>2</sub>/M progression. **(a)** Endogenous SIRT4 was detected in HeLa cells in G<sub>2</sub> and subsequent mitotic stages using a polyclonal antibody against SIRT4 (sc-135053; Santa Cruz Biotechnology, Heidelberg, Germany) and spinning disk microscopy. Antibody staining against Pericentrin and  $\alpha$ -tubulin was employed to visualize centrosomes and microtubules, respectively. DAPI was used to detect DNA. Bar: 10  $\mu$ m. **(b)** Quantification of centrosomal SIRT4 and Pericentrin levels during G<sub>2</sub>/M progression. Endogenous SIRT4 and Pericentrin were detected in HeLa cells as indicated above. Shown are mean signal intensities ( $\pm$ S.D.) which were analyzed using ImageJ software (v1.49k; Materials and Methods). Numbers of cells analyzed per cell cycle phase: G<sub>2</sub>,  $n = 8$ ; P, prophase,  $n = 17$ ; P/M, prometaphase,  $n = 42$ ; M, metaphase,  $n = 38$ ; A, anaphase,  $n = 15$ ; T, telophase,  $n = 32$ ; and C, cytokinesis,  $n = 13$ . To evaluate statistical significance (comparison of SIRT4 intensities between Prophase and G<sub>2</sub> or mitotic phases) one-way ANOVA followed-up by Tukey's test was performed (\*  $p < 0.05$ ; \*\*  $p < 0.01$ ; \*\*\*  $p < 0.001$ ; \*\*\*\*  $p < 0.0001$ ; n.s., not significant).

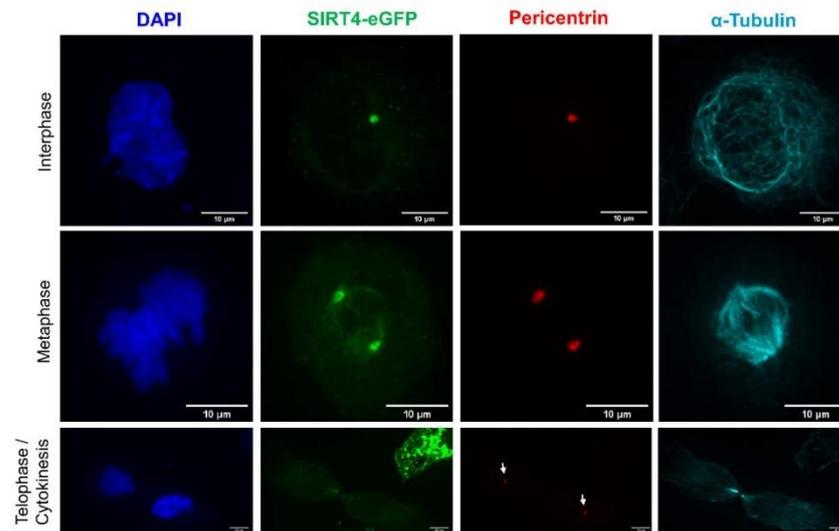


**Figure 2.** Centrosomal localization of SIRT4-eGFP during interphase and mitotic cell division. An expression construct for SIRT4-eGFP was transiently transfected into HeLa cells and SIRT4-eGFP was imaged by confocal spinning disk microscopy. The corresponding movies of these confocal pictures are provided in the supplementary information (Videos S2–S4). Antibodies against Pericentrin and  $\alpha$ -tubulin were employed to visualize centrosomes and microtubules, respectively. DAPI was used to detect DNA. Bar: 10  $\mu$ m.

### 3.2. Centrosomal Localization Kinetics of SIRT4 during Cell Cycle Progression

Next, we quantitatively analyzed SIRT4 at centrosomes during  $G_2$  and the course of mitotic cell division using Pericentrin as centrosomal marker. In HeLa cervix carcinoma cells, SIRT4 showed a dynamic centrosomal localization pattern where it displayed the highest signals in centrosomal staining during  $G_2$  and early mitosis, followed by a significant drop in signal intensity from prophase onwards until late mitosis/cytokinesis (Figure 1a,b). At the same time, centrosomal Pericentrin levels were comparable between  $G_2$  and metaphase, but significantly dropped thereafter in the second half of mitosis (Figure 1a,b), similar to the centrosomal dynamics of Pericentrin as originally described by Dictenberg et al. [51]. Similarly, SIRT4-eGFP that was transiently expressed in HeLa cells localized at centrosomes in interphase cells (Figure 2 and Video S2), prominently decorated Pericentrin at spindle poles in metaphase cells (Figure 2, Video S3), and lastly disappeared from centrosomes during telophase/cytokinesis (Figure 2, Video S4). Parallel control imaging experiments failed to detect eGFP localization at centrosomes (Video S5). Thus, centrosomal localization of SIRT4 or ectopically expressed SIRT4-eGFP seems to be dynamically regulated during cell cycle progression with a peak in  $G_2$  and early mitosis.

### 3.3. Subcellular Fractionation Reveals a Cytosolic, Extra-Mitochondrial Pool of SIRT4, But Not SIRT3

Given the extramitochondrial localization of SIRT4 at centrosomes, we next analyzed the intracellular SIRT4 protein distribution by subjecting total cell lysates to a subcellular fractionation protocol via differential centrifugation steps (Material and Methods). The method yielded in a highly cleared cytosolic fraction together with a mitochondrial-enriched particulate fraction as controlled by marker proteins specific for subcellular compartments. Interestingly, in addition to their mitochondrial localization, both endogenous SIRT4 (Figure 3) as well as ectopically expressed SIRT4-eGFP (Figure S7) were also found at substantial levels in the cytosolic fraction. In the case of SIRT5, we also observed ectopically expressed, C-terminally Flag-tagged SIRT5 in the cleared cytosolic fraction (Figure S8),

consistent with previous findings [31]. In contrast, endogenous SIRT3 or C-terminally Flag-tagged SIRT3 were only found in the mitochondrial enriched fraction (Figure 3 and Figure S8, respectively). Taken together, our findings obtained from confocal microscopic imaging and subcellular fractionation analyses both indicate that substantial levels of SIRT4, but not SIRT3, localize outside mitochondria in the cytoplasm.

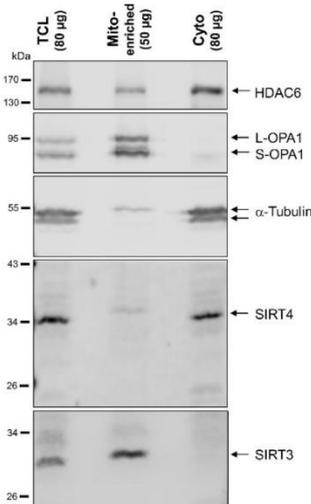


**Figure 3.** Subcellular fractionation analysis of endogenous SIRT4 and SIRT3 protein levels in HEK293 cells. Total cell lysates (TCL; 80 µg) and the respective mitochondria enriched (Mito-enriched; 50 µg) and cytosolic (Cyto; 80 µg) fractions were subjected to immunoblot analysis. Subcellular marker proteins detected were OPA1 (long and short forms of OPA1; mitochondria),  $\alpha$ -tubulin (cytoplasm), and HDAC6 (predominantly cytoplasmic localization).

#### 3.4. Ectopic Overexpression of SIRT4 or the Extra-Mitochondrial Localized Deletion Mutant SIRT4( $\Delta$ N28) Inhibits Mitotic Progression and Cell Proliferation

Given the stress induced/DNA damage-associated upregulation of SIRT4 and its anti-proliferative role [37,40], we next aimed to link extramitochondrially localized SIRT4 to a possible inhibitory function on cell cycle progression and proliferation. HEK293 cells stably expressing SIRT4-eGFP, SIRT4( $\Delta$ N28)-eGFP, the catalytically inactive mutant SIRT4(H161Y)-eGFP, or eGFP as control, were subjected to continuous live cell imaging analyses during cell division. As depicted and quantitatively analyzed in Figure 4, expression of all three SIRT4 variants led to a significant prolongation of mitosis with strongest impacts of SIRT4-eGFP and the exclusively outside mitochondria localized SIRT4( $\Delta$ N28)-eGFP fusion protein. In accordance with these findings, cellular proliferation was significantly reduced by all three SIRT4 variants as compared to eGFP-expressing cells (Figure 4c). Of note, expression of SIRT4( $\Delta$ N28)-eGFP was associated with an almost three-fold increase in bi- or multinucleated cells (Figure S9). The observation that SIRT4(H161Y)-eGFP, albeit catalytically inactive, still delays mitosis and inhibits proliferation indicates that SIRT4 possibly targets structural or regulatory factors in cell cycle progression (and/or mitochondrial function that then impacts on mitosis) through both catalytically dependent and independent mechanisms.

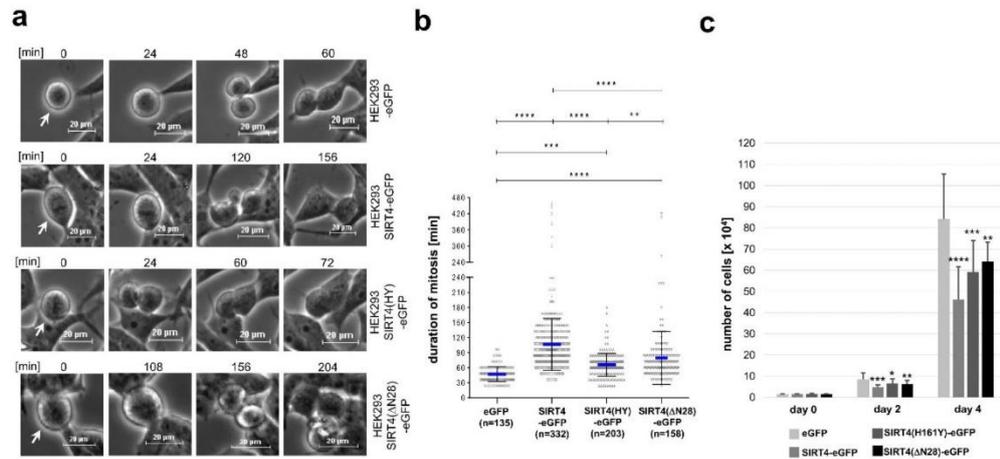


**Figure 4.** Ectopic expression of SIRT4 prolongs mitotic progression and inhibits cell proliferation. (a) HEK293 cell lines stably expressing SIRT4-eGFP, the enzymatically inactive mutant SIRT4(H161Y)-eGFP, or SIRT4( $\Delta$ N28)-eGFP lacking the N-terminal mitochondrial targeting signal were analyzed by live cell imaging. Cell lines were cultured in CO<sub>2</sub>-independent, HEPES containing media. Pictures of cells undergoing cell division were taken in intervals of 12 min. (b) Duration of mitosis was calculated from cell rounding/early mitosis to cytokinesis/cell reattachment. To evaluate statistical significance one-way ANOVA followed-up by Tukey's test was performed (\*\*  $p < 0.01$ ; \*\*\*  $p < 0.001$ ; \*\*\*\*  $p < 0.0001$ ). (c) Proliferation kinetics of HEK293 cells expressing SIRT4-eGFP or the indicated SIRT4 mutants. Cells were seeded at day 0 (15,000 cells/well) in triplicates and total cell numbers were counted at the indicated time points ( $n = 3-5$  independent experiments). To evaluate statistical significance one-way ANOVA followed-up by Tukey's test was performed (\*  $p < 0.05$ ; \*\*  $p < 0.01$ ; \*\*\*  $p < 0.001$ ; \*\*\*\*  $p < 0.0001$ ).

### 3.5. The Mitotic SIRT4 Interactome Comprises Microtubule-Associated Structural and Regulatory Proteins

To better understand the mechanism(s) through which SIRT4 impacts on mitosis, we next analyzed the SIRT4 interactome in mitotic SIRT4-eGFP-expressing HEK293 cells as compared to eGFP-expressing control cells. Cells were synchronized in G<sub>2</sub> by Ro3306-mediated, reversible inhibition of cyclin-dependent kinase 1 (CDK1) followed by release into mitosis for 45 min. Native SIRT4 containing protein complexes were isolated by anti-eGFP nanobody-based co-immunoprecipitation from total cell lysates followed by mass spectrometric characterization of SIRT4-interacting proteins (Table S1 and Figure S10). Protein network analyses revealed several known (e.g., DNA damage response [37]; mitochondrial respiratory chain components and glutamate metabolism regulators [34]; regulation of mitochondrial organization [42,48]) as well as novel functions and components associated with the mitotic SIRT4 interactome (e.g., tRNA aminoacylation and mitochondrial translation; cell cycle regulation; microtubule regulation) (Figure S10). In particular, as depicted in Figure 5, we identified several mitochondrial SIRT4-interacting proteins and potential substrates (OPA1 [42]; ATP5F1A [34]; ANT2 [21]; IDE [52]) as well as mostly novel, extra-mitochondrial localized SIRT4 interactors. The latter comprise  $\alpha$ - and  $\beta$ -tubulin as subunits of microtubules, components of the centrosomally localized  $\gamma$ TURC complex ( $\gamma$ -tubulin, TUBGCP2, TUBGCP3) [53,54] that nucleates microtubules at their minus poles, the microtubule deacetylase HDAC6 that is critically involved in the regulation of microtubule stability and dynamics [9], and the G<sub>2</sub>/M cell cycle regulator CDK1 [55]. These SIRT4 interactions were confirmed by nanobody-mediated co-immunoprecipitation (Figure 5b and Figure S11) and confocal colocalization analyses (Figure S11). The observed mitotic interaction pattern of SIRT4 appears specific, given that SIRT4 failed to co-immunoprecipitate with other centrosomal or mitotic spindle localized proteins like Pericentrin (Figure S12) or the TACC protein family member TACC3 [42], respectively.

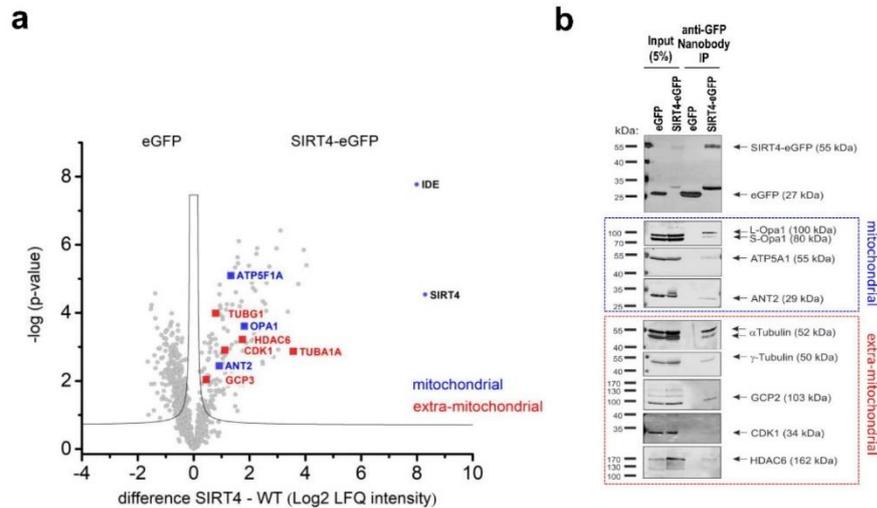


**Figure 5.** Analysis of the mitotic SIRT4 interactome by mass spectrometry. **(a)** Volcano plot analysis of mitochondrial and extra-mitochondrial proteins interacting with SIRT4. HEK293 cells stably expressing eGFP or SIRT4-eGFP ( $n = 4$  replicates each) were arrested in  $G_2$  by the reversible CDK1 inhibitor RO3306 followed by release into mitosis (45 min after RO3306 wash out). Total cell lysates were subjected to anti-eGFP nanobody co-immunoprecipitations followed by their mass spectrometric analysis. **(b)** Anti-eGFP nanobody co-immunoprecipitations of selected mitochondrial and extra-mitochondrial SIRT4 interacting proteins as compared to eGFP controls. Total cell lysates analyzed in **(a)** were employed.

### 3.6. SIRT4 Interacts with Microtubules and Negatively Regulates Acetyl- $\alpha$ -Tubulin (K40) Levels

Given the link between SIRT4 and proteins of the microtubule network, we next addressed the interaction of SIRT4 with microtubules and its role in regulation of microtubule dynamics. We performed microtubule pulldown assays and observed SIRT4-eGFP in the pelleted fraction of Taxol-stabilized microtubules (Figure 6a). In contrast to this, eGFP as control was almost exclusively detected in the soluble fraction of Taxol-stabilized microtubules (Figure 6a). Consistent with these findings, (i) an  $\alpha$ -tubulin specific antibody coimmunoprecipitated  $\alpha$ -tubulin and SIRT4-eGFP, but not eGFP (Figure 6b), and (ii)  $\alpha$ -tubulin co-localized with endogenous SIRT4 at MTOCs in mitotic cells as detected by spinning disk microscopy (Figure 6c). Given the putative protein interaction of SIRT4 with the microtubule deacetylase HDAC6 (Figure 5), we next analyzed the levels of K40-acetylated  $\alpha$ -tubulin upon ectopic expression of SIRT4-eGFP or mutants thereof. Interestingly, as indicated in Figure 7, SIRT4-eGFP, but not the catalytically inactive mutant SIRT4(H161Y)-eGFP or SIRT4( $\Delta$ N28)-eGFP, led to a profound decrease in the ratio of K40-acetylated  $\alpha$ -tubulin vs. total  $\alpha$ -tubulin levels in  $G_2$  synchronized HEK293 cells as compared to asynchronously growing cells. Thus, our findings indicate that full-length SIRT4 impacts in an enzymatically dependent manner on microtubule dynamics in  $G_2/M$  by decreasing microtubule stability, which presumably translates into inhibition of mitotic progression and proliferation (Figure 4).

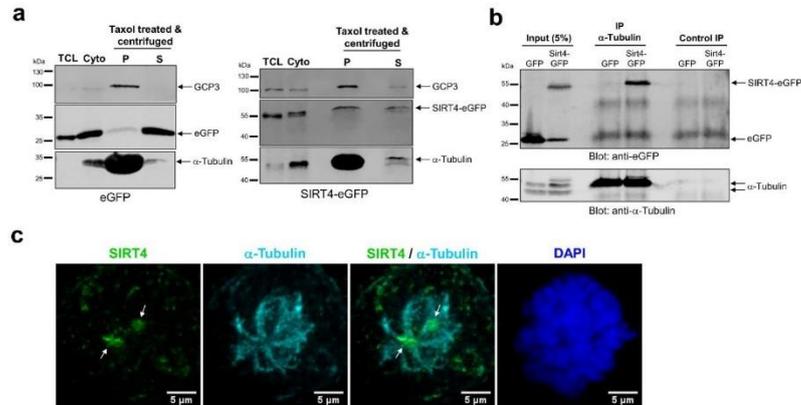


**Figure 6.** SIRT4 precipitates with microtubules and co-immunoprecipitates with  $\alpha$ -tubulin in HEK293 cells. (a) SIRT4-eGFP, but not eGFP, is present in the pelleted fraction (P) of microtubules which were Taxol-stabilized in the cytosolic fraction (Cyto) followed by pelleting via centrifugation through a sucrose cushion. TCL, Total cell lysate; S, supernatant. Tubulin Gamma Complex Associated Protein 3 (TUBGCP3 or GCP3) was detected as co-marker for microtubules (b). An  $\alpha$ -tubulin specific antibody co-immunoprecipitates SIRT4-eGFP, but not eGFP, from total cell lysates of stably transfected HEK293 cells. As control, immunoprecipitation without  $\alpha$ -tubulin antibody was performed. (c) Localization of SIRT4 at spindle poles/Microtubule Organizing Centers (MTOCs) of mitotic HeLa cells using a polyclonal antibody against SIRT4 (sc-135053, Santa Cruz Biotechnology, Heidelberg, Germany) and analysis by spinning disk microscopy. Antibodies against  $\alpha$ -Tubulin were employed to visualize microtubules. DAPI was used to detect DNA. Bar: 5  $\mu$ m.

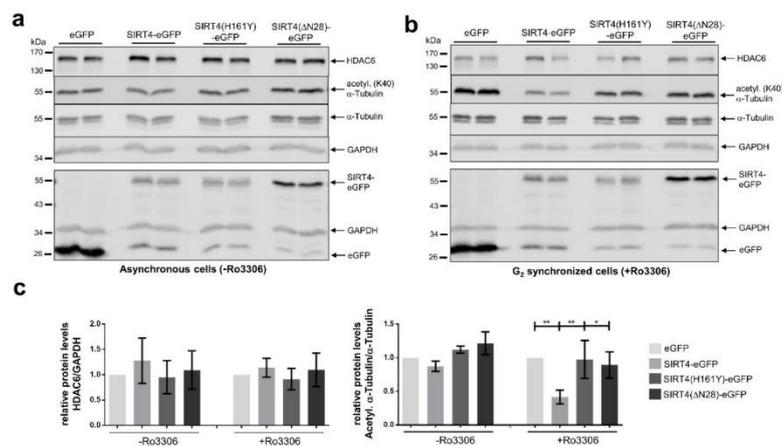


**Figure 7.** Ectopic expression of SIRT4 impacts negatively on acetylated  $\alpha$ -tubulin (K40) during mitosis. HEK293 cells stably expressing eGFP, SIRT4-eGFP, or mutants thereof were either asynchronously grown (a) or subjected to Ro3306-mediated G<sub>2</sub> synchronization (b) followed by immunoblot analysis of HDAC6, acetylated  $\alpha$ -tubulin (K40), and  $\alpha$ -tubulin. Expression of eGFP, SIRT4-eGFP, or mutants thereof was analyzed in a second immunoblot (lower panels in a and b). Probing against GAPDH was employed as loading control. Relative HDAC6 amounts and acetylated  $\alpha$ -tubulin (K40)/ $\alpha$ -tubulin levels were quantified by densitometric analysis (c). To evaluate statistical significance one-way ANOVA followed-up by Tukey's test was performed (three independent experiments; \*  $p < 0.05$ ; \*\*  $p < 0.01$ ). All P-values of the analysis of acetylated  $\alpha$ -tubulin (K40)/ $\alpha$ -tubulin levels (+Ro3306) refer to comparison with SIRT4-eGFP.

#### 4. Discussion

This study provides insights into a potential role of extra-mitochondrially localized SIRT4 in mitotic cell division. Our findings show that (i) SIRT4 localizes not only in mitochondria, but also in the cytosol, where it is found at centrosomes especially in early mitotic phases; (ii) as revealed by mass spectrometric, co-immunoprecipitation, and microtubule pulldown analyses, SIRT4 co-pellets with Taxol-stabilized microtubules and interacts with microtubule components, in particular  $\alpha$ -tubulin, with components of the centrosome associated  $\gamma$ TURC complex ( $\gamma$ -tubulin, GCP2, GCP3), and with the  $\alpha$ -tubulin deacetylase HDAC6; (iii) linked to the SIRT4-HDAC6 interaction, increased SIRT4 expression results in decreased acetyl- $\alpha$ -tubulin (K40) levels, which are typically associated with decreased stability and altered dynamics of mitotic microtubules; (iv) at the cellular level, ectopic expression of SIRT4 or SIRT4( $\Delta$ N28) lacking the N-terminal mitochondrial targeting signal prolongs mitotic progression and inhibits cell proliferation. Consistent with the subcellular localization profile of endogenous SIRT4 and ectopically expressed SIRT4-eGFP (Figures 1 and 2), it has been recently reported that ectopic SIRT4 expressed even at very low levels shows a dual localization in mitochondria as well as in the cytosol and nucleus. The authors attributed this to a low mitochondrial import kinetics of SIRT4 [36]. Thus, we propose that SIRT4 may exert its cell cycle inhibitory and tumor suppressor function through both mitochondria, i.e., bioenergetics-dependent, and mitochondria-independent, i.e., centrosome/mitotic spindle apparatus-linked mechanisms. Interestingly, the dual mitochondrial and centrosomal localization of SIRT4 (shown in this work) and its increased nuclear localization upon mitochondrial stress [36] is reminiscent of a function of SIRT4 as a “moonlighting protein” that per definition localizes at more than one cellular compartment/structure with similar or different functions [56]. Further examples of mitochondrially and centrosomal localized moonlighting proteins include C21orf33/GATD3A (glutamine amidotransferase like class 1 domain containing 3A), which has been identified within the human protein atlas project [57], and the mitochondrial porin VDAC3 (voltage-dependent anion-selective channel protein 3) that localizes at centrosomes and regulates centriole assembly [58].

In terms of the regulation of extramitochondrial SIRT4, we observed the highest centrosomal SIRT4 levels in G<sub>2</sub> and early mitosis (Figure 1), indicating that centrosomal recruitment of SIRT4 and possibly its dissociation toward mitotic exit (Videos S2–S4) represents a regulated process. In contrast, total SIRT4 protein levels did not greatly change during cell cycle progression when cells were released from double thymidine block-mediated G<sub>1</sub>/S synchronization [59], although we cannot exclude that the cytosolic (i.e., extramitochondrial) pool of SIRT4 does. The low import kinetics of SIRT4 into mitochondria [36] could be further reduced during G<sub>2</sub>/M when mitochondria increasingly undergo cyclin B1-CDK1 driven fission [60] to become evenly distributed around the mitotic spindle [61] for cell division. Elevated cytosolic SIRT4 levels in G<sub>2</sub>/M might then result in increased recruitment of SIRT4 to the centrosome, a hypothesis that remains to be further tested.

A candidate regulator of centrosomal SIRT4 localization is CDK1, given that both proteins co-immunoprecipitate with each other (Figure 5) and partially colocalize at centrosomes in G<sub>2</sub> [59]. Interestingly, an additional intramitochondrial role was uncovered for CDK1 where it interacts with and phosphorylates SIRT3 to enhance mitochondrial metabolism [62,63]. Given these findings it will be important to analyze the nature and function of a possible CDK1-SIRT4 axis in mitotic vs. non-mitotic cells. Overall, our findings add to the increasing evidence for a centrosomal localization of deacetylases (HDACs and sirtuins) [64] and their critical function(s) in centrosome biology, microtubule dynamics, and mitotic regulation. For example, the SIRT1-Plk2 (Polo-like kinase 2) and SIRT1-CCDC84-SAS6 axes control centriole duplication [65] and prevent centrosome overduplication [66], respectively. Expression of SIRT2, which is involved in the regulation of microtubule dynamics [8,10], is regulated in a cell cycle-dependent manner where SIRT2 localizes to centrosomes and the mitotic spindle [67]. Phosphorylation of SIRT2 by cyclin A-CDK2 reduces binding of SIRT2 to centrosomes and promotes G<sub>2</sub>/M progression [68]. In line with this, increased SIRT2 levels due to mitotic stress cause an extension

of the mitotic phase [69] presumably through the regulatory role of SIRT2 toward the anaphase promoting factor/cyclosome (APC/C) and hence cyclin B1 degradation [70].

Our proteome analysis suggests a role of SIRT4 in the regulation of microtubule dynamics and function. SIRT4 precipitates with microtubules and co-immunoprecipitates with  $\alpha$ -Tubulin (Figure 6). Here, SIRT4 may regulate the acetylation status and dynamics of microtubules which at least in part may mediate the inhibitory impact of ectopically expressed SIRT4 on cell division and proliferation (Figure 4), a hypothesis that remains to be further tested. Ectopic expression of SIRT4, but not the enzymatically inactive mutant SIRT4(H161Y), strongly inhibits the levels of acetylated  $\alpha$ -tubulin (K40) in G<sub>2</sub>-synchronized HEK293 cells (Figure 7). The absent effect of SIRT4( $\Delta$ N28)-eGFP expression on K40-acetylated  $\alpha$ -tubulin levels (Figure 7) was unexpected, given that SIRT4( $\Delta$ N28)-eGFP coimmunoprecipitates with  $\alpha$ -tubulin (Figure S11). Thus, either SIRT4 requires its N-terminus for its extramitochondrial function toward modulation of K40-acetylated  $\alpha$ -tubulin levels, or the mitochondrial import of SIRT4 is a prerequisite for its effects on acetylated  $\alpha$ -tubulin (K40) levels. Alternatively, SIRT4 impacts through additional acetyl- $\alpha$ -tubulin (K40) independent mechanism(s) on euploidy (Figure S9) and mitotic progression and proliferation (Figure 4). The latter possibility is supported by the reduced, but still significant inhibitory impact of SIRT4( $\Delta$ N28) on mitotic duration and proliferation as compared to the full effect of wild-type SIRT4.

Another interaction partner of SIRT4 represents the deacetylase HDAC6 that was also identified as bona fide SIRT4 interactor in the proteomic screen by Mathias et al. [24]. HDAC6 is mainly found in the nucleus and cytosol and also localizes at the centrosome and basal body where it is involved in ciliary disassembly [71]. HDAC6 targets besides HSP90 and cortactin also K40-acetylated  $\alpha$ -tubulin, resulting in decreased microtubule stability and altered microtubule dynamics [9,10]. It is currently unclear to which extent SIRT4 negatively regulates acetylated  $\alpha$ -tubulin (K40) levels directly as deacetylase or indirectly via interaction with the known microtubule deacetylase HDAC6. The latter mechanism has been e.g., described for the tumor suppressor RITA (RBP-J and tubulin-associated protein) that interacts with HDAC6 and thereby modulates levels of K40-acetylated  $\alpha$ -tubulin and microtubule dynamics [72].

Additional acetyl- $\alpha$ -tubulin (K40) independent mechanism(s) of SIRT4 in mitotic regulation may be based on other mitotic SIRT4 interaction partners. For example, SIRT4 also interacts (Figure 5 and Figure S11) and co-localizes (Figure S11) with  $\gamma$ -tubulin, TUBGCP2, and TUBGCP3, which represent core components of the  $\gamma$ TURC. The latter is located at the outer region of the pericentriolar material (PCM) [73,74] and functions as nucleator of microtubules at their minus poles [53,54]. It remains to be determined whether SIRT4 regulates recruitment of the  $\gamma$ TURC to centrosomes and/or its microtubule nucleation activity. However, besides phosphorylation, only few other post-translational modifications have been so far described for  $\gamma$ TURC components, including an acetylation of GCP2 at Lys827 with currently unknown function [75,76]. Lastly, the partial localization of SIRT4-eGFP at the midzone of telophase cells and at the cytokinetic bridge (Video S4; [59]) could indicate a potential involvement of SIRT4 in cytokinesis. Interestingly, based on our proteomic screen (Table S1) SIRT4 may interact with RACK1 (Receptor of activated protein C kinase 1), that functions as major regulator of endosomal trafficking during cytokinesis [77,78].

The NAD<sup>+</sup>-SIRT3 axis has been also implicated in the regulation of microtubule dynamics and chromosomal alignment during mitosis [32,33]. However, this function of SIRT3 is likely mitochondrial-based, given that SIRT3 is predominantly found in mitochondria (Figure 3 and Figure S8) and neither localizes at centrosomes nor at the mitotic spindle (Figure S6).

Recent overviews of the literature revealed that SIRT4, although first described as a metabolic tumor suppressor [37], may display both tumor suppressor and oncogenic/cancer promoting activities, depending on the tumor type and checkpoint activating conditions [79,80]. Our data on the centrosomal localization of SIRT4 and a putative SIRT4-microtubule dynamics axis are rather consistent with an additional extramitochondrial tumor suppressor function of SIRT4. Consistent with this, SIRT4 protein levels increase not only upon treatment with DNA damaging agents effective in S-phase [81], but also

through antimetotics like inhibitors of microtubule polymerization (Nocodazole or Vinblastine) or inhibition of microtubule dynamics (Paclitaxel) (Figure S13). Therefore, increased levels of SIRT4 may be critical to link mitotic stress to inhibition of cell proliferation as exemplified by ectopic expression of SIRT4-eGFP (Figure 4).

## 5. Conclusions

Our findings provide a first evidence suggesting that SIRT4 also takes over an extramitochondrial role in the regulation of mitotic cell division. Thus, stress-induced SIRT4 as in the case of DNA damage and senescence induction may exert its anti-proliferative role through both mitochondrial/metabolism dependent and mitochondria independent functions, the latter associated with its localization and function at the mitotic spindle apparatus.

**Supplementary Materials:** The following including Supplementary Material and Methods and Supplementary References are available online at <http://www.mdpi.com/2073-4409/9/9/1950/s1>. Figure S1: Centrosomal localization of endogenous SIRT4 in HeLa cells as determined by single staining analysis. Figure S2: Centrosomal localization of endogenous SIRT4 in HT1080 cells as determined by single staining analysis. Figure S3: Centrosomal/mitotic spindle pole associated localization of endogenous SIRT4 in HeLa cells as determined by single staining analysis. Figure S4: Subcellular localization of SIRT4-eGFP (upper panels) and SIRT4( $\Delta$ N28)-eGFP (lower panels) in transiently transfected HT1080 fibrosarcoma cells (interphase) as imaged by spinning disk microscopy. Figure S5: Detection of SIRT4 at the mitotic spindle apparatus and in mitochondria. Figure S6: SIRT3 localizes in mitochondria, but is absent from centrosomes. Figure S7: Subcellular fractionation analysis of ectopically expressed SIRT4-eGFP in HEK293 cells, Figure S8: Subcellular fractionation analysis of ectopically expressed sirtuin proteins. Figure S9: HEK293 cells ectopically expressing SIRT4( $\Delta$ N28)-eGFP display an increased percentage of polyploidy. Figure S10: Network analysis of the SIRT4-interactome of mitotically synchronized HEK293 cells using the ClueGO software. Figure S11: SIRT4-eGFP interacts and subcellularly colocalizes with the  $\gamma$ TUSC components GCP2 and GCP3. Figure S12: Anti-eGFP nanobody-based immunoprecipitation analysis of mitotic SIRT4-eGFP interactors. Figure S13: Mitotic stress leads to upregulation of SIRT4 protein levels. Table S1: Differential analysis of SIRT4-interacting proteins in mitotically synchronized HEK293 cells stably expressing SIRT4-eGFP as compared to eGFP expressing control cells. Table S2: List of antibodies used for immunoblot analysis. Table S3: List of antibodies used for confocal imaging analysis. Video S1: Subcellular localization of SIRT4( $\Delta$ N28)-eGFP in transiently transfected HeLa cells (interphase) as imaged by spinning disk microscopy. Video S2: Subcellular localization of SIRT4-eGFP in transiently transfected HeLa cells (interphase) as imaged by spinning disk microscopy. Video S3: Subcellular localization of SIRT4-eGFP in transiently transfected HeLa cells (metaphase) as imaged by spinning disk microscopy. Video S4: Subcellular localization of SIRT4-eGFP in transiently transfected HeLa cells (telophase/cytokinesis) as imaged by spinning disk microscopy. Video S5: Subcellular localization of eGFP in transiently transfected HeLa cells (metaphase) as imaged by spinning disk microscopy.

**Author Contributions:** Initiated the project, L.B., A.L., S.A.-H., and R.P.P.; designed the study, L.B., A.L., and R.P.P.; designed, performed, and analyzed the experiments L.B., A.L., C.B., S.A.-H., I.F., P.V., A.K., and R.P.P.; obtained and analyzed the mass spectrometric data, N.O., A.S., and K.S.; provided expertise and generated retrovirally transduced cell line models, C.W. and H.H.; provided expertise and tools for microscopic and cell cycle analysis, C.M., D.S., and R.U.J.; provided essential reagents and methods for protein complex and mitochondrial analysis and critically corrected the manuscript, J.S., A.S.R., and M.R.A.; wrote the manuscript, L.B. and R.P.P. All authors have read and agreed to the published version of the manuscript.

**Funding:** This work was funded by the Stiftung für Altersforschung (grant 701.810.783) of the Heinrich Heine-University Düsseldorf (to R.P.P.) and by the research commission (grants 9772643 and 9772690) of the Medical Faculty of the Heinrich Heine-University Düsseldorf (to R.P.P. and M.R.A., respectively).

**Acknowledgments:** We thank Hakima Ezzahoini for technical assistance and Katharina Raba (Core Flow Cytometry Facility, ITZ) for FACS sorting of stable cell lines.

**Conflicts of Interest:** The authors declare no conflict of interest.

## References

1. Bornens, M. The centrosome in cells and organisms. *Science* **2012**, *335*, 422–426. [[CrossRef](#)] [[PubMed](#)]
2. Conduit, P.T.; Wainman, A.; Raff, J.W. Centrosome function and assembly in animal cells. *Nat. Rev. Mol. Cell Biol.* **2015**, *16*, 611–624. [[CrossRef](#)] [[PubMed](#)]
3. Thakur, H.C.; Singh, M.; Nagel-Steger, L.; Prumbaum, D.; Fansa, E.K.; Gremer, L.; Ezzahoini, H.; Abts, A.; Schmitt, L.; Raunser, S.; et al. Role of centrosomal adaptor proteins of the TACC family in the regulation of microtubule dynamics during mitotic cell division. *Biol. Chem.* **2013**, *394*, 1411–1423. [[CrossRef](#)] [[PubMed](#)]

4. Zimmerman, W.C.; Sillibourne, J.; Rosa, J.; Doxsey, S.J. Mitosis-specific anchoring of gamma tubulin complexes by pericentriol controls spindle organization and mitotic entry. *Mol. Biol. Cell* **2004**, *15*, 3642–3657. [[CrossRef](#)]
5. Desai, A.; Mitchison, T.J. Microtubule polymerization dynamics. *Annu. Rev. Cell Dev. Biol.* **1997**, *13*, 83–117. [[CrossRef](#)]
6. Janke, C.; Bulinski, J.C. Post-translational regulation of the microtubule cytoskeleton: Mechanisms and functions. *Nat. Rev. Mol. Cell Biol.* **2011**, *12*, 773–786. [[CrossRef](#)]
7. Janke, C.; Montagnac, G. Causes and consequences of microtubule acetylation. *Curr. Biol.* **2017**, *27*, R1287–R1292. [[CrossRef](#)]
8. Skoge, R.H.; Dolle, C.; Ziegler, M. Regulation of SIRT2-dependent alpha-tubulin deacetylation by cellular NAD levels. *DNA Repair* **2014**, *23*, 33–38. [[CrossRef](#)]
9. Li, L.; Yang, X.J. Tubulin acetylation: Responsible enzymes, biological functions and human diseases. *Cell. Mol. Life Sci.* **2015**, *72*, 4237–4255. [[CrossRef](#)]
10. Skoge, R.H.; Ziegler, M. SIRT2 inactivation reveals a subset of hyperacetylated perinuclear microtubules inaccessible to HDAC6. *J. Cell Sci.* **2016**, *129*, 2972–2982. [[CrossRef](#)]
11. Chang, H.C.; Guarente, L. SIRT1 and other sirtuins in metabolism. *Trends Endocrinol. Metab.* **2014**, *25*, 138–145. [[CrossRef](#)] [[PubMed](#)]
12. Donmez, G.; Guarente, L. Aging and disease: Connections to sirtuins. *Aging Cell* **2010**, *9*, 285–290. [[CrossRef](#)] [[PubMed](#)]
13. German, N.J.; Haigis, M.C. Sirtuins and the metabolic hurdles in cancer. *Curr. Biol.* **2015**, *25*, R569–R583. [[CrossRef](#)] [[PubMed](#)]
14. Guarente, L. Sirtuins in aging and disease. *Cold Spring Harb. Symp. Quant. Biol.* **2007**, *72*, 483–488. [[CrossRef](#)]
15. Haigis, M.C.; Sinclair, D.A. Mammalian sirtuins: Biological insights and disease relevance. *Annu. Rev. Pathol.* **2010**, *5*, 253–295. [[CrossRef](#)]
16. Li, X.; Kazgan, N. Mammalian sirtuins and energy metabolism. *Int. J. Biol. Sci.* **2011**, *7*, 575–587. [[CrossRef](#)]
17. Pirinen, E.; Lo Sasso, G.; Auwerx, J. Mitochondrial sirtuins and metabolic homeostasis. *Best Pract. Res. Clin. Endocrinol. Metab.* **2012**, *26*, 759–770. [[CrossRef](#)]
18. van de Ven, R.A.; Santos, D.; Haigis, M.C. Mitochondrial sirtuins and molecular mechanisms of aging. *Trends Mol. Med.* **2017**, *23*, 320–331. [[CrossRef](#)]
19. Verdin, E.; Hirschey, M.D.; Finley, L.W.; Haigis, M.C. Sirtuin regulation of mitochondria: Energy production, apoptosis, and signaling. *Trends Biochem. Sci.* **2010**, *35*, 669–675. [[CrossRef](#)]
20. de Moura, M.B.; Uppala, R.; Zhang, Y.; Van Houten, B.; Goetzman, E.S. Overexpression of mitochondrial sirtuins alters glycolysis and mitochondrial function in HEK293 cells. *PLoS ONE* **2014**, *9*, e106028.
21. Ho, L.; Titus, A.S.; Banerjee, K.K.; George, S.; Lin, W.; Deota, S.; Saha, A.K.; Nakamura, K.; Gut, P.; Verdin, E.; et al. SIRT4 regulates ATP homeostasis and mediates a retrograde signaling via AMPK. *Aging* **2013**, *5*, 1–15. [[CrossRef](#)] [[PubMed](#)]
22. Verma, M.; Shulga, N.; Pastorino, J.G. Sirtuin-4 modulates sensitivity to induction of the mitochondrial permeability transition pore. *Biochim. Biophys. Acta* **2013**, *1827*, 38–49. [[CrossRef](#)] [[PubMed](#)]
23. Haigis, M.C.; Mostoslavsky, R.; Haigis, K.M.; Fahie, K.; Christodoulou, D.C.; Murphy, A.J.; Valenzuela, D.M.; Yancopoulos, G.D.; Karow, M.; Blander, G.; et al. SIRT4 inhibits glutamate dehydrogenase and opposes the effects of calorie restriction in pancreatic beta cells. *Cell* **2006**, *126*, 941–954. [[CrossRef](#)] [[PubMed](#)]
24. Mathias, R.A.; Greco, T.M.; Oberstein, A.; Budayeva, H.G.; Chakrabarti, R.; Rowland, E.A.; Kang, Y.; Shenk, T.; Cristea, I.M. Sirtuin 4 is a lipamidase regulating pyruvate dehydrogenase complex activity. *Cell* **2014**, *159*, 1615–1625. [[CrossRef](#)]
25. Betsinger, C.N.; Cristea, I.M. Mitochondrial function, metabolic regulation, and human disease viewed through the prism of sirtuin 4 (SIRT4) functions. *J. Proteome Res.* **2019**, *18*, 1929–1938. [[CrossRef](#)]
26. Gu, L.; Zhu, Y.; Lin, X.; Tan, X.; Lu, B.; Li, Y. Stabilization of FASN by ACAT1-mediated GNPAT acetylation promotes lipid metabolism and hepatocarcinogenesis. *Oncogene* **2020**, *39*, 2437–2449. [[CrossRef](#)]
27. Guo, L.; Zhou, S.-R.; Wei, X.-B.; Liu, Y.; Chang, X.-X.; Liu, Y.; Ge, X.; Dou, X.; Huang, H.-Y.; Qian, S.-W.; et al. Acetylation of mitochondrial trifunctional protein  $\alpha$ -subunit enhances its stability to promote fatty acid oxidation and is decreased in nonalcoholic fatty liver disease. *Mol. Cell. Biol.* **2016**, *36*, 2553–2567. [[CrossRef](#)]

28. Pannek, M.; Simic, Z.; Fuszard, M.; Meleshin, M.; Rotili, D.; Mai, A.; Schutkowski, M.; Steegborn, C. Crystal structures of the mitochondrial deacylase Sirtuin 4 reveal isoform-specific acyl recognition and regulation features. *Nat. Commun.* **2017**, *8*, 1513. [[CrossRef](#)]
29. Abmayr, S.M.; Workman, J.L. Histone lysine de-beta-hydroxybutyrylation by SIRT3. *Cell Res.* **2019**, *29*, 694–695. [[CrossRef](#)]
30. Iwahara, T.; Bonasio, R.; Narendra, V.; Reinberg, D. SIRT3 functions in the nucleus in the control of stress-related gene expression. *Mol. Cell Biol.* **2012**, *32*, 5022–5034. [[CrossRef](#)]
31. Nishida, Y.; Rardin, M.J.; Carrico, C.; He, W.; Sahu, A.K.; Gut, P.; Najjar, R.; Fitch, M.; Hellerstein, M.; Gibson, B.W.; et al. SIRT5 regulates both cytosolic and mitochondrial protein malonylation with glycolysis as a major target. *Mol. Cell* **2015**, *59*, 321–332. [[CrossRef](#)] [[PubMed](#)]
32. Choi, B.S.; Park, J.E.; Jang, C.Y. Sirt3 controls chromosome alignment by regulating spindle dynamics during mitosis. *Biochem. Biophys. Res. Commun.* **2014**, *444*, 662–669. [[CrossRef](#)] [[PubMed](#)]
33. Harkcom, W.T.; Ghosh, A.K.; Sung, M.S.; Matov, A.; Brown, K.D.; Giannakakou, P.; Jaffrey, S.R. NAD<sup>+</sup> and SIRT3 control microtubule dynamics and reduce susceptibility to antimicrotubule agents. *Proc. Natl. Acad. Sci. USA* **2014**, *111*, E2443–E2452. [[CrossRef](#)] [[PubMed](#)]
34. Yang, W.; Nagasawa, K.; Munch, C.; Xu, Y.; Satterstrom, K.; Jeong, S.; Hayes, S.D.; Jedrychowski, M.P.; Vyas, F.S.; Zaganjor, E.; et al. Mitochondrial sirtuin network reveals dynamic SIRT3-dependent deacetylation in response to membrane depolarization. *Cell* **2016**, *167*, 985–1000. [[CrossRef](#)]
35. Liu, L.; Xie, R.; Yang, C.; McKeenan, W.L. Dual function microtubule- and mitochondria-associated proteins mediate mitotic cell death. *Cell Oncol.* **2009**, *31*, 393–405.
36. Ramadani-Muja, J.; Gottschalk, B.; Pfeil, K.; Burgstaller, S.; Rauter, T.; Bischof, H.; Waldeck-Weiermair, M.; Bugger, H.; Graier, W.F.; Malli, R. Visualization of sirtuin 4 distribution between mitochondria and the nucleus, based on bimolecular fluorescence self-complementation. *Cells* **2019**, *8*, 1583. [[CrossRef](#)]
37. Jeong, S.M.; Xiao, C.; Finley, L.W.; Lahusen, T.; Souza, A.L.; Pierce, K.; Li, Y.H.; Wang, X.; Laurent, G.; German, N.J.; et al. SIRT4 has tumor-suppressive activity and regulates the cellular metabolic response to DNA damage by inhibiting mitochondrial glutamine metabolism. *Cancer Cell* **2013**, *23*, 450–463. [[CrossRef](#)]
38. Kim, H.S.; Patel, K.; Muldoon-Jacobs, K.; Bisht, K.S.; Aykin-Burns, N.; Pennington, J.D.; van der Meer, R.; Nguyen, P.; Savage, J.; Owens, K.M.; et al. SIRT3 is a mitochondria-localized tumor suppressor required for maintenance of mitochondrial integrity and metabolism during stress. *Cancer Cell* **2010**, *17*, 41–52. [[CrossRef](#)]
39. Zeng, J.; Jiang, M.; Wu, X.; Diao, F.; Qiu, D.; Hou, X.; Wang, H.; Li, L.; Li, C.; Ge, J.; et al. SIRT4 is essential for metabolic control and meiotic structure during mouse oocyte maturation. *Aging Cell* **2018**, *17*, e12789. [[CrossRef](#)]
40. Lang, A.; Grether-Beck, S.; Singh, M.; Kuck, F.; Jakob, S.; Kefalas, A.; Altinluk-Hambüchen, S.; Graffmann, N.; Schneider, M.; Lindecke, A.; et al. MicroRNA-15b regulates mitochondrial ROS production and the senescence-associated secretory phenotype through sirtuin 4/SIRT4. *Aging* **2016**, *8*, 484–505. [[CrossRef](#)]
41. Han, Y.; Zhou, S.; Coetzee, S.; Chen, A. SIRT4 and its roles in energy and redox metabolism in health, disease and during exercise. *Front. Physiol.* **2019**, *10*, 1006. [[CrossRef](#)]
42. Lang, A.; Anand, R.; Altinluk-Hambüchen, S.; Ezzahoini, H.; Stefanski, A.; Iram, A.; Bergmann, L.; Urbach, J.; Bohler, P.; Hansel, J.; et al. SIRT4 interacts with OPA1 and regulates mitochondrial quality control and mitophagy. *Aging* **2017**, *9*, 2163–2189. [[CrossRef](#)] [[PubMed](#)]
43. Drews, L.; Zimmermann, M.; Poss, R.E.; Brilhaus, D.; Bergmann, L.; Wiek, C.; Piekorz, R.P.; Weber, A.P.M.; Mettler-Altmann, T.; Reichert, A.S. Ammonia inhibits energy metabolism in astrocytes in a rapid and GDH2-dependent manner. *bioRxiv* **2019**, 683763. [[CrossRef](#)]
44. Schneider, L.; Essmann, F.; Kletke, A.; Rio, P.; Hanenberg, H.; Wetzel, W.; Schulze-Osthoff, K.; Nürnberg, B.; Piekorz, R.P. The transforming acidic coiled coil 3 protein is essential for spindle-dependent chromosome alignment and mitotic survival. *J. Biol. Chem.* **2007**, *282*, 29273–29283. [[CrossRef](#)]
45. Rothbauer, U.; Zolghadr, K.; Muyldermans, S.; Schepers, A.; Cardoso, M.C.; Leonhardt, H. A versatile nanotrap for biochemical and functional studies with fluorescent fusion proteins. *Mol. Cell. Proteom.* **2008**, *7*, 282–289. [[CrossRef](#)] [[PubMed](#)]
46. Anand, R.; Strecker, V.; Urbach, J.; Wittig, I.; Reichert, A.S. Mic13 is essential for formation of crista junctions in mammalian cells. *PLoS ONE* **2016**, *11*, e0160258. [[CrossRef](#)]

47. Gomez-Baldo, L.; Schmidt, S.; Maxwell, C.A.; Bonifaci, N.; Gabaldon, T.; Vidalain, P.O.; Senapedis, W.; Kletke, A.; Rosing, M.; Barnekow, A.; et al. TACC3-TSC2 maintains nuclear envelope structure and controls cell division. *Cell Cycle* **2010**, *9*, 1143–1155. [[CrossRef](#)]
48. Lang, A.; Piekorz, R.P. Novel role of the SIRT4-OPA1 axis in mitochondrial quality control. *Cell Stress* **2018**, *2*, 1–3. [[CrossRef](#)] [[PubMed](#)]
49. Ahuja, N.; Schwer, B.; Carobbio, S.; Waltregny, D.; North, B.J.; Castronovo, V.; Maechler, P.; Verdin, E. Regulation of insulin secretion by SIRT4, a mitochondrial ADP-ribosyltransferase. *J. Biol. Chem.* **2007**, *282*, 33583–33592. [[CrossRef](#)]
50. Lombard, D.B.; Alt, F.W.; Cheng, H.-L.; Bunkenborg, J.; Streeper, R.S.; Mostoslavsky, R.; Kim, J.; Yancopoulos, G.; Valenzuela, D.; Murphy, A.; et al. Mammalian Sir2 homolog SIRT3 regulates global mitochondrial lysine acetylation. *Mol. Cell. Biol.* **2007**, *27*, 8807–8814. [[CrossRef](#)]
51. Dictenberg, J.B.; Zimmerman, W.; Sparks, C.A.; Young, A.; Vidair, C.; Zheng, Y.; Carrington, W.; Fay, F.S.; Doxsey, S.J. Pericentrin and gamma-tubulin form a protein complex and are organized into a novel lattice at the centrosome. *J. Cell Biol.* **1998**, *141*, 163–174. [[CrossRef](#)] [[PubMed](#)]
52. Liu, M.; Wang, Z.; Ren, M.; Yang, X.; Liu, B.; Qi, H.; Yu, M.; Song, S.; Chen, S.; Liu, L.; et al. SIRT4 regulates PTEN stability through IDE in response to cellular stresses. *FASEB J.* **2019**, *33*, 5535–5547. [[CrossRef](#)] [[PubMed](#)]
53. Cota, R.R.; Teixido-Travesa, N.; Ezquerro, A.; Eibes, S.; Lacasa, C.; Roig, J.; Luders, J. MZT1 regulates microtubule nucleation by linking gammaTuRC assembly to adapter-mediated targeting and activation. *J. Cell Sci.* **2017**, *130*, 406–419. [[CrossRef](#)] [[PubMed](#)]
54. Tovey, C.A.; Tubman, C.E.; Hamrud, E.; Zhu, Z.; Dyas, A.E.; Butterfield, A.N.; Fyfe, A.; Johnson, E.; Conduit, P.T. Gamma-TuRC heterogeneity revealed by analysis of Mozart1. *Curr. Biol.* **2018**, *28*, 2314–2323. [[CrossRef](#)]
55. Crncec, A.; Hochegger, H. Triggering mitosis. *FEBS Lett.* **2019**, *593*, 2868–2888. [[CrossRef](#)]
56. Jeffery, C.J. Protein moonlighting: What is it, and why is it important? *Philos. Trans. R. Soc. Lond. B Biol. Sci.* **2018**, *373*. [[CrossRef](#)]
57. The Human Protein Atlas. Available online: [https://www.proteinatlas.org/search/subcell\\_location:Centriolar+satellite,Centrosome+AND+subcell\\_location:Mitochondria](https://www.proteinatlas.org/search/subcell_location:Centriolar+satellite,Centrosome+AND+subcell_location:Mitochondria) (accessed on 16 February 2020).
58. Majumder, S.; Slabodnick, M.; Pike, A.; Marquardt, J.; Fisk, H.A. VDAC3 regulates centriole assembly by targeting Mps1 to centrosomes. *Cell Cycle* **2012**, *11*, 3666–3678. [[CrossRef](#)]
59. Bergmann, L.; Piekorz, R.P. (Heinrich Heine University, Düsseldorf, Germany). Personal communication, 2020.
60. Kashatus, D.F.; Lim, K.H.; Brady, D.C.; Pershing, N.L.; Cox, A.D.; Counter, C.M. RALA and RALBP1 regulate mitochondrial fission at mitosis. *Nat. Cell Biol.* **2011**, *13*, 1108–1115. [[CrossRef](#)]
61. Chung, J.Y.; Steen, J.A.; Schwarz, T.L. Phosphorylation-induced motor shedding is required at mitosis for proper distribution and passive inheritance of mitochondria. *Cell Rep.* **2016**, *16*, 2142–2155. [[CrossRef](#)]
62. Liu, L.; Xie, B.; Fan, M.; Candas-Green, D.; Jiang, J.X.; Wei, R.; Wang, Y.; Chen, H.W.; Hu, Y.; Li, J.J. Low-level saturated fatty acid palmitate benefits liver cells by boosting mitochondrial metabolism via CDK1-SIRT3-CPT2 cascade. *Dev. Cell* **2019**, *52*, 196–209. [[CrossRef](#)]
63. Liu, R.; Fan, M.; Candas, D.; Qin, L.; Zhang, X.; Eldridge, A.; Zou, J.X.; Zhang, T.; Juma, S.; Jin, C.; et al. CDK1-mediated SIRT3 activation enhances mitochondrial function and tumor radioresistance. *Mol. Cancer Ther.* **2015**, *14*, 2090–2102. [[CrossRef](#)] [[PubMed](#)]
64. Ling, H.; Peng, L.; Seto, E.; Fukasawa, K. Suppression of centrosome duplication and amplification by deacetylases. *Cell Cycle* **2012**, *11*, 3779–3791. [[CrossRef](#)] [[PubMed](#)]
65. Ling, H.; Peng, L.; Wang, J.; Rahhal, R.; Seto, E. Histone deacetylase SIRT1 targets Plk2 to regulate centriole duplication. *Cell Rep.* **2018**, *25*, 2851–2865. [[CrossRef](#)] [[PubMed](#)]
66. Wang, T.; Zou, Y.; Huang, N.; Teng, J.; Chen, J. CCDC84 acetylation oscillation regulates centrosome duplication by modulating HsSAS-6 degradation. *Cell Rep.* **2019**, *29*, 2078–2091. [[CrossRef](#)]
67. North, B.J.; Verdin, E. Mitotic regulation of SIRT2 by cyclin-dependent kinase 1-dependent phosphorylation. *J. Biol. Chem.* **2007**, *282*, 19546–19555. [[CrossRef](#)]
68. Movahedi Naini, S.; Sheridan, A.M.; Force, T.; Shah, J.V.; Bonventre, J.V. Group IVA cytosolic phospholipase A2 regulates the G2-to-M transition by modulating the activity of tumor suppressor SIRT2. *Mol. Cell Biol.* **2015**, *35*, 3768–3784. [[CrossRef](#)]

69. Inoue, T.; Hiratsuka, M.; Osaki, M.; Yamada, H.; Kishimoto, I.; Yamaguchi, S.; Nakano, S.; Katoh, M.; Ito, H.; Oshimura, M. SIRT2, a tubulin deacetylase, acts to block the entry to chromosome condensation in response to mitotic stress. *Oncogene* **2007**, *26*, 945–957. [[CrossRef](#)]
70. Kim, H.S.; Vassilopoulos, A.; Wang, R.H.; Lahusen, T.; Xiao, Z.; Xu, X.; Li, C.; Veenstra, T.D.; Li, B.; Yu, H.; et al. SIRT2 maintains genome integrity and suppresses tumorigenesis through regulating APC/C activity. *Cancer Cell* **2011**, *20*, 487–499. [[CrossRef](#)]
71. Ran, J.; Yang, Y.; Li, D.; Liu, M.; Zhou, J. Deacetylation of alpha-tubulin and cortactin is required for HDAC6 to trigger ciliary disassembly. *Sci. Rep.* **2015**, *5*, 12917. [[CrossRef](#)]
72. Steinhauser, K.; Kloble, P.; Kreis, N.N.; Ritter, A.; Friemel, A.; Roth, S.; Reichel, J.M.; Michaelis, J.; Rieger, M.A.; Louwen, F.; et al. Deficiency of RITA results in multiple mitotic defects by affecting microtubule dynamics. *Oncogene* **2017**, *36*, 2146–2159. [[CrossRef](#)]
73. Woodruff, J.B.; Wueseke, O.; Hyman, A.A. Pericentriolar material structure and dynamics. *Philos. Trans. R. Soc. Lond. B Biol. Sci.* **2014**, *369*, 20130459. [[CrossRef](#)] [[PubMed](#)]
74. Pihan, G.A. Centrosome dysfunction contributes to chromosome instability, chromoanagenesis, and genome reprogramming in cancer. *Front. Oncol.* **2013**, *3*, 277. [[CrossRef](#)]
75. Choudhary, C.; Kumar, C.; Gnad, F.; Nielsen, M.L.; Rehman, M.; Walther, T.C.; Olsen, J.V.; Mann, M. Lysine acetylation targets protein complexes and co-regulates major cellular functions. *Science* **2009**, *325*, 834–840. [[CrossRef](#)] [[PubMed](#)]
76. Teixido-Travesa, N.; Roig, J.; Luders, J. The where, when and how of microtubule nucleation—One ring to rule them all. *J. Cell Sci.* **2012**, *125*, 4445–4456. [[CrossRef](#)] [[PubMed](#)]
77. Ai, E.; Skop, A.R. Endosomal recycling regulation during cytokinesis. *Commun. Integr. Biol.* **2009**, *2*, 444–447. [[CrossRef](#)] [[PubMed](#)]
78. Skop, A.R.; Liu, H.; Yates, J., 3rd; Meyer, B.J.; Heald, R. Dissection of the mammalian midbody proteome reveals conserved cytokinesis mechanisms. *Science* **2004**, *305*, 61–66. [[CrossRef](#)]
79. Carafa, V.; Altucci, L.; Nebbioso, A. Dual tumor suppressor and tumor promoter action of sirtuins in determining malignant phenotype. *Front. Pharmacol.* **2019**, *10*, 38. [[CrossRef](#)]
80. Huang, G.; Zhu, G. Sirtuin-4 (SIRT4), a therapeutic target with oncogenic and tumor-suppressive activity in cancer. *Onco Targets Ther.* **2018**, *11*, 3395–3400. [[CrossRef](#)]
81. Jeong, S.M.; Lee, A.; Lee, J.; Haigis, M.C. SIRT4 suppresses tumor formation in genetic models of Myc-induced B cell lymphoma. *J. Biol. Chem.* **2013**, *289*, 4135–4144. [[CrossRef](#)]



© 2020 by the authors. Licensee MDPI, Basel, Switzerland. This article is an open access article distributed under the terms and conditions of the Creative Commons Attribution (CC BY) license (<http://creativecommons.org/licenses/by/4.0/>).

## Subcellular localization and mitotic interactome analyses identify SIRT4 as a centrosomally localized and microtubule associated protein

Laura Bergmann, Alexander Lang, Christoph Bross, Simone Altinoluk-Hambuechen, Iris Fey, Nina Overbeck, Anja Stefanski, Constanze Wiek, Andreas Kefalas, Patrick Verhuelson, Christian Mielke, Dennis Sohn, Kai Stühler, Helmut Hanenberg, Reiner U. Jänicke, Jürgen Scheller, Andreas S. Reichert, Mohammad Reza Ahmadian, and Roland P. Piekorz

### Contents:

#### Supplementary Tables

**Table S1.** Differential analysis of SIRT4-interacting proteins in mitotically synchronized HEK293 cells stably expressing SIRT4-eGFP as compared to eGFP expressing control cells.\*

**Table S2.** List of antibodies used for immunoblot analysis.

Table S2. Antibodies for immunoblot analysis.

Primary antibodies	Supplier	Species	Dilution	Reference
Flag M2	Sigma-Aldrich	mouse	1:500	F3165
eGFP	Roche	mouse	1:2.000	11814460001
SIRT4	Proteintech	mouse	1:40.000	66543-1-Ig
SIRT3	Cell Signaling Technology	rabbit	1:500	5490
HDAC6	Santa Cruz	rabbit	1:1000	sc-11420
HDAC6	Cell Signaling Technology	rabbit	1:1000	7558
acetyl. Tubulin (K40)	Abcam	mouse	1:500	ab24610
$\alpha$ -Tubulin	Abcam	rabbit	1:1000	ab52866
OPA1	BD	mouse	1:1000	612607
OPA1		rabbit	1:1000	Barrera M et al. FEBS Lett.2016; 590:3309–22. <a href="https://doi.org/10.1002/1873-3468.12384">https://doi.org/10.1002/1873-3468.12384</a>
ATP5A1	Proteintech	rabbit	1:1000	14676-1-AP
ANT2	Cell Signaling Technology	rabbit	1:1000	14671
$\gamma$ -Tubulin	Sigma-Aldrich	mouse	1:1000	T8557
GCP2	GeneTex	rabbit	1:1000	GTX102281
GCP3	Santa Cruz	mouse	1:1000	sc-373758
Pericentrin	Abcam	rabbit	1:1000	ab4448
GAPDH	Santa Cruz	mouse	1:1000	sc-47724
Na <sup>+</sup> / K <sup>+</sup> ATPase	Sigma-Aldrich	mouse	1:1000	A276
CDK1	BD	mouse	1:500	610037

\* Data only accessible online

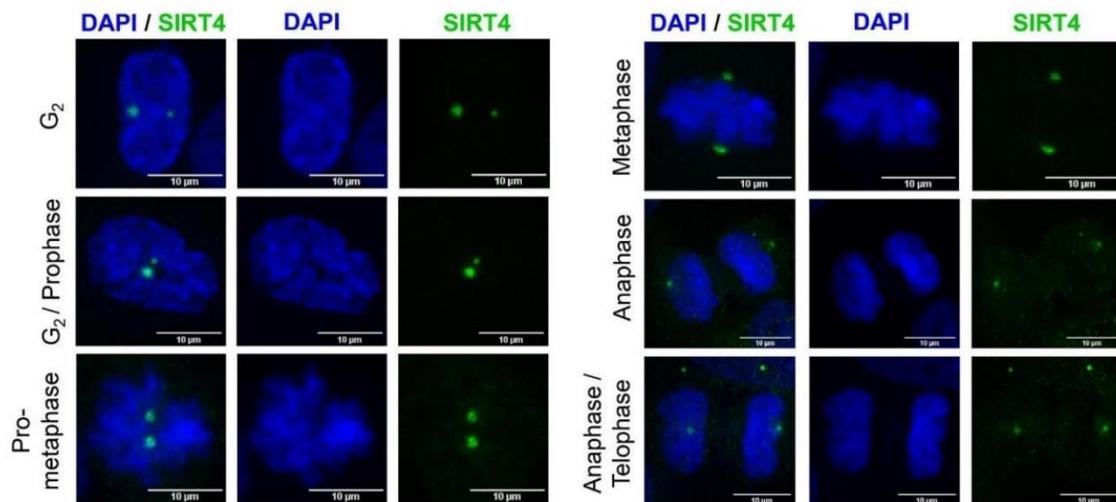
**Table S3.** List of antibodies used for confocal imaging analysis.

Primary antibodies	Supplier	Species	Dilution	Reference
eGFP	Roche	mouse	1:1000	11814460001
$\alpha$ -Tubulin	Santa Cruz	rat	1:500	sc-53029
$\alpha$ -Tubulin	Acris	rat	1:500	SM 568P
$\gamma$ -Tubulin	Sigma-Aldrich	mouse	1:500	T6557
Pericentrin	Abcam	rabbit	1:1000	ab4448
Pericentrin	Abcam	mouse	1:1000	ab28144
SIRT4	Santa Cruz	rabbit	1:500	sc-135053
SIRT4	Sigma Aldrich	mouse	1:500	SAB1407208
TUBGCP2	Santa Cruz	mouse	1:500	sc-377117
TUBGCP3	Santa Cruz	mouse	1:500	sc-373758
SIRT3	Cell Signaling Technology	rabbit	1:500	5490
MTCO2	Abcam	mouse	1:500	ab3298

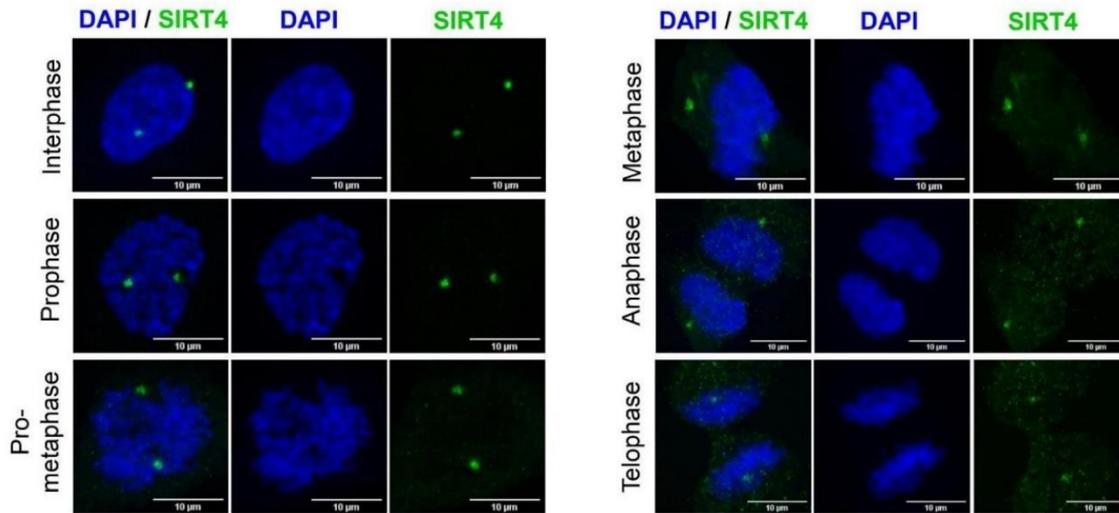
  

Secondary antibodies	Supplier	Species	Species reactivity	Dilution	Reference
Alexa Fluor 633	Invitrogen - Thermo Fisher Scientific	goat IgG	anti-rat	1:1000	A-21094
Alexa Fluor 488	Invitrogen - Thermo Fisher Scientific	goat IgG	anti-rabbit	1:1000	A-11034
Alexa Fluor 546	Invitrogen - Thermo Fisher Scientific	goat IgG	anti-rabbit	1:1000	A-11035
Alexa Fluor 488	Invitrogen - Thermo Fisher Scientific	goat IgG	anti-mouse	1:1000	A-11029
Alexa Fluor 546	Invitrogen - Thermo Fisher Scientific	goat IgG	anti-mouse	1:1000	A-11003

### Supplementary Figures



**Fig. S1.** Centrosomal localization of endogenous SIRT4 in HeLa cells as determined by single staining analysis. SIRT4 was detected using spinning disk microscopy and a polyclonal antibody against SIRT4 (sc-135053, Santa Cruz Biotechnology). DAPI was used to visualize DNA. Bar: 10  $\mu$ m.



**Fig. S2.** Centrosomal localization of endogenous SIRT4 in HT1080 cells as determined by single staining analysis. SIRT4 was detected using spinning disk microscopy and a polyclonal antibody against SIRT4 (sc-135053, Santa Cruz Biotechnology). DAPI was used to visualize DNA. Bar: 10  $\mu\text{m}$ .

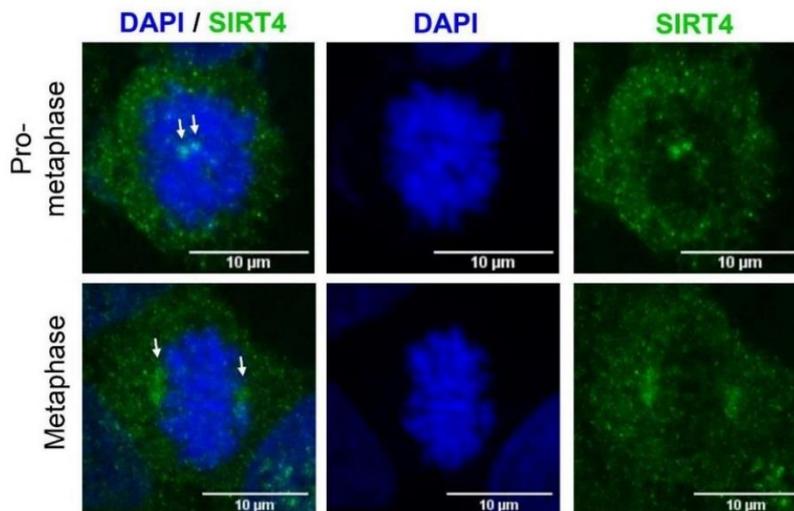


**Fig. S3.** Centrosomal/mitotic spindle pole associated localization of endogenous SIRT4 in HeLa cells as determined by single staining analysis. SIRT4 was detected using spinning disk microscopy and a monoclonal antibody against SIRT4 (SAB1407208, Sigma-Aldrich). DAPI was used to visualize DNA. Bar: 10  $\mu\text{m}$ .

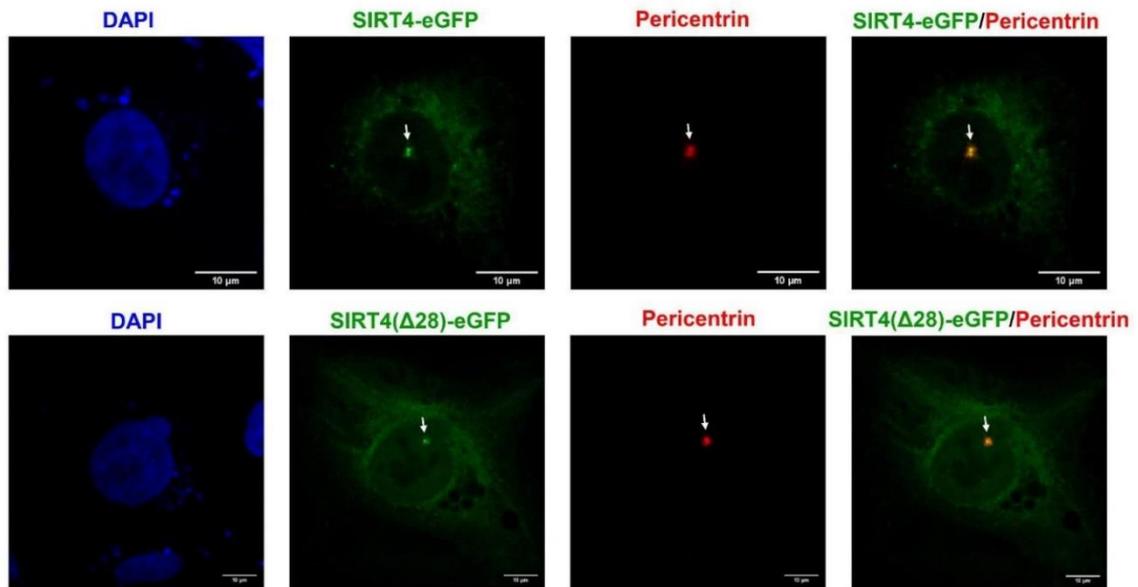


**Fig. S4.** Subcellular localization of SIRT4-eGFP (upper panels) and SIRT4( $\Delta$ N28)-eGFP (lower panels) in transiently transfected HT1080 fibrosarcoma cells (interphase) as imaged by spinning disk microscopy. Antibodies against Pericentrin were employed to visualize centrosomes. DAPI was used to detect DNA. Bars: 10  $\mu$ m.

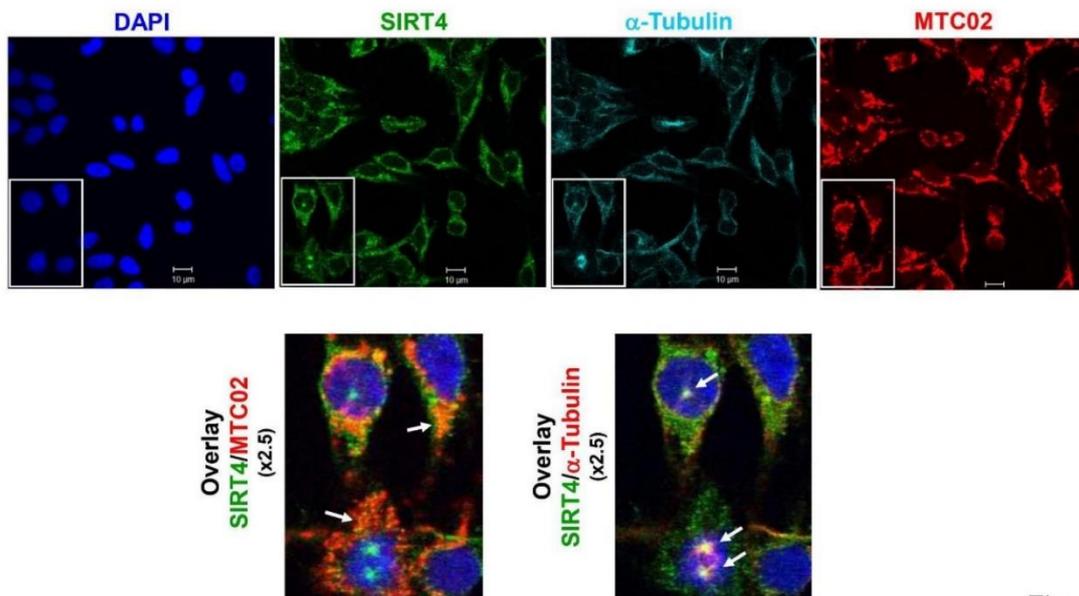


**Fig. S5.** Detection of SIRT4 at the mitotic spindle apparatus and in mitochondria. Endogenous SIRT4 was detected in HEK293 cells using standard confocal microscopy (cLSM510-Meta, Zeiss) and a polyclonal antibody against SIRT4 (sc-135053, Santa Cruz Biotechnology). Antibodies against MTC02 and  $\alpha$ -tubulin were employed to visualize mitochondria and microtubules, respectively. DAPI was used to detect DNA. Magnifications of SIRT4 co-localizing with either MTC02 or  $\alpha$ -tubulin are depicted and indicated by arrows. Bar: 10  $\mu$ m.

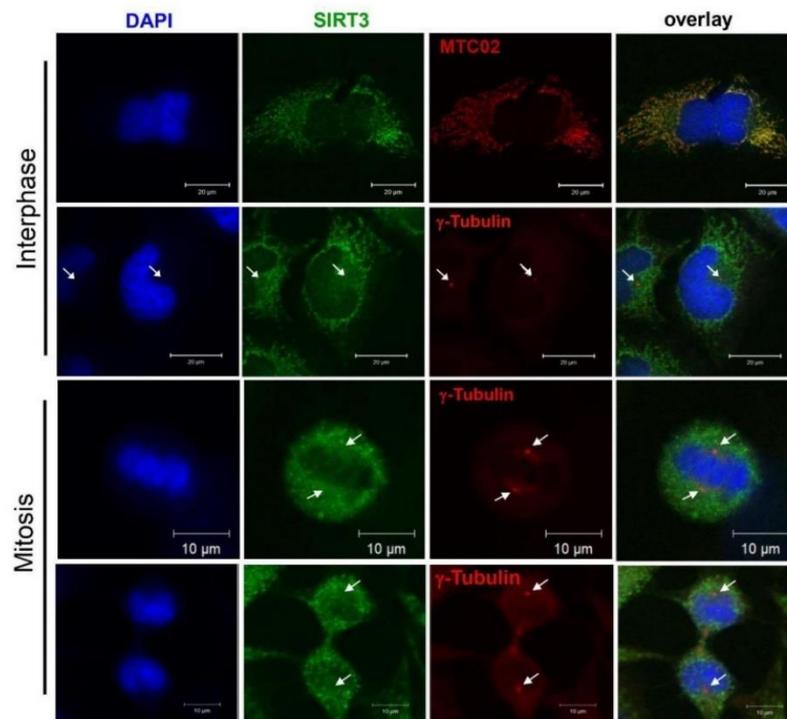


**Fig. S6.** SIRT3 localizes in mitochondria, but is absent from centrosomes. Endogenous SIRT3 was detected in HeLa cells using confocal microscopy (cLSM510-Meta, Zeiss) and a rabbit monoclonal antibody against SIRT3 (#5490, Cell Signaling). MTC02 and  $\alpha$ -tubulin co-stainings were employed to visualize mitochondria and centrosomes, respectively. DAPI was used to detect DNA. Bar: 20  $\mu$ m (interphase) and 10  $\mu$ m (mitosis).

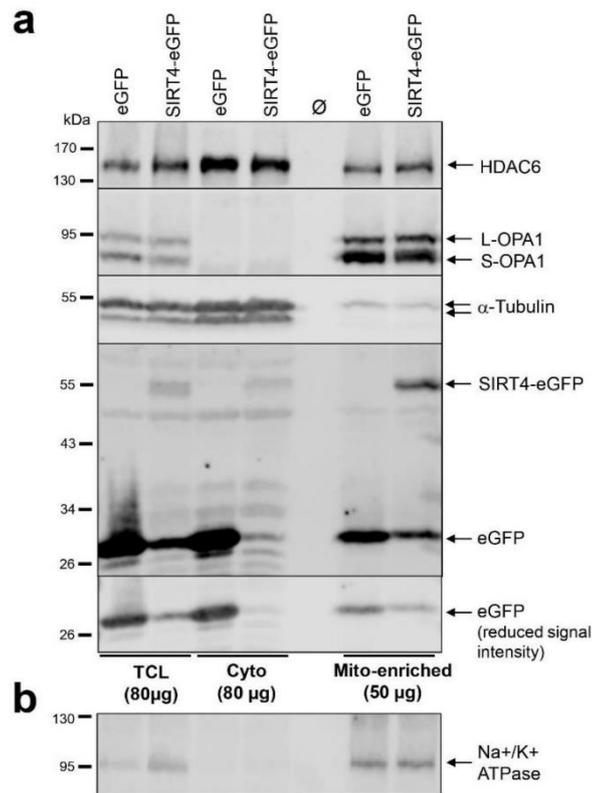


**Fig. S7.** Subcellular fractionation analysis of ectopically expressed SIRT4-eGFP in HEK293 cells. Total cell lysates (TCL; 80  $\mu$ g) and the respective mitochondrially enriched (Mito-enriched; 50  $\mu$ g) and cytosolic (Cyto; 80  $\mu$ g) fractions were subjected to immunoblot analysis. Subcellular marker proteins detected were OPA1 (long and short form; mitochondria),  $\alpha$ -tubulin (cytoplasm), and HDAC6 (predominantly cytoplasmic localized) (a) as well as Na/K ATPase as cell membrane marker (b). Antibodies against eGFP were employed to visualize eGFP and SIRT4-eGFP.

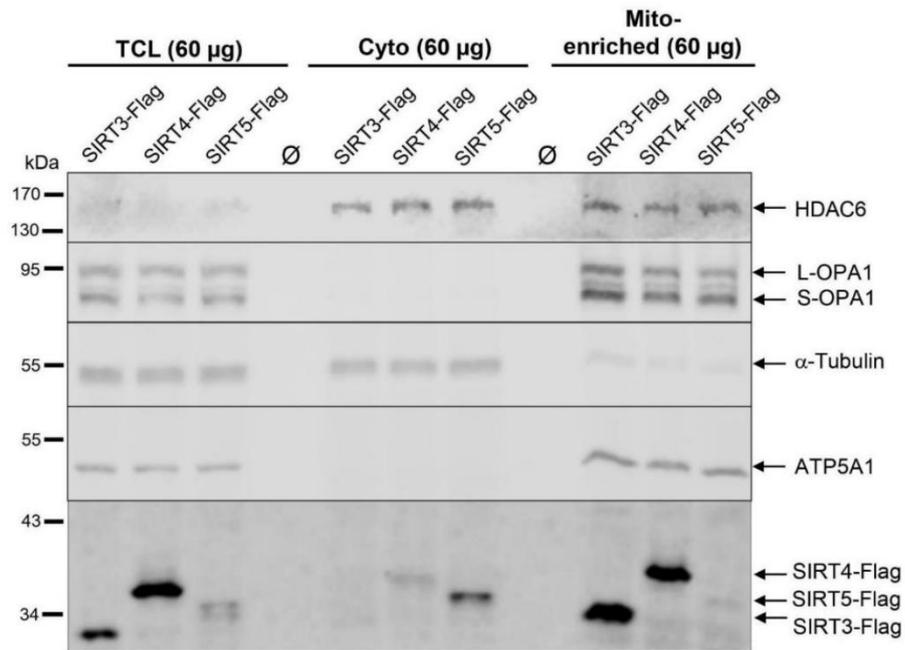


**Fig. S8.** Subcellular fractionation analysis of ectopically expressed sirtuin proteins. C-terminally Flag-tagged sirtuin isoforms SIRT3, SIRT4, and SIRT5 were ectopically expressed in HEK293 cells. Total cell lysates (TCL; 60 µg) and the respective mitochondrially enriched (Mito-enriched; 60 µg) and cytosolic (Cyto; 60 µg) fractions were subjected to immunoblot analysis. Subcellular marker proteins detected were OPA1 (long and short form; mitochondria) and ATP5A1 (mitochondria), α-tubulin (cytoplasm), and HDAC6 (predominantly cytoplasmic localized).

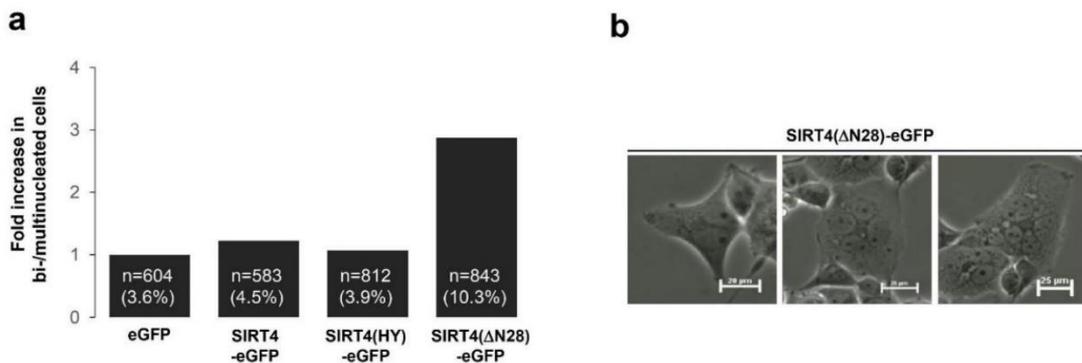


**Fig. S9.** HEK293 cells ectopically expressing SIRT4(ΔN28)-eGFP display an increased percentage of polyploidy. (a) Quantification of bi- or multinucleated HEK293 cells expressing SIRT4-eGFP or mutants thereof. The total numbers of cells analysed and the percentage of bi- or multinucleated cells are indicated (b). Representative pictures of polyploid SIRT4(ΔN28)-eGFP expressing HEK293 cells are depicted. Bar: 20 or 25 µm.

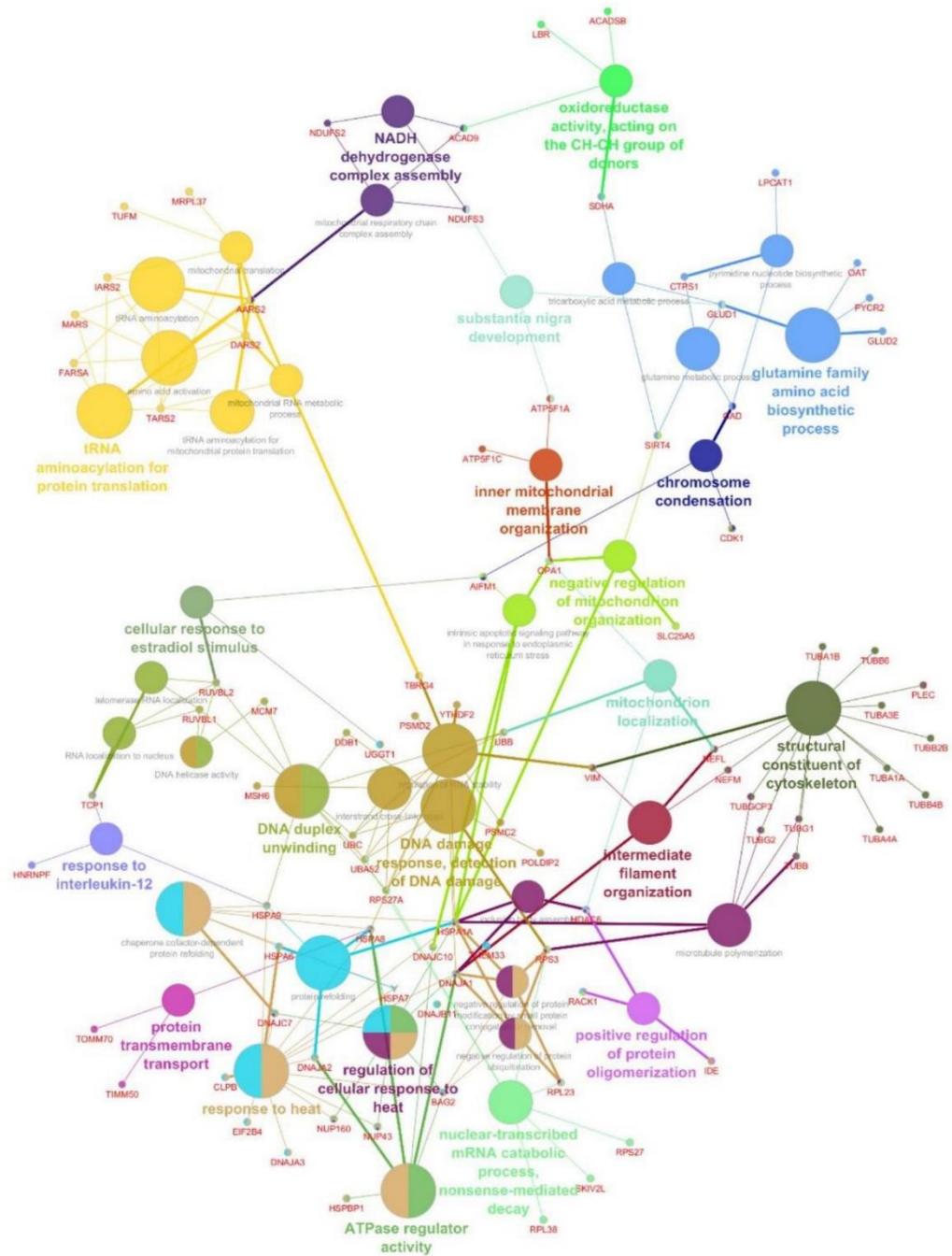


**Fig. S10.** Network analysis of the SIRT4-interactome of mitotically synchronized HEK293 cells using the ClueGO software.

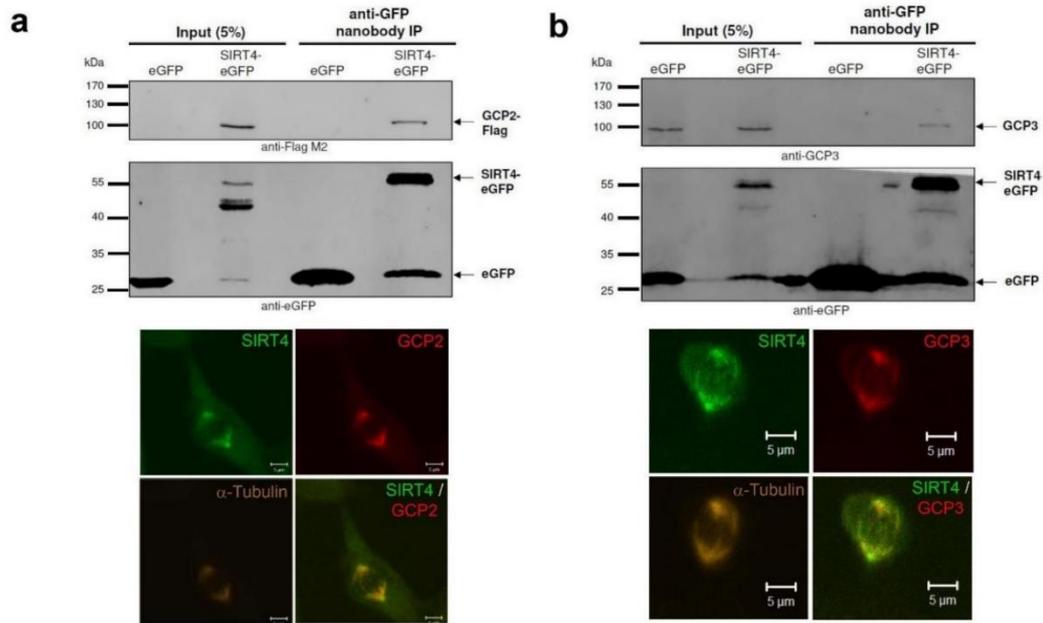


**Fig. S11.** SIRT4-eGFP interacts and subcellularly colocalizes with the  $\gamma$ TUSC components GCP2 and GCP3. **(a)** Upper panel: Anti-eGFP nanobody based immunoprecipitation analysis of SIRT4-eGFP interaction with ectopically expressed GCP2-Flag in HEK293 cells (upper panel). SIRT4 co-localizes with GCP2 at the mitotic spindle apparatus (lower panel). Endogenous SIRT4 and GCP2 were detected in HT1080 cells using standard confocal microscopy (cLSM510-Meta, Zeiss) and staining with a polyclonal antibody against SIRT4 (sc-135053, Santa Cruz Biotechnology) and a monoclonal antibody against GCP2 (sc. 377117, Santa Cruz Biotechnology). Microtubules were detected by  $\alpha$ -Tubulin staining. DAPI was used to visualize DNA. Bar: 5  $\mu$ m. **(b)** Upper panel: Anti-eGFP nanobody based immunoprecipitation analysis of SIRT4-eGFP interaction with endogenous GCP3 in HEK293 cells (upper panel). SIRT4 co-localizes with GCP3 at the mitotic spindle apparatus. Endogenous SIRT4 and GCP3 were detected in HT1080 cells using standard confocal microscopy (cLSM510-Meta, Zeiss) and staining with a polyclonal antibody against SIRT4 (sc-135053, Santa Cruz Biotechnology) and a monoclonal antibody against GCP3 (sc. 373758, Santa Cruz Biotechnology). Microtubules were detected by  $\alpha$ -Tubulin staining. DAPI was used to visualize DNA. Bar: 5  $\mu$ m.

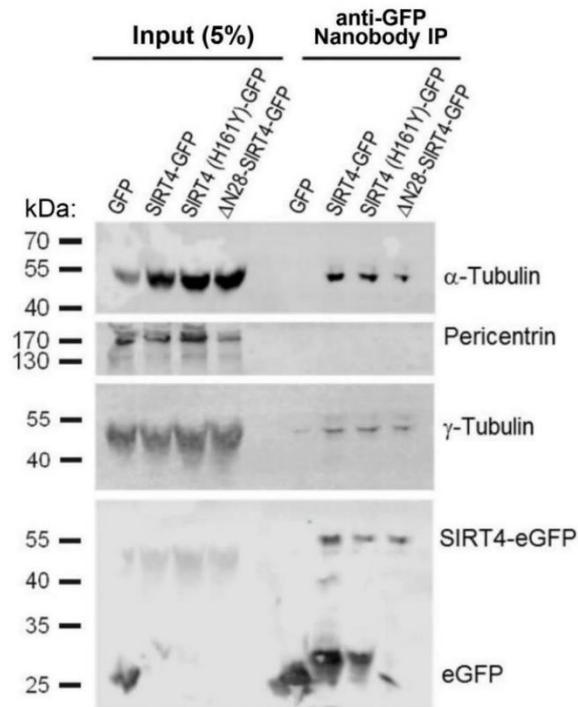


**Fig. S12.** Anti-eGFP nanobody based immunoprecipitation analysis of mitotic SIRT4-eGFP interactors. HEK293 cells stably expressing SIRT4-eGFP, mutants thereof [enzymatically inactive SIRT4(H161Y)-eGFP or SIRT4( $\Delta$ N28)-eGFP lacking the N-terminal mitochondrial targeting signal], or eGFP as control were analysed.  $\alpha$ -tubulin and  $\gamma$ -tubulin, but not Pericentrin, co-immunoprecipitate with SIRT4-eGFP.

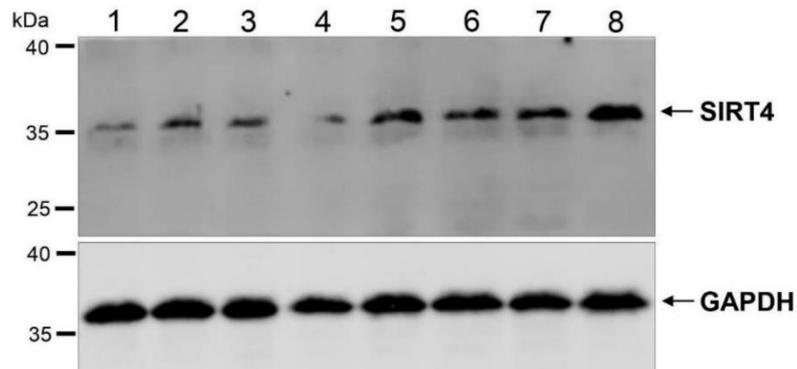


**Fig. S13.** Mitotic stress leads to upregulation of SIRT4 protein levels. HEK293 cells were either treated for 24 h with DMSO (control, lane 1) or various antimetotics or DNA damage inducing agents (suppl. Material and Methods), including Nocodazole (100 ng/ml, lane 2), Paclitaxel (10 nM, lane 3), MLN8237 (0.5  $\mu$ M, lane 4), Vinblastine (1  $\mu$ M, lane 5), Hydroxyurea (20 mM, lane 6), Mitomycin C (5  $\mu$ g/ml, lane 7), and Actinomycin D (1  $\mu$ g/ml). Antibodies against GAPDH were employed to control protein loading.

### Supplementary Videos\*

**Video S1:** Subcellular localization of SIRT4( $\Delta$ N28)-eGFP in transiently transfected HeLa cells (interphase) as imaged by spinning disk microscopy. Antibodies against Pericentrin and  $\alpha$ -tubulin were employed to visualize centrosomes and microtubules, respectively. DAPI was used to detect DNA. Lower panels: Movies are embedded as GIF files into PowerPoint.

**Video S2:** Subcellular localization of SIRT4-eGFP in transiently transfected HeLa cells (interphase) as imaged by spinning disk microscopy. Antibodies against Pericentrin and  $\alpha$ -tubulin were employed to visualize centrosomes and microtubules, respectively. DAPI was used to detect DNA. Movies are embedded as GIF files into PowerPoint.

**Video S3:** Subcellular localization of SIRT4-eGFP in transiently transfected HeLa cells (metaphase) as imaged by spinning disk microscopy. To increase detection of the SIRT4-eGFP fusion protein a primary antibody against GFP was employed. Antibodies against Pericentrin and  $\alpha$ -tubulin were employed to visualize centrosomes and microtubules, respectively. DAPI was used to detect DNA. Movies are embedded as GIF files into PowerPoint.

**Video S4:** Subcellular localization of SIRT4-eGFP in transiently transfected HeLa cells (telophase/cytokinesis) as imaged by spinning disk microscopy. To increase detection of the SIRT4-eGFP fusion protein a primary antibody against GFP was employed. Antibodies against Pericentrin and  $\alpha$ -tubulin were employed to visualize centrosomes and microtubules, respectively. DAPI was used to detect DNA. Movies are embedded as GIF files into PowerPoint.

**Video S5:** Subcellular localization of eGFP in transiently transfected HeLa cells (metaphase) as imaged by spinning disk microscopy. To increase detection of the eGFP protein a primary antibody against GFP was employed. Endogenous SIRT4 was detected using a polyclonal antibody against SIRT4 (sc-135053, Santa Cruz Biotechnology). Antibodies against  $\alpha$ -tubulin were employed to visualize microtubules. DAPI was used to detect DNA. Movies are embedded as GIF files into PowerPoint.

### Supplementary Materials and Methods

**Expression constructs and generation of stable cell lines.** Plasmids for eukaryotic expression of TUBGCP2 (pCMV6-GCP2-Flag) and TUBGCP3 (pCMV6-GCP3-Flag) were obtained from Sino Biological Inc. Expression plasmids for C-terminally Flag-tagged Sirtuins were obtained from Origene (pCMV6-SIRT4-Myc-Flag) and Addgene (pcDNA3.1-SIRT3-Flag: #13814; pcDNA3.1-SIRT5-Flag: #13816; [1]). HEK293 cell lines stably expressing flagged SIRT isoforms were generated using standard transfection protocols followed by selection [400  $\mu$ g/ml Geneticin/G418 (Genaxxon)]. Cell lines were passaged in media containing 400  $\mu$ g/ml Geneticin/G418 as permanent selection agent.

**Treatment of HEK293 cells with DNA damage inducing and antimetabolic agents.** Cells were treated with various agents, including Nocodazole and Vinblastin (inhibitors of microtubule polymerization), Paclitaxel (stabilizes microtubules and inhibits their dynamics), MLN8237 (inhibitor of the mitotic kinase Aurora A), Mitomycin C (DNA crosslinker), Hydroxyurea (ribonucleotide reductase inhibitor), and Actinomycin D (blocks DNA dependent RNA polymerase). Cell lysates were subjected to immunoblot analysis after lysing cells in buffer containing 0.5% NP-

---

\* Data only accessible online

40 as described in the main manuscript. Antibodies used for immunoblot analysis are listed in Table S2.

**Sample preparation for proteomic analysis.** Proteins were extracted from frozen cell pellets as described elsewhere[2]. Briefly, cells were lysed and homogenized in urea buffer with a TissueLyser (Qiagen, Hilden, Germany) and supernatants were collected after centrifugation for 15 min at 14.000 x g and 4°C. Protein concentration was determined using the Pierce 660 nm Protein Assay (Fischer Scientific, Schwerte, Germany) and 10 µg protein per sample were loaded on a SDS-PAGE for in-gel-digestion. The isolated gel pieces were reduced (50 µl, 10 mM DTT), alkylated (50 µl, 50 mM iodoacetamide), and underwent afterwards tryptic digestion (6 µl, 200 ng trypsin in 100 mM ammonium bicarbonate). The peptides were resolved in 15 µl 0.1 % trifluoroacetic acid and subjected to liquid chromatography.

**LC-MS analysis.** For the LC-MS analysis a QExactive plus (Thermo Scientific, Bremen, Germany) connected with an Ultimate 3000 Rapid Separation liquid chromatography system (Dionex / Thermo Scientific, Idstein, Germany) equipped with an Acclaim PepMap 100 C18 column (75 µm inner diameter, 25 cm length, 2 mm particle size from Thermo Scientific, Bremen, Germany) was applied. The length of the isocratic LC gradient was 120 minutes. The mass spectrometer was operating in positive mode and coupled with a nano electrospray ionization source. Capillary temperature was set to 250°C and source voltage to 1.4 kV. In the QExactive plus mass spectrometer for the survey scans a mass range from 200 to 2000 m/z at a resolution of 70,000 was used. The automatic gain control was set to 3.000.000 and the maximum fill time was 50 ms. The 10 most intensive peptide ions were isolated and fragmented by high-energy collision dissociation (HCD).

**Computational mass spectrometric data analysis.** Peptide and protein identification and quantification was done by using MaxQuant (version 1.5.3.8, MPI for Biochemistry, Planegg, Germany) applying standard parameters. As human samples were analyzed, searches were conducted using a specific proteome database (UP000005640, downloaded 06/20/16) from UniProt. Methionine oxidation and acetylation at protein N-termini were set as variable modification and carbamidomethylations at cysteines were considered as fixed modification. Peptides and proteins were accepted with a false discovery rate set to 1%. Unique and razor peptides were used for label-free quantification and peptides with variable modifications were included in the quantification. The minimal ratio count was set to two and the matched between runs option was enabled. The normalized intensities as provided by MaxQuant were analyzed by using Perseus framework (version 1.5.0.15, MPI for Biochemistry, Planegg, Germany). Only proteins containing at least two unique peptides and a minimum of 3 valid values in each group were taken into consideration for protein quantification. Proteins which were identified only by site or marked as contaminant (from the MaxQuant contaminant list) were excluded from the analysis. For the calculation of enriched proteins in the two groups Student's t-tests were applied. The significance analysis was applied on  $\log_2$  transformed values using a S0 constant = 0 and a 1 % false discovery rate-based cutoff. The mass spectrometry proteomics data have been deposited to the ProteomeXchange Consortium *via* the PRIDE partner repository [3] with the data set identifier PXD017319. SIRT4-interacting proteins were functionally grouped and subjected to gene ontology and pathway/network analysis using the ClueGO software[4].

### Supplementary References

- 1 North, B.J.; Marshall, B.L.; Borra, M.T.; Denu, J.M.; Verdin, E. The human Sir2 ortholog, SIRT2, is an NAD<sup>+</sup>-dependent tubulin deacetylase. *Mol Cell* **2003**, *11*, 437-444, doi:10.1016/s1097-2765(03)00038-8.
- 2 Poschmann, G.; Seyfarth, K.; Besong Agbo, D.; Klafki, H.W.; Rozman, J.; Wurst, W.; Wiltfang, J.; Meyer, H.E.; Klingenspor, M.; Stuhler, K. High-fat diet induced isoform changes of the Parkinson's disease protein DJ-1. *J Proteome Res* **2014**, *13*, 2339-2351, doi:10.1021/pr401157k.
- 3 Vizcaino, J.A.; Csordas, A.; Del-Toro, N.; Dianes, J.A.; Griss, J.; Lavidas, I.; Mayer, G.; Perez-Riverol, Y.; Reisinger, F.; Ternent, T., et al. 2016 update of the PRIDE database and its related tools. *Nucleic Acids Res* **2016**, *44*, 11033, doi:10.1093/nar/gkw880.
- 4 Bindea, G.; Mlecnik, B.; Hackl, H.; Charoentong, P.; Tosolini, M.; Kirilovsky, A.; Fridman, W.H.; Pages, F.; Trajanoski, Z.; Galon, J. ClueGO: a Cytoscape plug-in to decipher functionally grouped gene ontology and pathway annotation networks. *Bioinformatics* **2009**, *25*, 1091-1093, doi:10.1093/bioinformatics/btp101.

## 7. Abschlussdiskussion

Die in dieser Arbeit präsentierten Daten geben Einblick in eine mögliche Rolle von extramitochondrial lokalisiertem SIRT4 in der mitotischen Zellteilung. Die Ergebnisse weisen darauf hin, dass SIRT4 neben seiner bekannten Funktion im mitochondrialen Metabolismus auch als neues Zentrosomen- und Mikrotubuli-assoziiertes Protein fungiert, das an der Regulation des mitotischen Zellzyklusverlaufs beteiligt ist. So könnte bei replikativem/mitotischem Stress nicht nur das mitochondrial lokalisierte SIRT4 (über eine metabolische Hemmung und/oder ROS-Generation [264]), sondern auch extramitochondriales SIRT4 (über eine Veränderung der mitotischen Regulation und/oder der Mikrotubuli-Dynamik) die antiproliferative(n) Tumorsuppressorfunktion(en) von SIRT4 auslösen.

### 7.1. Subzelluläre Lokalisierung von SIRT4

Obwohl Sirtuine eine vorherrschende Lokalisierung innerhalb der Zelle aufweisen, wird diese flexibel in Abhängigkeit von Zelltyp, Stressstatus und molekularen Wechselwirkungen unterschiedlich moduliert. Zum Beispiel hat SIRT1 zwei Kernexportsignale [193], und auch für SIRT2 konnte eine doppelte subzelluläre Lokalisierung entweder im Kern oder im Zytoplasma nachgewiesen werden [106]. Verantwortlich für die mitochondriale Lokalisierung der Sirtuine 3, 4 und 5 sind ihre N-terminalen, mitochondrialen Zielsequenzen (*mitochondrial targeting sequence* - MTS) [152]. Für SIRT3 konnte allerdings eine Lokalisationsänderung von Mitochondrien zum Kern beobachtet werden, wenn es zusammen mit SIRT5 exprimiert wird. Veränderungen der MTS von SIRT3 führte die Autoren zu der Schlussfolgerung, dass die MTS nicht nur notwendig ist, um SIRT3 in die Mitochondrien zu importieren, sondern auch, um den nukleären Import von SIRT3 in Anwesenheit von SIRT5 zu medieren [265].

Diese Beobachtungen unterstützen die Hypothese, dass auch SIRT4 nicht strikt an seine Lokalisation im Mitochondrium gebunden ist, sondern ebenfalls über vergleichbare Modulationen und Bedingungen, analog zu den zuvor genannten Sirtuinen, eine differenzierte subzelluläre Verteilung einnimmt.

Durch die Fusion von eGFP an den C-Terminus von SIRT4 konnte in dieser Arbeit die frühe subzelluläre Verteilung von SIRT4 nach Expression in HeLa-Zellen beobachtet

werden. Konfokal mikroskopische Analysen des überexprimierten SIRT4-eGFP wurden sechs bzw. 24 Stunden nach der Transfektion durchgeführt. Während nach 24 Stunden eine überwiegende Lokalisation von SIRT4-eGFP in den Mitochondrien festgestellt wurde, zeigten die Analysen nach sechs Stunden zunächst eine Lokalisation des SIRT4-eGFP Fluoreszenzsignals innerhalb des Zytoplasms. Die Mehrzahl der Zellen wies Aggregate mit dominanter Aggregation am Zentrosom auf. Gelegentlich wurden auch Zellen mit einem gleichverteilten Fluoreszenzsignal innerhalb des Zellkerns beobachtet. Die ungleichmäßige Verteilung des SIRT4-eGFP kurz nach der Überexpression zeigt eine hochempfindliche Dynamik der Lokalisation innerhalb der Zelle, da diese nicht nur vom Zeitpunkt des Zellzyklus abhängig zu sein scheint, sondern auch von der Gesamtexpression sowie dem SIRT4-eGFP Proteingehalt im Zytoplasma.

Diese Beobachtungen stehen in Übereinstimmung mit den Ergebnissen von Ramadani-Muja *et al.*, welche über eine Verteilung von SIRT4-sfGFP von 60% in den Mitochondrien und 40% extramitochondrial berichten [188]. Zusätzlich wiesen die Autoren mit einer speziellen „*self-complementing split fluorescent protein*“ Technologie die eindeutige Akkumulation von überexprimiertem SIRT4 im Kern nach [188]. Dazu passend treten in der massenspektroskopischen Analyse für SIRT4 [263] unter anderem Interaktionspartner wie die Importin Untereinheit  $\beta 1$  (KPNB1), Transportin-1 (TNP01) und Importin-5 (IPO5) auf, welche an den nukleären Imports von Proteinen beteiligt sind. Da diese vordergründig mit nukleären Lokalisierungssignalen (NLS) interagieren, ist anzunehmen, dass auch SIRT4 ein solches Signal besitzt. Unter Stressbedingungen kann es zu einer Stagnation/Verzögerung des Imports von Proteinen in die Mitochondrien kommen, was zur Anreicherung dieser Proteine im Zytoplasma führt [266, 267]. Wenn diese Proteine nicht direkt abgebaut werden (oder nicht direkt abgebaut werden können), können sie Signalwege initiieren, um dem Zellstress entgegenzuwirken [268]. Als Vorbereitung der Zelle auf die Mitose werden die Mitochondrien zunehmend gespalten, um einzelne Mitochondrien zu transportieren und gleichmäßig über das Mikrotubuli-Netzwerk auf die Zellpole zu verteilen [269]. Eine geringe Importkinetik von SIRT4 in die Mitochondrien [188] könnte unter physiologischen Bedingungen und in Verbindung mit der Vorbereitung der Zellen auf die Mitose ein Auslöser der extramitochondrialen SIRT4-Regulation sein. So könnte es durch die mitochondriale Spaltung zu einer Verringerung des Imports der Mitochondrien Matrix Proteine kommen, was die SIRT4-Proteinspiegel im Zytoplasma

erhöht, was wiederum als Signal für die Rekrutierung von SIRT4 an das Zentrosom gelten könnte. Ein zu hoher Anstieg der SIRT4-Mengen im Zytosol hingegen könnte einen Import in den Zellkern aktivieren, der dann als akutes Stresssignal wirken würde. In den hier durchgeführten Experimenten führten die transienten Transfektionen am nächsten Tag zu einer Zelltodesrate von ca. 20%. Unter der Annahme, dass sich SIRT4 unter Stressbedingungen im Zellkern anreichert, könnte das beobachtete SIRT4-eGFP Signal im Zellkern eine zelluläre Antwort auf den durch die Transfektion induzierten Stress sein.

### **7.1.2. SIRT4( $\Delta$ N28) und die Bedeutung des N-Terminus von SIRT4**

Die SIRT4( $\Delta$ N28)-Mutante ist eine SIRT4-Variante, der die MTS fehlt und die daher nicht mehr in die Mitochondrien importiert werden kann [261]. Mit dieser Mutante sollte das extramitochondriale Lokalisationsverhalten von SIRT4 untersucht werden. Für die mit C-terminal fusioniertem eGFP SIRT4( $\Delta$ N28)-eGFP-Mutante konnte weiterhin eine Co-Lokalisation des Fluoreszenz Signals mit dem zentrosomalen Marker Pericentrin beobachtet sowie eine Häufung des nukleären Signals detektiert werden ([263], Abbildung S4). Sechs Stunden nach Expression der SIRT4( $\Delta$ N28)-eGFP Variante konnte die Bildung von Aggregaten in den Zellen mit Akkumulation am Zentrosom ([263], suppl. Movie 1) beobachtet werden. Bei Zellen, die SIRT4( $\Delta$ N28)-eGFP weitaus niedriger exprimierten, war eine deutliche Co-Lokalisation am Zentrosom ohne Aggregatbildung zu erkennen. Da SIRT4( $\Delta$ N28)-eGFP nicht in das Mitochondrium importiert wird, imitiert diese Variante eine Form von erhöhten SIRT4-Mengen im Zytosol, die als akutes Stresssignal zu einem verstärkten Zellkernimport des Enzyms führen könnte. Das häufiger auftretende Kernsignal bei der SIRT4( $\Delta$ N28)-eGFP-Variante lässt vermuten, dass ebenso wie bei SIRT3 [265, 270] auch bei SIRT4 die MTS eine Rolle bei der Relokalisation in den Nukleus bei Zellstress einnimmt.

In Co-Immunopräzipitationsexperimenten sowie in der massenspektroskopischen Analyse konnte beobachtet werden, dass SIRT4-Proteine miteinander co-präzipitieren, was eine Erklärung für die Aggregate in den konfokalen Mikroskopie-Aufnahmen wäre. Ein weiterer potenzieller Effekt der MTS könnte sein, dass weniger SIRT4 Proteinaggregate außerhalb des Mitochondriums gebildet werden. Dieser Effekt wäre auf die sich abstoßenden positiven Ladungen, aus denen die MTS hauptsächlich besteht [188, 271], zurückzuführen.

Ein Faktor, der zur SIRT2-Lokalisierung und -Funktion beiträgt, ist das differenzielle Spleißen der SIRT2-mRNA, wodurch unterschiedliche SIRT2-Isoformen mit unterschiedlichen funktionellen Domänen und PTMs erzeugt werden [272, 273]. Zurzeit sind drei SIRT2-Isoformen bekannt. Die Isoformen 1 und 2 gelten als zytoplasmatisch lokalisiert [272], während die Isoform 5 als die nukleäre SIRT2 Variante beschrieben wird, welche hauptsächlich im Nukleus lokalisiert und dort wahrscheinlich eine nicht enzymatisch aktive Funktion erfüllt [211]. Dabei interagiert SIRT2 mit verschiedenen Importinen, unter anderem Importin-7 (IPO7), welches für die SIRT2 vermittelte Deacetylierung von Histon H3(K13) bei einer bakteriellen Infektion notwendig ist [273]. Die Importbindung und der Nukleärtransport von SIRT2 wird dabei über den unstrukturierten C-Terminus negativ reguliert [274].

Auch für das murine SIRT3 wurden zwei verschiedene Isoformen mit und ohne MTS beschrieben, die beide im Mitochondrium lokalisieren. Beide Formen werden als enzymatisch aktiv beschrieben und eine Überexpression beider Isoformen zeigt deren nukleäre Lokalisierung [266]. Dies eröffnet die Möglichkeit, dass auch analog für SIRT4 eine primär zytoplasmatische Isoform besteht, in der die MTS Einfluss auf das Lokalisationsverhalten hat.

Diese Befunde lassen insgesamt vermuten, dass die MTS neben ihrer dominanten Funktion, Proteine in die Mitochondrien zu transferieren, auch eine wichtige Rolle bei der multi-subzellulären Umverteilung von funktionellen Sirtuinen in Abhängigkeit von Zellzyklus und Stressfaktoren spielt.

## **7.2. Extramitochondriales SIRT4 und seine Rolle im Zellzyklus**

Die Ergebnisse von Bergmann *et al.* [263] zeigen zusammenfassend, dass (I) SIRT4 subzellulär nicht nur in Mitochondrien, sondern auch im Zytosol lokalisiert, wo es vor allem in frühen mitotischen Phasen an Zentrosomen nachgewiesen werden kann; (II) wie durch massenspektrometrische und Co-Immunopräzipitationsanalysen gezeigt, co-pelletiert SIRT4 mit Mikrotubuli und mit Mikrotubuli-bindenden Proteinen, insbesondere  $\alpha$ -Tubulin, Komponenten des  $\gamma$ TuRC ( $\alpha$ -Tubulin, GCP2, GCP3) und interagiert mit der  $\alpha$ -Tubulin-Deacetylase HDAC6; (III) in Übereinstimmung mit letzterem führt eine erhöhte SIRT4-Expression zu verminderten Acetyl- $\alpha$ -Tubulin

(K40)-Mengen, was mit einer verminderten Stabilität und einer veränderten Dynamik der mitotischen Mikrotubuli verbunden ist; (IV) auf zellulärer Ebene verlängert die ektopische Expression von SIRT4 oder SIRT4( $\Delta$ N28) die mitotische Progression und hemmt die Zellproliferation.

### **7.2.1. SIRT4 am Zentrosom und dessen Einfluss auf die Mikrotubuli-Dynamik**

Der  $\gamma$ TuRC befindet sich in der äußeren Region des perizentriolären Materials, während Pericentrin im gesamten PCM von innen nach außen integriert ist und zur Wagenradstruktur des Zentrosoms beiträgt [18, 31].

Aufgrund des Einflusses von SIRT4 auf den Acetylierungszustand von Acetyl- $\alpha$ -Tubulin (K40) und der Co-Immunopräzipitation mit Komponenten des  $\gamma$ TuRC, nicht aber mit Pericentrin [263], ist eine naheliegende Vermutung und Arbeitshypothese, dass SIRT4 Teil des  $\gamma$ TuRC ist oder an diesen angrenzt und dort an der Regulation und Polymerisation der mitotischen Mikrotubuli beteiligt ist [263]. In Abbildung 10 ist schematisch die potenzielle Lokalisation von SIRT4 im PCM abgebildet. Grundlage hierfür bilden vor allem auch mikroskopische Aufnahmen, welche das Signal von endogenem SIRT4 am Initiationspunkt der Mikrotubuli-Polymerisation zeigen.

Da SIRT4 bereits während der Interphase am Zentrosom lokalisiert, ist es möglich, dass SIRT4 in der späten G<sub>1</sub>- oder S-Phase rekrutiert wird, in welcher die Zentriolen verdoppelt werden und die Zentrosomen reifen, bevor diese sich teilen. Zudem wurde die höchste zentrosomale SIRT4-Signalintensität für Zellen in der G<sub>2</sub>- und Prophase definiert [263], in der die Trennung der reifen Zentrosomen stattfindet [18]. In einem weiteren Schritt könnte durch eine Korrelation des SIRT4-Signals mit Zellzyklusphasen spezifischen G<sub>2</sub>/M Markern genauer determiniert werden, ob die SIRT4-Rekrutierung im Übergang von der G<sub>1</sub>- zur S-Phase stattfindet. Dies würde eine bessere Aufgliederung ermöglichen, ob und wie sich die SIRT4-Mengen am Zentrosom gemäß den mitotischen Phasen ändern.

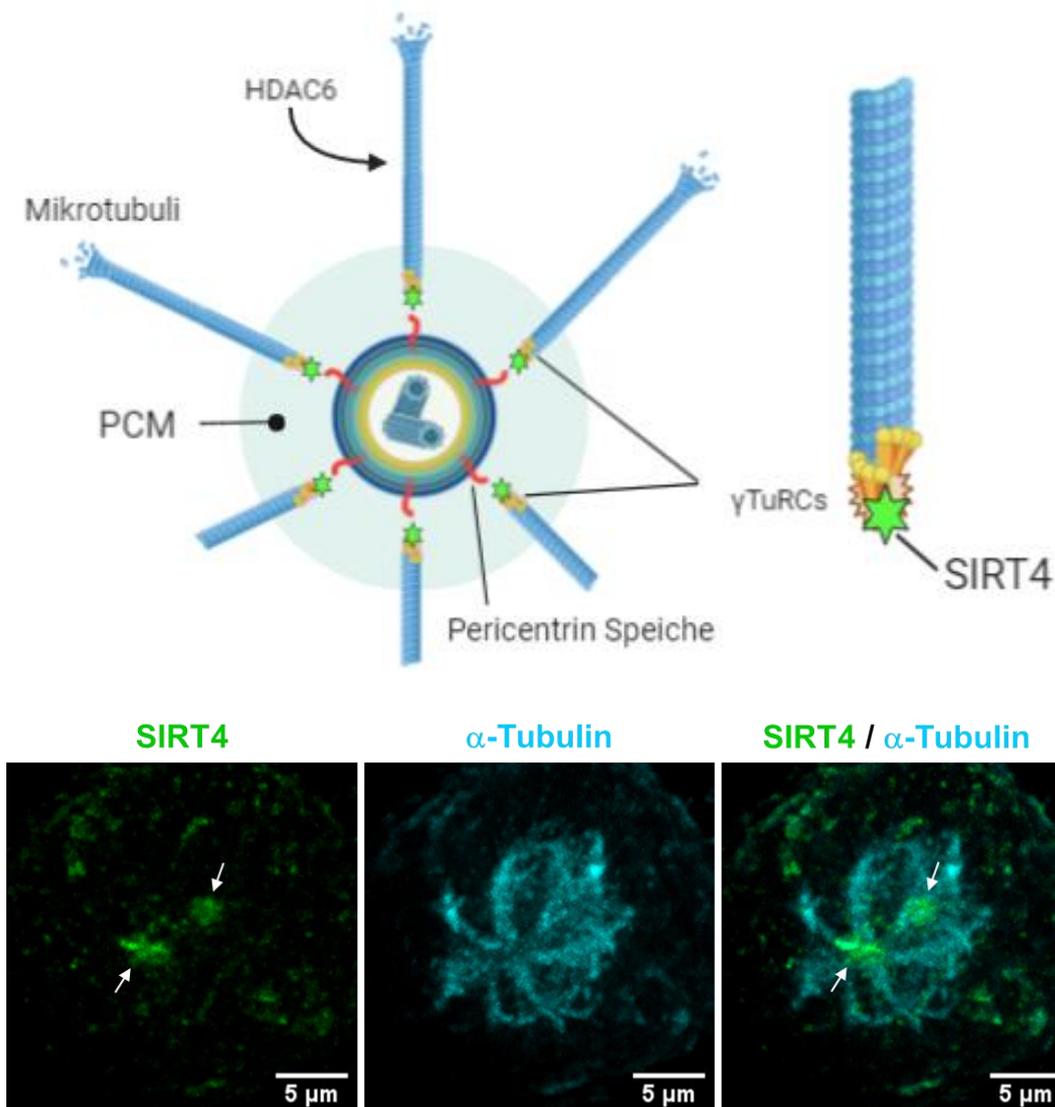


**Abbildung 10:** Schematische Einordnung von SIRT4 am Zentrosom. Abgeleitet anhand der konfokalen *Spinning Disk* Aufnahmen und in Kombination mit den Co-Immunopräzipitationsdaten [263] ist zu vermuten, dass SIRT4 Teil des PCM oder aber Bestandteil des  $\gamma$ TuRC ist, um dort Einfluss auf die Nukleierung und Polymerisation der Spindelmikrotubuli zu nehmen [263]. Erstellt mit Biorender.com

Mikrotubuli-Nukleationspunkte entstehen in der Zelle an definierten Stellen und viele verschiedene Signalwege müssen ineinandergreifen, um eine bestimmte Zytoskelettarchitektur auszubilden [50, 275, 276]. Jeder Mikrotubuli-Nukleationsweg erfordert einen einzigartigen Satz von Nukleationseffektoren zur Rekrutierung und Regulierung von mehreren  $\gamma$ TuRC an unterschiedlichen zellulären Standorten [50, 276]. Dabei unterliegen Mikrotubuli verschiedenen kovalenten Änderungen. Eine wichtige posttranslationale Schlüsselmodifikation ist die reversible Acetylierung von dem Lysin 40 (K40) des  $\alpha$ -Tubulin, die mit stabilen Mikrotubuli einhergeht und von Protisten bis zum Menschen konserviert ist [71, 277]. Bei Säugetieren wird das Ausmaß der Acetylierung hauptsächlich durch die  $\alpha$ -Tubulin-Acetyltransferase 1

( $\alpha$ Tat1) [278, 279] und HDAC6 [277, 280] bestimmt. Durch Maus-*Knock-Out*-Studien dieser Enzyme konnte die Modifikation der Mikrotubuli-Acetylierung mit neurologischen Störungen, Krebs, Herzkrankheiten und anderen pathologischen Zuständen in Verbindung gebracht werden [71, 281].

Konfokale Mikroskopie-Aufnahmen zeigen SIRT4 bereits in der Interphase am Zentrosom, wobei hier nicht klar ist, in welcher Phase vor der G<sub>2</sub>/M-Phase SIRT4 an das Zentrosom rekrutiert wird. Diese zeigen die höchste SIRT4 Intensität während der G<sub>2</sub>- und Prophase mit einem raschen Abfall ab der Prometaphase, in welcher sich die Spindelmikrotubuli zur Chromosomen-Segregation voll ausgebildet haben und letztere zu den Zellpolen hinziehen. Eine Rolle des zytoplasmatischen SIRT4 könnte hier darin bestehen, die Spindelmikrotubuli-Entstehung am Zentrosom zurückzuhalten, sodass es nicht zu einer abnormalen und zu frühen Spindelausprägung kommt.

Ein Hinweis auf die Regulierung der Mikrotubulientstehung am  $\gamma$ TuRC durch SIRT4 ist die Beobachtung, dass die ektopische SIRT4-Expression spezifisch in G<sub>2</sub>/M arretierten Zellen zu erniedrigten Mengen an acetyliertem  $\alpha$ -Tubulin (K40) führt [263]. Die erhöhten SIRT4 Level am Zentrosom könnten also über Regulierung der Mikrotubuli-Modifikation (Ac K40) entweder direkt oder indirekt über den in der massenspektroskopischen Analyse und durch Co-Immunopräzipitationsexperimente bestätigten Interaktor HDAC6 Einfluss auf die Mikrotubulidynamik haben. Von Interesse wäre es, die Level des acetylierten- $\alpha$ -Tubulin über die weiteren mitotischen Phasen hinweg mit der zentrosomalen Lokisationskinetik von SIRT4 zu betrachten und zu schauen, ob diese mit dem konfokal ermittelten Intensitätssignal korrelieren.

Für SIRT4 wurden verschiedene enzymatische Aktivitäten beschrieben, einschließlich der Lysin-Deacetylierung [163]. Letztere steht mit der Regulation des Zellzyklus in Verbindung und es gibt zunehmend Hinweise auf eine Sirtuin-vermittelte Deacetylierung als Regulator der zentrosomalen Funktion und der mitotischen Zellzyklusprogression [234, 236, 237, 239]. Gegenwärtig kann nicht ausgeschlossen werden, dass SIRT4 zentrosomale/mitotische Proteine durch die beschriebenen enzymatischen Aktivitäten wie dem ADP-Ribosyltransfer oder eine Deacylierung modifiziert und so zu einer Regulation der mitotischen Progression beiträgt. Dabei könnte SIRT4 eine ähnliche Rolle wie MZT1 ausführen. Dieses Protein interagiert ebenfalls mit GCP-Komponenten des  $\gamma$ TuRC, vorrangig GCP3, und dient als *priming*

Faktor für den  $\gamma$ TuRC, um eine räumliche Regulierung der Mikrotubuli Nukleation zu ermöglichen [52, 282, 283].

Insgesamt verstärken die hier präsentierten Ergebnisse die Evidenz für eine zentrosomale Lokalisation von Deacetylasen (HDACs und Sirtuine) [284] sowie ihre Rolle in der Zentrosomenbiologie, der Mikrotubuli-Dynamik und der mitotischen Regulation. Beispielsweise kontrollieren die SIRT1-Plk2 und SIRT1-CCDC84-SAS6 Achsen die Zentriolen-Duplikation [239], um die Zentrosomen-Amplifikation zu regulieren [285]. Die Expression von SIRT2, das an der Regulation der Mikrotubuli-Dynamik beteiligt ist [72, 73], wird zellzyklusabhängig reguliert, wobei SIRT2 am Zentrosom und der mitotischen Spindel lokalisiert [192]. Die Phosphorylierung von SIRT2 durch Zyklin A-CDK2 reduziert die Bindung von SIRT2 an das Zentrosom und fördert die G<sub>2</sub>/M-Progression [238]. Zusätzlich bewirkt eine erhöhte SIRT2-Konzentration eine Verlängerung der mitotischen Phase [213]. Letzteres wird der regulatorischen Rolle von SIRT2 gegenüber dem *Anaphase Promoting Complex/Cyclosome* und damit dem Abbau von Zyklin B1 zugeschrieben [235]. Zyklin B1 ist schließlich entscheidend, um die Progression von der Metaphase in die Anaphase zu starten.

### **7.2.2. SIRT4 vermittelte Hemmung der Zellproliferation**

In dieser Arbeit konnte gezeigt werden, dass die Überexpression von SIRT4 zu einer Verlangsamung der mitotischen Progression sowie zu einer Hemmung der Proliferation von HEK293-Zellen führt [263]. Dies stimmt mit der Charakterisierung von SIRT4 als Tumorsuppressor [181, 251] überein. Die Überexpression der mutierten Varianten SIRT4(H161Y) und SIRT4( $\Delta$ N28) zeigten ebenfalls eine um etwa ein Drittel der Zeit verzögerte Mitose im Vergleich zu den eGFP-exprimierenden Kontrollzellen. Dies ging ebenfalls mit einer verminderten Zellproliferation einher.

In diesen Modellen kann die Verzögerung der Mitose, die wahrscheinlich zu einem verminderten Wachstum der Zellpopulation führte, von verschiedenen Faktoren abhängen. Die enzymatische Aktivität von SIRT4 scheint einen verzögernden Einfluss auf die Mitose zu haben, da der Effekt in der enzymatisch defekten SIRT4(H161Y)-Mutante zwar noch zu beobachten, jedoch deutlich reduziert war.

Da die SIRT4( $\Delta$ N28)-Mutante nicht mehr in die Mitochondrien importiert wird, simuliert diese durch die damit einhergehende Akkumulation von SIRT4-Protein im Zytoplasma die bereits in Kapitel 7.1 beschriebene Zellstresssituation im Sinne der mitochondrialen Importstagnation. Es ist zu berücksichtigen, ob der Einfluss eines katalytisch aktiven SIRT4 auf die Mitose und den gesamten Zellzyklusverlauf von einer mitochondrialen Funktion bzw. mehreren Funktionen abhängt, da letztere in diesem Fall weder von SIRT4(H161Y) noch von der potentiell katalytisch aktiven SIRT4( $\Delta$ N28)-Mutante ausgeführt werden kann.

Da noch nicht klar ist, von welchem enzymatischen/molekularem Mechanismus die extramitochondriale Funktion von SIRT4 abhängt, ist es möglich, dass SIRT4(H161Y) mitochondrial inaktiv, aber für die extramitochondriale Funktion aktiv ist und daher eine Reduktion der mitotischen Progression und der Zellproliferation bewirkt.

Im Weiteren war zu beobachten, dass SIRT4( $\Delta$ N28)-eGFP immer noch am Zentrosom lokalisiert, aber keinen Einfluss mehr auf die K40 acetylierten- $\alpha$ -Tubulin-Level hat. Eine Erklärung ist, dass das Motiv für die zentrosomale Rekrutierung noch intakt ist, aber aufgrund des fehlenden N-Terminus das Protein nicht richtig gefaltet wird, oder mit anderen Effektoren nicht mehr interagieren kann und damit für seine zentrosomale Funktion inaktiv ist.

Die hier untersuchten SIRT4-Mutanten werfen so die Möglichkeit auf, dass der gesamte antiproliferative Effekt von SIRT4 durchaus eine Kombination von mitochondrial-abhängigen und mitochondrial-unabhängigen Effekten darstellt, der sich in den Wachstumskurven und der mitotischen Progression auf die beiden Mutanten aufgeteilt zeigt und sich im Wildtyp kombiniert auswirkt.

## 7.3. SIRT4 als Regulator zwischen Mitochondrien-Aktivität und Mitose

### 7.3.1. Die SIRT4-OPA1-Achse in der Vorbereitung für die Mitose

Die Mitose ist ein hochregulierter Vorgang im Zellzyklus. Dabei beginnen die Vorbereitungen für eine erfolgreiche Mitose bereits in der Interphase. Die Mitochondrien spielen hierbei nicht nur in der Energieproduktion, sondern auch in ihrer Distribution eine wichtige Rolle. Vor der Zellteilung orchestriert die Zelle Prozesse, welche die Generierung zweier funktioneller Tochterzellen gewährleisten. Einer dieser Vorgänge ist die ordnungsgemäße Verteilung der Mitochondrien, da diese in den Tochterzellen aus dem vererbten Pool *de novo* gebildet werden. Zu diesem Zweck erhöhen die Mitochondrien ihre Anzahl vor der Mitose durch mitochondriale Biogenese und Spaltung [143, 286].

Während die Mitochondrien in der Interphase mit dem Mikrotubuli-Zytoskelett assoziiert sind, müssen sie in Vorbereitung zur Mitose über den Vorgang der mitochondrialen Fission vereinzelt und über das Mikrotubulinetzwerk auf die Zellperipherie symmetrisch aufgeteilt werden. Chung *et al.* [269] konnten zeigen, dass die Entkopplung der Mitochondrien von den Mikrotubuli nach deren Transport durch den Abbau der entsprechenden Motorproteine an der Mitochondrienoberfläche stattfindet. Bei artifizierlicher Erhöhung der Motorproteine konnte nach der Mitose eine asymmetrische Verteilung der Mitochondrien beobachtet werden. Bei einer erzwungenen ‚Befestigung‘ der Mitochondrien an die Spindel-Mikrotubuli kann es zum kompletten mitotischen Stillstand oder aber zu mehrkernigen Tochterzellen, d.h. Polyploidie, kommen [269]. Somit zeigt sich hier ein Zusammenhang zwischen dem Ereignis der mitochondrialen Fission und multinukleären Tochterzellen, die schließlich laut Literaturlage [287, 288] zur Krebsentstehung beitragen können.

SIRT4 ist über die OPA1-Achse an der Regulation der mitochondrialen Dynamik und der Qualitätskontrolle mechanistisch beteiligt [261]. Die Überexpression von SIRT4-eGFP führte dabei zu verlängerten und fusionierten Mitochondrien und stabilisierte die mitochondrialen Netzwerke. Eine unvollständige oder nicht durchgeführte Vereinzelung der Mitochondrien kann zu Mitosefehlern oder sogar zu einem kompletten Stopp der mitotischen Progression führen [269]. Auf diese Weise könnten

erhöhte mitochondriale SIRT4 Mengen einen direkten Einfluss auf die Regulierung der Mitose haben.

Die mitochondriale Fission hängt sowohl von der Relokalisation der großen GTPase DRP1 an die äußere mitochondriale Membran als auch von der Phosphorylierung von DRP1 am S616 durch die mitotische Kinase CDK1 ab [143, 289].

In der massenspektroskopischen Analyse und über Co-Immunopräzipitation konnte CDK1 als SIRT4-Interaktor identifiziert werden [263]. Da bereits für SIRT1 [240] und SIRT3 [155] bekannt ist, dass diese mit CDK1 interagieren, wirft dies die Frage auf, ob SIRT4 ebenfalls in einem regulatorischen Verhältnis mit CDK1 oder *vice versa* steht. Hierbei kann es sein, dass es sich um mitochondriales SIRT4 oder das hier vorgestellte zytoplasmatische SIRT4 oder beide Varianten handelt, die durch CDK1 vermittelte Phosphorylierung reguliert werden.

Ebenso interagiert SIRT5 mit einem Zellzyklus Regulator, dem Zyklin F [290]. In dem von Mills *et al.* vorgestellten Modell wird beschrieben, dass die SIRT5-Proteinkonzentration unter einen Schwellenwert sinken muss, damit die Zellen die G<sub>1</sub>-Phase verlassen können, um in die S-Phase überzuwechseln. Die SIRT5 Proteinmengen werden dabei über eine Zyklin F vermittelten ubiquitinären Abbau reguliert. Des Weiteren wird postuliert, dass hohe SIRT5-Spiegel zur Etablierung und/oder Aufrechterhaltung der Ruhe- oder G<sub>0</sub>-Phase beitragen können.

Diese Beobachtungen verstärken weiter die essenzielle Rolle der Sirtuine in der Zellzyklus-Progression.

Für SIRT4 ergab eine Untersuchung zur Apoptose in Prostatakrebs, dass die mitochondrialen SIRT4-Mengen über eine PAK6-SIRT4-ANT2-Komplex vermittelte Ubiquitinierung reguliert werden. Dabei sind die detaillierten Mechanismen, einschließlich der Identifizierung der genauen ubiquitinierten Seitenketten von SIRT4 und allen beteiligten Interaktionspartnern, die zur Regulierung der SIRT4-Mengen führen, in diesem Zusammenhang noch nicht bekannt [291]. Entsprechend könnte eine Phosphorylierung von SIRT4 durch CDK1 zu einer Ubiquitinierung mit anschließendem Abbau von SIRT4 eine Negativ-Regulation wie bei SIRT5 [290] darstellen. Dies würde die mitochondriale Fission einleiten, sodass die Mitochondrien sich in Vorbereitung auf die Mitose teilen können. Diese Form der Regulierung ist für die Histon-Methyltransferase des Histon 3 (EZH2) gezeigt worden. EZH2 wird an Threonin 345 und Threonin 487 durch CDK1 in einer zellzyklusabhängigen Weise

phosphoryliert, was zu einer verstärkten Ubiquitinierung und einem anschließenden proteasomalen Abbau führt [292-294].

### **7.3.2. Die SIRT4-CDK1 Achse im Mitochondrium und deren Einfluss auf Metabolismus und Zellzyklus**

Die G<sub>1</sub>/S- und G<sub>2</sub>/M-Kontrollpunkte im Zellzyklus erfordern aufgrund eines hohen Energiebedarfs eine ausgeprägte Bioenergieversorgung, die auch für die Phasenübergänge im Zellzyklus benötigt wird [295]. In proliferierenden Säugetierzellen wird mitochondriales ATP über oxidative Phosphorylierungsmaschinen (Elektronentransportkette), die aus den 5 Multi-Untereinheit-Komplexen, Komplex I - Komplex V (CI-CV), bestehen, generiert. CI ist mit 46 Untereinheiten der größte Komplex und ist der Haupteintrittspunkt der Elektronen in die Atmungskette. Ein funktioneller CI ist nicht nur für die gesamte mitochondriale Atmung erforderlich [296, 297], sondern auch für eine erfolgreiche Zellzyklusprogression [298].

Die Zellzyklus Kinase CDK1 ist hauptsächlich zytoplasmatisch und nukleär lokalisiert. Dennoch konnte über die letzten Jahre ein signifikanter Pool an enzymatisch aktivem CDK1/ZyclinB Komplex in der Matrix der Mitochondrien lokalisiert sowie ein zugehöriges *Cluster* mitochondrialer Proteine identifiziert werden. Dazu gehören die Untereinheiten der Komplexe CI und CII und der MnSOD, welche alle von CDK1 phosphoryliert werden [291, 299]. Es konnte aufgezeigt werden, dass aktives CDK1 die mitochondriale Atmung erhöht, wodurch mehr ATP erzeugt wird, welches den erhöhten Energiebedarf der Zelle während des G<sub>2</sub>/M-Übergangs deckt und die Gesamtzykluszeit verkürzt.

Dabei lokalisiert der CDK1/ZyclinB-Komplex in der Mitochondrien Matrix, wo es den Atmungskomplex CI phosphoryliert und so zu einem erhöhtem O<sub>2</sub>-Konsum führt. Unter Umständen findet sich hier CDK1 als regulatorischer Gegenspieler von SIRT4 wieder, welches den Atmungskomplex 1 bei Überexpression negativ reguliert [261] und so den O<sub>2</sub>-Umsatz in den Mitochondrien reduziert. Während SIRT4 die Energieproduktion in den Mitochondrien negativ reguliert und somit seine Funktion als Tumorsuppressor ausführt, könnte hier der CDK1/ZyclinB-Komplex als Vorbereitung auf die Mitose den inhibitorischen SIRT4-Effekt durch Phosphorylierung aufheben. Die Phosphorylierung

würde zu dem bereits diskutierten Ubiquitin-vermittelten Abbau von SIRT4 führen, was mit den niedrigen SIRT4-Proteinmengen in vielen Tumorarten einhergeht [300-302].

Während die GDH durch SIRT3 aktiviert wird, führt die ADP-Ribosyltransferase-Aktivität von SIRT4 zu einer Inhibierung der GDH [162, 169]. Dies ermöglicht durch eine wechselseitige Kontrolle der anaplerotischen Reaktion des Citratzyklus und somit eine metabolische Kontrolle der mitochondrialen Signalwege. Die enzymatische Aktivität von SIRT3 wird über die Thr150/Ser159-Phosphorylierung in dessen NAD<sup>+</sup>-Bindestellenmotiv durch CDK1/ZyclinB weiter verstärkt [155]. Dieses Motiv der NAD<sup>+</sup>-Bindestelle findet sich ebenfalls in der Sequenz von SIRT4, jedoch mit dem Unterschied, dass die beiden Proline, welche typischerweise die Phosphorylierungsstellen Threonin und Serin flankieren und das minimale Konsensus-Motiv für CDK1 markieren [303], zu Glutaminsäure umgewandelt sind [siehe Anhang 13.1]. Dies ist ein Indikator dafür, dass über evolutive Prozesse SIRT3 und SIRT4 in ihren Aufgaben im Mitochondrium spezifiziert wurden, sodass keine Erhöhung der enzymatischen Aktivität durch CDK1 bei SIRT4 stattfinden kann, ohne dabei die NAD<sup>+</sup>-Bindung und damit die katalytische Aktivität von SIRT4 komplett auszuschalten. Bei gleichem Bindemotiv käme es demnach ebenfalls zu einer Aktivierung der enzymatischen Aktivität von SIRT4 durch CDK1, wodurch die SIRT3 Aktivität wieder ausgeglichen werden würde. Insgesamt käme es somit zu keinem Netto-Mehrgewinn in der bioenergetischen GDH-Regulation.

Die Phosphorylierungsstelle in der NAD<sup>+</sup>-Bindedomäne von SIRT5 zeigt ebenfalls kein Konsensus-Motiv für CDK1 auf, was wiederum für eine spezifische Regulation von SIRT3 durch CDK1 an dieser Position spricht [siehe Anhang 13.1].

Eine Zellzyklus-spezifische Regulation von SIRT4 durch CDK1 ist dennoch nicht auszuschließen, da sich für SIRT4 eine theoretische CDK1 Phosphorylierungsstelle mit minimalem Konsensus-Motiv an der Position Serin 36, welche bereits von Costantini *et al.* postuliert wurde [304], sowie an der Position Threonin 176 findet [siehe Anhang 13.1].

Demnach könnte SIRT4 über eine duale Funktion im Zellzyklus einen Einfluss auf die Mitose haben. Während der Interphase wird SIRT4 in das Mitochondrium importiert, um dort seine Aufgaben im Metabolismus auszuführen, schematisch zusammengestellt in Abbildung 11.

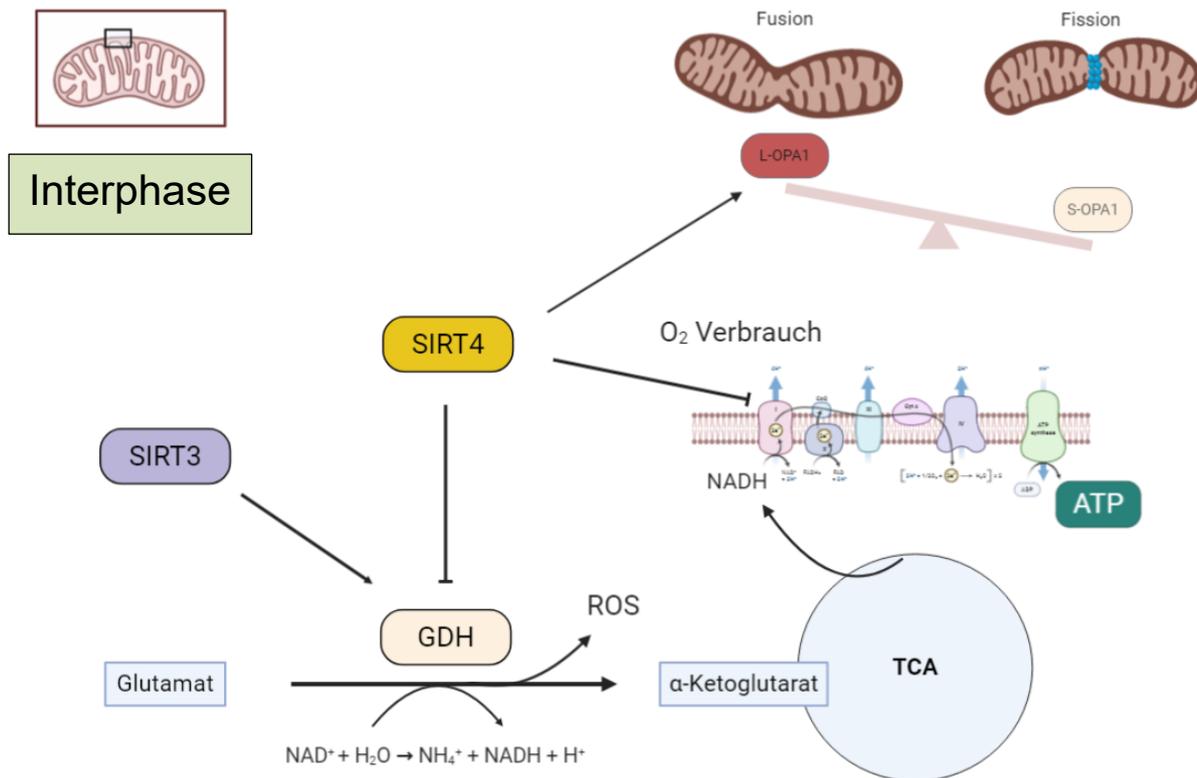


**Abbildung 11:** Vorgeschlagenes Modell der mitochondrialen SIRT4-Wirkmechanismen während der Interphase. Während der Interphase nimmt SIRT4 Einfluss auf die mitochondriale Bioenergetik, indem es antagonistisch zu SIRT3 die anaplerotische Reaktion des Citratzyklus über eine Inhibition der GDH reguliert. Ebenfalls wird der Atmungskomplex I negativ durch SIRT4 reguliert, wodurch die Energieproduktion gedrosselt wird [162]. Gleichzeitig nimmt SIRT4 Einfluss auf die Aufrechterhaltung eines verzweigten mitochondrialen Netzwerkes über Regulation des L-OPA1/S-OPA1 Gleichgewichts. Erstellt mit BioRender.com

Bei der Vorbereitung der Mitose kommt es nun zu einer Regulierung der subzellulären Lokalisation von SIRT4, die ebenfalls eine zunehmende Vereinzelung der Mitochondrien zur Folge hat. Dies ist in Abbildung 12 schematisch zusammengefasst. Während das ins Mitochondrium importierte CDK1 SIRT3 phosphoryliert und damit das Reaktionsgleichgewicht Richtung  $\alpha$ -Ketoglutarat verschiebt, führt eine Inhibition bzw. ein möglicher zellzyklus-regulierter Abbau von SIRT4 auch zu einer Erhöhung der Energieproduktion in den Mitochondrien, da die GDH und der CI der Atmungskette nicht länger negativ reguliert werden. So kann das für die mitotische Progression notwendige ATP generiert werden, um die Verteilung der Organellen zu gewährleisten [299, 305, 306].

Zusätzlich wird durch die Verschiebung des Gleichgewichtes zu S-OPA1 die mitochondriale Fission eingeleitet, die schließlich eine korrekte Verteilung der Mitochondrien in Vorbereitung auf die Mitose ermöglicht.

Durch die Vereinzelung und den Transport der Mitochondrien an die Zellpole kann es zu einem Stopp des SIRT4-Imports in das Mitochondrium kommen, wodurch sich die

zytoplasmatische SIRT4-Konzentration erhöht. Die erhöhte Konzentration im Zytoplasma könnte darauffolgend ein Auslöser sein, welcher zur Anreicherung von SIRT4 in den Zellkern oder aber zur Rekrutierung von SIRT4 an das Zentrosom führt. Auch am Zentrosom könnte dann wie bei EZH2 [292-294] eine durch CDK1 vermittelte Regulation von SIRT4, die mitotische Progression durch die Ausbildung der Spindelmikrotubuli, gesteuert werden.

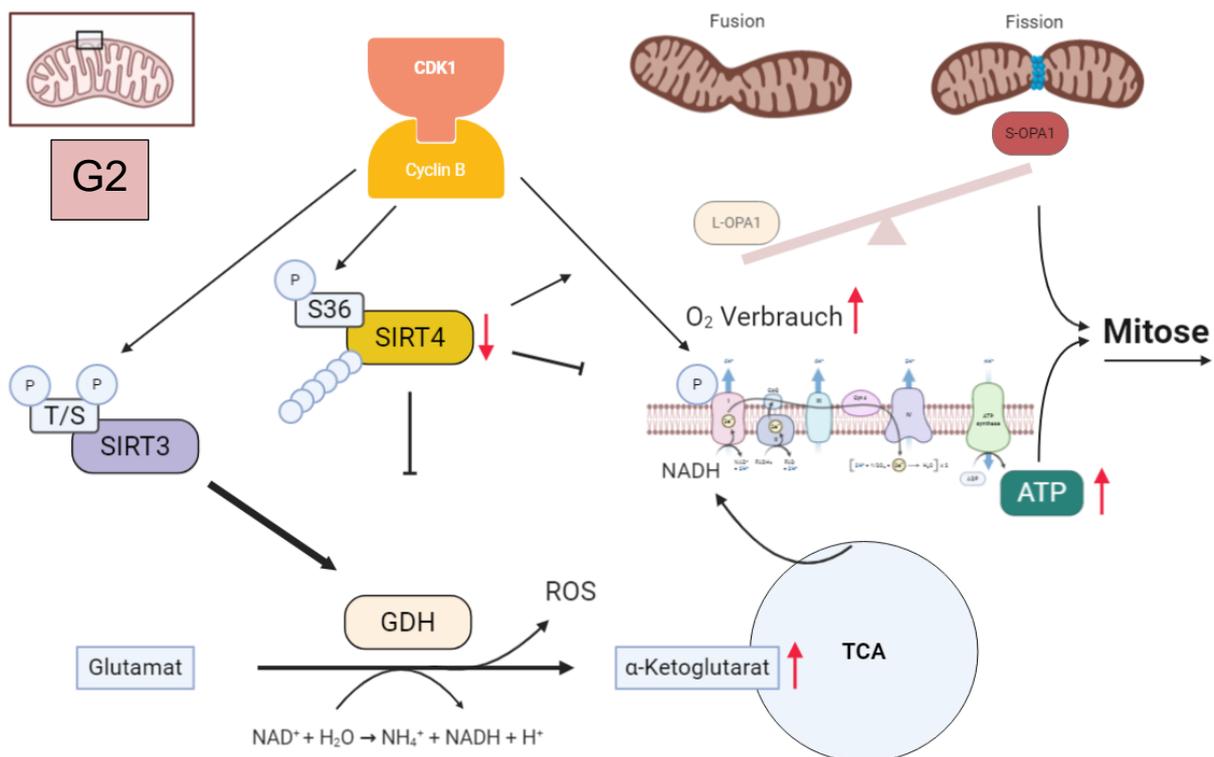


**Abbildung 12:** Vorgeschlagenes Modell der mitochondrialen SIRT4-Wirkmechanismen während der G<sub>2</sub>/M-Phase. In Vorbereitung auf die Mitose kommt es zur Translokation und Anreicherung von CDK1/ZyclinB in die Mitochondrien, wo es eine Reihe von Substraten (z.B. Mn-abhängige Superoxiddismutase, MnSOD) durch Phosphorylierung aktiviert, darunter auch die Untereinheiten des mitochondrialen Atmungskettenkomplexes I. Dies dient der Verbesserung der mitochondrialen Funktion und Energieproduktion, was den energiensensitiven G<sub>2</sub>/M-Übergang antreibt. CDK1 aktiviert ebenfalls über Phosphorylierung SIRT3, während gleichzeitig eine mögliche Phosphorylierung von SIRT4 zu dessen Abbau führen könnte. Dadurch wird das Gleichgewicht der anaplerotischen Reaktion deutlich stärker auf die Seite von α-Ketoglutarat verschoben. In Zusammenhang mit einer Aktivierung des Atmungskettenkomplexes I kommt es zur erhöhten ATP Produktion, die für die mitotischen Vorgänge benötigt wird. Durch den Abbau oder die Deaktivierung von SIRT4 wird ebenfalls das Gleichgewicht auf die S-OPA1-Seite verschoben, wodurch eine verstärkte Fission des mitochondrialen Netzwerkes stattfinden kann, welche für die Distribution um den mitotischen Spindelapparat und auf die Tochterzellen notwendig ist. Erstellt mit BioRender.com

## 7.4. SIRT4 als metabolischer Tumorsuppressor

Literaturübersichten zeigen, dass SIRT4, obwohl initial als metabolischer Tumorsuppressor beschrieben [258], auch onkogene/krebsfördernde Aktivitäten in Abhängigkeit von Tumortyp und zellzyklus-aktivierenden Bedingungen aufweist [307, 308]. Erhöhte SIRT4-Spiegel sind z.B. mit einer schlechten Prognose bei Brustkrebs verbunden [309]. Des Weiteren fördert die Überexpression von SIRT4 das Überleben von HepG2-Hepatomzellen bei stress-induziertem Zelltod unter DNA-schädigenden Bedingungen [310]. Andererseits werden die SIRT4-Proteinmengen z.B. bei Magen- und Lungenkrebs herunterreguliert [251, 302, 311, 312]. Letzteres steht im Einklang mit Befunden, dass SIRT4-*Knock-Out*-Mäuse spontan Tumore wie Lungen-Adenokarzinome entwickeln [251] und die Überexpression von SIRT4 die zelluläre Proliferation von Tumorzelltypen wie Darmkrebs sowohl in Kultur als auch *in vivo* hemmt [251, 302, 311, 312].

Die duale mitochondriale und zentrosomale Lokalisation von SIRT4 ist konsistent mit einer Funktion als *Moonlighting*-Protein, das per Definition an zwei verschiedenen zellulären Kompartimenten/Strukturen mit vergleichbaren oder unterschiedlichen Funktionen lokalisiert [313]. Weitere Beispiele für mitochondrial und zentrosomal lokalisierte *Moonlighting*-Proteine sind *Glutamin amidotransferase like class 1 domain containing 3A* (C21orf33/GATD3A), das im Rahmen des menschlichen Proteinatlas-Projekts identifiziert wurde [314], und das mitochondriale spannungsabhängige anionenselektive Kanalprotein 3 (Porin VDAC3), welches am Zentrosom lokalisiert und den Zusammenbau der Zentriole reguliert [315].

Die metabolische Rolle von SIRT4 im Mitochondrium und dessen potenzielle zentrosomale Aktivität und damit verbundene Auswirkung auf die mitotisch bedingte Chromosomen-Verteilung, steht in direktem Zusammenhang mit der Rolle von SIRT4 als Tumorsuppressor. Bei metabolischem Stress wird die Energieproduktion heruntergefahren und die Progression des Zellzyklus verlangsamt oder sogar direkt gestoppt. Daher sind die Mengen an produzierter Energie in den Mitochondrien ein direktes Feedback für die Zellzykluskontrolle [299].

Ein Marker für mitochondrialen und metabolischen Stress [316] stellt Glutamin dar, welches von der GDH in  $\alpha$ -Ketoglutarat umgewandelt wird, um den Citratzyklus zu

speisen und somit die Energiezufuhr für die Zelle zu gewährleisten. Dieser Schritt wird direkt von SIRT4 über die GDH-Inhibition negativ reguliert.

Der tumorsuppressive Charakter von SIRT4 würde dadurch in Erscheinung treten, dass bei einer Reduktion der SIRT4-Mengen die GDH innerhalb der Mitochondrien nicht inhibiert würde und es so zu einer dauerhaft erhöhten ATP Produktion kommt. Dies beschreibt bei einigen Tumorarten das Phänomen der „Glutamin-Sucht“ [316-318]. Dadurch können Krebszellen ihren erhöhten Energiebedarf für die stetige Zellteilung und Proliferation aufrechterhalten.

Auch eine erhöhte Vereinzelnung der Mitochondrien, die im Zusammenhang mit einer SIRT4-Reduktion steht, ermöglicht es Zellen schneller wieder in die Mitose einzutreten. Damit nimmt SIRT4 eine Rolle in der Zellzyklus- und mitotischen Progression über die Regulierung der mitochondrialen Fission über OPA1 [149, 319] und DRP1 [289, 306] abhängige Signalwege / Mechanismen ein [320].

Beim Fehlen von SIRT4 am Spindelapparat könnte es zu einer unkontrollierten Entwicklung des Zentrosoms oder aber der Spindelmikrotubuli kommen, was schließlich zu Fehlern bei der Chromosomenverteilung führt und ebenso zur Zelltransformation beitragen könnte. Auch die erhöhte Möglichkeit der asymmetrischen Mitochondrien-Verteilung, die in multinukleären Zellen resultieren kann, erhöht das kanzerogene Potential einer Zelle nach der Mitose. Dieser Befund deckt sich wiederum mit der Beobachtung, dass SIRT4-*Knock-Out*-Mäuse eine vermehrte Tumorbildung mit entsprechend auftretender Aneuploidie aufweisen [251]. Hierbei greifen die Mechanismen, ob es durch SIRT4-Depletion zur Tumorbildung kommt oder ob die Runterregulierung von SIRT4 eine Folgeadaptation eines aggressiveren Tumors ist, reziprok ineinander. Es liegt nahe, dass SIRT4 in seiner Rolle im Zellzyklus ein Bindeglied zwischen Mitochondrien und Mitose darstellt, welches auf die Chromosomenverteilung und Chromosomenintegrität bei der Zellteilung Einfluss nimmt. Daher kann SIRT4 seine tumorsupprimierende und zellzyklushemmende Funktion sowohl durch mitochondriale, bioenergetische als auch Mitochondrien-unabhängige, Zentrosom/mitotische Spindelapparat-lokalisierte Mechanismen ausüben.

## 8. Abkürzungsverzeichnis

Acetyl-CoA	Acetyl-Coenzym A
ADP	Adenosindiphosphat
APC	<i>Anaphase Promoting Complex</i>
APC/C	<i>Anaphase Promoting Complex/Cyclosome</i>
ATP	Adenosintriphosphat
CCCP	Carbonylcyanide-m-chlorophenylhydrazon
CDK	<i>cyclin-dependent kinases</i>
CDK5RAP2	<i>CDK5 regulatory subunit-associated protein 2</i>
Cep152	<i>Centrosomal protein of 152 kDa</i>
Cep192	<i>Centrosomal protein of 192 kDa</i>
CuZnSOD	Kupfer-Zink-abhängige Superoxiddismutase
DNA	Desoxyribonukleinsäure
DRP1	<i>Dynamin-1-like Protein</i>
eGFP	<i>enhanced green fluorescent protein</i>
eNOS	endotheliale Stickstoffmonoxid-Synthase
FOXO1	<i>Forkhead-Box Protein O1</i>
G6PD	Glukose-6-Phosphat-Dehydrogenase
GATD3A	<i>Glutamin amidotransferase like class 1 domain containing 3A</i>
GCP	$\gamma$ -Tubulinkomplex-Proteinen
GDH	Glutamat-Dehydrogenase
GTP	Guanosintriphosphat
GTPase	Guanosintriphosphatase
HDAC6	Histondeacetylase 6
HE	hepatische Enzephalopathie
HEK293	<i>Human Embryonic Kidney 293</i>
HIF	<i>Hypoxia-inducible factor</i>
IDH2	Isocitrate-Dehydrogenase 2
K40	Lysin 40
L-OPA1	<i>Long form - Optic Atrophy 1</i>
LRP130	<i>Leucin-rich Protein 130</i>
MAP	Mikrotubuli-assoziiertes Protein

MFN	Mitofusin
MnSOD	Mangan-abhängige Superoxiddismutase
MOZART	<i>mitotic-spindle organizing protein associated with a ring of <math>\gamma</math>-tubulin</i>
mRNA	<i>messenger ribonucleic acid</i>
mtDNA	Mitochondriale DNA
MTOC	<i>microtubule organizing centre</i>
mtROS	mitochondriale ROS
MTS	mitochondriales Translokationssignal
NAD	Nicotinamid-Adenin-Dinukleotid
NADPH	Nicotinamidadenindinukleotidphosphat
NHEJ	non-homologous end joining
NLS	nukleäres Lokalisierungssignal
NSCLC	<i>non-small cell lung cancer</i>
PARP-1	Poly-(ADP-ribose)-polymerase 1
PARPs	Poly-(ADP)-Ribosyltransferasen
PCM	perizentrioläres Material
PDC	Pyruvat-Dehydrogenase Komplex
PDH	Pyruvat-Dehydrogenase
PGAM-1	Phosphoglyceratmutase-1
Plk	<i>polo-like kinase</i>
Porin VDAC3	spannungsabhängiges anionenselektives Kanalprotein 3
PPAR	Peroxisom-Proliferator-aktivierten Rezeptor
PTM	posttranslationale Modifikationen
RNA	Ribonukleinsäure
ROS	<i>reactive oxygen species</i>
SAC	<i>Spindel-Assembly-Checkpoint</i>
SASP	Seneszenz-assoziiierter sekretorischer Phänotyp
SDH	Succinat-Dehydrogenase
SIR2	<i>Silent Information Regulator 2</i>
SIRT	Sirtuin
SMS	Seneszenz-assoziiertes Sekretom
S-OPA1	<i>Short form - Optic Atrophy 1</i>
SPD-2	<i>Spindle-defective protein 2</i>
SPD-5	<i>Spindle-defective protein 5</i>

S-Phase	Synthese-Phase
TACC3	<i>transforming acidic coiled-coil-containing protein 3</i>
TUBGCP	$\gamma$ -Tubulinkomplex-Proteinen
TUBGCP2	$\gamma$ -Tubulin-Komplex-Komponente 2
TUBGCP3	$\gamma$ -Tubulin-Komplex-Komponente 3
WAT	<i>white adipose tissue</i>
$\alpha$ Tat1	$\alpha$ -Tubulin-Acetyltransferase 1
$\gamma$ TuC	$\gamma$ - <i>Tubulin complex</i>
$\gamma$ TuRC	$\gamma$ - <i>Tubulin ring complex</i>
$\gamma$ TuSC	$\gamma$ - <i>Tubulin small complex</i>

## 9. Literaturverzeichnis

1. Reed, S.I., Ratchets and clocks: the cell cycle, ubiquitylation and protein turnover. *Nat Rev Mol Cell Biol*, 2003. **4**(11): p. 855-64.
2. Lindqvist, A., V. Rodriguez-Bravo, and R.H. Medema, The decision to enter mitosis: feedback and redundancy in the mitotic entry network. *J Cell Biol*, 2009. **185**(2): p. 193-202.
3. Lince-Faria, M., et al., Spatiotemporal control of mitosis by the conserved spindle matrix protein Megator. *J Cell Biol*, 2009. **184**(5): p. 647-57.
4. Liu, X., et al., Targeting mitosis exit: A brake for cancer cell proliferation. *Biochim Biophys Acta Rev Cancer*, 2019. **1871**(1): p. 179-191.
5. Pines, J., Mitosis: a matter of getting rid of the right protein at the right time. *Trends Cell Biol*, 2006. **16**(1): p. 55-63.
6. Moonen, L., P.C. D'Haese, and B.A. Vervaet, Epithelial Cell Cycle Behaviour in the Injured Kidney. *Int J Mol Sci*, 2018. **19**(7).
7. Umeda, M., S.S. Aki, and N. Takahashi, Gap 2 phase: making the fundamental decision to divide or not. *Curr Opin Plant Biol*, 2019. **51**: p. 1-6.
8. Ciciarello, M., R. Mangiacasale, and P. Lavia, Spatial control of mitosis by the GTPase Ran. *Cell Mol Life Sci*, 2007.
9. Lodish H, B.A., Zipursky SL, et al. , *Molecular Cell Biology*. 6th ed. 2008, New York: W. H. Freeman.
10. Sanchez, L., M. Kodiha, and U. Stochaj, Monitoring the disruption of nuclear envelopes in interphase cells with GFP-beta-galactosidase. *J Biomol Tech*, 2005. **16**(3): p. 235-8.
11. Barbacid, M., et al., Cell cycle and cancer: genetic analysis of the role of cyclin-dependent kinases. *Cold Spring Harb Symp Quant Biol*, 2005. **70**: p. 233-40.
12. Malumbres, M., Cyclins and related kinases in cancer cells. *J BUON*, 2007. **12 Suppl 1**: p. S45-52.
13. Satyanarayana, A. and P. Kaldis, Mammalian cell-cycle regulation: several Cdks, numerous cyclins and diverse compensatory mechanisms. *Oncogene*, 2009. **28**(33): p. 2925-39.
14. Sherr, C.J. and J.M. Roberts, CDK inhibitors: positive and negative regulators of G1-phase progression. *Genes Dev*, 1999. **13**(12): p. 1501-12.
15. Sherr, C.J. and J.M. Roberts, Living with or without cyclins and cyclin-dependent kinases. *Genes Dev*, 2004. **18**(22): p. 2699-711.
16. Weinberg, R.A., The retinoblastoma protein and cell cycle control. *Cell*, 1995. **81**(3): p. 323-30.

17. Dyson, N., The regulation of E2F by pRB-family proteins. *Genes Dev*, 1998. **12**(15): p. 2245-62.
18. Pihan, G.A., Centrosome dysfunction contributes to chromosome instability, chromoanagenesis, and genome reprogramming in cancer. *Front Oncol*, 2013. **3**: p. 277.
19. Bornens, M., The centrosome in cells and organisms. *Science*, 2012. **335**(6067): p. 422-6.
20. Conduit, P.T., A. Wainman, and J.W. Raff, Centrosome function and assembly in animal cells. *Nat Rev Mol Cell Biol*, 2015. **16**(10): p. 611-24.
21. Thakur, H.C., et al., Role of centrosomal adaptor proteins of the TACC family in the regulation of microtubule dynamics during mitotic cell division. *Biol Chem*, 2013. **394**(11): p. 1411-23.
22. Andersen, J.S., et al., Proteomic characterization of the human centrosome by protein correlation profiling. *Nature*, 2003. **426**(6966): p. 570-4.
23. Neumann, B., et al., Phenotypic profiling of the human genome by time-lapse microscopy reveals cell division genes. *Nature*, 2010. **464**(7289): p. 721-7.
24. Zimmerman, W.C., et al., Mitosis-specific anchoring of gamma tubulin complexes by pericentrin controls spindle organization and mitotic entry. *Mol Biol Cell*, 2004. **15**(8): p. 3642-57.
25. Graf, R., Comparative Biology of Centrosomal Structures in Eukaryotes. *Cells*, 2018. **7**(11).
26. Stearns, T. and M. Winey, The cell center at 100. *Cell*, 1997. **91**(3): p. 303-9.
27. Douglas, M.E. and M. Mishima, Still entangled: assembly of the central spindle by multiple microtubule modulators. *Semin Cell Dev Biol*, 2010. **21**(9): p. 899-908.
28. Carvalho-Santos, Z., et al., Evolution: Tracing the origins of centrioles, cilia, and flagella. *J Cell Biol*, 2011. **194**(2): p. 165-75.
29. Carvalho-Santos, Z., et al., Stepwise evolution of the centriole-assembly pathway. *J Cell Sci*, 2010. **123**(Pt 9): p. 1414-26.
30. Lattao, R., L. Kovacs, and D.M. Glover, The Centrioles, Centrosomes, Basal Bodies, and Cilia of *Drosophila melanogaster*. *Genetics*, 2017. **206**(1): p. 33-53.
31. Woodruff, J.B., O. Wueseke, and A.A. Hyman, Pericentriolar material structure and dynamics. *Philos Trans R Soc Lond B Biol Sci*, 2014. **369**(1650).
32. Desai, A. and T.J. Mitchison, MICROTUBULE POLYMERIZATION DYNAMICS. *Annual Review of Cell and Developmental Biology*, 1997. **13**(1): p. 83-117.
33. Cooke, C.A., M.M. Heck, and W.C. Earnshaw, The inner centromere protein (INCENP) antigens: movement from inner centromere to midbody during mitosis. *J Cell Biol*, 1987. **105**(5): p. 2053-67.
34. Arnold, T.R., R.E. Stephenson, and A.L. Miller, Rho GTPases and actomyosin: Partners in regulating epithelial cell-cell junction structure and function. *Exp Cell Res*, 2017. **358**(1): p. 20-30.

35. Steigemann, P., et al., Aurora B-mediated abscission checkpoint protects against tetraploidization. *Cell*, 2009. **136**(3): p. 473-84.
36. Hummer, S. and T.U. Mayer, Cdk1 negatively regulates midzone localization of the mitotic kinesin Mklp2 and the chromosomal passenger complex. *Curr Biol*, 2009. **19**(7): p. 607-12.
37. Fu, J., I.M. Hagan, and D.M. Glover, The centrosome and its duplication cycle. *Cold Spring Harb Perspect Biol*, 2015. **7**(2): p. a015800.
38. Bergalet, J., et al., Inter-dependent Centrosomal Co-localization of the cen and ik2 cis-Natural Antisense mRNAs in *Drosophila*. *Cell Rep*, 2020. **30**(10): p. 3339-3352 e6.
39. Ryder, P.V., J. Fang, and D.A. Lerit, c entrocartin RNA localization to centrosomes is regulated by FMRP and facilitates error-free mitosis. *J Cell Biol*, 2020. **219**(12).
40. Pederson, T., The centrosome: built on an mRNA? *Nat Cell Biol*, 2006. **8**(7): p. 652-4.
41. Pelletier, L., et al., The *Caenorhabditis elegans* centrosomal protein SPD-2 is required for both pericentriolar material recruitment and centriole duplication. *Curr Biol*, 2004. **14**(10): p. 863-73.
42. Bonaccorsi, S., M.G. Giansanti, and M. Gatti, Spindle self-organization and cytokinesis during male meiosis in asterless mutants of *Drosophila melanogaster*. *J Cell Biol*, 1998. **142**(3): p. 751-61.
43. Hamill, D.R., et al., Centrosome maturation and mitotic spindle assembly in *C. elegans* require SPD-5, a protein with multiple coiled-coil domains. *Dev Cell*, 2002. **3**(5): p. 673-84.
44. Nigg, E.A. and A.J. Holland, Once and only once: mechanisms of centriole duplication and their deregulation in disease. *Nat Rev Mol Cell Biol*, 2018. **19**(5): p. 297-312.
45. Kanai, M., et al., Involvement of poly(ADP-Ribose) polymerase 1 and poly(ADP-Ribosyl)ation in regulation of centrosome function. *Mol Cell Biol*, 2003. **23**(7): p. 2451-62.
46. Boehler, C. and F. Dantzer, PARP-3, a DNA-dependent PARP with emerging roles in double-strand break repair and mitotic progression. *Cell Cycle*, 2011. **10**(7): p. 1023-4.
47. Scarpa, E.S., G. Fabrizio, and M. Di Girolamo, A role of intracellular mono-ADP-ribosylation in cancer biology. *FEBS J*, 2013. **280**(15): p. 3551-62.
48. Kanai, M., et al., Haploinsufficiency of poly(ADP-ribose) polymerase-1-mediated poly(ADP-ribosyl)ation for centrosome duplication. *Biochem Biophys Res Commun*, 2007. **359**(3): p. 426-30.
49. Rale, M.J., R.S. Kadzik, and S. Petry, Phase Transitioning the Centrosome into a Microtubule Nucleator. *Biochemistry*, 2018. **57**(1): p. 30-37.
50. Kollman, J.M., et al., Microtubule nucleation by gamma-tubulin complexes. *Nat Rev Mol Cell Biol*, 2011. **12**(11): p. 709-21.
51. Tovey, C.A. and P.T. Conduit, Microtubule nucleation by gamma-tubulin complexes and beyond. *Essays Biochem*, 2018. **62**(6): p. 765-780.

52. Cota, R.R., et al., MZT1 regulates microtubule nucleation by linking gammaTuRC assembly to adapter-mediated targeting and activation. *J Cell Sci*, 2017. **130**(2): p. 406-419.
53. Choi, Y.K. and R.Z. Qi, Assaying microtubule nucleation by the gamma-tubulin ring complex. *Methods Enzymol*, 2014. **540**: p. 119-30.
54. Gunawardane, R.N., et al., Characterization and reconstitution of Drosophila gamma-tubulin ring complex subunits. *J Cell Biol*, 2000. **151**(7): p. 1513-24.
55. Murphy, S.M., et al., GCP5 and GCP6: two new members of the human gamma-tubulin complex. *Mol Biol Cell*, 2001. **12**(11): p. 3340-52.
56. Murphy, S.M., L. Urbani, and T. Stearns, The mammalian gamma-tubulin complex contains homologues of the yeast spindle pole body components spc97p and spc98p. *J Cell Biol*, 1998. **141**(3): p. 663-74.
57. Hutchins, J.R., et al., Systematic analysis of human protein complexes identifies chromosome segregation proteins. *Science*, 2010. **328**(5978): p. 593-9.
58. Teixido-Travesa, N., et al., The gammaTuRC revisited: a comparative analysis of interphase and mitotic human gammaTuRC redefines the set of core components and identifies the novel subunit GCP8. *Mol Biol Cell*, 2010. **21**(22): p. 3963-72.
59. Tovey, C.A., et al., gamma-TuRC Heterogeneity Revealed by Analysis of Mozart1. *Curr Biol*, 2018. **28**(14): p. 2314-2323 e6.
60. Brouhard, G.J. and L.M. Rice, Microtubule dynamics: an interplay of biochemistry and mechanics. *Nat Rev Mol Cell Biol*, 2018. **19**(7): p. 451-463.
61. Gelfand, V.I. and A.D. Bershadsky, Microtubule dynamics: mechanism, regulation, and function. *Annu Rev Cell Biol*, 1991. **7**: p. 93-116.
62. Burbank, K.S. and T.J. Mitchison, Microtubule dynamic instability. *Curr Biol*, 2006. **16**(14): p. R516-7.
63. Mahadevan, L. and T.J. Mitchison, Cell biology: powerful curves. *Nature*, 2005. **435**(7044): p. 895-7.
64. Nogales, E. and H.W. Wang, Structural mechanisms underlying nucleotide-dependent self-assembly of tubulin and its relatives. *Curr Opin Struct Biol*, 2006. **16**(2): p. 221-9.
65. Zilberman, Y., et al., Regulation of microtubule dynamics by inhibition of the tubulin deacetylase HDAC6. *J Cell Sci*, 2009. **122**(Pt 19): p. 3531-41.
66. Howard, J. and A.A. Hyman, Dynamics and mechanics of the microtubule plus end. *Nature*, 2003. **422**(6933): p. 753-8.
67. Joshi, H.C., Microtubule dynamics in living cells. *Curr Opin Cell Biol*, 1998. **10**(1): p. 35-44.
68. Kirschner, M.W., Biological implications of microtubule dynamics. *Harvey Lect*, 1987. **83**: p. 1-20.

69. Janke, C. and J.C. Bulinski, Post-translational regulation of the microtubule cytoskeleton: mechanisms and functions. *Nat Rev Mol Cell Biol*, 2011. **12**(12): p. 773-86.
70. Janke, C. and G. Montagnac, Causes and Consequences of Microtubule Acetylation. *Curr Biol*, 2017. **27**(23): p. R1287-R1292.
71. Li, L. and X.J. Yang, Tubulin acetylation: responsible enzymes, biological functions and human diseases. *Cell Mol Life Sci*, 2015. **72**(22): p. 4237-55.
72. Skoge, R.H., C. Dolle, and M. Ziegler, Regulation of SIRT2-dependent alpha-tubulin deacetylation by cellular NAD levels. *DNA Repair (Amst)*, 2014. **23**: p. 33-8.
73. Skoge, R.H. and M. Ziegler, SIRT2 inactivation reveals a subset of hyperacetylated perinuclear microtubules inaccessible to HDAC6. *J Cell Sci*, 2016. **129**(15): p. 2972-82.
74. Hanahan, D. and R.A. Weinberg, The hallmarks of cancer. *Cell*, 2000. **100**(1): p. 57-70.
75. Hanahan, D. and R.A. Weinberg, Hallmarks of cancer: the next generation. *Cell*, 2011. **144**(5): p. 646-74.
76. L., H., Uber asymmetrische Zelltheilung in Epithelkrebsen und deren biologische Bedeutung. *Arch Pathol Anat Physiol Klin Med Hypotheses*, 1890. **119**:299–326.
77. L., H., Ueber pathologische Mitosen. *Arch Pathol Anat Physiol Klin Med Hypotheses*, 1891. **123**:356–70.
78. Collado, M. and M. Serrano, The power and the promise of oncogene-induced senescence markers. *Nat Rev Cancer*, 2006. **6**(6): p. 472-6.
79. Campisi, J. and F. d'Adda di Fagagna, Cellular senescence: when bad things happen to good cells. *Nat Rev Mol Cell Biol*, 2007. **8**(9): p. 729-40.
80. van Deursen, J.M., The role of senescent cells in ageing. *Nature*, 2014. **509**(7501): p. 439-46.
81. Schmidt, S., et al., The centrosome and mitotic spindle apparatus in cancer and senescence. *Cell Cycle*, 2010. **9**(22): p. 4469-73.
82. Lopez-Otin, C., et al., The hallmarks of aging. *Cell*, 2013. **153**(6): p. 1194-217.
83. Tchkonja, T., et al., Cellular senescence and the senescent secretory phenotype: therapeutic opportunities. *J Clin Invest*, 2013. **123**(3): p. 966-72.
84. Kuilman, T., et al., The essence of senescence. *Genes Dev*, 2010. **24**(22): p. 2463-79.
85. Coppe, J.P., et al., Senescence-associated secretory phenotypes reveal cell-nonautonomous functions of oncogenic RAS and the p53 tumor suppressor. *PLoS Biol*, 2008. **6**(12): p. 2853-68.
86. Rodier, F., et al., Persistent DNA damage signalling triggers senescence-associated inflammatory cytokine secretion. *Nat Cell Biol*, 2009. **11**(8): p. 973-9.

87. Kuilman, T. and D.S. Peeper, Senescence-messaging secretome: SMS-ing cellular stress. *Nat Rev Cancer*, 2009. **9**(2): p. 81-94.
88. Huck, J.J., et al., MLN8054, an inhibitor of Aurora A kinase, induces senescence in human tumor cells both in vitro and in vivo. *Mol Cancer Res*, 2010. **8**(3): p. 373-84.
89. Tritarelli, A., et al., p53 localization at centrosomes during mitosis and postmitotic checkpoint are ATM-dependent and require serine 15 phosphorylation. *Mol Biol Cell*, 2004. **15**(8): p. 3751-7.
90. Schmidt, S., et al., The centrosomal protein TACC3 controls paclitaxel sensitivity by modulating a premature senescence program. *Oncogene*, 2010. **29**(46): p. 6184-92.
91. Mikule, K., et al., Loss of centrosome integrity induces p38-p53-p21-dependent G1-S arrest. *Nat Cell Biol*, 2007. **9**(2): p. 160-70.
92. Srsen, V., et al., Inhibition of centrosome protein assembly leads to p53-dependent exit from the cell cycle. *J Cell Biol*, 2006. **174**(5): p. 625-30.
93. Qi, F. and F. Zhang, Cell Cycle Regulation in the Plant Response to Stress. *Front Plant Sci*, 2019. **10**: p. 1765.
94. Hartwell, L.H. and T.A. Weinert, Checkpoints - Controls That Ensure the Order of Cell-Cycle Events. *Science*, 1989. **246**(4930): p. 629-634.
95. Rieder, C.L. and H. Maiato, Stuck in division or passing through: what happens when cells cannot satisfy the spindle assembly checkpoint. *Dev Cell*, 2004. **7**(5): p. 637-51.
96. Weaver, B.A. and D.W. Cleveland, Decoding the links between mitosis, cancer, and chemotherapy: The mitotic checkpoint, adaptation, and cell death. *Cancer Cell*, 2005. **8**(1): p. 7-12.
97. Gascoigne, K.E. and S.S. Taylor, Cancer cells display profound intra- and interline variation following prolonged exposure to antimetabolic drugs. *Cancer Cell*, 2008. **14**(2): p. 111-22.
98. Brito, D.A. and C.L. Rieder, Mitotic checkpoint slippage in humans occurs via cyclin B destruction in the presence of an active checkpoint. *Curr Biol*, 2006. **16**(12): p. 1194-200.
99. Sinclair, D.A. and L. Guarente, Extrachromosomal rDNA circles--a cause of aging in yeast. *Cell*, 1997. **91**(7): p. 1033-42.
100. Kaeberlein, M., M. McVey, and L. Guarente, The SIR2/3/4 complex and SIR2 alone promote longevity in *Saccharomyces cerevisiae* by two different mechanisms. *Genes Dev*, 1999. **13**(19): p. 2570-80.
101. Verdin, E., The many faces of sirtuins: Coupling of NAD metabolism, sirtuins and lifespan. *Nat Med*, 2014. **20**(1): p. 25-7.
102. Tan, G., et al., Apoptosis induced by low-dose paclitaxel is associated with p53 upregulation in nasopharyngeal carcinoma cells. *Int J Cancer*, 2002. **97**(2): p. 168-72.
103. Tissenbaum, H.A. and L. Guarente, Increased dosage of a sir-2 gene extends lifespan in *Caenorhabditis elegans*. *Nature*, 2001. **410**(6825): p. 227-30.

104. Baur, J.A., et al., Dietary restriction: standing up for sirtuins. *Science*. **329**(5995): p. 1012-3; author reply 1013-4.
105. Frankel, S., T. Ziafazeli, and B. Rogina, dSir2 and longevity in *Drosophila*. *Exp Gerontol*.
106. Haigis, M.C. and D.A. Sinclair, Mammalian sirtuins: biological insights and disease relevance. *Annu Rev Pathol*, 2010. **5**: p. 253-95.
107. Banerjee, K.K., et al., dSir2 in the adult fat body, but not in muscles, regulates life span in a diet-dependent manner. *Cell Rep*, 2012. **2**(6): p. 1485-91.
108. Osborne, B., et al., The role of mitochondrial sirtuins in health and disease. *Free Radic Biol Med*, 2016. **100**: p. 164-174.
109. Imai, S., et al., Transcriptional silencing and longevity protein Sir2 is an NAD-dependent histone deacetylase. *Nature*, 2000. **403**(6771): p. 795-800.
110. Sauve, A.A., et al., The biochemistry of sirtuins. *Annu Rev Biochem*, 2006. **75**: p. 435-65.
111. Landry, J., et al., The silencing protein SIR2 and its homologs are NAD-dependent protein deacetylases. *Proc Natl Acad Sci U S A*, 2000. **97**(11): p. 5807-11.
112. Pannek, M., et al., Crystal structures of the mitochondrial deacylase Sirtuin 4 reveal isoform-specific acyl recognition and regulation features. *Nat Commun*, 2017. **8**(1): p. 1513.
113. Saunders, L.R. and E. Verdin, Sirtuins: critical regulators at the crossroads between cancer and aging. *Oncogene*, 2007. **26**(37): p. 5489-504.
114. Frye, R.A., Phylogenetic classification of prokaryotic and eukaryotic Sir2-like proteins. *Biochem Biophys Res Commun*, 2000. **273**(2): p. 793-8.
115. Haigis, M.C. and L.P. Guarente, Mammalian sirtuins--emerging roles in physiology, aging, and calorie restriction. *Genes Dev*, 2006. **20**(21): p. 2913-21.
116. Poljsak, B. and I. Milisav, NAD<sup>+</sup> as the Link Between Oxidative Stress, Inflammation, Caloric Restriction, Exercise, DNA Repair, Longevity, and Health Span. *Rejuvenation Res*, 2016. **19**(5): p. 406-415.
117. Lang, A., Die Rolle des Sirtuins SIRT4 in mitochondrialer Funktion und Qualitätskontrolle, zellulärer Seneszenz und Alterung. <https://docserv.uni-duesseldorf.de/>, 2017: p. 21.
118. Consortium, U., <https://www.uniprot.org/>. Stand Januar 2021.
119. Li, X. and N. Kazgan, Mammalian sirtuins and energy metabolism. *Int J Biol Sci*, 2011. **7**(5): p. 575-87.
120. Pirinen, E., G. Lo Sasso, and J. Auwerx, Mitochondrial sirtuins and metabolic homeostasis. *Best Pract Res Clin Endocrinol Metab*, 2012. **26**(6): p. 759-70.
121. van de Ven, R.A.H., D. Santos, and M.C. Haigis, Mitochondrial Sirtuins and Molecular Mechanisms of Aging. *Trends Mol Med*, 2017. **23**(4): p. 320-331.

122. Chang, H.C. and L. Guarente, SIRT1 and other sirtuins in metabolism. *Trends Endocrinol Metab*, 2014. **25**(3): p. 138-45.
123. Donmez, G. and L. Guarente, Aging and disease: connections to sirtuins. *Aging Cell*, 2010. **9**(2): p. 285-90.
124. German, N.J. and M.C. Haigis, Sirtuins and the Metabolic Hurdles in Cancer. *Curr Biol*, 2015. **25**(13): p. R569-83.
125. Guarente, L., Sirtuins in aging and disease. *Cold Spring Harb Symp Quant Biol*, 2007. **72**: p. 483-8.
126. van der Bliek, A.M., M.M. Sedensky, and P.G. Morgan, Cell Biology of the Mitochondrion. *Genetics*, 2017. **207**(3): p. 843-871.
127. Drose, S., U. Brandt, and I. Wittig, Mitochondrial respiratory chain complexes as sources and targets of thiol-based redox-regulation. *Biochim Biophys Acta*, 2014. **1844**(8): p. 1344-54.
128. Wallace, D.C., A mitochondrial paradigm of metabolic and degenerative diseases, aging, and cancer: a dawn for evolutionary medicine. *Annu Rev Genet*, 2005. **39**: p. 359-407.
129. Lowell, B.B. and G.I. Shulman, Mitochondrial dysfunction and type 2 diabetes. *Science*, 2005. **307**(5708): p. 384-7.
130. Antico Arciuch, V.G., et al., Mitochondrial regulation of cell cycle and proliferation. *Antioxid Redox Signal*, 2012. **16**(10): p. 1150-80.
131. Chan, D.C., Mitochondrial fusion and fission in mammals. *Annu Rev Cell Dev Biol*, 2006. **22**: p. 79-99.
132. Zhao, J., et al., Mitochondrial dynamics regulates migration and invasion of breast cancer cells. *Oncogene*, 2013. **32**(40): p. 4814-24.
133. Archer, S.L., Mitochondrial dynamics--mitochondrial fission and fusion in human diseases. *N Engl J Med*, 2013. **369**(23): p. 2236-51.
134. Grandemange, S., S. Herzig, and J.C. Martinou, Mitochondrial dynamics and cancer. *Semin Cancer Biol*, 2009. **19**(1): p. 50-6.
135. Roberts, E.R. and K.J. Thomas, The role of mitochondria in the development and progression of lung cancer. *Comput Struct Biotechnol J*, 2013. **6**: p. e201303019.
136. Lima, A.R., et al., Dynamin-Related Protein 1 at the Crossroads of Cancer. *Genes (Basel)*, 2018. **9**(2).
137. Elmore, S.P., et al., The mitochondrial permeability transition initiates autophagy in rat hepatocytes. *FASEB J*, 2001. **15**(12): p. 2286-7.
138. Lemasters, J.J., Selective mitochondrial autophagy, or mitophagy, as a targeted defense against oxidative stress, mitochondrial dysfunction, and aging. *Rejuvenation Res*, 2005. **8**(1): p. 3-5.
139. McBride, H. and V. Soubannier, Mitochondrial function: OMA1 and OPA1, the grandmasters of mitochondrial health. *Curr Biol*, 2010. **20**(6): p. R274-6.

140. Twig, G. and O.S. Shirihai, The interplay between mitochondrial dynamics and mitophagy. *Antioxid Redox Signal*, 2011. **14**(10): p. 1939-51.
141. Weber, T.A. and A.S. Reichert, Impaired quality control of mitochondria: aging from a new perspective. *Exp Gerontol*, 2010. **45**(7-8): p. 503-11.
142. Westermann, B., Mitochondrial fusion and fission in cell life and death. *Nat Rev Mol Cell Biol*, 2010. **11**(12): p. 872-84.
143. Kashatus, D.F., et al., RALA and RALBP1 regulate mitochondrial fission at mitosis. *Nat Cell Biol*, 2011. **13**(9): p. 1108-15.
144. Boland, M.L., A.H. Chourasia, and K.F. Macleod, Mitochondrial dysfunction in cancer. *Front Oncol*, 2013. **3**: p. 292.
145. van der Blik, A.M., Q. Shen, and S. Kawajiri, Mechanisms of mitochondrial fission and fusion. *Cold Spring Harb Perspect Biol*, 2013. **5**(6).
146. Lennon, F.E. and R. Salgia, Mitochondrial dynamics: biology and therapy in lung cancer. *Expert Opin Investig Drugs*, 2014. **23**(5): p. 675-92.
147. Rehman, J., et al., Inhibition of mitochondrial fission prevents cell cycle progression in lung cancer. *FASEB J*, 2012. **26**(5): p. 2175-86.
148. Thomas, K.J. and M.R. Jacobson, Defects in mitochondrial fission protein dynamin-related protein 1 are linked to apoptotic resistance and autophagy in a lung cancer model. *PLoS One*, 2012. **7**(9): p. e45319.
149. Del Dotto, V., et al., OPA1 Isoforms in the Hierarchical Organization of Mitochondrial Functions. *Cell Rep*, 2017. **19**(12): p. 2557-2571.
150. Wai, T. and T. Langer, Mitochondrial Dynamics and Metabolic Regulation. *Trends Endocrinol Metab*, 2016. **27**(2): p. 105-17.
151. Youle, R.J. and A.M. van der Blik, Mitochondrial fission, fusion, and stress. *Science*, 2012. **337**(6098): p. 1062-5.
152. Michishita, E., et al., Evolutionarily conserved and nonconserved cellular localizations and functions of human SIRT proteins. *Mol Biol Cell*, 2005. **16**(10): p. 4623-35.
153. Tang, X., et al., Mitochondrial Sirtuins in cardiometabolic diseases. *Clin Sci (Lond)*, 2017. **131**(16): p. 2063-2078.
154. Yang, W., et al., Mitochondrial Sirtuin Network Reveals Dynamic SIRT3-Dependent Deacetylation in Response to Membrane Depolarization. *Cell*, 2016. **167**(4): p. 985-1000 e21.
155. Liu, R., et al., CDK1-Mediated SIRT3 Activation Enhances Mitochondrial Function and Tumor Radioresistance. *Mol Cancer Ther*, 2015. **14**(9): p. 2090-102.
156. Torrens-Mas, M., et al., Sirtuin 3 silencing impairs mitochondrial biogenesis and metabolism in colon cancer cells. *Am J Physiol Cell Physiol*, 2019. **317**(2): p. C398-C404.

157. Schwer, B., et al., The human silent information regulator (Sir)2 homologue hSIRT3 is a mitochondrial nicotinamide adenine dinucleotide-dependent deacetylase. *J Cell Biol*, 2002. **158**(4): p. 647-57.
158. Shi, T., et al., SIRT3, a mitochondrial sirtuin deacetylase, regulates mitochondrial function and thermogenesis in brown adipocytes. *J Biol Chem*, 2005. **280**(14): p. 13560-7.
159. Onyango, P., et al., SIRT3, a human SIR2 homologue, is an NAD-dependent deacetylase localized to mitochondria. *Proc Natl Acad Sci U S A*, 2002. **99**(21): p. 13653-8.
160. Hebert, A.S., et al., Calorie restriction and SIRT3 trigger global reprogramming of the mitochondrial protein acetylome. *Mol Cell*, 2013. **49**(1): p. 186-99.
161. Fernandez-Marcos, P.J., et al., Muscle or liver-specific Sirt3 deficiency induces hyperacetylation of mitochondrial proteins without affecting global metabolic homeostasis. *Sci Rep*, 2012. **2**: p. 425.
162. Haigis, M.C., et al., SIRT4 inhibits glutamate dehydrogenase and opposes the effects of calorie restriction in pancreatic beta cells. *Cell*, 2006. **126**(5): p. 941-54.
163. Laurent, G., et al., SIRT4 coordinates the balance between lipid synthesis and catabolism by repressing malonyl CoA decarboxylase. *Mol Cell*, 2013. **50**(5): p. 686-98.
164. Mathias, R.A., et al., Sirtuin 4 is a lipoamidase regulating pyruvate dehydrogenase complex activity. *Cell*, 2014. **159**(7): p. 1615-25.
165. Du, J., et al., Sirt5 is a NAD-dependent protein lysine demalonylase and desuccinylase. *Science*, 2011. **334**(6057): p. 806-9.
166. Park, J., et al., SIRT5-mediated lysine desuccinylation impacts diverse metabolic pathways. *Mol Cell*, 2013. **50**(6): p. 919-30.
167. Rardin, M.J., et al., SIRT5 regulates the mitochondrial lysine succinylome and metabolic networks. *Cell Metab*, 2013. **18**(6): p. 920-33.
168. Nishida, Y., et al., SIRT5 Regulates both Cytosolic and Mitochondrial Protein Malonylation with Glycolysis as a Major Target. *Mol Cell*, 2015. **59**: p. 321-332.
169. Schlicker, C., et al., Substrates and regulation mechanisms for the human mitochondrial sirtuins Sirt3 and Sirt5. *J Mol Biol*, 2008. **382**(3): p. 790-801.
170. Fan, J., et al., Tyr phosphorylation of PDP1 toggles recruitment between ACAT1 and SIRT3 to regulate the pyruvate dehydrogenase complex. *Mol Cell*, 2014. **53**(4): p. 534-48.
171. Ozden, O., et al., SIRT3 deacetylates and increases pyruvate dehydrogenase activity in cancer cells. *Free Radic Biol Med*, 2014. **76**: p. 163-172.
172. Bell, E.L. and L. Guarente, The SirT3 divining rod points to oxidative stress. *Mol Cell*, 2011. **42**(5): p. 561-8.

173. Sundaresan, N.R., et al., Sirt3 blocks the cardiac hypertrophic response by augmenting Foxo3a-dependent antioxidant defense mechanisms in mice. *J Clin Invest*, 2009. **119**(9): p. 2758-71.
174. Zhang, L., et al., Differential protein acetylation assists import of excess SOD2 into mitochondria and mediates SOD2 aggregation associated with cardiac hypertrophy in the murine SOD2-tg heart. *Free Radic Biol Med*, 2017. **108**: p. 595-609.
175. Tao, R., et al., Sirt3-mediated deacetylation of evolutionarily conserved lysine 122 regulates MnSOD activity in response to stress. *Mol Cell*, 2010. **40**(6): p. 893-904.
176. Qiu, X., et al., Calorie Restriction Reduces Oxidative Stress by SIRT3-Mediated SOD2 Activation. *Cell Metab*. **12**(6): p. 662-7.
177. Lin, Z.F., et al., SIRT5 desuccinylates and activates SOD1 to eliminate ROS. *Biochem Biophys Res Commun*, 2013. **441**(1): p. 191-5.
178. Zhou, L., et al., SIRT5 promotes IDH2 desuccinylation and G6PD deglutarylation to enhance cellular antioxidant defense. *EMBO Rep*, 2016. **17**(6): p. 811-22.
179. Boylston, J.A., et al., Characterization of the cardiac succinylome and its role in ischemia-reperfusion injury. *J Mol Cell Cardiol*, 2015. **88**: p. 73-81.
180. Luo, Y.X., et al., SIRT4 accelerates Ang II-induced pathological cardiac hypertrophy by inhibiting manganese superoxide dismutase activity. *Eur Heart J*, 2017. **38**(18): p. 1389-1398.
181. Lang, A., et al., MicroRNA-15b regulates mitochondrial ROS production and the senescence-associated secretory phenotype through sirtuin 4/SIRT4. *Aging (Albany NY)*, 2016. **8**: p. 534-559.
182. Nakagawa, T., et al., SIRT5 Deacetylates carbamoyl phosphate synthetase 1 and regulates the urea cycle. *Cell*, 2009. **137**(3): p. 560-70.
183. Abmayr, S.M. and J.L. Workman, Histone lysine de-beta-hydroxybutyrylation by SIRT3. *Cell Res*, 2019. **29**(9): p. 694-695.
184. Iwahara, T., et al., SIRT3 functions in the nucleus in the control of stress-related gene expression. *Mol Cell Biol*, 2012. **32**(24): p. 5022-34.
185. Choi, B.S., J.E. Park, and C.Y. Jang, Sirt3 controls chromosome alignment by regulating spindle dynamics during mitosis. *Biochem Biophys Res Commun*, 2014. **444**(4): p. 662-9.
186. Harkcom, W.T., et al., NAD<sup>+</sup> and SIRT3 control microtubule dynamics and reduce susceptibility to antimicrotubule agents. *Proc Natl Acad Sci U S A*, 2014. **111**(24): p. E2443-52.
187. Zeng, J., et al., SIRT4 is essential for metabolic control and meiotic structure during mouse oocyte maturation. *Aging Cell*, 2018. **17**(4): p. e12789.
188. Ramadani-Muja, J., et al., Visualization of Sirtuin 4 Distribution between Mitochondria and the Nucleus, Based on Bimolecular Fluorescence Self-Complementation. *Cells*, 2019. **8**(12).

189. Mathias, R.A., T.M. Greco, and I.M. Cristea, Identification of Sirtuin4 (SIRT4) Protein Interactions: Uncovering Candidate Acyl-Modified Mitochondrial Substrates and Enzymatic Regulators. *Methods Mol Biol*, 2016. **1436**: p. 213-39.
190. Liu, L., et al., Dual function microtubule- and mitochondria-associated proteins mediate mitotic cell death. *Cell Oncol*, 2009. **31**(5): p. 393-405.
191. Guarente, L., Calorie restriction and sirtuins revisited. *Genes Dev*, 2013. **27**(19): p. 2072-85.
192. North, B.J. and E. Verdin, Mitotic regulation of SIRT2 by cyclin-dependent kinase 1-dependent phosphorylation. *J Biol Chem*, 2007. **282**(27): p. 19546-55.
193. Tanno, M., et al., Nucleocytoplasmic shuttling of the NAD<sup>+</sup>-dependent histone deacetylase SIRT1. *J Biol Chem*, 2007. **282**(9): p. 6823-32.
194. Jeong, S.M. and M.C. Haigis, Sirtuins in Cancer: a Balancing Act between Genome Stability and Metabolism. *Mol Cells*, 2015. **38**(9): p. 750-8.
195. Firestein, R., et al., The SIRT1 deacetylase suppresses intestinal tumorigenesis and colon cancer growth. *PLoS One*, 2008. **3**(4): p. e2020.
196. Oberdoerffer, P., et al., SIRT1 redistribution on chromatin promotes genomic stability but alters gene expression during aging. *Cell*, 2008. **135**(5): p. 907-18.
197. Li, K., et al., Regulation of WRN protein cellular localization and enzymatic activities by SIRT1-mediated deacetylation. *J Biol Chem*, 2008. **283**(12): p. 7590-8.
198. Dobbin, M.M., et al., SIRT1 collaborates with ATM and HDAC1 to maintain genomic stability in neurons. *Nat Neurosci*, 2013. **16**(8): p. 1008-15.
199. Lin, Y.H., et al., KAP1 Deacetylation by SIRT1 Promotes Non-Homologous End-Joining Repair. *PLoS One*, 2015. **10**(4): p. e0123935.
200. Wang, R.H., et al., Impaired DNA damage response, genome instability, and tumorigenesis in SIRT1 mutant mice. *Cancer Cell*, 2008. **14**(4): p. 312-23.
201. Rodgers, J.T., et al., Nutrient control of glucose homeostasis through a complex of PGC-1alpha and SIRT1. *Nature*, 2005. **434**(7029): p. 113-8.
202. Liu, Y., et al., A fasting inducible switch modulates gluconeogenesis via activator/coactivator exchange. *Nature*, 2008. **456**(7219): p. 269-73.
203. Gerhart-Hines, Z., et al., Metabolic control of muscle mitochondrial function and fatty acid oxidation through SIRT1/PGC-1alpha. *EMBO J*, 2007. **26**(7): p. 1913-23.
204. Purushotham, A., et al., Hepatocyte-specific deletion of SIRT1 alters fatty acid metabolism and results in hepatic steatosis and inflammation. *Cell Metab*, 2009. **9**(4): p. 327-38.
205. Hallows, W.C., W. Yu, and J.M. Denu, Regulation of glycolytic enzyme phosphoglycerate mutase-1 by Sirt1 protein-mediated deacetylation. *J Biol Chem*, 2012. **287**(6): p. 3850-8.
206. Qiang, L., et al., Brown remodeling of white adipose tissue by Sirt1-dependent deacetylation of Ppargamma. *Cell*, 2012. **150**(3): p. 620-32.

207. Picard, F., et al., Sirt1 promotes fat mobilization in white adipocytes by repressing PPAR-gamma. *Nature*, 2004. **429**(6993): p. 771-6.
208. Mattagajasingh, I., et al., SIRT1 promotes endothelium-dependent vascular relaxation by activating endothelial nitric oxide synthase. *Proc Natl Acad Sci U S A*, 2007. **104**(37): p. 14855-60.
209. Planavila, A., et al., Sirt1 acts in association with PPARalpha to protect the heart from hypertrophy, metabolic dysregulation, and inflammation. *Cardiovasc Res*, 2011. **90**(2): p. 276-84.
210. North, B.J., et al., The human Sir2 ortholog, SIRT2, is an NAD<sup>+</sup>-dependent tubulin deacetylase. *Mol Cell*, 2003. **11**(2): p. 437-44.
211. Rack, J.G., et al., Constitutive nuclear localization of an alternatively spliced sirtuin-2 isoform. *J Mol Biol*, 2014. **426**(8): p. 1677-91.
212. Dryden, S.C., et al., Role for human SIRT2 NAD-dependent deacetylase activity in control of mitotic exit in the cell cycle. *Mol Cell Biol*, 2003. **23**(9): p. 3173-85.
213. Inoue, T., et al., SIRT2, a tubulin deacetylase, acts to block the entry to chromosome condensation in response to mitotic stress. *Oncogene*, 2007. **26**(7): p. 945-57.
214. Inoue, T., et al., SIRT2 downregulation confers resistance to microtubule inhibitors by prolonging chronic mitotic arrest. *Cell Cycle*, 2009. **8**(8): p. 1279-91.
215. Jiang, W., et al., Acetylation regulates gluconeogenesis by promoting PEPCK1 degradation via recruiting the UBR5 ubiquitin ligase. *Mol Cell*, 2011. **43**(1): p. 33-44.
216. Wang, Y.P., et al., Regulation of G6PD acetylation by SIRT2 and KAT9 modulates NADPH homeostasis and cell survival during oxidative stress. *EMBO J*, 2014. **33**(12): p. 1304-20.
217. Zhao, Y., et al., Cytosolic FoxO1 is essential for the induction of autophagy and tumour suppressor activity. *Nat Cell Biol*, 2010. **12**(7): p. 665-75.
218. Rothgiesser, K.M., et al., SIRT2 regulates NF-kappaB dependent gene expression through deacetylation of p65 Lys310. *J Cell Sci*, 2010. **123**(Pt 24): p. 4251-8.
219. North, B.J. and E. Verdin, Interphase nucleo-cytoplasmic shuttling and localization of SIRT2 during mitosis. *PLoS One*, 2007. **2**(8): p. e784.
220. Wang, F. and Q. Tong, SIRT2 suppresses adipocyte differentiation by deacetylating FOXO1 and enhancing FOXO1's repressive interaction with PPARgamma. *Mol Biol Cell*, 2009. **20**(3): p. 801-8.
221. Seo, K.S., et al., SIRT2 regulates tumour hypoxia response by promoting HIF-1alpha hydroxylation. *Oncogene*, 2015. **34**(11): p. 1354-62.
222. Campisi, J., Senescent cells, tumor suppression, and organismal aging: good citizens, bad neighbors. *Cell*, 2005. **120**(4): p. 513-22.
223. Lombard, D.B., Sirtuins at the breaking point: SIRT6 in DNA repair. *Aging (Albany NY)*, 2009. **1**(1): p. 12-6.

224. Mostoslavsky, R., et al., Genomic instability and aging-like phenotype in the absence of mammalian SIRT6. *Cell*, 2006. **124**(2): p. 315-29.
225. Michishita, E., et al., Cell cycle-dependent deacetylation of telomeric histone H3 lysine K56 by human SIRT6. *Cell Cycle*, 2009. **8**(16): p. 2664-6.
226. Cheng, W.H., M. Muftuoglu, and V.A. Bohr, Werner syndrome protein: functions in the response to DNA damage and replication stress in S-phase. *Exp Gerontol*, 2007. **42**(9): p. 871-8.
227. Michishita, E., et al., SIRT6 is a histone H3 lysine 9 deacetylase that modulates telomeric chromatin. *Nature*, 2008. **452**(7186): p. 492-6.
228. Zhong, L., et al., The histone deacetylase Sirt6 regulates glucose homeostasis via Hif1alpha. *Cell*, 2010. **140**(2): p. 280-93.
229. Vazquez, B.N., et al., SIRT7 promotes genome integrity and modulates non-homologous end joining DNA repair. *EMBO J*, 2016. **35**(14): p. 1488-503.
230. Barber, M.F., et al., SIRT7 links H3K18 deacetylation to maintenance of oncogenic transformation. *Nature*, 2012. **487**(7405): p. 114-8.
231. Hubbi, M.E., et al., Sirtuin-7 inhibits the activity of hypoxia-inducible factors. *J Biol Chem*, 2013. **288**(29): p. 20768-75.
232. Ford, E., et al., Mammalian Sir2 homolog SIRT7 is an activator of RNA polymerase I transcription. *Genes Dev*, 2006. **20**(9): p. 1075-80.
233. Patel, V.P. and C.T. Chu, Decreased SIRT2 activity leads to altered microtubule dynamics in oxidatively-stressed neuronal cells: implications for Parkinson's disease. *Exp Neurol*, 2014. **257**: p. 170-81.
234. Zhang, H., et al., SIRT2 directs the replication stress response through CDK9 deacetylation. *Proc Natl Acad Sci U S A*, 2013. **110**(33): p. 13546-51.
235. Kim, H.S., et al., SIRT2 maintains genome integrity and suppresses tumorigenesis through regulating APC/C activity. *Cancer Cell*, 2011. **20**(4): p. 487-99.
236. Vaquero, A., et al., SirT2 is a histone deacetylase with preference for histone H4 Lys 16 during mitosis. *Genes Dev*, 2006. **20**(10): p. 1256-61.
237. Serrano, L., et al., The tumor suppressor SirT2 regulates cell cycle progression and genome stability by modulating the mitotic deposition of H4K20 methylation. *Genes Dev*, 2013. **27**(6): p. 639-53.
238. Movahedi Naini, S., et al., Group IVA Cytosolic Phospholipase A2 Regulates the G2-to-M Transition by Modulating the Activity of Tumor Suppressor SIRT2. *Mol Cell Biol*, 2015. **35**(21): p. 3768-84.
239. Ling, H., et al., Histone Deacetylase SIRT1 Targets Plk2 to Regulate Centriole Duplication. *Cell Rep*, 2018. **25**(10): p. 2851-2865 e3.
240. Deota, S., et al., Allosteric Regulation of Cyclin-B Binding by the Charge State of Catalytic Lysine in CDK1 Is Essential for Cell-Cycle Progression. *J Mol Biol*, 2019. **431**(11): p. 2127-2142.

241. Baur, J.A., et al., Are sirtuins viable targets for improving healthspan and lifespan? *Nat Rev Drug Discov*, 2012. **11**(6): p. 443-61.
242. Gertz, M. and C. Steegborn, Using mitochondrial sirtuins as drug targets: disease implications and available compounds. *Cell Mol Life Sci*, 2016. **73**(15): p. 2871-96.
243. Currais, A., et al., Elevating acetyl-CoA levels reduces aspects of brain aging. *Elife*, 2019. **8**.
244. Jeck, W.R., A.P. Siebold, and N.E. Sharpless, Review: a meta-analysis of GWAS and age-associated diseases. *Aging Cell*, 2012. **11**(5): p. 727-31.
245. Barzilai, N., et al., The critical role of metabolic pathways in aging. *Diabetes*, 2012. **61**(6): p. 1315-22.
246. Finkel, T. and N.J. Holbrook, Oxidants, oxidative stress and the biology of ageing. *Nature*, 2000. **408**(6809): p. 239-47.
247. Finley, L.W., et al., SIRT3 opposes reprogramming of cancer cell metabolism through HIF1alpha destabilization. *Cancer Cell*, 2011. **19**(3): p. 416-28.
248. Sebastian, C., et al., The histone deacetylase SIRT6 is a tumor suppressor that controls cancer metabolism. *Cell*, 2012. **151**(6): p. 1185-99.
249. Ahuja, N., et al., Regulation of insulin secretion by SIRT4, a mitochondrial ADP-ribosyltransferase. *J Biol Chem*, 2007. **282**(46): p. 33583-92.
250. Argmann, C. and J. Auwerx, Insulin secretion: SIRT4 gets in on the act. *Cell*, 2006. **126**(5): p. 837-9.
251. Jeong, S.M., et al., SIRT4 has tumor-suppressive activity and regulates the cellular metabolic response to DNA damage by inhibiting mitochondrial glutamine metabolism. *Cancer cell*, 2013. **23**(4): p. 450-463.
252. Nasrin, N., et al., SIRT4 regulates fatty acid oxidation and mitochondrial gene expression in liver and muscle cells. *J Biol Chem*, 2010. **285**: p. 31995-32002.
253. Fu, L., et al., SIRT4 inhibits malignancy progression of NSCLCs, through mitochondrial dynamics mediated by the ERK-Drp1 pathway. *Oncogene*, 2017. **36**(19): p. 2724-2736.
254. Carafa, V., A. Nebbioso, and L. Altucci, Sirtuins and disease: the road ahead. *Front Pharmacol*, 2012. **3**: p. 4.
255. Csibi, A., et al., The mTORC1 pathway stimulates glutamine metabolism and cell proliferation by repressing SIRT4. *Cell*, 2013. **153**(4): p. 840-54.
256. Jeong, S.M., et al., SIRT4 protein suppresses tumor formation in genetic models of Myc-induced B cell lymphoma. *J Biol Chem*, 2014. **289**(7): p. 4135-44.
257. Kim, H.S., et al., SIRT3 is a mitochondria-localized tumor suppressor required for maintenance of mitochondrial integrity and metabolism during stress. *Cancer Cell*, 2010. **17**(1): p. 41-52.

258. Jeong, S.M., et al., SIRT4 has tumor-suppressive activity and regulates the cellular metabolic response to DNA damage by inhibiting mitochondrial glutamine metabolism. *Cancer Cell*, 2013. **23**(4): p. 450-63.
259. Bastians, H., Causes of Chromosomal Instability. *Recent Results Cancer Res*, 2015. **200**: p. 95-113.
260. Zeng, J., et al., SIRT4 is essential for metabolic control and meiotic structure during mouse oocyte maturation. *Aging Cell*, 2018: p. e12789.
261. Lang, A., et al., SIRT4 interacts with OPA1 and regulates mitochondrial quality control and mitophagy. *Aging (Albany NY)*, 2017. **9**(10): p. 2163-2189.
262. Drews, L., et al., Ammonia inhibits energy metabolism in astrocytes in a rapid and glutamate dehydrogenase 2-dependent manner. *Dis Model Mech*, 2020. **13**(10).
263. Bergmann, L., et al., Subcellular Localization and Mitotic Interactome Analyses Identify SIRT4 as a Centrosomally Localized and Microtubule Associated Protein. *Cells*, 2020. **9**(9).
264. Han, Y., et al., SIRT4 and Its Roles in Energy and Redox Metabolism in Health, Disease and During Exercise. *Front Physiol*, 2019. **10**: p. 1006.
265. Nakamura, Y., et al., Localization of mouse mitochondrial SIRT proteins: shift of SIRT3 to nucleus by co-expression with SIRT5. *Biochem Biophys Res Commun*, 2008. **366**(1): p. 174-9.
266. Bao, J., et al., Characterization of the murine SIRT3 mitochondrial localization sequence and comparison of mitochondrial enrichment and deacetylase activity of long and short SIRT3 isoforms. *J Cell Biochem*, 2010. **110**(1): p. 238-47.
267. Filipuzzi, I., et al., Stenomycin selectively inhibits TIM23-dependent mitochondrial protein import. *Nat Chem Biol*, 2017. **13**(12): p. 1239-1244.
268. Melber, A. and C.M. Haynes, UPR(mt) regulation and output: a stress response mediated by mitochondrial-nuclear communication. *Cell Res*, 2018. **28**(3): p. 281-295.
269. Chung, J.Y., J.A. Steen, and T.L. Schwarz, Phosphorylation-Induced Motor Shedding Is Required at Mitosis for Proper Distribution and Passive Inheritance of Mitochondria. *Cell Rep*, 2016. **16**(8): p. 2142-2155.
270. Scher, M.B., A. Vaquero, and D. Reinberg, SirT3 is a nuclear NAD<sup>+</sup>-dependent histone deacetylase that translocates to the mitochondria upon cellular stress. *Genes Dev*, 2007. **21**(8): p. 920-8.
271. Harbauer, A.B., et al., The protein import machinery of mitochondria-a regulatory hub in metabolism, stress, and disease. *Cell Metab*, 2014. **19**(3): p. 357-72.
272. Maxwell, M.M., et al., The Sirtuin 2 microtubule deacetylase is an abundant neuronal protein that accumulates in the aging CNS. *Hum Mol Genet*, 2011. **20**(20): p. 3986-96.
273. Pereira, J.M., et al., Infection Reveals a Modification of SIRT2 Critical for Chromatin Association. *Cell Rep*, 2018. **23**(4): p. 1124-1137.
274. Eldridge, M.J.G., et al., Active nuclear import of the deacetylase Sirtuin-2 is controlled by its C-terminus and importins. *Sci Rep*, 2020. **10**(1): p. 2034.

275. Luders, J. and T. Stearns, Microtubule-organizing centres: a re-evaluation. *Nat Rev Mol Cell Biol*, 2007. **8**(2): p. 161-7.
276. Lin, T.C., A. Neuner, and E. Schiebel, Targeting of gamma-tubulin complexes to microtubule organizing centers: conservation and divergence. *Trends Cell Biol*, 2015. **25**(5): p. 296-307.
277. Matsuyama, A., et al., In vivo destabilization of dynamic microtubules by HDAC6-mediated deacetylation. *EMBO J*, 2002. **21**(24): p. 6820-31.
278. Akella, J.S., et al., MEC-17 is an alpha-tubulin acetyltransferase. *Nature*, 2010. **467**(7312): p. 218-22.
279. Shida, T., et al., The major alpha-tubulin K40 acetyltransferase alphaTAT1 promotes rapid ciliogenesis and efficient mechanosensation. *Proc Natl Acad Sci U S A*, 2010. **107**(50): p. 21517-22.
280. Hubbert, C., et al., HDAC6 is a microtubule-associated deacetylase. *Nature*, 2002. **417**(6887): p. 455-8.
281. Aguilar, A., et al., Alpha-tubulin K40 acetylation is required for contact inhibition of proliferation and cell-substrate adhesion. *Mol Biol Cell*, 2014. **25**(12): p. 1854-66.
282. Lin, T.C., et al., MOZART1 and gamma-tubulin complex receptors are both required to turn gamma-TuSC into an active microtubule nucleation template. *J Cell Biol*, 2016. **215**(6): p. 823-840.
283. Nakamura, M., et al., Arabidopsis GCP3-interacting protein 1/MOZART 1 is an integral component of the gamma-tubulin-containing microtubule nucleating complex. *Plant J*, 2012. **71**(2): p. 216-25.
284. Ling, H., et al., Suppression of centrosome duplication and amplification by deacetylases. *Cell Cycle*, 2012. **11**(20): p. 3779-91.
285. Wang, T., et al., CCDC84 Acetylation Oscillation Regulates Centrosome Duplication by Modulating HsSAS-6 Degradation. *Cell Rep*, 2019. **29**(7): p. 2078-2091 e5.
286. Martinez-Diez, M., et al., Biogenesis and dynamics of mitochondria during the cell cycle: significance of 3'UTRs. *PLoS One*, 2006. **1**: p. e107.
287. Mirzayans, R., B. Andrais, and D. Murray, Roles of Polyploid/Multinucleated Giant Cancer Cells in Metastasis and Disease Relapse Following Anticancer Treatment. *Cancers (Basel)*, 2018. **10**(4).
288. Levine, M.S. and A.J. Holland, The impact of mitotic errors on cell proliferation and tumorigenesis. *Genes Dev*, 2018. **32**(9-10): p. 620-638.
289. Taguchi, N., et al., Mitotic phosphorylation of dynamin-related GTPase Drp1 participates in mitochondrial fission. *J Biol Chem*, 2007. **282**(15): p. 11521-9.
290. Mills, C.A., et al., Sirtuin 5 is Regulated by the SCF-Cyclin F Ubiquitin Ligase and is Involved in Cell Cycle Control. *Mol Cell Biol*, 2020.
291. Li, T., et al., Mitochondrial PAK6 inhibits prostate cancer cell apoptosis via the PAK6-SIRT4-ANT2 complex. *Theranostics*, 2020. **10**(6): p. 2571-2586.

292. Wei, Y., et al., CDK1-dependent phosphorylation of EZH2 suppresses methylation of H3K27 and promotes osteogenic differentiation of human mesenchymal stem cells. *Nat Cell Biol*, 2011. **13**(1): p. 87-94.
293. Sun, S., et al., Circular RNA circ-ADD3 inhibits hepatocellular carcinoma metastasis through facilitating EZH2 degradation via CDK1-mediated ubiquitination. *Am J Cancer Res*, 2019. **9**(8): p. 1695-1707.
294. Wu, S.C. and Y. Zhang, Cyclin-dependent kinase 1 (CDK1)-mediated phosphorylation of enhancer of zeste 2 (Ezh2) regulates its stability. *J Biol Chem*, 2011. **286**(32): p. 28511-9.
295. Sweet, S. and G. Singh, Accumulation of human promyelocytic leukemic (HL-60) cells at two energetic cell cycle checkpoints. *Cancer Res*, 1995. **55**(22): p. 5164-7.
296. Petrosillo, G., et al., Mitochondrial complex I dysfunction in rat heart with aging: critical role of reactive oxygen species and cardiolipin. *Free Radic Biol Med*, 2009. **46**(1): p. 88-94.
297. Roessler, M.M., et al., Direct assignment of EPR spectra to structurally defined iron-sulfur clusters in complex I by double electron-electron resonance. *Proc Natl Acad Sci U S A*, 2010. **107**(5): p. 1930-5.
298. Owusu-Ansah, E., et al., Distinct mitochondrial retrograde signals control the G1-S cell cycle checkpoint. *Nat Genet*, 2008. **40**(3): p. 356-61.
299. Wang, Z., et al., Cyclin B1/Cdk1 coordinates mitochondrial respiration for cell-cycle G2/M progression. *Dev Cell*, 2014. **29**(2): p. 217-32.
300. Nakahara, Y., et al., Downregulation of SIRT4 Expression Is Associated with Poor Prognosis in Esophageal Squamous Cell Carcinoma. *Oncology*, 2016. **90**(6): p. 347-55.
301. Xing, J., et al., SIRT4 enhances the sensitivity of ER-positive breast cancer to tamoxifen by inhibiting the IL-6/STAT3 signal pathway. *Cancer Med*, 2019. **8**(16): p. 7086-7097.
302. Fu, L., et al., SIRT4 inhibits malignancy progression of NSCLCs, through mitochondrial dynamics mediated by the ERK-Drp1 pathway. *Oncogene*, 2017. **36**(19): p. 2724-2736.
303. Suzuki, K., et al., Identification of non-Ser/Thr-Pro consensus motifs for Cdk1 and their roles in mitotic regulation of C2H2 zinc finger proteins and Ect2. *Sci Rep*, 2015. **5**: p. 7929.
304. Sharma, A., S. Costantini, and G. Colonna, The protein-protein interaction network of the human Sirtuin family. *Biochim Biophys Acta*, 2013. **1834**(10): p. 1998-2009.
305. Horbay, R. and R. Bilyy, Mitochondrial dynamics during cell cycling. *Apoptosis*, 2016. **21**(12): p. 1327-1335.
306. Xie, B., et al., Cyclin B1/CDK1-regulated mitochondrial bioenergetics in cell cycle progression and tumor resistance. *Cancer Lett*, 2019. **443**: p. 56-66.

307. Carafa, V., L. Altucci, and A. Nebbioso, Dual Tumor Suppressor and Tumor Promoter Action of Sirtuins in Determining Malignant Phenotype. *Front Pharmacol*, 2019. **10**: p. 38.
308. Huang, G. and G. Zhu, Sirtuin-4 (SIRT4), a therapeutic target with oncogenic and tumor-suppressive activity in cancer. *Onco Targets Ther*, 2018. **11**: p. 3395-3400.
309. Shi, Q., et al., Decreased sirtuin 4 expression is associated with poor prognosis in patients with invasive breast cancer. *Oncol Lett*, 2016. **12**(4): p. 2606-2612.
310. Jeong, S.M., S. Hwang, and R.H. Seong, SIRT4 regulates cancer cell survival and growth after stress. *Biochem Biophys Res Commun*, 2016. **470**(2): p. 251-256.
311. Huang, G., et al., Clinical and therapeutic significance of sirtuin-4 expression in colorectal cancer. *Oncol Rep*, 2016.
312. Miyo, M., et al., Tumour-suppressive function of SIRT4 in human colorectal cancer. *Br J Cancer*, 2015. **113**(3): p. 492-9.
313. Jeffery, C.J., Protein moonlighting: what is it, and why is it important? *Philos Trans R Soc Lond B Biol Sci*, 2018. **373**(1738).
314. Proteinatlas-Projekt,  
[https://www.proteinatlas.org/search/subcell\\_location:Centriolar+Satellit,Zentrosom+AND+Subzell-Lokation:Mitochondrien](https://www.proteinatlas.org/search/subcell_location:Centriolar+Satellit,Zentrosom+AND+Subzell-Lokation:Mitochondrien).
315. Majumder, S., et al., VDAC3 regulates centriole assembly by targeting Mps1 to centrosomes. *Cell Cycle*, 2012. **11**(19): p. 3666-78.
316. Chen, M.K., et al., Influence of progressive tumor growth on glutamine metabolism in skeletal muscle and kidney. *Ann Surg*, 1993. **217**(6): p. 655-66; discussion 666-7.
317. Wise, D.R., et al., Myc regulates a transcriptional program that stimulates mitochondrial glutaminolysis and leads to glutamine addiction. *Proc Natl Acad Sci U S A*, 2008. **105**(48): p. 18782-7.
318. Klimberg, V.S. and J.L. McClellan, Claude H. Organ, Jr. Honorary Lectureship. Glutamine, cancer, and its therapy. *Am J Surg*, 1996. **172**(5): p. 418-24.
319. Patten, D.A., et al., OPA1-dependent cristae modulation is essential for cellular adaptation to metabolic demand. *EMBO J*, 2014. **33**(22): p. 2676-91.
320. Lee, Y.J., et al., Roles of the mammalian mitochondrial fission and fusion mediators Fis1, Drp1, and Opa1 in apoptosis. *Mol Biol Cell*, 2004. **15**(11): p. 5001-11.

## 10. Danksagung

Ich möchte mich herzlichst bei allen bedanken, die mich bei der Erarbeitung und Zusammenstellung dieser Arbeit unterstützt und begleitet haben.

Besonders möchte ich mich bei Reza Ahmadian und Lutz Schmitt dafür bedanken, dass sie die Rollen als Gutachter übernommen haben und mir damit den Rahmen zur Erarbeitung dieser Dissertation ermöglichten.

Großer Dank gilt auch Jürgen Scheller, der durch zusätzliche Finanzierung dafür gesorgt hat, dass ich diese Arbeit fertigstellen konnte. Vor allem aber auch, weil er zu genau den richtigen Zeitpunkten die genau richtigen Worte der Motivation in seiner eigenen Art parat hatte!

Ich möchte mich bei allen im Institut für BCMII bedanken, die mir im Labor im Kleinen sowie auch im Großen ausgeholfen haben. Ich habe viel von Leuten gelernt und übernommen, aber auch an andere weitergegeben. Die Zusammenarbeit und Erfahrungen, die ich über die Jahre gesammelt habe, sind genauso essenziell für die Erstellung dieser Arbeit gewesen wie das bloße Wälzen der Literatur. Vielen lieben Dank an alle meine Kollegen die mich in den unterschiedlichsten Bereichen unterstützt haben. Dabei möchte ich mich besonders bei Petra für die Hilfe bei allem organisatorischen und bei Feri für die Unterstützungen in allen technischen Belangen bedanken. Herausstellen möchte ich auch Iris, mit der ich viel im Labor zusammengearbeitet habe und ohne deren Unterstützung und Know-how viele Experimente nie möglich gewesen wären.

Danke auch an alle mit denen ich in Kooperationen zusammengearbeitet habe und die mir Einblick in ihre Projekte und Forschungsgebiete gegeben haben.

Besonderer Dank weiterhin auch an Andreas Reichert für die ausgiebige Nutzung des konfokalen Mikroskops seiner Arbeitsgruppe ohne das ein signifikanter Teil der Daten und Ergebnisse sonst nicht möglich gewesen wäre.

Schließlich möchte ich mich herzlich bei Roland Piekorz bedanken. Mentor, direkter Betreuer und vor allem auch Sparringspartner in vielen Diskussionen mit dem ich über die Jahre eng an dem Projekt zusammengearbeitet habe. Seine Betreuung und Anleitung, gerade aber auch unsere teils hitzigen Diskussionen haben meine Entwicklung was den wissenschaftlichen Diskurs angeht und meine Selbstsicherheit in meine Experimente und Datenlage gestärkt und geprägt.

Ich möchte mich herzlich bei allen Korrekturlesern bedanken, die mit frischem Blick auf die Arbeit geschaut haben und mir nicht nur bei Rechtschreibung und Kommasetzung unter die Arme gegriffen haben, sondern auch immer wieder Anstöße zur verständlicheren Formulierung gegeben haben. Dabei möchte ich insbesondere Marik, Luzia, Gudrun und Norbert als Unterstützer erwähnen!

Es gibt unzählige Leute, die ich hier noch auflisten könnte, die auf verschiedenste Weise mitgeholfen haben, bei denen ich mir Rat und Mut geholt habe und Frust und Stress abladen konnte.

Danke euch allen!

# 11. Lebenslauf

## Laura Bergmann

---

Anschrift	Gumbertstraße 166 40229 Düsseldorf
E-Mail	Laura.Bergmann@hhu.de
Geboren	16.03.1991 (Faro, Portugal)

## Berufliche Erfahrungen

---

01.10.2020 – 30.09.2021	Quality Specialist Contract Manufacturing GTO Wilkinson Sword GmbH
01.05.2017 – 30.09.2020	Promotionsstudent at Universitätsklinikum Düsseldorf Institut für Biochemie und Molekularbiologie II
26.10.2016 – 31.01.2017	Internship an dem Universitätsklinikum Düsseldorf Institut für Pharmakologie und Klinische Pharmakologie UKD
04.09.2016 – 15.10.2016	Freiwilligenarbeit in Südafrika Konservator bei White Shark Projects, Gansbaai
01.04.2015 – 31.01.2016	Internship bei Henkel in der Abteilung Laundry & Home Care Research / Enzymes / Characterization
02.01.2014 – 31.12.2014	Studentische Hilfskraft Universitätsklinikum Düsseldorf AG Infektiologie und Typ 1 Diabetes
10.09.2007 – 21.09.2007	Praktikum im Museum für Naturkunde, Berlin Bereich: Paläobiologie der Ammoniten

## Hochschulbildung

---

05.2017 – 09.2020	Promotion an der Heinrich-Heine-Universität Düsseldorf im Institut für Molekularbiologie und Biochemie II Thesis: „Die Rolle des Sirtuins SIRT4 in der Zellzyklusprogression und mitotischen Zellteilung“
10.2013 – 04.2016	Masterstudium in Biochemie (M. Sc.) Heinrich-Heine-Universität Düsseldorf; Notendurchschnitt: 2,1 Thesis: „Klonierung, Expression und Charakterisierung von Tannin abbauenden Enzymen“
10.2010 – 09.2013	Bachelorstudium in Biochemie (B. Sc.) Heinrich-Heine-Universität Düsseldorf; Notendurchschnitt: 2,0 Thesis: „Charakterisierung von ADEP-resistenten ClpP Mutanten“

## Publikationen

---

- 2020 **Bergmann L**, Lang A, Bross C, Altinoluk-Hambüchen S, Feyl, Overbeck N, Stefanski A, Wiek C, Kefalas A, Verhülsdonk P, Mielke C, Sohn D, Stühler K, Hanenberg H, Jänicke RU, Scheller J, Reichert AS, Ahmadian MR, Piekorz RP
- Subcellular Localization and Mitotic Interactome Analyses Identify SIRT4 as a Centrosomally Localized and Microtubule Associated Protein**
- Cells. 2020 Aug 24;9(9):1950. doi: 10.3390/cells9091950. PMID: 32846968; PMCID: PMC7564595.
- 2020 Drews L, Zimmermann M, Westhoff P, Brilhaus D, Poss RE, **Bergmann L**, Wiek C, Brenneisen P, Piekorz RP, Mettler-Altman T, Weber APM, Reichert AS.
- Ammonia inhibits energy metabolism in astrocytes in a rapid and glutamate dehydrogenase 2-dependent manner**
- Dis Model Mech. 2020 Nov 4;13(10): dmm047134. doi: 10.1242/dmm.047134. PMID: 32917661; PMCID: PMC7657470
- 2018 Singh M, Bergmann L, Lang A, Pexa K, Kuck F, Stibane D, Janke L, Ezzahoini H, Lindecke A, Wiek C, Hanenberg H, Köhrer K, von Gall C, Reinke H, Piekorz RP
- $\alpha_{13}$  signaling is associated with sexual dimorphic expression of the clock-controlled output gene *Dbp* in murine liver**
- Oncotarget. 2018 Jul 13;9(54):30213-30224. doi: 10.18632/oncotarget.25727. PMID: 30100984; PMCID: PMC6084400.
- 2017 Lang A, Anand R, Altinoluk-Hambüchen S, Ezzahoini H, Stefanski A, Iram A, **Bergmann L**, Urbach J, Böhler P, Hänsel J, Franke M, Stühler K, Krutmann J, Scheller J, Stork B, Reichert AS and Piekorz RP
- SIRT4 interacts with OPA1 and regulates mitochondrial quality control and mitophagy**
- Aging (Albany NY). 2017; 9:2160-2186. DOI: 10.18632/aging.101307

## 12. Eidesstattliche Erklärung

Ich versichere an Eides statt, dass die Dissertation von mir selbstständig und ohne unzulässige fremde Hilfe unter der Beachtung der „Grundsätze zur Sicherung guter wissenschaftlicher Praxis an der Heinrich-Heine-Universität Düsseldorf“ erstellt worden ist.

Düsseldorf, den 05.04.2022

  
Laura Bergmann



## 13. Anhang

### 13.1. Aminosäuresequenzen und Alignments der Sirtuine 2, 3, 4 und 5

CDK1: Serine/Threonin (S/T) Kinase [303]:

Katalysiert den Transfer eines Phosphates von ATP auf einen Prolin (P)-orientierten S oder T Rest. Substrate beinhalten entweder ein optimales (S/T\*-P-x-K/R) oder ein minimales (S/T\*-P) CDK1 Konsensus-Motiv.

Zusätzlich sind in wenigen Fällen auch non-Ser/Thr-Pro Konsensus-Motive bekannt:

Minimal Sequenz: [S/T-X-X-R/K](#)

Bevorzugte:(P)-X-S/T-X-[R/K]

#### **SIRT4 Aminosäure Sequenz** ([www.uniprot.org/uniprot/Q9Y6E7](http://www.uniprot.org/uniprot/Q9Y6E7))

MKMSFALTFRSAKGRWIANPSQPCSKASIGLVFVPA**SP**PLDPEKVKELQRFITLSKRLLVM  
T**GAGISTESGIPDYRSE**KVGLYARTDRRPIQHGFVRSAPIRQRYWARNFVGPQFSSHQ  
PNPAHWALST**WEKLGKLYWLV**TQNVDALHTKAGSRRLTELHGCMDRVLCDCGEQ**TE**RGV  
LQERFQVLNPTWSAEAHGLAPDGDVFLSEEQVRSFQVPTCVQCGHLLKPDVVFVGGDTVNP  
DKVDFVHKRVKEADSLLVGSSLVQVYSGYRIFILTAWEEKLPIAILNIGPTRSDDLACLKL  
NSRCGELLPLIDPC

#### **SIRT3 Aminosäure Sequenz** ([www.uniprot.org/uniprot/Q9NTG7](http://www.uniprot.org/uniprot/Q9NTG7))

MAFWGWRAAAALRLWGRVVERVEAGGGVGPQACGCRLLVGGRRDDVSAGLRGSHGARGE  
LDPARPLQRPPRPEVPRAFRRQPRAAAPSSFFSSIKGRRSISFVSGASSVVGSGG**SSDK**  
GKLSLQDVAELIRARACQRVVVMV**GAGISTPSGIPDFRS**PGSGLYSNLQQYDLPYPEAIF  
ELPFFFHNPKPFFTLAKELYPGNYKPNVTHYFLRLLHDKGLLLRLYTQNIIDGLERVSGIP  
ASKLVEAHGTAFASATCTVCQRPFPGEDIRADVMADRVPRCPVCTGVVVKPDIVFFGEPLPQ  
RFLLVVDFPMADLLILGTSLEVEPFASLTEAVRS**SVPR**LLINRDLVGPLAWH**PRSR**DV  
AQLGDVVHGVESLVELLGWTEEMRDLVQRETGKLDGPK

#### **SIRT5 Aminosäure Sequenz** ([www.uniprot.org/uniprot/Q9NXA8](http://www.uniprot.org/uniprot/Q9NXA8))

MRPLQIVPSRLISQLYCGLKP**PASTRNQ**ICLKMARPSSSMADFRKFFAKAKHIVIISGAG  
VSAESGVPTFRGAGGYWRKWQAQDLA**TE**LAFAHNPSRVWEFYHYRREVMGSKEPNAGHRA  
IAECETRLGKQRRVVVITQNIIDELHRKAGTKNLEIHG**SLFK**TRCTSCGVVAENYK**SE**I  
CPALSGKGAPEPGTQDASIPVEKLPCEEEAGCGLLRPHVVWFGENLDPAILVEVDRELA  
HCDLCLVVGTSVVVYPAAMFAPQVAARGVPVAEFNTET**TE**ATNFRFRHFQGPCGTTLPEA  
LACHENETVS

CLUSTAL O(1.2.4) multiple sequence alignment erstellt über Uniprot:  
<https://www.uniprot.org/align/>

```

SP|Q9NTG7|SIR3_HUMAN MAFWGWRAAAAALRLWGRVVERVEAGGVGVPFQACGCRLVLGGRDDVSAGLRGSHGARGE 60
SP|Q9Y6E7|SIR4_HUMAN -----
SP|Q9NXA8|SIR5_HUMAN -----

SP|Q9NTG7|SIR3_HUMAN LDPARPLQRPPRPEVPRAFR--RQPRAAAPSFSSIKGRRSISFSVVGASSVVGSGGSS 118
SP|Q9Y6E7|SIR4_HUMAN -----MKMSFALTFRSAKGRWIANPSQPCSKAS-----IGLFVPASE----- 37
SP|Q9NXA8|SIR5_HUMAN -----MR-----PLQIVPSRLISQLY-----CGLKPPASTRNQ---IC 30
          :                               ** * .           .: **

          NAD+-Bindemotiv
          |-----|
          |GAGISTPSGIPDFRSESGGLYSNLQQYDLPYPE 177
          |GAGISTESGIPDYRSEKVGLYARTDRRPIQHGD 94
          |GAGVSAESGVPTFRGAGG-YWRKWQAQDLATE- 88
          |ICLVGAGISTSAGIPDFRSESTGLYDNLEKYH
          ..: : : ..: : : ***:* : **:* :* . : . : :

SP|Q9NTG7|SIR3_HUMAN AIFELPFFFHNPKEPFTLAK--ELYPGNYKPNVTHYFLRL----LHDKGLLLRRLYTQNI 231
SP|Q9Y6E7|SIR4_HUMAN FVR----SAPIRQRYWARNFVWQPFSSHQPNPAHWALST----WEKLGKLYLWLTQNV 146
SP|Q9NXA8|SIR5_HUMAN -LA----FAHNPSRVWEFYHYRREVMSKEPNAGHRAIAECETRLGKQRRVVVITQNI 143
          : . : . . : ** * : . * : ***:*

SP|Q9NTG7|SIR3_HUMAN GLERVSGIPASKLVEAHGTFFASATCTVCQRPFPGED I----- 268
SP|Q9Y6E7|SIR4_HUMAN ALHTKAGS--RRLTELHGCMRDLVCLDCGEQTERGVLQERFQVLNPTWSAEAHGLAPDGD 204
SP|Q9NXA8|SIR5_HUMAN ELHRKAGT--KNLLEIHGSLFKTRCTSCGVVAENYK----SEICPALSGK--G-APEPG 193
          * . : * . * * * : . * *

SP|Q9NTG7|SIR3_HUMAN ----RADVMADRVPRC--PVCTGVVKPDIVFFGEPLPQRFLLVH-VDFPMADLLLILGTS 321
SP|Q9Y6E7|SIR4_HUMAN VFLSEEQVRSFQVPTC--VQCGGHLKPDVVFFGDTVNPDKVDFVHKRVKEADSLLVGSS 262
SP|Q9NXA8|SIR5_HUMAN TQ--DASIPVEKLP RCEEAGCGGLLRPHVWVFGENLDPALIEVDRELAHCDLCLVVGTS 251
          . : : * * * * : * : * . . * * : * : *

SP|Q9NTG7|SIR3_HUMAN LEVEPFASL TEAV-RSSVPRLLINRDLVG-----PLAWHPRSRDVAQLGDVVHGVESLVE 375
SP|Q9Y6E7|SIR4_HUMAN LQVYSGYR FILTAW EKKLP IAILNIGPTRSDDLACLKLSRCGELLPLIDPC----- 314
SP|Q9NXA8|SIR5_HUMAN SVVYPAAMFAPQVAARGVPVAEFNTETTEATNRF RHFHQGPCGTTLPEALACHENETVS- 310
          * : . : * : * . : : .

SP|Q9NTG7|SIR3_HUMAN LLGWTEEMRDLVQRETGKLDGDPDK 399
SP|Q9Y6E7|SIR4_HUMAN -----
SP|Q9NXA8|SIR5_HUMAN -----

```

## SIRT2 Aminosäure Sequenz (www.uniprot.org/uniprot/Q8IXJ6)

MAEPDPSHPLETQAGKVQEAQDSDSSEGGAGGEADMDFLRNLFSSQTLSLGSQKERLLDELTLLEGVARYMQSER  
 CRRVICLVGAGISTSAGIPDFRSPSTGLYDNLEKYHLPYPEAIFEISYFKKHPEPFFALAKELYPGQFKPTICHY  
 FMRLKDKGLLLRCYTNIDTLERIAAGLEQEDLVEAHGTFYTSVCVSASCRHEYPFSWMKEKIFSEVTEKCEDCQ  
 SLVKPDIVFFGESLPAFFSCMQSDFLKVDLLVMGTSLVQVQPFASLISKAPLSTPRLLINKEKAGQSDPFLGMI  
 MGLGGGMDFDSSKAYRDVAWLGECDQGCCLALAEALLGWKKELEDLVRREHASIDAQSGAGVNPSTSASEKKSPP  
 AKDEARTTEREKPO

CLUSTAL O(1.2.4) multiple sequence alignment erstellt über Uniprot:  
<https://www.uniprot.org/align/>

```
SP|Q9Y6E7|SIR4_HUMAN -----MKMSFALTFRSAKGRWIANPSQPCS 25
SP|Q8IXJ6|SIR2_HUMAN MAEPDPSHPLETQAGKVQEAQDSDSSEGGAGGEADMDFLRNLF----- 46
                        .*.*  .: *
```

NAD<sup>+</sup>-Bindemotiv

```
SP|Q9Y6E7|SIR4_HUMAN KASIGLVFVPASPPLDPEKVKELQRFI--TLKRLLVMTGAGISTESGIPDYRSEKVGGLYA 83
SP|Q8IXJ6|SIR2_HUMAN -QTLGLGSQKERLLDELTLLEGVARYMQSERCRRVICLVGAGISTSAGIPDFRSPSTGLYD 105
                        :.* . ** .:: *:: .::: :*** **.:***.** .**
```

```
SP|Q9Y6E7|SIR4_HUMAN RTDRRPIQHGDVFRSAPIRQRYWARNFVGPQ-----FSSHQPNPAHWALSTWEKLGKL 137
SP|Q8IXJ6|SIR2_HUMAN NLEKYHLPYPEAIF---EISYFKKHPEPFFALAKELYPGQFKPTICHYFMRLKDKGLL 161
                        . : : : : . * : : : . . . : * . * : : . * *
```

```
SP|Q9Y6E7|SIR4_HUMAN YWLVTQNVDAHHTKAGSR--RLTELHGCMRVLCLD--CGEQTPRGVLQERFQVLNPTWS 193
SP|Q8IXJ6|SIR2_HUMAN LRCYTNIDTLERIAAGLEQEDLVEAHGTFYTSVCVSASCRHEYP----- 205
                        ***:*.* ** . *.* ** : *:. * .: *
```

```
SP|Q9Y6E7|SIR4_HUMAN AEAHGLAPDGDVFLSEEQVRSFQVPTCVQC GGHLKPDVVFVGDVTPNDKVDVHKRVKEA 253
SP|Q8IXJ6|SIR2_HUMAN -----LSWMKEKIFSEVTEKCEDCQSLVKPDIVFFGESLPAFFSCMQSDFLK 254
                        : *:: * .*. * : :***:***::: . . :. . . :
```

```
SP|Q9Y6E7|SIR4_HUMAN DSLLVVGSLSLVYSGYRFLTAWKELPIALINIGP-TRSD----- 294
SP|Q8IXJ6|SIR2_HUMAN DLLVMGTSLVQVQPFASLISKAPL-STPRLLINKEKAGQSDPFLGMIMGLGGGMDFDSSK 313
* ***:*.**** :* . * . * ::* :**
```

```
SP|Q9Y6E7|SIR4_HUMAN -----LACLKLNRCGELLPLIDP----- 314
SP|Q8IXJ6|SIR2_HUMAN AYRDVAWLGECDQGCCLALAEALLGWKKELEDLVRREHASIDAQSGAGVNPSTSASEKKS 373
                        .** * . * * *
```

```
SP|Q9Y6E7|SIR4_HUMAN -----
SP|Q8IXJ6|SIR2_HUMAN PPAKDEARTTEREKPO 389
```